

Galaxy masses

Stéphane Courteau*

Queen's University, Department of Physics, Engineering Physics and Astronomy, Kingston, Ontario, Canada

Michele Cappellari

Sub-department of Astrophysics, Department of Physics, University of Oxford, Denys Wilkinson Building, Keble Road, Oxford OX1 3RH, United Kingdom

Roelof S. de Jong

Leibniz-Institut für Astrophysik Potsdam (AIP), An der Sternwarte 16, 14482 Potsdam, Germany

Aaron A. Dutton

Max-Planck-Institut für Astronomie, Königstuhl 17, 69117 Heidelberg, Germany

Eric Emsellem

European Southern Observatory, Karl-Schwarzschild-Strasse 2, 85748, Germany and Université Lyon 1, Observatoire de Lyon, Centre de Recherche Astrophysique de Lyon and Ecole Normale Supérieure de Lyon, 9 avenue Charles André, F-69230 Saint-Genis Laval, France

Henk Hoekstra

Leiden Observatory, Leiden University, P.O. Box 9513, NL-2300 RA Leiden, The Netherlands

L. V. E. Koopmans

University of Groningen, Kapteyn Astronomical Institute, P.O. Box 800, 9700 AV, Groningen, The Netherlands

Gary A. Mamon

Institut d'Astrophysique de Paris (UMR 7095: CNRS & UPMC), 98 bis Bd Arago, F-75014 Paris, France

Claudia Maraston

University of Portsmouth, Institute of Cosmology and Gravitation, Dennis Sciama Building, Burnaby Road, Portsmouth, United Kingdom

Tommaso Treu

University of California, Santa Barbara, Department of Physics, Santa Barbara, California, USA

Lawrence M. Widrow

Queen's University, Department of Physics, Engineering Physics and Astronomy, Kingston, Ontario, Canada

(published 14 January 2014)

Galaxy masses play a fundamental role in our understanding of structure formation models. This review addresses the variety and reliability of mass estimators that pertain to stars, gas, and dark matter. The different sections on masses from stellar populations, dynamical masses of gas-rich and gas-poor galaxies, with some attention paid to our Milky Way, and masses from weak and strong lensing methods all provide review material on galaxy masses in a self-consistent manner.

DOI: [10.1103/RevModPhys.86.47](https://doi.org/10.1103/RevModPhys.86.47)

PACS numbers: 98.35.Ce, 98.62.Ve, 06.30.Dr

*courteau@astro.queensu.ca

CONTENTS

I. Introduction	48	VI. Weak Lensing by Galaxies	86
II. From Light to Mass: Modeling the Stellar M^*/L Ratio	49	A. Introduction	86
A. Modeling galaxies and their stellar populations:		B. Theory of weak lensing	87
A historical introduction	49	C. Shear	88
B. Basics of stellar population models	50	D. Magnification	89
C. Stellar mass from M^*/L versus color diagnostics	53	E. Galaxy-mass cross-correlation function	89
1. Effect of star formation history	54	F. Properties of dark-matter halos	90
2. Stellar initial mass function	56	G. Halo shapes	91
3. Model ingredients	56	H. Future prospects	92
D. Data fitting techniques	58	VII. The Dark and Luminous Mass Distribution of Early-type Galaxies Using Strong Gravitational Lensing	92
E. Robustness of stellar mass derivations	59	A. Introduction	92
F. Future prospects	60	B. Basic lensing theory	93
III. Dynamical Masses of Gas-rich Galaxies	60	1. The thin-lens approximation	93
A. Mass estimates from rotation curves	61	2. The lens equation	94
B. Inner parts	63	3. Axisymmetric lenses	95
C. Mass modeling	64	4. Lensing and stellar dynamics	95
1. Mass modeling limitations	65	C. Observational results	96
D. Other galaxy-mass constraints	66	1. Sloan Lens ACS Survey	96
1. Maximal and submaximal disks	66	2. The density profiles of ETGs	96
2. Velocity dispersion measurements	67	3. The stellar IMF and dark-matter fraction in ETGs	97
3. Scaling relations residuals	67	4. Mass substructure in ETGs	99
4. Fluid-dynamical modeling	68	5. Luminous dwarf galaxies	99
5. Gravitational lensing	68	6. Dark substructures	100
6. Two-body interactions and the mass of the local group	68	D. Future prospects	101
E. Future prospects	69	Acknowledgments	102
IV. Dark Matter and Mass Models of the Milky Way	69	References	102
A. Introduction	69		
B. Multicomponent models for the Milky Way	70		
C. Further observational constraints on the Milky Way potential	72		
1. Circular speed at the Sun's position in the Galaxy	72		
2. Local escape speed	72		
3. Kinematic tracers	72		
4. Vertical force and surface density in the solar neighborhood	73		
D. Future prospects	74		
V. Dynamical Masses of Gas-poor Galaxies	75		
A. Introduction	75		
B. Simple mass estimators	75		
C. Methods based on dynamical modeling	77		
1. Jeans analysis	78		
2. Spherical modeling	78		
3. Axisymmetric modeling	79		
D. Distribution function analysis	80		
1. Spherical distribution function modeling	80		
2. Toward flattened systems	81		
3. General orbit-based modeling	81		
E. Results	82		
1. Integrated stellar light: The inner regions and the IMF	82		
2. Globular clusters and planetary nebulae: The outer regions	83		
3. Other tracers and combined approaches	84		
4. The mass-anisotropy degeneracy	84		
5. Discrete star velocities for dwarf spheroidal galaxies	85		
F. Future prospects	86		

I. INTRODUCTION

The distribution of matter in cosmological structures is a fundamental property of nature as the mass of a system is likely the major driver of its evolution. This is especially true for stars whose evolution depend almost fully on their initial mass (and chemical composition) on the main sequence, as embodied by the (idealistic) Vogt-Russell theorem. Mass also plays a fundamental role in galaxy evolution. Galaxies have largely been shaped through mergers and galaxy interactions in hierarchical fashion whereby small systems merged into bigger ones. At early times, star formation was most effective in massive galaxies but as the Universe aged, star formation was likely quenched in those massive systems but continued in smaller galaxies, a phenomenon now called “downsizing.” The oldest stars are thus found in the most massive systems. The complex interplay between star formation efficiency and quenching is likely modulated by a galaxy’s total mass.

Measurements of the distribution of matter in the Universe enable a variety of tests of structure formation models on different scales. For instance, the distribution of galaxy masses on all scales enables the closest possible, though not direct, comparison of predicted mass functions for baryonic and nonbaryonic matter in the Universe. The relative fraction of baryonic to nonbaryonic matter is also indicative of fundamental, yet poorly understood, processes in galaxy formation which typically give rise to tight scaling relations based on the stellar and dynamical masses of galaxies.

Because galaxy masses play such a critical role in our understanding of the formation and evolution of cosmic structures, we review the variety and reliability of mass estimators for gas-poor and gas-rich galaxies and discuss

our ability to derive from those estimators meaningful constraints of theoretical galaxy formation models. While certain techniques enable only the measurement of galaxy masses on large scales, others allow the decomposition of individual mass components such as gas, stars, and dark matter (DM) at different galactocentric radii. The latter methods probe the gravitational potential through the dynamics of visible tracers where baryons are (sub)dominant. Although many galaxies may be safely assumed to be virialized, uncertainties in their mass estimates remain, for instance due to anisotropies in the velocity distributions. Furthermore, baryon-dominated regions remain poorly understood, which complicates a direct comparison of galaxy formation models to observational data.

Many techniques exist for the determination of galaxy masses. The most popular involves the measurement of Doppler shifts of nebular and/or stellar atomic lines due to internal dynamics. Stellar motions can also be resolved in the closest galaxies, such as our Milky Way, Andromeda, and other local group stellar systems; galaxy masses of more distant systems otherwise rely for now on integrated spectra. Another mass estimator consists of converting the galaxy light profile into a mass profile using a suitable stellar mass-to-light ratio (usually derived from stellar population models). A more global approach has also involved the mapping of gravitational lensing effects, both strong and weak. This list is not meant to be complete, as we review below. However, in all cases, galaxy-mass estimates account for matter encompassed within a specified radius and are thus always a lower limit to the total galaxy mass.

This review has evolved from discussions which took place during the celebrations of Vera Rubin’s career at Queen’s University in June 2009.¹ We were all present at that conference. This review was inspired by, and is meant as a modern revision of, early treatises on the masses and mass-to-light ratios of galaxies by [Burbidge and Burbidge \(1975\)](#) and [Faber and Gallagher \(1979\)](#), respectively.

The review is organized as follows: We first present in Sec. II the central topic of stellar M/L determinations from stellar population models. This is followed by a discussion of the mass estimates for gas-rich galaxies in Sec. III, including the special (resolved) case of the Milky Way in Sec. IV. Gas-poor galaxies are addressed in Sec. V, and weak and strong lensing techniques are presented in Secs. VI and VII, respectively. Conclusions, with a view toward future developments, are presented at the end of each section.

This review is naturally incomplete; conspicuously missing topics include the measurement of stellar and dynamical masses of high-redshift galaxies ([Förster Schreiber *et al.*, 2006](#); [Bezanson *et al.*, 2011](#); [Alaghband-Zadeh *et al.*, 2012](#)), the direct comparison of stellar and dynamical mass estimates ([de Jong and Bell, 2007](#); [Taylor *et al.*, 2010](#)), mass function determinations [e.g., stellar mass functions: [Bundy *et al.* \(2006\)](#), [Pozzetti *et al.* \(2010\)](#), and [Maraston *et al.* \(2012\)](#)] [e.g., dynamical mass functions: [Papastergis *et al.* \(2011\)](#), [Trujillo-Gomez *et al.* \(2011\)](#), and [Papastergis *et al.* \(2012\)](#)], constraints on halo masses by statistical techniques such as

those involving satellite kinematics ([More *et al.*, 2011a](#); [Wojtak and Mamon, 2013](#)), group catalogs ([Yang, Mo, and van den Bosch, 2009](#)), and abundance matching ([Behroozi, Wechsler, and Conroy, 2013](#)) to name a few.

Furthermore, this review is restricted to mass analyses based on Newtonian dynamics. Alternatives exist, the most popular being modified Newtonian dynamics (MOND) ([Milgrom, 1983](#)), but a proper treatment of them is beyond the scope of this review. Readers interested in alternative models, MOND or others, are referred to [Famaey and McGaugh \(2012\)](#).

II. FROM LIGHT TO MASS: MODELING THE STELLAR M^*/L RATIO

A. Modeling galaxies and their stellar populations: A historical introduction

The stellar mass M^* of a galaxy is a key physical parameter of galaxy formation and evolution studies as it traces the galaxy formation process. The stellar mass of a galaxy grows through processes such as the internal conversion of gas and dust into stars via star formation, or external events like major interactions with other galaxies and subsequent merging which may induce further star formation, as well as minor events such as accretion of satellites. Moreover, knowledge of the galaxy stellar mass is crucial in order to decompose the contributions from stars and dark matter to the dynamics of galaxies. Modern galaxy formation models embedded in a Λ -cold-dark-matter universe can also predict the evolution of the galaxy-mass assembly over cosmic time ([De Lucia *et al.*, 2007](#)).

Galaxies shine because their stars radiate the energy they produced via nuclear reactions in their cores. The theory of stellar evolution describes the amount of energy released by a star given its initial mass. Hence, by modeling the light emitted by all the stars in a galaxy over all wavelengths [the so-called “integrated spectral energy distribution (SED)”] one can in principle derive the stellar mass that is responsible for such radiation. However, a certain fraction of evolved stars no longer shines yet still contributes to the galaxy-mass budget in the form of stellar remnants such as white dwarfs, neutron stars, and black holes. The sum of *living* stars plus remnants makes up the “stellar mass” M^* of a galaxy.

Despite our detailed knowledge of stellar evolution, the modeling of a galaxy spectrum (which is the superposition of all spectra from individual stars) is a challenging exercise since the exact stellar composition of a galaxy and its overall stellar generations are unknown *a priori*. These depend on the history of star formation, chemical enrichment, accretion, and interaction. Unlike stellar clusters whose vast majority of stars are coeval and share the same chemical composition, galaxies are a complicated ensemble of stellar generations. Recent extensive reviews of SED modeling of galaxies have appeared in [Walcher *et al.* \(2011\)](#) and [Conroy \(2013\)](#).

As recognized early on by [Oort \(1926\)](#) and [Baade \(1944\)](#), our own Milky Way is composed of various populations of stars, each featuring different dynamics, chemical properties, and formation epochs. Thus, from a stellar content viewpoint, galaxies can be broken into *stellar populations* with shared definable properties. The “simple stellar population” (SSP) is defined as a group of coeval stars with homogeneous

¹See <http://www.astro.queensu.ca/GalaxyMasses09> for workshop presentations and photographs.

chemistry (at birth) and similar orbits and kinematics. A recent, comprehensive textbook on stellar populations in galaxies is due to [Greggio and Renzini \(2011\)](#).

Star clusters, either open or globular, are the closest realization of SSPs in nature. The main unknown of an SSP is the stellar initial mass function (IMF), which gives the mass spectrum of the stellar generation at birth. The latter is not known from first principles. Empirical determinations of the IMF based on solar neighborhood data were first modeled by [Salpeter \(1955\)](#) as a power law with exponent of ~ -2.35 . An IMF must be assumed when calculating the properties of population models. While galaxies are not SSPs, they can be viewed as a sum of all present SSPs, that is, galaxies = $\sum_j \text{SSP}_j$. The distribution of stellar generations in time and chemical enrichment is called the “star formation history” (SFH). Several analytical laws describe plausible SFHs which depend on the time scale of the star formation rate (SFR), such as exponentially declining models, or τ models, models with constant star formation, models with time-increasing star formation, etc. Examples of such SFHs are shown in [Fig. 1](#).

Ultimately, the stellar content of a galaxy over time t may be thought of as

$$\text{galaxy} = \sum_{\text{time}} \text{SFR}(t) \times \text{SSP}(t, Y, Z, \text{IMF}), \quad (1)$$

with Y the helium abundance and Z the abundance of heavier elements (metallicity). Note that Y , Z , and the IMF may vary between different stellar generations, i.e., among different SSPs, but they do not vary within an SSP by definition.

It is useful to note that little is known about the physical processes that drive the rate of star formation and the

emerging mass spectrum (the IMF). We know that stars form from dense, cold gas that is shock compressed (e.g., in disks, during galaxy interactions, or dynamical instabilities), but a theory that predicts the SFR and the IMF in different galaxies and as a function of time has yet to be written. For these reasons, these two physical quantities are parametrized in population models and observations to guide ongoing developments. Indeed, our limited knowledge about the SFR and IMF is a major impediment in the precise determination of a galaxy’s stellar mass.

Historically, the problem of modeling a galaxy spectrum has been approached in two ways. In the so-called “optimized population synthesis” ([Spinrad and Taylor, 1971](#); [Faber, 1972](#); [O’Connell, 1976](#); [Pickles, 1985](#); [Bica and Alloin, 1986](#)), empirical stellar spectra are combined in proportions such that the resulting composite spectrum can best reproduce the galaxy spectrum. These proportions can be *ad hoc*, hence neither necessarily obeying stellar evolution time scales nor a realistic stellar IMF. The obtained best-fit model can provide an excellent representation of the galaxy spectrum, but it cannot be evolved with time. Hence the optimized spectral fitting does not allow one to study galaxy evolution in a cosmological context. Still it can provide important insights on the types of stars which are effectively present in a stellar system ([MacArthur, González, and Courteau, 2009](#)). Optimized synthesis can also be used to obtain an instantaneous description of a galaxy spectrum in order to achieve accurate estimates of the broadening of absorption lines for velocity dispersion measurements (see [Sec. V](#)).

The alternative approach makes use of stellar evolutionary models, which describe the detailed time evolution of the luminosity and temperature of stars of different mass. Integrated spectra for galaxies are calculated by adding up the contributions of the individual model stars after assuming an IMF and a SFH. These so-called “evolutionary population synthesis models,” based on stellar evolution theory, can be evolved in time back and forth and galaxy evolution can be studied at arbitrary cosmic distances with the same underlying theory. Comparison between these models and observational data provides estimates for the average formation epoch, metallicity, and SFH of a galaxy, thus enabling an evaluation of the stellar mass through the model mass-to-light, or M^*/L , ratio. These models, pioneered by [Tinsley \(1972\)](#), [Tinsley and Gunn \(1976\)](#), [Renzini and Voli \(1981\)](#), and [Bruzual \(1983\)](#), from which galaxy stellar masses are derived, are described extensively in [Sec. II.B](#), focusing on the quantities that directly affect the stellar mass derivation, using various models available in the literature. We also address the impact of different model fitting techniques on extracted results and conclude with an assessment of the accuracy of galaxy stellar mass estimates.

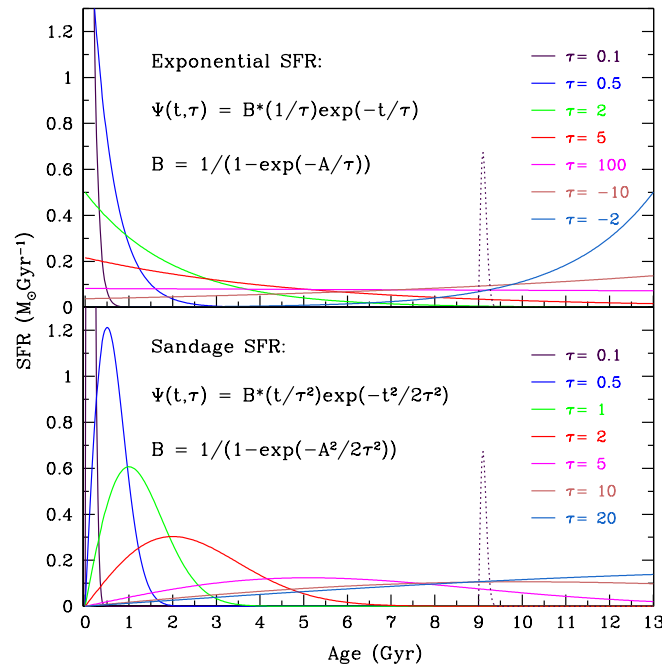


FIG. 1 (color online). Time evolution of the exponential (upper panel) and [Sandage \(1986a\)](#) (lower panel) star formation histories (solid curves). The dotted curve is a Sandage-style burst of star formation in which 10% of the total mass of stars are formed. From [MacArthur *et al.*, 2004](#).

B. Basics of stellar population models

Evolutionary population synthesis (EPS) models provide the expected SED of a stellar population as a function of key parameters, such as

- (1) the formation epoch, or the time elapsed since the beginning of star formation, normally referred to as the *age* t of the population, measured in years;

- (2) the SFH, often parametrized with analytic functions, e.g., $\text{SFR} \propto e^{-t/\tau}$ (see Fig. 1);
- (3) the chemical composition, often referred to as metallicity and expressed as the fractional abundance Z of elements heavier than He and H ($[Z/H]$), or as the fractional abundance of iron ($[Fe/H]$);
- (4) the chemical abundance ratios, or the ratios of all key elements with respect to those values measured in the Sun: e.g., the ratio of magnesium to iron $[Mg/Fe]$, the ratio of oxygen to iron $[O/Fe]$; etc.;
- (5) the IMF.

These are the main parameters controlling the time evolution of the population. Further assumptions need to be made for stars evolving over specific evolutionary phases, which will be mentioned below.

The model ingredients are the stellar evolutionary tracks and/or isochrones, the stellar spectral libraries, the parametrization for the mass loss which affects several late stages of evolution such as the thermally pulsing asymptotic giant branch (TP-AGB), the red giant branch (RGB), the horizontal branch (HB), and also the main sequence (MS) in young populations.

A further model feature is the computational procedure, which may be an integration by mass of the luminosity contributions [the so-called isochrone synthesis technique (Bruzual and Charlot, 1993)] or a technique based on Renzini's *fuel consumption theorem* (Renzini, 1981; Buzzoni, 1989; Maraston, 1998, 2005). This theorem states that the number of stars at each burning stage is proportional to the time it takes to exhaust the nuclear fuel burned at that stage. This can be interpreted as the conservation of energy for stellar populations. In population synthesis models, it is a useful tool to quantify the contribution of rapid, and very luminous, stellar phases as found at the tip of the RGB, the AGB, and the RGB bump [cf. discussion in Maraston (2005)]. Numerical experiments have shown that calculations based on the fuel consumption theorem and isochrone synthesis agree well (Charlot and Bruzual, 1991), provided the mass bin of the mass integration in the isochrone synthesis case is small [Maraston (1998) finds $10^{-6} M_{\odot}$ for the tip of the RGB]. Moreover, the fuel consumption theorem is useful for including in synthetic integrated models those stellar phases for which a complete isochrone may not be available, such as the AGB, the horizontal branch with different morphologies, and the hot stars responsible for producing the UV upturn in ellipticals.

A detailed description of the individual population models can be found in the corresponding papers, e.g., Vazdekis *et al.* (1996), Fioc and Rocca-Volmerange (1997), Bruzual and Charlot (2003), Maraston (2005), and Conroy, Gunn, and White (2009), in addition to the reviews cited in Sec. II.A.

The basic model EPS unit is the SSP. In the following SSPs are first used to illustrate the fundamental dependencies of M^*/L on age and metallicity, with composite models treated later on.

The most important driver of an SSP's luminosity evolution is its age, since the most massive stars live quickly but are orders of magnitude more luminous than smaller mass stars. For most IMFs the mass of a stellar population is dominated by the faintest stars and changes relatively little with time

after the first Gyr of age (see Fig. 2), but the luminosity of a population is dominated by its brightest stars showing large changes over time. Besides the main sequence, which provides a substantial contribution to the light at virtually every age, the brightest stars are found in different post-main sequence evolutionary phases. Which phase dominates depends upon the age of the stellar population and the wavelength of observation. In young populations ($t \lesssim 200$ Myr), helium burning stars dominate the light, while at intermediate age ($200 \text{ Myr} < t \lesssim 2 \text{ Gyr}$), the TP-AGB stars take over (in some models, see below); at old ages, RGB stars outshine all other stars. AGB and RGB phases are mostly bright in the near-IR (NIR), while MS stars contribute mostly to optical bands [see Fig. 11 in Maraston (1998)].

The luminosity of an SSP is therefore a strong function of time. This rate varies with wavelength given the contributions from different evolutionary phases. The overall luminosity evolution is more significant in the blue or optical spectral range where MS stars dominate, scaling roughly logarithmically with time (Tinsley, 1972), as compared to the NIR light of old populations ($t \gtrsim 2\text{--}3 \text{ Gyr}$), where the slowly evolving RGB stars dominate. The rate of luminosity change at NIR wavelengths is large near 0.3–1 Gyr for some models including the TP-AGB phase (Maraston, 1998, 2005; Marigo *et al.*, 2008), since the onset of this phase implies a rapid increase of the NIR luminosity due to the cool and luminous TP-AGB stars. This effect is model dependent. Global age and metallicity effects on the M^*/L in various bands for SSP models are shown in Fig. 2.

The stellar population's metallicity also affects stellar evolution time scales and mostly the stellar SEDs. Metal-rich stars are cooler (because of a higher opacity in their stellar envelopes) and fainter (because the turnoff mass is smaller and most outgoing photons are trapped into their

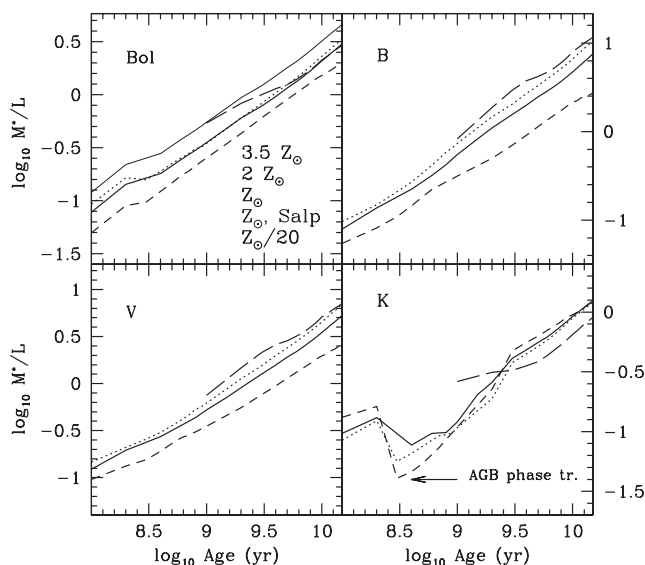


FIG. 2. The stellar bolometric M^*/L and M^*/L in various bands (B , V , K) as a function of age for SSPs (single-burst models) and the different indicated metallicities. All models for Kroupa IMF, except for the thin solid line in the top-left diagram for a Salpeter IMF. The stellar mass M^* accounts for stellar mass losses, as in Maraston (1998, 2005). See also text for details. From Maraston, 2005.

envelope), hence the higher M^*/L of a metal-rich population due to a lower luminosity (while M^* changes little). This trend is visible in Fig. 2. Metallicity effects are significantly milder at NIR bandpasses; at very high metallicity (see the 3.5 solar metallicity track in Fig. 2, long dashed line), the trend reverses in NIR bands, since the luminosity of such a metal-enriched population is concentrated at longer wavelengths [see Maraston (2005) for a full discussion]. As is well known, ageing of a stellar population has the same effect as increasing metals since, as the most massive stars die out, the temperature distribution skews toward cooler values. The combined age and metallicity effects on dwarf and giant stars result in the so-called “age-metallicity (A/Z) degeneracy” in the optical region of their spectrum (Faber, 1972; Renzini and Buzzoni, 1986; Worthey, 1994; Maraston and Thomas, 2000). At optical wavelengths, the effect is such that a population of stars that is 3 times more metal rich mimics a population twice its age; this is the “3/2 rule” of Worthey (1994). This A/Z degeneracy at optical wavelengths obviously holds for M^*/L ratios as well. The optical A/Z degeneracy can be lifted by including data at longer wavelengths where giant stars dominate the spectrum and increasing metallicity results in redder colors, with a small dependence on age (with the exception of the AGB time). Worthey (1994) proposed that the spectral region around $1 \mu\text{m}$ (i.e., between the I , J bandpasses, depending slightly on age and IMF) is the most insensitive to metallicity. This notion has been exploited with color-color diagrams involving optical and at least one NIR passband to analyze the stellar populations of integrated stellar systems (de Jong, 1996; Bell and de Jong, 2000; Maraston *et al.*, 2001; MacArthur *et al.*, 2004; Roediger *et al.*, 2011). This concept of using an extended wavelength range has also been exploited for the study of high-redshift galaxies where the time spanned since the big bang is short and the age dependencies can be disregarded. In particular, the TP-AGB phase appears in galaxy spectra and the inclusion of the NIR allows galaxy ages to be better constrained (Maraston *et al.*, 2006).

The total stellar mass M^* of an SSP also evolves with time. It typically decreases with time since the most massive stars progressively die leaving stellar remnants with mass smaller than the initial ones. M^* is a strong function of the IMF. Figure 3 shows the evolution of M^* for several widely used empirically based IMFs, namely, Salpeter (1955), Kroupa (2001), and Chabrier (2003). These IMFs follow the same Salpeter power-law slope for stellar masses larger than $0.6M_\odot$, but have, to varying degrees, less stars than predicted by this Salpeter law slope below this mass limit (hence bottom light). Note that the IMFs of Salpeter (1955), Kroupa (2001), and Chabrier (2003) were all based on solar neighborhood data.

Also shown are two additional, not empirically based IMFs meant to illustrate extreme cases of a dwarf-dominated (labeled “bottom heavy”) and a giant-dominated (labeled “top heavy”) IMF. These are single-sloped IMFs with exponents 3.5 and 1 in the notation in which the Salpeter’s one is 2.35 and are meant to illustrate galaxies dominated by low-mass and high-mass stars, respectively. Evidence for these extreme IMFs has been advocated in the literature. For example, van Dokkum and Conroy (2012) suggested a

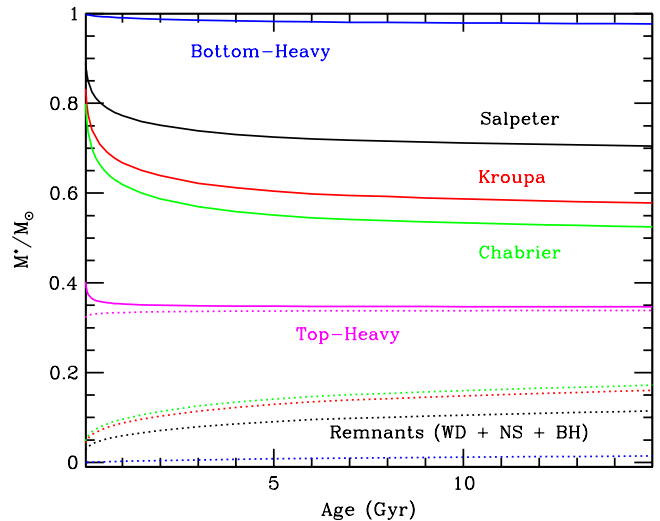


FIG. 3 (color online). Evolution of the stellar mass fractions for stellar populations with the same total initial mass (normalized to $1M_\odot$) and different initial mass functions. “Bottom-heavy” and “Top-heavy” are extreme cases of single-sloped IMFs with exponents 3.5 and 1 in the notation in which the Salpeter slope is 2.35. M^* evolves because stars die progressively and leave remnants with mass lower than the initial mass. Also shown are the fractions of M^* in remnants, namely, white dwarfs (WD), neutron stars (NS), and black holes (BH). Based on Maraston (2005) models.

dwarf-dominated IMF in massive early-type galaxies (ETGs) to explain the strength of near-IR lines. Similarly, dynamical modeling studies (Cappellari *et al.*, 2012, see also Sec. V) and gravitational lensing studies (Auger, Treu, Gavazzi *et al.*, 2010; Treu *et al.*, 2010; Brewer *et al.*, 2012, see also Sec. VII) of ETGs find evidence for the same type of IMF, with larger mass-to-light ratios than those predicted by Chabrier-like IMFs.

At the other end of the mass spectrum, Baugh *et al.* (2007) found that a top-heavy IMF in high-redshift bursts helps in explaining the colors of massive dusty and bursty distant galaxies (so-called “submillimeter” galaxies).

For the same total initial mass, the stellar masses of top-heavy IMFs evolve faster with time because of their larger proportion of massive stars. Most of the evolution occurs within the first Gyr, following the much faster evolution time scales of stars more massive than roughly $2M_\odot$. Over a Hubble time, the amount of mass loss averages 30 to 40% of the initial mass. For composite population models with ongoing star formation, the decrement is reduced to $\sim 20\%$ (Maraston *et al.*, 2006). In the Maraston models, the total remnant mass is budgeted among white dwarfs, neutron stars, and black holes, following the analytical prescription of Renzini and Ciotti (1993). Maraston (1998) explored IMFs with various exponents to show that M^* is maximally large for dwarf-dominated as well as top-heavy IMFs, while the minimum M^* is achieved with a bottom light² IMFs such as

²Note that bottom light refers to an IMF that is not as rich in dwarf stars as the Salpeter one, namely, has a different slope above $0.6M_\odot$. This is different from a top-heavy IMF, which is strongly dominated by giant stars due to a smaller exponent value all over the mass range

the Scalo (1986) and Kroupa (2001), or Chabrier (2003)-type IMFs [see Figs. 16 and 17 in Maraston (1998)]. A population born with a dwarf-dominated (or bottom-heavy) IMF has a large M^* since most stars have a small mass, hence their extended lifetime and they contribute their total mass to M^* . A giant-dominated (or top-heavy) IMF has a large M^* given by the large number of massive remnants left by the evolved massive stars. These considerations are important as the value of M^* and the assumptions regarding the IMF directly impact the evaluation of the total stellar mass and the dark-matter content in galaxies.

It should be noted that the predicted M^* may differ among different population synthesis models [see model comparisons between Bruzual and Charlot (2003) and Maraston (2005) in Fig. 3 of MacArthur *et al.* (2010)]. This discrepancy may reflect a different accounting of stellar remnants. Hence, in comparing stellar masses obtained with different EPS models, one should also consider if and how the remnant masses are accounted for. For example, the Worthey (1994) models considered the mass contribution of the sole living stars, while Bruzual and Charlot (1993) considered a constant M^* , etc.

Other factors may complicate the broad-brush stellar evolution picture discussed. For example, stars in exotic evolutionary phases (such as hot horizontal branch at high metallicity and blue straggler stars) may alter the luminosity in the blue spectral range. These events probably affect mostly globular cluster (GC) studies, as the relative contribution of these phases to the total light of a galaxy should not be very significant. Also, one should not rely on a single band, especially a blue band, to determine stellar masses. The reddest side of the spectrum is equally challenging with the evolution along the TP-AGB being woefully uncertain due to the unknown mass loss. Debate pertaining to the reliability of optical and NIR stellar mass estimates is currently ongoing (Bruzual, 2007; Marigo *et al.*, 2008; Conroy, Gunn, and White, 2009; Zibetti, Charlot, and Rix, 2009; Conroy and Gunn, 2010; MacArthur *et al.*, 2010; Lyubenova *et al.*, 2012; Conroy, 2013; Zibetti *et al.*, 2013).

A resolution of the significance of the TP-AGB phase to stellar mass estimates cannot be achieved in this review. However, a sound estimate of the stellar mass appears to be provided by the $g-i$ color (Zibetti, Charlot, and Rix, 2009; Taylor *et al.*, 2011). The effect of the TP-AGB phase on stellar mass derivations stemming from the use of models with and without a substantial TP-AGB contribution is highlighted when appropriate.

Extinction from dust also affects broadband luminosities, hence M^*/L ratios and stellar population colors. However, in optical passbands the expected dust effects on M^*/L and population color run parallel to the expected stellar population color- M^*/L relations and the mass estimates are only weakly affected (Bell and de Jong, 2001). Likewise, line indices are only slightly affected by dust (MacArthur, 2005) and can help disentangle extinction from population effects. For full stellar mass estimation dust extinction should be included in analyses, but dust is not further addressed here. Finally, most stellar systems will not be approximated by single-burst or SSP models, rather by composite populations with multiple ages and metallicities. The unknown galaxy

star formation histories complicate the interpretation of integrated light observations and will be discussed in Sec. II.C.1.

In the following we focus on mass determinations in relation to fitting of the broadband spectrum, as this situation is common to low- as well as high-redshift studies, where high resolution spectral fitting is presently unfeasible. Note also that comparison of galaxy-mass determinations obtained via broadband or spectral fitting agrees well when the signal-to-noise ratio of the spectrum is high (Chen *et al.*, 2012).

C. Stellar mass from M^*/L versus color diagnostics

The list at the beginning of Sec. II.B makes it clear that the big 4 variables that stand between the observed photometric distribution of star light and our interpretation in terms of stellar mass are (i) the correctness of stellar evolution models along stellar phases, (ii) the SFH, (iii) the chemical enrichment history, and (iv) the IMF. These are all interconnected astrophysically and phenomenologically. Part of this interconnection could be labeled the fifth variable of the “environment.” In most cases when analyzing galaxies, little information is available on the big 4, with perhaps the exclusion of (i) which can be calibrated and tested in local stars. Hence, usually a variety of models are assumed including different formalizations for (ii)–(iv). The significance of these assumptions is shown next.

Following Bell and de Jong (2001), we illustrate how M^*/L ratios in the B and the K bands correlate with $(B-R)$ and $(I-K)$ colors (as tracers of age and/or metallicity), and the mostly age sensitive $H\delta_A$ index. Figure 2 shows that M^*/L values in other optical passbands behave similarly to the M^*/L_B plots, just with a slightly different slope.

Figure 4 shows grids of model colors M^*/L and a spectroscopic index for SSPs of various ages and metallicities. Once a population is older than about 0.1 Gyr, M^*/L_B vs $(B-R)$ displays a good correlation, which is fairly independent of metallicity. The M^*/L_K vs $(B-R)$ is more ambiguous with age as M^*/L_K evolves slowly after the TP-AGB phase transition (meaning, after some Gyr of age). The relations of M^*/L with $(I-K)$ color cannot be used alone to derive M^* because the model loci are nearly vertical after 0.1 Gyr, meaning that at a given metallicity M^*/L is nearly independent of color. As mentioned, the luminosity in the NIR after a few 100 Myr is dominated by evolved (AGB and later RGB) stars. The lower NIR M^*/L at early ages (~ 10 Myr) is due to short-lived, bright red supergiants. Note that this caveat is relevant only for very recent star formation, basically from HII regions.

Perhaps the best approach to measuring M^*/L is to fit SEDs simultaneously in at least three passbands, with one in the NIR, hence breaking the age-metallicity degeneracy. Modulo model uncertainties as detailed in the following sections, convergence to the right M^*/L value may be achieved [as shown by Zibetti, Charlot, and Rix (2009) or by Maraston *et al.* (2001) for massive star clusters and Maraston *et al.* (2006) for high-redshift galaxies].

Finally, the rightmost column of Fig. 4 shows an example of M^*/L trends with an absorption line index. The $H\delta_A$ Balmer line index (Worthey and Ottaviani, 1997) was chosen as it has been used specifically for the estimation of M^* for the SDSS galaxies (Kauffmann *et al.*, 2003). This index is

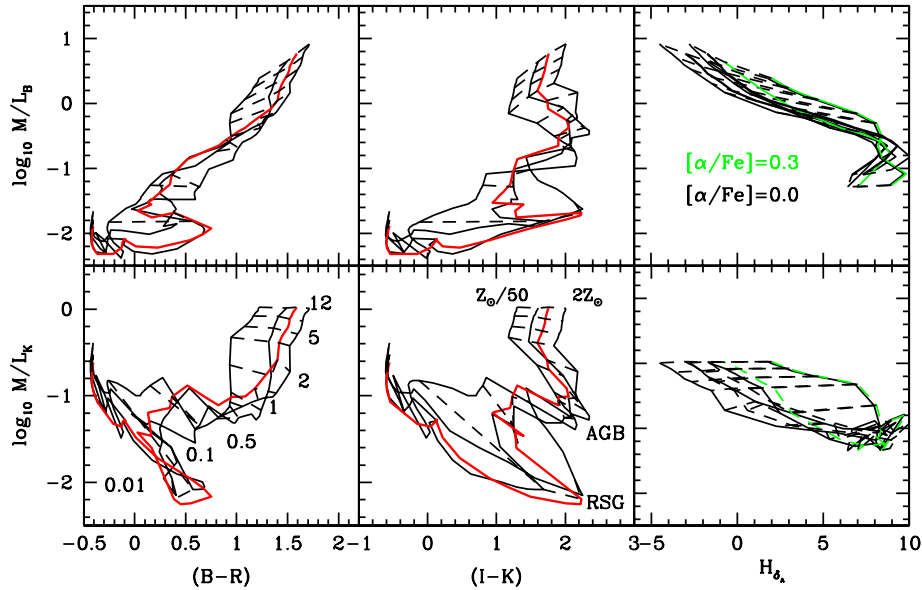


FIG. 4 (color online). Trends of Maraston (2005) SSP models with various ages and metallicities, and a Salpeter IMF. M^*/L values in B and K bands (top to bottom) are shown vs $(B-R)$, $(I-K)$, and the $H\delta_A$ line index (left to right). The latter models are from Thomas, Maraston, and Johansson (2011); colored lines connect models for the $[\alpha/\text{Fe}]$ ratio of +0.3 and solar-scaled models. Models with the same age (in Gyr) are connected with dashed lines, models with the same metallicity with solid lines ($Z = 0.001, 0.01, 0.02, 0.04$). Other colored lines highlight solar metallicity ($Z = 0.02$).

sensitive to the age of the stellar population, being the strongest around 0.3–0.5 Gyr (depending on metallicity) when A -type stars dominate the spectrum and smaller at both older and younger ages [see Fig. 8 in Maraston *et al.* (2001)]. This degeneracy for $H\delta_A$ can be broken (for a single-burst population) by using an extra spectral indicator with a monotonic behavior with age. Two further complications should be noted. Because of its temperature dependence, the index is also affected by old, although hot, stars such as metal-poor blue HB stars (Maraston *et al.*, 2003). Moreover, the index has been shown to be sensitive to the $[\alpha/\text{Fe}]$ ratio, because of strong Fe lines present in the pseudocontinua (Thomas, Maraston, and Korn, 2004). For instance, the index is stronger in $[\alpha/\text{Fe}]$ -enhanced populations (such as those of massive ETGs) than in solar-scaled ones. The trend with abundance ratios is shown in Fig. 4, where the colored grid displays models for the same total metallicity Z , but enhanced $[\alpha/\text{Fe}] = 0.3$. The consideration of these effects when dealing with massive galaxies is important, as a strong index can otherwise be explained only by a lower age, which in turn would induce a mismatch in the derivation of the M^*/L ratio. Ideally in the future it should be possible to complete the last panel of Fig. 4 by considering the abundance-ratio effects on colors and mass to light. Broadbrush, the model grid distribution shown in $H\delta_A$ vs M^*/L is similar to the $(B-R)$ vs M^*/L distributions, except for the very youngest ages. The same degeneracies are therefore also present in composite age models and we will no longer show the $H\delta_A$ models separately.

Single-burst models are ideal cases that apply well to star clusters, but not to galaxies, where a prolonged star formation is in general more appropriate. The determination of M^* in these cases is much more difficult, as the latest generations dominate the light and drive down the M^*/L hence M^* , which leads to an underestimate of the stellar mass (Bell and de Jong,

2001; MacArthur, González, and Courteau, 2009; Maraston *et al.*, 2010). These issues are discussed in Sec. II.C.1.

1. Effect of star formation history

Stellar systems like galaxies are expected to have a wide range of SFHs. The effect of prolonged star formation history on the model grids is visualized in Fig. 5 by using exponentially declining SFR models or τ models [as introduced by Bruzual (1983)], with $\text{SFR}(t) \propto \exp(-t/\tau)$, where τ indicates the e -folding time scale of star formation and can be both positive and negative. This model is a reasonable first approximation of the star formation history of a spiral galaxy or, for very low τ 's, of a passive system. Negative τ values represent galaxies which have increasing SFRs, especially galaxies with recent star bursts (Bell and de Jong, 2000).

The model M^*/L ratios in the optical are nearly degenerate versus $(B-R)$ in Fig. 5. This degeneracy is somewhat broken in $(B-R)$ versus the near-IR M^*/L_K , especially for the lowest metallicities ($Z < 0.004$). However, realizing that chemical evolution caused by modest amounts of star formation raises the system metallicity rapidly to at least 0.1 solar (or $Z = 0.002$, in a closed box, conversion of $\sim 20\%$ of gas mass into stars raises the average metallicity to over 0.1 solar), the range of relevant metallicities becomes narrower in most applications, making the color- M^*/L_K relation tighter.

Tracing mainly evolved stellar populations, $(I-K)$ is largely metallicity sensitive, weakly sensitive on age, and $(I-K)$ on its own (without any other passbands) is not useful for mass estimation as Fig. 5 shows. Moreover, the details of evolved stellar evolution stages are still relatively poorly modeled and the exact shapes of these $(I-K)$ diagrams are highly dependent on models used, as shown in Sec. II.C.3.

Not all stellar systems are ~ 12 Gyr old, either because they are observed at higher redshift when the Universe was

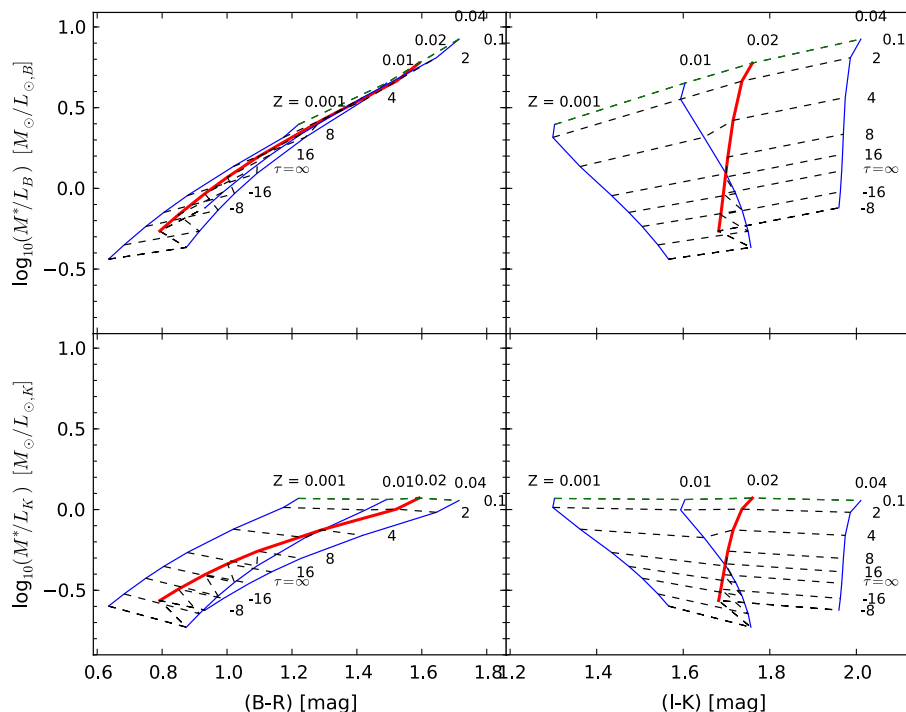


FIG. 5 (color online). Trends in M^*/L ratios using exponentially declining star formation rate models. The models are the same as in Fig. 4, except that instead of a single burst an exponentially declining star formation rate is used observed at age 12 Gyr after star formation began. Models with the same e -folding time scale τ are connected with dashed lines, where positive τ stands for the decreasing star formation rate with time, negative τ for the increasing star formation rate, and $\tau = \infty$ is a constant star formation rate model. Solid lines connect models with equal indicated metallicity, where the colored line highlights solar metallicity. Based on Maraston (2005) models.

much younger or because they may have had their major epoch of star formation significantly delayed. The effect of a younger final age on exponential SFR models is shown in Fig. 6. This figure shows the same range of τ values as in Fig. 5, although now after 12, 8.5, 6, 3, and 2 Gyr (and for clarity only for solar and 1/20 solar models). For concordance cosmology, this corresponds to roughly redshifts $z = 0, 0.3, 0.7, 1.5,$ and 2 when starting star formation 12 Gyr ago. Model colors are shown in the rest frame.

The main conclusion from the color- M^*/L diagrams in Fig. 6 is that a final age change mainly results in a simple offset since the slope of the relation stays nearly constant especially for solar metallicities. The age-metallicity degeneracy stays intact in the optical relations. Only at the youngest ages and lowest metallicities, and predominantly in M^*/L_K , does the slope of the relation change.

So far only smooth SFHs have been considered in this section, but star formation will be more bursty in nature for especially smaller systems. A recent burst of star formation will dramatically lower the M^*/L of a total stellar system as well as change its SED to make it look much younger, because a young population is so much more luminous. The size of the effect will depend on the size of the star burst relative to the underlying population and the age difference between the populations. This effect may be most relevant for small galaxies, where any burst of stars is significant, and for stellar masses dominated by an old population, where any trickle of young stars will dramatically alter their properties. For instance, the rejuvenation caused by a “frosting” of young stars has been used to explain the apparent line indices based on

young ages of morphological ETGs that are thought to be mostly old (de Jong and Davies, 1997; Trager *et al.*, 2000), although hot horizontal branch stars produce the same effect on the observed line strengths (Maraston and Thomas, 2000).

Figure 7 shows the effect of adding 10% of the final mass of the system in a star burst of 0.2 Gyr duration. The models start with the canonical set of 12 Gyr old exponential SFR models of Fig. 5 to which 1, 2, 3, 4, or 6 Gyr old star bursts are added. For clarity, only the solar and 1/20 solar results are shown.

A number of features are apparent from Fig. 7. First, the effects of star bursts are largest in both color and M^*/L when starting with an old, small τ population (independent of metallicity). Second, almost any burst of star formation will bias models toward lower M^*/L values at a given color compared to smooth star formation models. At a given $(B-R)$ color, the maximum offset from a smooth SFH due to a late star burst is less than 0.5 dex, but in most combinations it is less than 0.3 dex. This effect is stronger for higher metallicities. Finally, when starting off from a fairly young underlying population ($\tau > 5$ Gyr) the effects of the modeled star bursts are only larger than 0.1 dex in M^*/L for bursts younger than 1–2 Gyr. In this case the population may actually become redder than the underlying population in $(B-R)$ after a few Gyr after the burst, because the star burst will increase the luminosity-weighted average age of the total population. When starting from mostly old populations ($\tau < 5$ Gyr), the effect of a star burst on the M^*/L may be long lived (4–6 Gyr).

If most galaxies had irregular star formation in their last 2–5 Gyr with variations in the star formation rate of factors

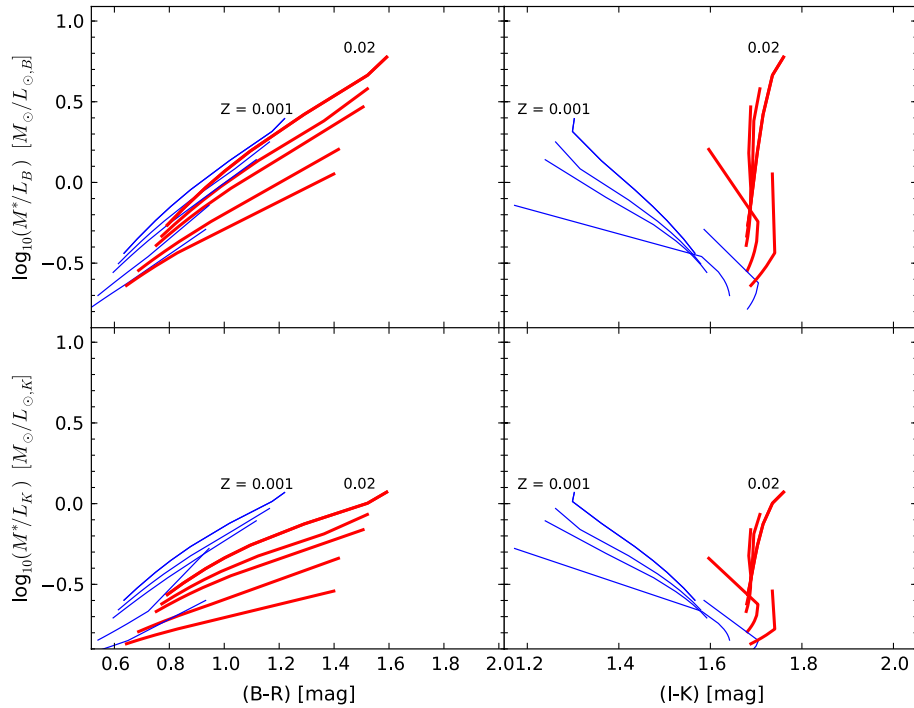


FIG. 6 (color online). M^*/L ratios for exponentially declining star formation rate models with a different final age. The models are the same as in Fig. 5, except that the populations are now observed 12, 8.5, 6, 3, 2 Gyr (top to bottom) after star formation commenced. The top ends of the lines are the ends with the smallest positive τ values, i.e., the oldest average age. For clarity, only the solar metallicity ($Z = 0.02$, thick lines) and the 1/20th solar metallicity ($Z = 0.001$, thin lines) are plotted and the dashed lines connecting the same τ values are not shown as in Fig. 5. In principle these models form similar grids with different offsets. Based on Maraston (2005) models.

greater than 2, most galaxies are expected to lie below the smooth exponential SFR model SED- M^*/L relations. One can calculate this offset and increase in scatter by using models that include a varying amount of star formation and incorporate this in the derived SED- M^*/L relations. Alternatively, one can reduce the scatter induced by these recent star bursts by including an SED tracer of a stellar population younger than 2–3 Gyr when fitting the SED. One has to choose a tracer that is not degenerate in age and metallicity with the other SED tracers used. Some options include a $(U-B)$ color or a higher order Balmer line. The combination of such recent star formation indicators and SED templates with an irregular SFR should yield a scatter reduction in M^*/L by ~ 0.1 dex if many objects with irregular SFR are contained in the sample.

More bandpasses (at least four) can provide additional degeneracy lift. For example, in the Maraston models a very red $(I-K)$ color corresponds only to the TP-AGB dominated ages of ~ 1 Gyr, which is more pronounced in a small τ model. Most models behave similarly in the optical bands, while the NIR is driven by the treatment of evolved phases, for which there is a strong variance within existing models (see also Sec. II.C.3).

2. Stellar initial mass function

As noted in Sec. II.A, the IMF is a major uncertainty in SP modeling and M^*/L ratios are strongly dependent on it. The IMF of external galaxies is in principle unknown [although see Tortora, Romanowsky, and Napolitano (2013)], but most IMFs determined for the Milky Way in the solar

neighborhood show a very similar behavior, namely, a turnover in their logarithmic slope at about 0.6 solar mass. The exact details of this turnover in the IMF slope around this mass scale are poorly constrained [see, e.g., Scalo (1986), Kroupa (2001), and Chabrier (2003)], but critically determine the total mass of the system. Figure 8 visualizes the solar metallicity M^*/L versus color relation using different IMFs, specifically the same as in Fig. 3. The predicted relations are clearly very similar in shape for exponential SFR models and the plausible Salpeter or Kroupa IMF (the Chabrier and Kroupa IMF's behave similarly). These different IMFs result primarily in offsets in zero point of the M^*/L versus color relations. These offsets are independent of metallicity and nearly the same whether one measures M^*/L_B or M^*/L_K .

The M^*/L ratio versus color slope remains unchanged even assuming a rather extreme bottom-light IMF, but the offset is much larger (a factor of ~ 10) for the latter (Fig. 8). However, this IMF is ruled out by strong gravitational lensing and stellar dynamics which permit only M^*/L ratios up to a factor of ~ 2 higher than that predicted for a Salpeter IMF (Brewer *et al.*, 2012; Cappellari *et al.*, 2012).

3. Model ingredients

As discussed in Sec. II.A, EPS models include several ingredients and assumptions (stellar evolutionary tracks, stellar spectral libraries, IMF, etc.), which may be treated differently in different models. It is beyond the scope of this review to investigate the effects of each ingredient and its uncertainty on the models [for reviews see, e.g., Charlot, Worthey, and Bressan (1996), Maraston (2005), Conroy, Gunn, and White (2009),

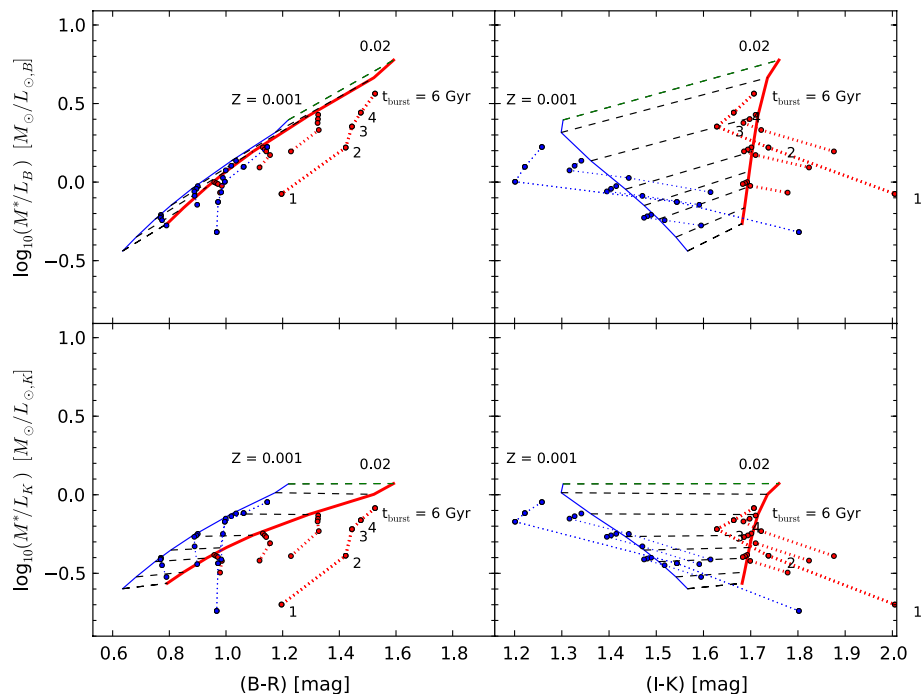


FIG. 7 (color online). M^*/L ratios for exponentially declining star formation rate models with an additional star burst. The starting models without star burst are the same 12 Gyr old exponentially decaying SFR models as in Fig. 5, except that for clarity only the solar metallicity ($Z = 0.02$, thick lines) and the 1/20 solar ($Z = 0.001$, thin lines) are plotted. For τ values ∞ , 8, 4, 1 a 10% final mass fraction star burst of 0.2 Gyr duration is added that occurred 1, 2, 3, 4, 6 Gyr ago (solid circles connected with dotted lines). Based on Maraston (2005) models.

and Leitherer and Ekström (2012)]. Rather, M^*/L versus color relations for the different EPS are compared here using exponential SFR models. The GALAXEV (Bruzual and Charlot, 2003), Projet d’Etude des GALaxies par Synthèse Evolutive (Fioc and Rocca-Volmerange, 1997; PEGASE), and Flexible Stellar Population Synthesis (Conroy, Gunn, and White, 2009; FSPS) models are used with a Chabrier IMF, while the Maraston models use a Kroupa IMF.

Not surprisingly, the GALAXEV (BC03) and PEGASE results are very similar in all color- M^*/L diagrams, since

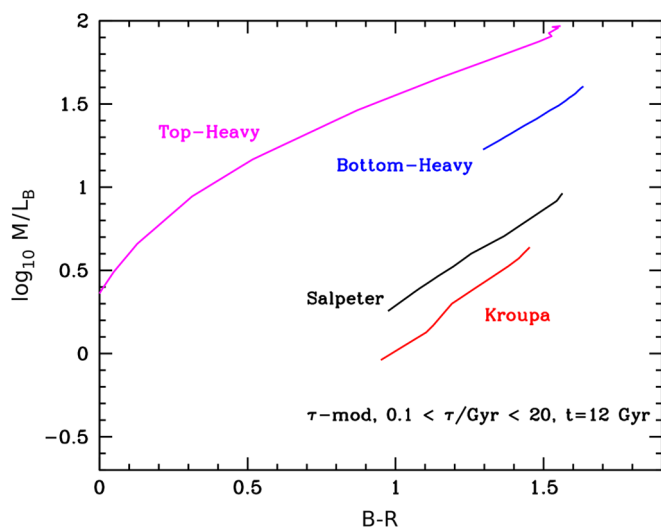


FIG. 8 (color online). M^*/L ratios vs $(B-R)$ for exponentially declining star formation rate models of age 12 Gyr and solar metallicity, with a Salpeter, Kroupa, and the same top-heavy and bottom-heavy IMFs as in Fig. 3.

they use the same Padova stellar evolutionary tracks and similar spectral libraries. At optical wavelengths, nearly all models agree to within 0.1 dex in $(B-R)$ versus an M^*/L measured in an optical band.

As discussed by Charlot, Worthey, and Bressan (1996) and Maraston (2005), the treatment of TP-AGB and RGB stars leads to the largest discrepancies in the NIR which is reshaped here with the $(I-K)$ vs M^*/L diagram. The $(I-K)$ colors of old (small τ) populations with the same metallicity can differ by 0.2 mag (magnitude), and up to 0.5 mag for young populations. The reason for this discrepancy is two-fold. First, they are due to a different treatment of the (uncertain) late stages of stellar evolution (red supergiant, AGB, RGB). In these late stages, stars suffer mass loss that cannot be connected to the basic stellar parameters from first principles and must be parametrized and calibrated with data. This uncertainty involves energetics, stellar temperatures, and stellar spectra for the AGB, and mostly stellar temperatures and spectra for the RGB. The importance of the TP-AGB phase of stellar evolution became clear, when it was shown that the BC03, PEGASE, Starburst99, and Maraston (2005) models yielded systematic differences of several tenths of magnitude in the NIR at intermediate ages of 0.2 to 2 Gyr (Maraston, 2005; Maraston *et al.*, 2006; Bruzual, 2007), mostly attributable to differences in the treatment of TP-AGB stars. Second, numerical instabilities of luminosity integration along short-lived phases in the isochrone synthesis approach (Maraston, 1998, 2005) may explain why models based on the same stellar evolution tracks exhibit large fluctuations.

The models in Fig. 9 with a small TP-AGB contribution (i.e., BC03, PEGASE) display bluer values of $(I-K)$ colors at young ages (low M^*/L). The Vazdekis models behave

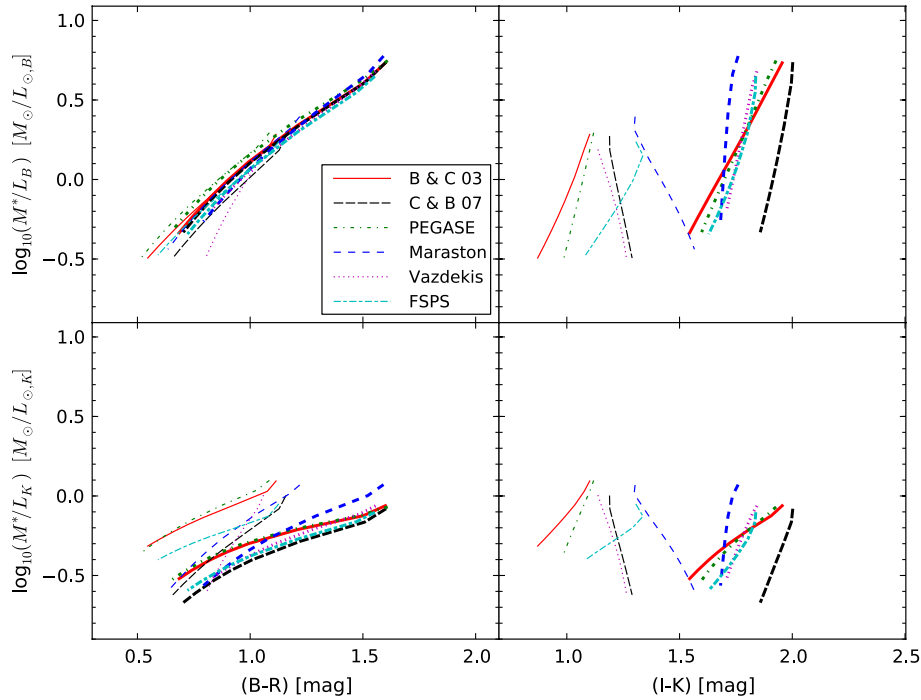


FIG. 9 (color online). M^*/L ratios for exponential SFR models of age 12 Gyr using SSPs from different models. The models compared are GALAXEV 2003 (Bruzual and Charlot, 2003) with Padova 1994 tracks, GALAXEV [2007, an updated version of Bruzual and Charlot (2003) with different treatment of the TP-AGB phase], PEGASE 2.0 (Fioc and Rocca-Volmerange, 1997), and the FSPS models (Conroy, Gunn, and White, 2009) all based on Padova stellar models and a Chabrier (2003) IMF, and the Maraston (2005) and the Vazdekis *et al.* (1996) models using a Kroupa (2001). Solar metallicity ($Z = 0.02$, thick lines) and 1/5 solar metallicity ($Z = 0.004$, thin lines) models are used, except for the Maraston models, where this metallicity is not available and a lower metallicity model of $Z = 0.001$ is plotted. The Chabrier and Kroupa IMFs give essentially the same results for broadband colors; hence by using these IMFs all the model sets can be compared even though some models are available only with either Chabrier or Kroupa IMFs.

similarly, but they are redder only because they include only ages >0.1 Gyr. Models with a substantial TP-AGB contribution (Maraston, 2005, 2007 version of the Bruzual and Charlot GALAXEV models) display redder colors at young ages or large or negative τ 's. At solar metallicity, old ages or small τ 's (upper right corner of the diagram), models based on Padova tracks (GALAXEV, FSPS, PEGASE), are redder than the Maraston models based on the Cassisi, Castellani, and Castellani (1997) tracks because the former have a redder RGB [see Fig. 9 in Maraston (2005) and discussion therein].

D. Data fitting techniques

The variety of techniques to derive M^*/L values by fitting spectra has increased dramatically in the last decade (Walcher *et al.*, 2011). Methods depend on the data available, ranging from two bandpasses (Bell and de Jong, 2001), multiple broadband colors (Bell *et al.*, 2003; Maraston *et al.*, 2012), a few line indices (Kauffmann *et al.*, 2003; Thomas *et al.*, 2011) to full spectral fitting (Blanton and Roweis, 2007; Tojeiro *et al.*, 2009; Chen *et al.*, 2012). Broadband imaging is often preferred over spectroscopy when large numbers of galaxies are required, when 2D stellar maps are created (Zibetti, Charlot, and Rix, 2009), or in low S/N situations as in high-redshift studies (Daddi *et al.*, 2005; Shapley *et al.*, 2005; Maraston *et al.*, 2006; Cimatti *et al.*, 2008). While more data points should in theory increase the accuracy of the

M^*/L estimation, this may not always be true in practice due to two reasons. First, EPS models have larger systematic uncertainties at certain wavelengths (Fig. 9). Such intrinsic model uncertainties should be taken into account while fitting the data, however this is rarely done (as it is not easy to quantify) and typically only the error in the measurement is used when weighing the different data points in the fit. Second, using more data points can also lead to systematic biases if the set of model templates is too limited to fit the complexity of the data. For example, for wavelengths longward of the K passband, the SED is dominated by dust reemission which is very difficult to model. Without a good description of dust reemission, the fitting of far-IR data is meaningless and can even impede a proper understanding of shorter wavelength data. Another case is when smooth (e.g., exponentially declining) SFHs are used with data sets that include indicators very sensitive to recent star formation. In such cases, templates should include at least a combination of a smooth SFH and a late star burst.

Methods furthermore vary according to the number of templates fitted to the data, namely, the range and type of SFHs and metallicity distributions (single burst, multiple burst, exponential SFH, etc.). This can lead to significant offsets whether one assumes that the most significant SF burst occurred 12 Gyr ago (Bell and de Jong, 2001) or more recently (Trager *et al.*, 2000). Integrated light SEDs rarely contain enough information to discriminate between burst time scales 8–13 Gyr ago, which can lead to offsets as high as 0.2 dex in M^* .

Finally, many mathematically different techniques have been used to fit models to data, ranging from simple minimum χ^2 fitting (Bell *et al.*, 2003) to maximum likelihood (Kauffmann *et al.*, 2003; Taylor *et al.*, 2011), and Bayesian methods (Auger *et al.*, 2009). For large data samples, information compression techniques are often used to reduce computational time, such as principle component analysis (Chen *et al.*, 2012), non-negative matrix factorization (Blanton and Roweis, 2007), and the linear compression technique used in Panter *et al.* (2007). The optimum amount of reduction allowed while retaining all information available will depend on the data quality and model used and may be hard to determine (Tojeiro *et al.*, 2007; Graff, Hobson, and Lasenby, 2011).

E. Robustness of stellar mass derivations

Determining the accuracy and robustness of stellar mass estimation from SED fitting is nontrivial since some of the intrinsic key properties of galaxies, most notably the SFH and the stellar IMF, are unknown. Nonetheless, estimates of uncertainties and systematic biases of a particular fitting method can be obtained by testing the results on mock galaxies. These mock galaxies are often based on semianalytic galaxy formation models, providing hundreds of thousands of test galaxies with a wide range of (hopefully realistic) SFHs. Such comparisons can also provide guidance on the minimal and optimal data sets to use when fitting real data (Pforr, Maraston, and Tonini, 2012; Wilkins *et al.*, 2013).

Sections II.C and II.D above make it clear that several parameters affect the accuracy and biases of stellar mass estimates, the most important being the IMF, data quality, the EPS model, SFHs and chemical evolution, dust, and redshift. More detailed analyses can be found in Conroy, Gunn, and White (2009), Gallazzi and Bell (2009), Pforr, Maraston, and Tonini (2012), and Wilkins *et al.* (2013), and references therein.

First, the IMF is the main systematic uncertainty in M^*/L estimation. However, as long as the IMF slope does not change for $M > 1M_{\odot}$, as is the case for Salpeter (1955), Kennicutt (1983), and Kroupa (2001), or Chabrier (2003) IMFs, the incognita from the initial mass function results only in a constant offset in stellar mass as the luminosity does not vary and only the total mass of a stellar population changes. A significant change of the IMF slope above $M > 1M_{\odot}$ implies a nonconstant offset (Pforr, Maraston, and Tonini, 2012).

Constraints on the IMF normalization can be derived by comparing stellar population mass estimates to dynamical or lensing mass estimates such as described in the remainder of this review, with the simple notion that the mass in stars should not exceed the total measured one. Such a comparison is done in Bell and de Jong (2001) using disk galaxy rotation curves. However, only upper limits can be obtained, since a fraction of the luminous mass can always be traded off to a (smooth) dark-matter component with a similar mass distribution such as the light. Only when there is a dynamical substructure on scales smaller than those expected for dark matter can one obtain lower limits to the stellar mass normalizations. Examples include the dynamics of bar and spiral

structure in disk galaxies, the effect of bulges on galaxy rotation curves, and the vertical velocity dispersion in disk galaxies (see Sec. III). de Jong and Bell (2007) performed such a comparison between dynamical and stellar population mass estimates and showed that the $SED-M^*/L$ relation normalization can be constrained to within ~ 0.2 dex (66% confidence level). If the IMF varies among galaxy types, as argued for instance by Auger, Treu, Gavazzi *et al.* (2010), Treu *et al.* (2010), Cappellari *et al.* (2012), and Conroy and van Dokkum (2012) (see also Secs. V.E.1 and VII.C.3), the IMF effect becomes much more complicated and unpredictable, let alone any evolution of the IMF with redshift (van Dokkum, 2008).

Proceeding with random uncertainties, the accuracy of mass estimation depends on the quality of the data. For example, Gallazzi and Bell (2009) determined that a spectral signal-to-noise ratio of $S/N > 20$ is required to get an accuracy of 0.1 dex in M^*/L when using a few optical indices. Tojeiro *et al.* (2009) performing full spectral fitting derived a ~ 0.1 dex uncertainty in M^* due to the quality of the data ($S/N \sim 10\text{--}15/\text{pixel}$). Chen *et al.* (2012) exploited low S/N high- z spectra from the SDSS-III/BOSS survey to argue that spectral fitting relying on a principal component analysis can lead to reliable results also for $S/N \sim 5$, although the actual parameters of the populations may not be well determined. Fitting the broadband signal instead of the spectrum for the low S/N case may be the best choice (Maraston *et al.*, 2012), and the two methods converge at high S/N .

The use of different EPS models also affects stellar masses, with an uncertainty of ~ 0.2 to 0.3 dex [on the logarithmic mass, Maraston *et al.* (2006), Conroy, Gunn, and White (2009), and Ilbert *et al.* (2010)], reaching at most 0.6 dex at $z \sim 2$ (Conroy, Gunn, and White, 2009) when TP-AGB stars dominate the spectrum and the models vary most (see Sec. II.C.3).

The adopted SFH in the models significantly contributes to the uncertainty and biases in M^*/L values (Maraston *et al.*, 2010) for high-redshift galaxies. The range in functional forms (if a function is used at all), the chosen oldest and youngest stars, and the inclusion and number of star bursts all affect the uncertainty and bias in the M^*/L determination.

For galaxies at low redshift with late star formation, Gallazzi and Bell (2009) found that the M^*/L may be overestimated by 0.1 dex when using spectral indices. Nearly similar accuracies can be obtained using one optical color, the choice of which may vary with redshift (Wilkins *et al.*, 2013). Using more than one color reduces the offsets slightly, but even more colors will not reduce the uncertainties and offsets (Gallazzi and Bell, 2009; Zibetti, Charlot, and Rix, 2009). This is in apparent contrast to Pforr, Maraston, and Tonini (2012), who argued that more passbands further reduce uncertainties and stress the benefits of near-IR data. This may be related to the limited set of templates adopted by Pforr *et al.* compared to the star formation histories in their mock catalog (if the templates do not fully span the range of “observed” galaxy parameters, more data help to get closer to the correct result) and possibly due to their inclusion of dust effects. Pforr, Maraston, and Tonini (2012) also showed that—when the template star formation history matches the real one—as is the case for positive τ models for high-redshift galaxies (Maraston *et al.*, 2010), the mass recovery from the

spectral fit is excellent and mostly independent of the waveband used in the fit.

Indeed, from the point of view of the SFH, high-redshift galaxies have less uncertain M^*/L as long as the redshifted data capture all necessary rest-frame wavelengths. This stems from a decrease in the number of possible SFHs (less time has passed since the initial star formation). Most notably the age difference between any old, underlying population and a recent burst is smaller, and the frosting or outshining effect by young stars is decreased (Maraston *et al.*, 2010). For similar quality multipassband data, this can reduce biases for dusty galaxies from 0.5 dex at $z = 0.5$ to 0.1 dex at $z = 2$ and uncertainties from 0.5 dex at $z = 0.5$ to 0.2 dex at $z = 2$ (Pforr, Maraston, and Tonini, 2012).

Finally, dust in galaxies significantly alters the SED (MacArthur, 2005). In case of very dusty systems spectroscopy clearly becomes the favored channel for M^*/L estimation. Access to both photometric and spectroscopic data enables a derivation of extinction values by comparing SED expectations derived from the spectral features to the observed photometry (Kauffmann *et al.*, 2003). Pforr, Maraston, and Tonini (2012) showed that including dust prescription in the SED fit dramatically increases the uncertainties and biases in stellar M^*/L estimates especially at low redshifts, with offsets being as large 0.5 dex and similarly sized rms uncertainties. When focusing on mass estimation, the conservative choice of neglecting dust as an additional parameter in the spectral fitting may lead to a more robust determination of stellar mass (Maraston *et al.*, 2012).

F. Future prospects

The stellar mass of galaxies M^* is a key parameter in studying the formation and evolution of galaxies over the cosmic time, tracing galaxy dynamics, and disentangling the contribution from dark matter to the overall galaxy potential. In this section, we reviewed the basic physics entering the derivation of M^* . This exploits the theory of stellar evolution to calculate the mass in stars from the amount of stellar light that galaxies emit. The modeling of the integrated galaxy light requires several assumptions regarding the distribution of ages and chemical compositions of the component stars (i.e., the galaxy star formation history), the distribution of stellar masses at birth (the stellar initial mass function), and the attenuation of light from dust. The fundamental tool to perform such modeling is called a “stellar population model.” We have described such models, highlighting their main uncertainties and how these affect the derivation of M^* . Using models from various authors we visualized the basic relations between M^* and the integrated spectral energy distribution, including color and spectral indices. Furthermore, we discussed the part of M^* which is composed of stellar remnants, such as white dwarfs, neutron stars, and black holes, which do not emit light but contribute to the total mass, and their dependence on the stellar initial mass function.

Finally, we briefly addressed the main techniques to calculate M^* found in the literature and discussed the typical uncertainties and biases of SED based on stellar mass estimates. While these depend on galaxy type, they are (i) for

star-forming galaxies, the unknown star formation history and the fact that a small fraction by mass of newly born stars can outshine the underlying older population dominating the mass, thus jeopardizing the mass derivation; and (ii) for both star-forming and passively evolving galaxies, the unknown IMF. Spectrophotometric data are most crucial for treating star-forming galaxies whereas the near-IR bands help in constraining the older, outshined component of the stellar population [see Fig. 3 in Maraston *et al.* (2010)].

Despite many unknowns, and excluding extreme cases of very dusty galaxies or galaxies with complicated and bursty star formation histories, relative stellar masses between galaxies can be regarded robust within 0.2–0.3 dex. The still poorly constraint IMF normalization will shift SED derived M^*/L values of all galaxies up or down by a few tenths of a dex, and if IMF variations occur across galaxy types and/or with redshift errors in SED, M^*/L estimation can be as large as 0.5 dex. Recent simulations have shown how fundamental model parameters such as the choice of SFH, adopted wavelength range, redshift, and inclusion of dust contribute to the uncertainties and can be used as a quantitative guide to assess uncertainties in M^* (Maraston *et al.*, 2010, 2012; Pforr, Maraston, and Tonini, 2012; Wilkins *et al.*, 2013).

The most urgently required model improvements include constraining residual uncertainties in stellar evolution, specifically regarding the temperature of the RGB and the energetics of the TP-AGB stars, and the effect of nonsolar abundance ratios on spectra. An improved understanding of star formation history effects for low- z galaxies would also be beneficial.

This section is by no means complete, but it provides the necessary background to understand several statements made in forthcoming sections. Other comprehensive reviews which address stellar mass estimates in galaxies include Conroy, Gunn, and White (2009), Greggio and Renzini (2011), Walcher *et al.* (2011), and Conroy (2013).

III. DYNAMICAL MASSES OF GAS-RICH GALAXIES

Galaxy masses were first inferred from spiral galaxy rotation curves, which were themselves first measured in the early 1900s (Scheiner, 1899; Slipher, 1914; Pease, 1918). The nebular lines from which velocity curves were derived already showed some evidence of a “tilt,” indicative of rotation, even though these early spectra sampled only the inner parts of the galaxy. In his most original 1922 paper and using Pease’s (1918) velocity curve of the Andromeda galaxy, Opik (1922) inferred a mass of $4.5 \times 10^9 M_\odot$ within $150''$ (~ 0.6 kpc) for $M31$. He did so by requiring that the $M31$ disk have a mass-to-light (hereafter M/L) ratio comparable to that of the solar neighborhood. This is the first reported measurement of galaxy mass. That same year, Kapteyn (1922) remarked in his study of the Milky Way’s local mass density that “We have the means of estimating the mass of dark matter in the Universe.” This appears to be the very first reference to the concept of “dark matter” in astrophysics. His dynamical analysis and determination of the density in the solar neighborhood is also the first of its kind. However, Kapteyn failed to find dynamical signatures for the elusive dark matter given the limitations of his data

and preliminary method, as reviewed by Oort (1932). The latter can be credited with the first discovery of dark matter in galaxies [see Zwicky (1933) for a similar discovery of dark matter in clusters of galaxies]. In his 1940 study of NGC 3115, Oort remarks “The distribution of mass in the system appears to bear almost no relation to that of the light.” This is yet another pioneering report of large mass-to-light ratios in galaxies.

About our own Galaxy, Rubin *et al.* (1962) remarked “For $R > 8.5$ kpc, the stellar [rotation] curve is flat, and does not decrease as is expected for Keplerian orbits.” Indeed, by the late 1960s, improved detectors at optical and radio frequencies yielded routine detections of flat galaxy rotation curves. Using a then-state-of-the-art image-tube spectrograph at the KPNO 84 in. telescope, Rubin and Ford (1970) obtained the first extended rotation curve of a galaxy (*M31*) out to 120' (~ 27 kpc). Roberts and Whitehurst (1975) confirmed the flatness of the *M31* rotation curve observed by Rubin and Ford with 21 cm velocities extending to 170' (~ 38 kpc). Roberts and Whitehurst, however, contended that dwarf *M* stars are adequate to explain the required mass and mass-to-light ratio. They, as well as most astronomers then, seem to have missed the note from Freeman (1970) that the HI rotation curves that were available at the time did not turn over at the radius expected from their surface photometry. Freeman’s 1970 paper, commonly cited for its study of exponential disks in galaxies (rather than the note above), was likely the very first to quantify the mismatch at large galactocentric radii between the observed rotation curve and the rotation curve expected from the light distribution and constant M/L .

The flatness of observed rotation curves in all galaxy types is now a well-established fact (Faber and Gallagher, 1979; Rubin *et al.*, 1985; Sofue and Rubin, 2001) but it is not by itself proof of dark matter in galaxies [see the contribution by Kalnajs in the 1982 Besancon conference proceedings (Athanassoula, 1983)]. Despite notable efforts by the likes of Kapteyn, Oort, Babcock, Mayall, de Vaucouleurs, Schwarzschild, the Burbidge’s, Roberts, Rubin, and others, and the realization that luminous galaxies are not a simple Keplerian environment, the firm manifestation of dark matter through galaxy rotation curves would await extended dynamical measurements at radio wavelengths (21 cm line of neutral hydrogen), especially with the Westerbork synthesis radio telescope (WSRT) (Rogstad and Shostak, 1972; Bosma, 1978; van der Kruit and Allen, 1978), and the ability to place upper limits on the contribution of the baryonic component to the total observed rotation curve (Bosma, 1978; Carignan and Freeman, 1985; van Albada *et al.*, 1985; Kent, 1986, 1987).

The first detailed and unambiguous demonstration of unseen mass in galaxy disks from the mass modeling of galaxy rotation curves came with Albert Bosma’s Ph.D. thesis in 1978. Using early disk analysis methods by Toomre (1963), Shu, Stachnik, and Yost (1971), and Nordsieck (1973), Bosma was able to decompose the extended rotation curves of 25 spiral galaxies to show for the first time that the total M/L ratio of galaxies grows with radius. To our knowledge, Faber and Gallagher (1979) were the first to link measurements for the local mass density (Oort, 1932, 1965), the velocity dispersion in galaxy clusters (Zwicky, 1933), and the notion of flat extended galaxy rotation curves (Bosma, 1978)

into a coherent picture of missing mass on galactic and extragalactic scales.

While measurements of gas and stellar motions for mass estimates of gas-rich galaxies are now fairly straightforward, it is of relevance to discuss the applicability and accuracy of their related mass estimators. Modern mass modeling of galaxy rotation curves, and the ability to disentangle baryonic and nonbaryonic components, are being reviewed next.

A modern review of the structure of galaxy disks can also be found in van der Kruit and Freeman (2011), hereafter vdKF11. We defer to that review in some cases below for more detailed discussions and/or derivations than can be provided here.

In their 2001 ARAA article, Sofue and Rubin wrote “Babcock and Oort share credit for uncovering the dark matter problem in individual spiral galaxies” for their work in the 1930s. The pioneering contributions in the 1960s–1980s of Toomre, Kalnajs, Shu, Freeman, Bosma, Carignan, Kent, van Albada, van der Kruit, Sancisi, and others addressing the problem of galaxy-mass models should also be underscored.

A. Mass estimates from rotation curves

The mass distribution in disk galaxies is typically determined from resolved rotation curves or integrated line profiles extracted from emission lines such as $H\alpha$, CO, and HI lines. With the current generation of detectors, the $H\alpha$ and CO lines yield high spectral resolution spectra over most of the optical disk; greater spatial coverage (often at the expense of spectral resolution) is usually obtained with resolved HI velocity curves. Integrated linewidths yield only an estimate of a total mass within some (uncertain) isophotal radius. A more accurate assessment of the extended galaxy-mass profile is obtained from 2D resolved HI velocity fields but the prohibitive exposure times constrain sample sizes (de Blok *et al.*, 2008). For nearby disks, $H\alpha$ velocity fields (e.g., with the instruments SparsePak, DensePak, PPAK) and CO velocity fields (e.g., with CARMA) are just as slow to obtain. The extent of the neutral gas in spiral galaxies, as traced by rotation curves, can often exceed twice that of the stars.

There is good agreement between resolved rotation curves extracted from $H\alpha$, HI, and CO lines (Sofue and Rubin, 2001; Simon *et al.*, 2003, 2005; Spekkens and Sellwood, 2007) and from [OII], [OIII], $H\beta$, [NII], and [SII] lines (Courteau and Sohn, 2003) within the optical disk of galaxies.

It is often assumed that HI linewidths sample the disk to large galactocentric radii, by analogy to resolved HI rotation curves; however, HI linewidths are a convolution of gas dynamics and exponentially declining gas surface densities (Cayatte *et al.*, 1994) such that the effective depth of integrated linewidths is likely representative of the gas distribution within the optical disk of a galaxy. This is in line with the many linear transformations that exist between $H\alpha$ rotation measures and HI linewidths (Mathewson, Ford, and Buchhorn, 1992; Courteau, 1997; Catinella, Haynes, and Giovanelli, 2007 to name a few).

The circular velocity of a spherical system in a potential Φ is given by

$$V_{\text{circ}}^2(r) = r \frac{d\Phi}{dr} = G \frac{M(r)}{r}, \quad (2)$$

where $M(r)$ is the enclosed mass within a sphere of radius r . For a flattened disk, as in most spiral galaxies, the left-hand side of Eq. (2) must be replaced by the more exact expression derived by Freeman (1970). In the absence of dark matter or bulge, it should be stated that the exact expression for the rotation curve of a self-gravitating exponential disk is described by (Freeman, 1970)

$$V_{\text{circ}}^2(R) = 4\pi G \Sigma_0 R_d y^2 [I_0(y)K_0(y) - I_1(y)K_1(y)], \quad (3)$$

where G is the gravitational constant, Σ_0 is the central surface brightness, R_d is the disk exponential scale length, $y \equiv R/2R_d$, and $I_i(y)$ and $K_i(y)$ are the modified Bessel functions of the first and second kind [Freeman (1970), see also vdKF11 and Fig 2.17 of Binney and Tremaine (2008)]. The rotation curve of a pure exponential, infinitesimally thin, disk peaks at $V_{2.2} \equiv V(R = 2.15R_d)$. For disks of finite thickness (say $z_0/R_d = 0.2$, where z_0 is the disk scale height), the rotation curve has a very similar shape but a $\sim 5\%$ lower peak (Casertano, 1983); this will slightly affect the “shape” term in the square brackets in Eq. (3), but leave the subsequent scalings untouched.

The reliability of $M(r)$ depends on how the rotational velocities V_{rot} reflect the assumed circular velocities. Several factors involving corrections for observational and physical effects come into play. First, the observed line-of-sight (LOS) velocity V_{LOS} must be corrected for projection via

$$V_{\text{rot}} = V_{\text{LOS}} / \sin i, \quad (4)$$

where i is the projected inclination of the galaxy disk [or a ring along that disk, for tilted-ring solutions (Teuben, 2002)]. Equation (4) applies for velocities along the major axis; for the general case along any other projection, see Teuben (2002).

The spatially resolved rotation curve or integrated line-width of a rotating system is obtained via the Doppler equation:

$$V_{\text{LOS}}(r) = c[\lambda(r) - \lambda_0]/\lambda_0, \quad (5)$$

where λ_0 is the observed wavelength of the galaxy center and r is the position along the slit. A linewidth W , usually equal to $2V_{\text{obs}}$, must also be corrected for internal turbulence and other effects (Haynes and Giovanelli, 1984; Catinella, Haynes, and Giovanelli, 2007).

The inclination angle i for an oblate spheroid is given by

$$i = \cos^{-1} \sqrt{\frac{(b/a)^2 - q_0^2}{1 - q_0^2}}, \quad (6)$$

where the semimajor (a) and semiminor (b) axes are determined from isophotal fitting of the galaxy image, and q_0 is the axial ratio of a galaxy viewed edge on [for late-type disks, $q_0 \approx 0.13$ (Hall *et al.*, 2012 and references therein)].

Inclination uncertainties in Eq. (2) can be most significant for systems with $i < 30^\circ$ or for distant galaxies whose disk is poorly resolved (in such cases, space-based observations or adaptive optics are needed to overcome the effect of atmospheric blur). Inclination estimates vary as a function of wavelength and are clearly affected by warps beyond the

optical disks (Briggs, 1990). Tilt uncertainty, such as due to warps, can account for a significant fraction of the mass budget in the outer parts of the disk. This is illustrated in Fig. 10 for the mass profiles of NGC 45, $M31$, and $M33$ obtained assuming a kinematical model with constant inclination and major axis position angle (open squares) or a full tilted-ring model (filled squares). The ratio of these curves is shown on the right side of Fig. 10 as a function of radius normalized by the disk exponential scale length h . While the value of h depends on the assumed distance to the galaxy and details of surface brightness profile fitting (Courteau *et al.*, 2011), Fig. 10 makes it clear that tilted-ring models are required for rotation curves extending beyond 5–6 optical disk scale lengths.

The effects of slit misalignment (erroneous position angles) for long-slit spectra on mass estimates are also addressed by Rhee *et al.* (2004), Spekkens, Giovanelli, and Haynes (2005), and Chemin *et al.* (2006).

Ideally, a totally enclosed galaxy mass should be determined using the most extended rotation curve and probing a regime where it is flat. Velocity curves can be modeled using a fitting function (Courteau, 1997; Giovanelli and Haynes, 2002). This is especially useful for low-mass systems whose observed rotation curves rarely reach a plateau (caution is

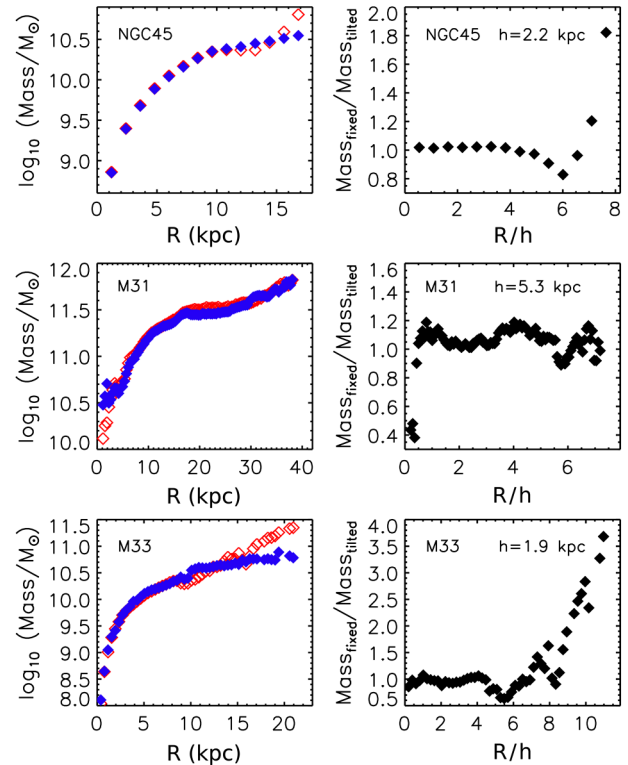


FIG. 10 (color online). Mass profiles from HI rotation curves of NGC 45 (Chemin, Carignan *et al.*, 2006), $M31$ (Chemin, Carignan, and Foster, 2009), and $M33$ (Chemin *et al.*, in preparation). Mass profiles on the left were obtained from rotation curves assuming a kinematical model with constant inclination and constant position angle of the major axis (open squares) or a full tilted-ring model (filled squares). The adopted distances are NGC 45 ($D = 5.9$ Mpc), $M31$ ($D = 785$ kpc), and $M33$ ($D = 800$ kpc). The ratio of these mass profiles is shown on the right side where the radial scale has been normalized by the optical exponential disk scale length h .

advised against extrapolations) or for noisy rotation curves with spiral structure wiggles. The reliability of mass estimates depends greatly on the stability of the velocity measure. For instance, V_{obs} is typically measured for one-sided resolved rotation curves at a fiducial marker such as $V(R_{\text{max}})$, where R_{max} is the radius at which V_{obs} reaches its peak value or $V_{23.5}$, the velocity measured at the 23.5 mag arcsec⁻² I-band isophote (Courteau, 1997), or at half of a suitably chosen width of an integrated line profile (Haynes and Giovanelli, 1984; Springob *et al.*, 2005). Different definitions of rotational velocities or linewidths can yield tighter galaxy scaling relations. For example, measurements of V_{obs} at either $V_{2.2}$ or $V_{23.5}$ yield the tightest scatter in various galaxy scaling relations for bright galaxies (Courteau, 1997). For the rising rotation curves of lower surface brightness systems, Catinella, Haynes, and Giovanelli (2007) noted that the $V_{2.2}$ values may not probe the rotation curve deeply enough and that these may therefore show a surface brightness dependence. $V_{23.5}$ would thus be a safer mass tracer, provided that the rotation curve is sampled that far.

Optical (typically H α) rotation curves for bright galaxies may show extended flattening out to 4–5 disk scale lengths (Courteau, 1997), such that a maximum $V_{\text{max}} = V(R_{\text{max}})$ can be estimated. HI rotation curves routinely extend to that radius, making the measurement of V_{max} straightforward from these data.

Beyond galaxy disks, little is known about the mass profiles of individual galaxies. By stacking galaxies of similar masses or luminosities, it is possible to use weak gravitational lensing (see Sec. VI) or satellite kinematics (More *et al.*, 2011a) to measure total masses within the virial radius of the dark-matter halo. This mass can be trivially converted into the circular velocity at the virial radius V_{200} . By comparing with the rotation velocities within the optical disk V_{opt} , one finds that on average for late-type galaxies $V_{\text{opt}}/V_{200} \approx 1.2$ (Dutton *et al.*, 2010; Reyes *et al.*, 2011). Thus, the dark matter near the virial radius may have slightly lower circular velocity than that of the inner baryons, and extended rotation curves are best decomposed into their major components (bar, bulge, disk, halo) rather than extrapolated. We discuss such decompositions in Sec. III.C.

The velocity function (or the number of galaxies per unit circular velocity per volume) of spiral galaxies has been measured directly for the Virgo cluster by Papastergis *et al.* (2011). The full spectrum of (projected) linewidths ranges from 20 km s⁻¹, where corrections for turbulence dominate measurement uncertainty, to more than 400 km s⁻¹.³

³The fastest reported galaxy “disk” is that of UGC 12591, an S0/Sa galaxy rotating at 500 km s⁻¹ and having a total mass within R_{25} equal to $1.4 \times 10^{12} M_{\odot}$ ($H_0 = 70 \text{ km s}^{-1} \text{ Mpc}^{-1}$) (Giovanelli *et al.*, 1986). Considering its x-ray emission and surprisingly low baryon mass fraction (3%–5%; Dai *et al.*, 2012), this galaxy is likely a massive spheroid that has accreted its, now rotating, neutral gas after assembling most of its stellar mass. The late merger-accretion event that formed the disk of UGC 12591 may have also turned on a massive outflow to drive its gas halo out to very large radii. As such, UGC 12591 should clearly not be compared to normal spiral galaxies.

For a spherically symmetric system, the total mass enclosed within a radius R can be written in solar units as

$$M(R) = 2.33 \times 10^5 R V_{\text{obs}}^2 / \sin^2(i) M_{\odot}, \quad (7)$$

where R is the radius along the major axis in kpc and V_{obs} is the observed rotation velocity in km s⁻¹. Galaxy masses are thus best measured for systems with accurate distances; galaxies in unvirialized clusters or close enough ($cz \lesssim 5000 \text{ km s}^{-1}$) to experience substantial deviations from the Hubble flow clearly suffer (linearly) from significant distance estimate errors.

Note that while the total enclosed mass $M(R)$ is corrected for projection through Eq. (7), the complete deprojection of a rotation curve into a radial mass profile requires a tilted-ring analysis of the light distribution to account for the combined effects of a bulge, bar, and disk (and sometimes a stellar halo) and isophotal warps (Fig. 10). Other physical effects discussed in Sec. III.B make this endeavor, especially in the inner parts of a galaxy, a rather challenging and uncertain one. To probe the total galaxy potential in its outskirts would require other tracers such as planetary nebulae (PNe), globular clusters, and satellites.

B. Inner parts

In addition to errors introduced by deprojection effects and distance uncertainty, fundamental physical complications thwart the direct interpretation of galaxy rotation curves via Eq. (7) in their inner parts. These include deviations from circular orbits due to barlike perturbations, differential dust opacity in the bulge and inner disk, density profile variations due to a triaxial halo, and more. We next address these briefly.

Because a large fraction of gas-rich galaxies have non-axisymmetric inner parts, noncircular velocities are often observed within the corotation radius of gas-rich galaxies (Lindblad, Lindblad, and Athanassoula, 1996; Weiner, Sellwood, and Williams, 2001; Courteau *et al.*, 2003; Spekkens and Sellwood, 2007; Valenzuela *et al.*, 2007; Sellwood and Sánchez, 2010). Once identified, correcting for noncircular motions is a daunting task. To relate those motions with a photometric bar requires detailed, model-dependent fluid-dynamical simulations (see Sec. III.D.4). Beyond the self-consistent treatment of the bar in these fluid-dynamical models, the correlation between the observed photometric bar strength (or length) and the amplitude of barlike noncircular motions has not been widely explored (Spekkens and Sellwood, 2007; Sellwood and Sánchez, 2010; Kuzio de Naray *et al.*, 2012); the latter requires high-quality 2D velocity fields and an empirical means to measure barlike flows. Furthermore, the contribution of a bar or oval distortion to noncircular motions depends on the angle between the bar axis and the major axis. The amplitude of a rotation curve will be biased high or low if a bar close to the minor or major axis is neglected (Spekkens and Sellwood, 2007; Sellwood and Sánchez, 2010).

As an example for the phenomenological description of the influence of a bar on measured rotation curves, we show in Fig. 11 a diagram adapted from Valenzuela *et al.* (2007). They used N -body simulations to show that noncircular motions, combined with gas pressure support and projection

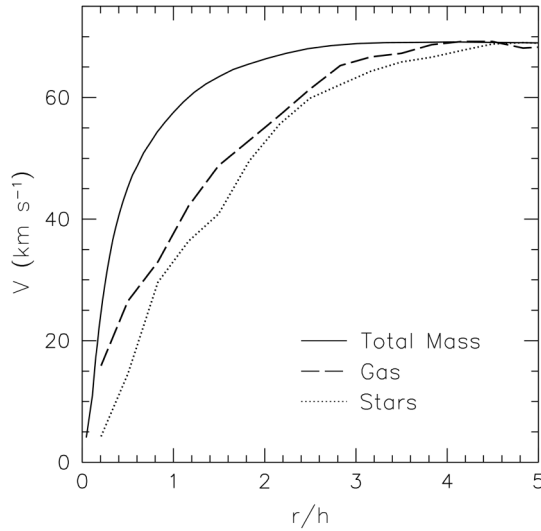


FIG. 11. Simulated velocity curves for a dwarf galaxy. The solid curve shows the spherical averaged circular velocity $(GM_{\text{tot}}/r)^{1/2}$. The long-dashed curve is for the azimuthally averaged rotation velocity of gas particles. The stellar rotation velocity is shown by the dotted curve. Curves for the gas and stars are substantially below the circular velocity for $r < 3h$, where h is the disk scale length. From Valenzuela *et al.*, 2007.

effects, can result in a large underestimation of the circular velocity in the central ~ 1 kpc region of a gas-rich dwarf galaxy. While those highlighted effects are stronger in barred systems, they are also present in axisymmetric disks. Their simulations show that $V_{\text{obs}} \approx V_{\text{circ}}$ only beyond three disk scale lengths.

The differential opacity in spiral disks (Bosma *et al.*, 1992; Giovanelli and Haynes, 2002) also calls for a careful interpretation of optical rotation curves. The effects of dust extinction on velocity curves, which tend to mimic solid-body rotation, can be significant at high tilt ($> 80^\circ$) and for wavelengths bluer than $H\alpha$ (Bosma *et al.*, 1992; Courteau, 1992) within one disk scale length. This “tapering” effect is also luminosity dependent, being stronger for the most luminous systems (Giovanelli and Haynes, 2002). This problem is mostly overcome by measuring rotation curves at near-infrared wavelengths (e.g., through the Pa α and Br γ hydrogen recombination lines) where extinction is minimized.⁴ Radio observations nearly alleviate this concern, although lower resolution at HI may affect the rise of the rotation curve in the central regions (Bosma, 1978; van den Bosch and Swaters, 2001), and the HI optical depth and related self-absorption effects are not negligible in more inclined galaxies (Rupen, 1991). The high-spatial resolution kinematics of galaxies’ inner regions from high- J CO line spectroscopy using the Atacama large millimeter array (ALMA) will soon lessen these issues, although similar concerns such as the above for more inclined galaxies apply. Effects due to triaxiality and flattening of the disk have been discussed by Dutton *et al.* (2005) and Binney and Tremaine (2008) (Fig. 2.13).

⁴Clearly, the issue of extinction is less conspicuous in nearly face-on systems (Andersen *et al.*, 2006).

For distant galaxies, the inner rise of the rotation curve is also critically damped by both resolution effects and enhanced central galaxy activity which contributes more dust per unit area at early times. Both dust extinction and resolution yield observed rotation curves that are shallower than the true velocity profile (Förster Schreiber *et al.*, 2006).

Because of the complex and somewhat uncertain modeling involved in correcting for noncircular motions and internal extinction, masses for nearby galaxies are often extracted beyond corotation or, equivalently, beyond two to three disk scale lengths (Kranz, Slyz, and Rix, 2003; Valenzuela *et al.*, 2007).

C. Mass modeling

An ultimate goal of galaxy-mass studies is the decomposition of a mass profile into its main components (the bulge, disk, and dark-matter halo) at all radii. Unlike gas-poor systems (Sec. V) whose spectral features are faint beyond one effective radius, mass modeling decompositions can be attempted for spiral galaxies since dynamical tracers are conspicuous from the center to the optical edge. Pioneering mass models have been derived by Casertano (1983), Wevers (1984), Carignan and Freeman (1985), van Albada *et al.* (1985), and others.

Mass modeling is possible because the gas particles and stars are sensitive to the full potential contributed by the baryons and dark matter. If the matter distribution is axially symmetric and in centrifugal equilibrium, then the total circular velocity is given by

$$V_{\text{circ}} \approx \sqrt{V_{\text{gas}}^2 + V_*^2 + V_{\text{halo}}^2}, \quad (8)$$

at each radius R in the plane of the galaxy, where V_{gas} , V_* , and V_{halo} are the observed rotation curves of the gas, stars, and halo components, respectively. The latter accounts for the baryons and presumed dark-matter particles in the halo. V_{halo} is usually inferred once the gas and stellar component have been subtracted from the observed overall rotation curve.

The velocity curves for the stars and gas found in the galaxy bulge and disk can be obtained by inverting their respective light (emission) profiles into mass profiles using suitable potentials and stellar M/L_* ratios. For instance, the stellar rotation curve is obtained by multiplying the light profile, ideally in a band where dust extinction effects are minimized, with an optimized M/L_* consistent with stellar population models (Sec. II).

The neutral atomic gas M_{HI} can be estimated from the total HI flux density S_{21} , measured from the 21-cm line in absorption and emission:

$$M_{\text{HI}} = 2.33 \times 10^5 S_{21} (D/\text{Mpc})^2 M_{\odot}, \quad (9)$$

where D is the physical distance to the source in Mpc and S_{21} is the integrated flux density of the source in Jy km s^{-1} . The total gas mass which accounts for helium and other metals is given by

$$M_{\text{gas}} = 1.33 M_{\text{HI}} \quad (10)$$

for an optically thin gas. An estimate of the molecular gas mass is more challenging since H_2 , the most abundant

molecule in the Universe by far, has no permanent electric dipole moment and thus cannot emit in the state in which it is typically found. Consequently, the second most abundant molecule, the CO molecule which has an electric dipole and is often optically thick, can be used since it is collisionally excited by H₂. However, the conversion from CO intensity to H₂ mass, via some “X_{CO}” factor, is notoriously uncertain (Bolatto *et al.*, 2008). Still, Braine *et al.* (1993) estimated the mass contribution of molecular gas to ~20% of the HI mass, and this fraction decreases in later-type systems. For these reasons, we do not consider the molecular mass content further.

Detailed mass models of spiral galaxies including the equations for the density profiles and associated rotation curves for the bulge, disk, and halo profiles can be found in Dutton *et al.* (2005), de Blok *et al.* (2008), and Tamm *et al.* (2012), and Sec. 11.1 of Mo, van den Bosch, and White (2010). Disks are often modeled as idealized infinitesimally thin, radially exponential, collections of dust, gas, and stars with surface density distributions (Freeman, 1970):

$$\Sigma(R) = \Sigma_0 \exp(-R/R_d), \quad (11)$$

where R_d is the scale length of the specific disk component. The total mass of the disk is $M_d = 2\pi\Sigma_0 R_d^2$. Dutton, Conroy *et al.* (2011) showed that disk scale lengths of the gas are on average 1.5 times greater than disk scale lengths measured in the R -band light. The case of a thicker disk (Casertano, 1983) adds only a small effect to the overall rotation curve (Mo, van den Bosch, and White, 2010). Real disks, however, often show spiral arm features, truncations, antitruncations, and other deviations from a pure exponential surface density distribution (van der Kruit and Freeman, 2011) that are best modeled through a free form reconstruction of the stellar mass by inversion of the light profile as discussed following Eq. (8).

The halo profile is obtained as the difference (in quadrature) between the observed rotation curve and the inferred baryonic components [Eq. (8)]. The halo is typically modeled as a pseudoisothermal profile (Burkert, 1995), a cosmologically motivated dark profile (Navarro, Frenk, and White, 1996, 1997, hereafter NFW), or an Einasto fitting function (Einasto, 1965). The halo profile can be conveniently parametrized via the following function (Kravtsov *et al.*, 1998):

$$\rho_{\text{halo}}(r) = \frac{\rho_0}{(r/r_s)^\alpha (1 + r/r_s)^{3-\alpha}}, \quad (12)$$

where ρ_0 is a central density, r_s is a scale radius, and α is a shape index. This density profile has an inner logarithmic slope of $-\alpha$. For $\alpha = 1$ this reduces to the NFW profile, and at the scale radius r_s , the slope of the density profile is -2 (isothermal). At large radii, the logarithmic slope is -3 .

1. Mass modeling limitations

The greatest source of uncertainty in mass modeling is the assessment of realistic stellar M/L_* ratios, followed by ill-constrained covariances among halo parameters as well as between halo and disk parameters, as we discuss next.

The computation of mass models through Eq. (8) usually involves four fundamental parameters: one for the stellar M/L_* , and three for the halo component [as in Eq. (12)]. In the language of NFW, those three quantities are the dark-matter halo shape index α , a velocity normalization V_{200} , and a concentration c .

Figure 12 highlights many of the challenges inherent to mass modeling such as the intrinsic degeneracy of current mass model solutions due to strong covariances between the disk and halo model parameters [see also van Albada *et al.* (1985)]. Figure 12 shows examples of modeled rotation curves for galaxies in three different mass ranges. The points are H α and HI velocity data from Blais-Ouellette (2000). The

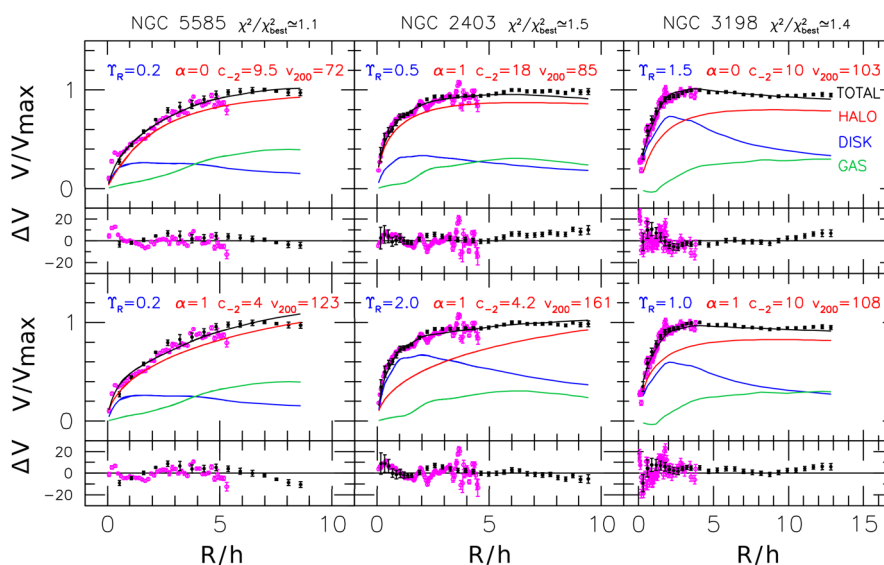


FIG. 12 (color online). Mass models for three spiral galaxies with a range of peak circular velocity. The X axis is in units of the optical disk scale length h . The velocity on the Y axis is normalized by the maximum observed orbital velocity. There are four free fitting parameters: Y_R is the stellar M/L_* (here in the R band) and α , c , and V_{200} describe the NFW dark-matter halo [see Dutton *et al.* (2005) for details]. Variations in the fitting parameter can result in the same data-model residuals, as gauged by the model residuals ΔV (shown in the lower windows) and the overall χ^2 -square statistic (shown above each figure column). The model decompositions in each column (two per galaxy) have the same overall χ^2 -square statistic, shown at the top. Mass models are thus nonunique. See text for details.

fitted components are shown for the gas, disk, and halo models. In each panel, one model parameter is held fixed while the others can adjust to achieve a best-fit solution (by minimizing the global data-model χ^2 statistic). In all cases, the model decompositions (two per galaxy) in a given column have the same overall χ^2 statistic. Variations in the fitting parameters can result in the same data-model residuals (ΔV , shown in the smaller horizontal windows) thus yielding nonunique solutions. The two right-side panels highlight the well-known disk-halo degeneracy between the stellar disk M/L_* , here expressed as Y_R in the R band, and the halo inner slope α [a cusp has $\alpha = 1$, a core has $\alpha = 0$; see Eq. (12)]. The two central panels show another facet of the disk-halo degeneracy assuming that all dark-matter halos are cuspy. The range of acceptable parameters is large. Finally, the left panels show that model degeneracies exist even among halo parameters, assuming a common best-fitting stellar M/L_* ratio (in agreement with stellar population models). Thus, in order to achieve realistic mass models, both accurate stellar M/L_* and well-constrained cosmological models are needed. Stellar M/L_* are only accurate to factors of 2 (Sec. II) and the current range of allowed halo parameters c , V_{200} , and α is still too broad to provide tight (unique) mass model solutions (Macciò, Dutton, and van den Bosch, 2008). The inner shape parameter α is especially difficult to constrain observationally due to the added complication that only a small number of rotation curve points constrain this value; see Dutton *et al.* (2005) and de Blok (2010) for reviews.

An additional complication to the mass modeling exercise is whether the *initial* distribution of dark-matter particles is affected by the gradual cooling of the baryons as a galaxy forms. If the potential variations due to the dissipating baryons occur slowly compared to the orbital period of a dark-matter particle in circular orbit, then the end state of the system is independent of the path taken (Blumenthal *et al.*, 1986; Gnedin *et al.*, 2004; Abadi *et al.*, 2010). Thus, contraction of the dark matter occurs when baryons collapse and come to the central region; if the gravitational potential increases, matter naturally follows. This “adiabatic” contraction of the halo due to the cooling baryons can be modeled as

$$r_f V_f(r_f) = r_i V_i(r_i), \quad (13)$$

where $V_i(r_i)$ and $V_f(r_f)$ are the initial and final rotation curves, respectively, and $rV(r)$ is the adiabatic invariant (Mo, van den Bosch, and White, 2010).⁵ The example of a modeled rotation curve with and without adiabatic contraction (AC) is shown in Fig. 13. This model has a fixed stellar $M/L_* = 1$ and halo $\alpha = 1$. The ratio of dark to baryonic mass within the optical disk of a galaxy can increase by almost 40% if AC is invoked. In more extreme cases, AC can transform an initial $\rho \propto r^{-1}$ NFW-type halo into a $\rho \propto r^{-2}$ isothermal halo.

⁵They advocated using $rV(r)$ as the adiabatic invariant, instead of the usual $rM(r)$ invariant, since disks are not spherical. Note also that the algorithm for compression due to adiabatic infall in a spherical halo model may take a different form when random motions are accounted for (Sellwood and McGaugh, 2005).

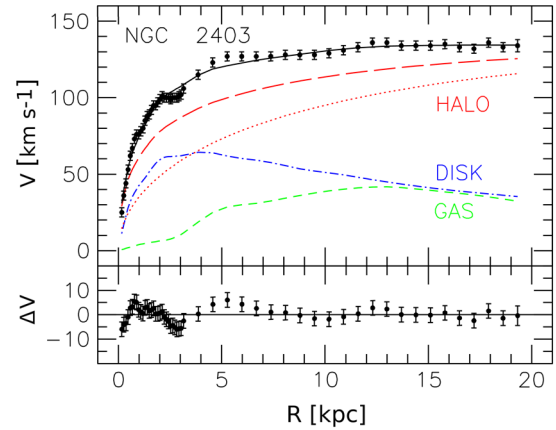


FIG. 13 (color online). Mass model for the bright spiral galaxy NGC 2403 with an adiabatically contracted halo model (long-dashed line) or not (initial model shown with dotted line). The disk and gas profiles correspond to the contracted final model. The data-fit residuals ΔV are shown in the lower panel. The ratio of dark to baryonic mass within the optical disk of a galaxy can increase by almost 40% within $V_{2,2}$ if AC is invoked. The observed velocity data (black points) are from Blais-Ouellette (2000). See text for details about the modeling technique.

While AC is undoubtedly at play in all forming galaxies, it is known that baryonic effects such as supernova feedback and dynamical fraction can, in principle, result in reduced halo contraction or even halo expansion (Navarro, Eke, and Frenk, 1996; El-Zant, Shlosman, and Hoffman, 2001). Only recently have these effects been demonstrated in fully cosmological simulations of galaxy formation (Johansson, Burkert, and Naab, 2009; Abadi *et al.*, 2010; Duffy *et al.*, 2010; Governato *et al.*, 2012; Macciò *et al.*, 2012; Martizzi *et al.*, 2012). Despite recent progress, cosmological simulations have not yet provided unique predictions for the response of dark-matter halos to galaxy formation. A wide range of possibilities (from adiabatic contraction to expansion, from cuspy to cored halos) should thus be accounted for when attempting mass models of galaxies.

D. Other galaxy-mass constraints

Besides mass modeling of individual galaxies, with all the limitations that this entails as we saw previously, potentially tighter constraints for the mass of baryonic and dark matter in disk galaxies may be achieved through dynamical or statistical arguments. As a way of introduction, we first present various methods to constrain the stellar M/L_* , independently of stellar population models.

1. Maximal and submaximal disks

The hypothesis that the bulge and disk could contribute “maximally” to the rotation curve was introduced by Carignan and Freeman (1985) and van Albada *et al.* (1985) in order to overcome the intrinsic uncertainties of stellar M/L_* ratios. A maximal disk obeys

$$\mathcal{F} \equiv V_{\text{disk}}(R_{\text{max}})/V_{\text{tot}}(R_{\text{max}}) > 0.85,$$

where V_{disk} is the inferred velocity of the disk (stars and gas), V_{tot} is the total observed velocity, and R_{max} is the radius at which V_{disk} reaches its peak value. For a pure exponential disk, this is $V_{2.2}$ (see Sec. III.A). In other words, for a maximal disk galaxy $V_{\text{disk}}^2(R_{\text{max}})/V_{\text{tot}}^2(R_{\text{max}}) \geq 0.72$ and the disk contributes at least 72% of the total rotational support at R_{max} . Note that this is just an arbitrary convention following Sackett (1997). A lesser contribution of the disk to the overall rotation curve at R_{max} is deemed “submaximal.” Since a galaxy with a submaximal disk with a significant bar or bulge component can still be baryon dominated within R_{max} , we define a galaxy to be maximal at R_{max} if $\mathcal{F} > 0.85$, where V_{disk} is the inferred velocity of the baryons (bulge and disk). Even in the presence of a maximal disk, rare are the galaxies that do not require a halo component to match fully extended rotation curves. For dwarf galaxies, maximal disks often involve stellar M/L_* ratios that are physically implausible (Swaters *et al.*, 2011).

The central panel of Fig. 12 provides a good example of a submaximal (top) versus a maximal (bottom) disk fit. Both fits are equally valid numerically [see also Kassín, de Jong, and Weiner (2006) and Noordermeer *et al.* (2007)]. Thus, without further constraints and especially extended HI rotation curves, the choice of a (sub)maximal disk solution remains ill constrained. Fortunately, arguments about the dynamical structure of disks and the existence of a velocity-luminosity (VL , aka “Tully-Fisher”) relation of spiral galaxies allow for new constraints to be implemented as discussed in Sec. III.D.3 (see also discussions on this topic by vdKF11). In general, those other techniques listed next point to galaxy disks whose stellar masses are significantly below the so-called maximal value.

2. Velocity dispersion measurements

For a self-gravitating, radially exponential disk with vertical profile of the form $\rho(R, z) = \rho(R, 0)\text{sech}^2(z/z_0)$, van der Kruit (1988) and Bottema (1993) showed that the peak circular velocity of the stellar disk V_{disk} , measured at $R = 2.2R_d$ can be related to the vertical velocity dispersion V_z and the intrinsic thickness (or scale height) of the disk z_0 via

$$V_{\text{disk}}(R_{\text{max}}) = c_{\text{max}} \langle V_z^2 \rangle_{R=0}^{1/2} \sqrt{\frac{R_d}{z_0}}, \quad (14)$$

where $c_{\text{max}} \simeq 0.88(1 - 0.28z_0/R_d)$ (Bershady *et al.*, 2011). A more detailed discussion of Eq. (14) is presented in vdKF11 (see their Sec. 3.2.4).

The power of Eq. (14) is that the disk M/L_* , derived via $V_{\text{disk}}(R_{\text{max}})$, can be determined independently of the dark-matter halo. However, the measurements involved are difficult since the scale height z_0 and the vertical component of the velocity dispersion V_z cannot be measured simultaneously. Thus this method is statistical in nature, at least for nearly edge-on (Kregel, van der Kruit, and Freeman, 2005) and nearly face-on (Andersen *et al.*, 2006; Andersen and Bershady, 2013) systems. Indeed, for face-on systems, V_z can be measured but z_0 must be inferred; and vice versa for edge-on systems. The tightness of the statistical correlations used to infer z_0 and V_z for face-on and edge-on galaxies, respectively, is reviewed by Bershady, Verheijen, Westfall

et al. (2010). Furthermore, Bershady *et al.* (2011) showed that the edge-on sample of Kregel, van der Kruit, and Freeman (2005) and the face-on sample (so-called “DiskMass survey”) of Bershady, Verheijen, Swaters *et al.* (2010) yield similar distributions of V_{disk} vs V_z . Systematic errors in M/L_* estimates based on Eq. (14) are thus relatively small.

Kregel, van der Kruit, and Freeman (2005) determined the intrinsic stellar disk kinematics through Eq. (14) for 15 intermediate and late-type edge-on spiral galaxies using a dynamical modeling technique and assuming that $\sigma_z/\sigma_r = 0.6 \pm 0.1$ (based on various arguments). For 12 of their 15 spirals, they found on average $\mathcal{F} = 0.53 \pm 0.04$. They also found that the contribution of the disk to $V_{2.2}$ is independent of barredness, in agreement with the Tully-Fisher (VL) analysis of barred galaxies⁶ by Courteau *et al.* (2003) and Sheth *et al.* (2012) and the N -body simulations of Valenzuela and Klypin (2003).

More recently, Bershady, Verheijen, Swaters *et al.* (2010) applied the velocity dispersion method on a sample of 46 nearly face-on (inclinations $\simeq 30$ deg) galaxies. This survey uses integral-field spectroscopy to measure stellar and gas kinematics using the custom-built SparsePak and PPAK instruments. For the high-surface-brightness galaxy UGC 463, Westfall *et al.* (2011) found the galaxy to be submaximal at 2.2 disk scale lengths with $\mathcal{F} = 0.61^{+0.07}_{-0.09}(\text{ran})^{+0.12}_{-0.18}(\text{sys})$. The ratio \mathcal{F} could be much smaller for lower surface brightness systems. In fact, Bershady *et al.* (2011) confirmed for 30 DiskMass systems covering a range of structural properties that the fraction \mathcal{F} ranges from 0.25 to 0.65 and increases with luminosity, rotation speed, and redder color. The DiskMass project does not include a dark-matter component in their analysis since their data in the plane of the disk are largely baryon dominated (even in areas where dark matter dominates the enclosed mass). The impact of the dark halo is to make the disks less maximal [as advocated by Bottema (1993)] at the 20% level.

3. Scaling relations residuals

Courteau and Rix (1999) suggested that submaximal disks provide a solution to the surface brightness independence of the VL relation [see also Zwaan *et al.* (1995)]. Courteau and Rix found that, on average, high-surface brightness spiral galaxies have $\mathcal{F} \simeq 0.6 \pm 0.1$, as recently verified by Bershady *et al.* (2011), Sec. III.D.2. Their argument relies on the assumption that the scatter in the VL relation and the size-luminosity relation is largely controlled by the disk scale length, that spiral galaxies have self-similar M/L profiles (different than having constant M/L ratios), and that dark-matter halos are adiabatically contracted. Dutton *et al.* (2007) revisited the Courteau and Rix method using a more detailed account of baryonic physics to find that $\mathcal{F} \simeq 0.72 \pm 0.05$ if AC is ignored or compensated for by other mechanisms

⁶The fact that barred and unbarred galaxies share the same Tully-Fisher relation (Courteau *et al.*, 2003) reflects that the angular momentum transferred from the bar to the halo is relatively small and easily absorbed by the halo. Thus, bars of all strengths belong to the same Tully-Fisher relation, as also verified by Sheth *et al.* (2012).

which may result from nonspherical, clumpy gas accretion, coupled with dynamical friction transfer of energy from the gas to the dark matter. Dutton *et al.* (2007) reproduced the Courteau and Rix (1999) result if AC is invoked. Either way, most spiral disks obey the submaximal disk constraints.

4. Fluid-dynamical modeling

Dynamical friction between a stellar bar and a dark-matter halo is believed to slow down the pattern speed of the bar, and therefore fast bars should imply maximal disks (Weinberg, 1985). A compilation of 17 barred galaxies analyzed via the “Tremaine-Weinberg” method was presented by Corsini (2011); the overall impression from these analyses favors maximal disks. Likewise, slow bars might imply maximal halos [e.g., for UGC 628, Chemin and Hernandez (2009)]. However, some of these claims have been challenged on account of numerical artifacts yielding, e.g., overefficient bar slow down (Valenzuela and Klypin, 2003). Indeed, Athanassoula (2003) and Athanassoula, Machado, and Rodionov (2013) argued that the decrease in the pattern speed does not depend only on the mass of the dark-matter halo, but also on other galaxy properties such as gas fraction or halo shape. Thus they argued that, on its own, the pattern speed decrease cannot set constraint to the halo mass.

Based on detailed fluid-dynamical modeling, a maximal disk solution was found by Englmaier and Gerhard (1999) for the Milky Way and by Weiner, Sellwood, and Williams (2001) for the NGC 4123. Both galaxies are barred [see Sellwood and Sánchez (2010) for other examples]. Conversely, the hydrodynamic gas simulations used by Kranz, Slyz, and Rix (2003) to model the spiral arm structure of five grand design nonbarred galaxies yield a wide range of \mathcal{F} , from closely maximal to 0.6. In their work, galaxy disks appear to be maximal if $V_{\max} > 200 \text{ km s}^{-1}$, submaximal otherwise. Although detailed comparisons of observed galaxy velocity fields with hydrodynamic gas simulations are challenging, future galaxy mass reviews ought to include more analyses of this kind.

5. Gravitational lensing

In the rare cases where a distant galaxy or quasar is lensed by a foreground galaxy, gravitational lensing can be used to place constraints on the projected ellipticity and mass within the Einstein radius. For disk-dominated lenses, this extra information coupled with spatially resolved kinematics can be used to break the disk-halo degeneracy (Dutton, Brewer *et al.*, 2011). Until recently, only a handful of spiral galaxy lenses were known, the best studied being B1600 + 434 (Jaunsen and Hjorth, 1997; Koopmans, de Bruyn, and Jackson, 1998; Maller *et al.*, 2000) and the “Einstein Cross” 2237 + 0305 (Huchra *et al.*, 1985; Trott and Webster, 2002; Trott *et al.*, 2010). However, since these lenses are bulge dominated, they are not ideally suited to constrain disk masses.

A number of recent searches for spiral lens galaxies (Féron *et al.*, 2009; Sygnet *et al.*, 2010; Treu *et al.*, 2011) have uncovered several new disk-dominated spiral lenses. A joint strong lensing and dynamics analysis of the disk-dominated gravitational lens SDSSJ2141-0001, discovered as part of the

Sloan Lens Advanced Camera for Surveys (SLACS) (Bolton, Bures *et al.*, 2008), yields a best fit $\mathcal{F} = 0.87^{+0.05}_{-0.09}$ (Barnabè *et al.*, 2012), where \mathcal{F} includes both disk and bulge. Since the bulge contributes $\sim 30\%$ of the stellar mass within 2.2 disk scale lengths, the *disk* is actually consistent (at the 1σ level) with being submaximal.

6. Two-body interactions and the mass of the local group

The relative motions of two orbiting bodies, and assumptions about their angular momentum and total energy, may also be used to infer the total mass of that system.

Looking at our own local group (LG) of galaxies, the Milky Way and M31 galaxies display largely unperturbed disks suggesting that they are likely on their first passage since having formed. Based on that observation, Kahn and Woltjer (1959) were able to compute the relative motion of the Milky Way and M31 as a two-body problem assuming purely radial infall (zero angular momentum). This method, referred to as the “Kahn-Woltjer timing argument” (TA) [see also Binney and Tremaine (2008)], led Kahn and Woltjer to measure a total mass for the LG in excess of the reduced mass of M31 and the Milky Way by a factor greater than 6, thus calling for a sizable amount of hitherto undetected intergalactic matter. Sandage (1986b), using a similar argument for the deceleration of nearby galaxies caused by the LG, found a lower value for the maximum mass for the LG, $M_{\text{LG}} = 5 \times 10^{12} M_{\odot}$, with a best-fit value of $4 \times 10^{11} M_{\odot}$. Courteau and van den Bergh (1999) also used various mass estimators to compute $M_{\text{LG}} = (2.3 \pm 0.6) \times 10^{12} M_{\odot}$ within 1.2 Mpc. More recently, Partridge, Lahav, and Hoffman (2013) revised the TA for the LG by accounting for a dark energy component and finding a total $M_{\text{LG}} = (6.19 \pm 0.56[\text{obs}] \pm 0.99[\text{sys}]) \times 10^{12} M_{\odot}$. The systematic error is obtained by testing the TA model against LG-like objects selected from a cosmological simulation. The effect of dark energy is to make the value of M_{LG} roughly 12% larger than similar TA mass estimates that neglect it.

A major limitation of the TA is its reliance on single-galaxy interactions with the Milky Way and assumptions about virialization of the LG (Phelps, Nusser, and Desjacques, 2013). The latter implemented a numerical action method, originally developed by Peebles (1989), which takes into account the peculiar motions of a large subset of LG galaxies while eliminating the mass degeneracy in the two-body TA. Their method yields estimates of $(2.5\text{--}5.0) \times 10^{12} M_{\odot}$ for the Milky Way and $(1.0\text{--}5.0) \times 10^{12} M_{\odot}$ for M31. If the putative transverse velocity of M31 (van der Marel *et al.*, 2012) is taken into account, the lower bound for the mass of the Milky Way drops from $2.5 \times 10^{12} M_{\odot}$ to $1.5 \times 10^{12} M_{\odot}$ in the 95% confidence region. The transverse velocity of M31 remains somewhat tentative owing to the uncertainty in our own orbit around the Milky Way center.

While the above values seem high, the action method effectively measures a maximal possible mass for each bound system. Smaller mass estimates will thus be obtained on smaller scales. For instance, independent estimates for the dynamical mass of the Milky Way within 100 kpc range of $M_{\text{MW}} = (0.4\text{--}1.4) \times 10^{12} M_{\odot}$ (see Sec. IV); likewise for M31 with $M_{\text{M31}} = (0.8\text{--}1.1) \pm 10^{12} M_{\odot}$ within the virial radius $R_{200} = 189\text{--}213$ kpc, depending on the modeled dark-matter distribution (Tamm *et al.*, 2012).

Since this review is mostly concerned with mass estimators for individual galaxies, we do not investigate the mass of the LG further. The TA should, however, be noted as a method to estimate the mass of the local group and/or that of the Milky Way or *M31* if one of the other masses is known independently. For more details on modern applications of the TA, see [Phelps, Nusser, and Desjacques \(2013\)](#) and references therein. We review independent mass estimates of the Milky Way in Sec. IV.

E. Future prospects

Mass modeling methods will require new constraints to break the disk-halo degeneracies as well as those internal to the halo model. Those may come from other mass estimators (not considered here due to space limits) based on, e.g., external tracers such as planetary nebulae, globular clusters, and satellites ([Yegorova, Pizzella, and Salucci, 2011](#)). Nonetheless, various independent methods outlined in Sec. III present evidence for the prevalence of submaximal disks in most spiral galaxies with

$$V_{\text{disk}}/V_{2.2} \approx 0.6 \pm 0.1. \quad (15)$$

However, galaxies do come with a range in disk-to-halo masses, with the most massive ($V_{\text{max}} > 200 \text{ km s}^{-1}$), high-surface-brightness spirals being close to having maximal disks. Almost all other galaxies, 90% of them being of dwarf type, are likely submaximal.

The dark matter near the virial radius likely has circular velocity at slightly lower speeds than the inner baryons. By comparing with the rotation velocities within the optical disk V_{opt} , one finds from satellite kinematics and weak lensing that on average for late-type galaxies $V_{\text{opt}}/V_{200} \approx 1.2$ ([Dutton *et al.*, 2010](#); [Reyes *et al.*, 2011](#)).

Looking ahead, very large kinematical surveys of spiral galaxies will enable a global characterization of rotation curve shapes for thousands of galaxies; e.g., MaNGA (“Mapping Nearby Galaxies at APO”; PI: Kevin Bundy) is a project to collect integral field unit (IFU) velocity maps at Apache Point Observatory from 2014 to 2020 for $\sim 10\,000$ northern galaxies with stellar masses above $10^9 M_{\odot}$ over a full range of gas contents, environments, and orientations. It will cover the range 360–1000 nm at a resolution of about 2500, with an emphasis on spectrophotometric calibration at all wavelengths. On shorter time scales, the Calar Alto Legacy Integral Field Area Survey (CALIFA) will already provide 2D PPAK IFU maps for ~ 600 nearby galaxies ([Sánchez *et al.*, 2012](#)). However, a shortcoming of the large IFU surveys in progress and planned is their low spectral resolution. This will not enable measurements of disk velocity dispersions except in the inner regions where disentangling effects of the bulge kinematics will make interpretation difficult without more sophisticated analysis methods. One such method is the “Jeans Anisotropic Multi-Gaussian Expansion” described in detail in Sec. V.C.3, although it will need to be augmented to consider the effects of dust extinction. CALIFA, and particularly MaNGA, will still truly refine our definition of velocity fields and the stellar populations in galaxies. Large samples of interferometric data will also be needed to extract velocity fields homogeneously for

comparisons with optical velocity fields. This will be addressed by upcoming HI surveys with square kilometer array pathfinders, notably WALLABY on the Australian Square Kilometer Array Pathfinder and its northern counterpart on WSRT. These projects may span ~ 5 years or more.

Despite the extensive new galaxy dynamics databases, the rigorous separation of baryonic and dark-matter profiles in galaxies will require accurate stellar M/L_* ’s from stellar population models and/or dynamical measurements [e.g., Eq. (14)] as well as precise constraints from Λ CDM structure formation models to resolve the many degeneracies between the luminous and dark-matter components.

IV. DARK MATTER AND MASS MODELS OF THE MILKY WAY

A. Introduction

As seen in Sec. III, galactic rotation curves are one piece of the multifaceted dark-matter puzzle. By the 1970s when the signatures for dark matter from flat rotation curves were first inferred, cosmologists began to understand that relics from the early Universe, in the form of subatomic particles, could contribute significantly to the present-day mass density of the Universe. Today, the leading dark-matter candidate is a stable, electrically neutral, supersymmetric particle with a mass between 1 GeV and 1 TeV. This weakly interacting massive particle (WIMP) would have been nonrelativistic during the formation of large-scale structure and hence represents an example of cold dark matter (CDM) [see, e.g., [Bertone, Hooper, and Silk \(2005\)](#)]. WIMPs naturally form halos with roughly the right structure to explain flat rotation curves ([Blumenthal *et al.*, 1984](#); [Dubinski and Carlberg, 1991](#); [Navarro, Frenk, and White, 1996](#)). Moreover, the halo mass function that is predicted by the standard CDM theory of structure formation is consistent with the observed hierarchy of virialized systems from dwarf galaxies to clusters ([Press and Schechter, 1974](#); [Bardeen *et al.*, 1986](#); [Tinker *et al.*, 2008](#)).

In the mid-1980s, several researchers pointed out that WIMPs might be detected in the laboratory ([Drukier and Stodolsky, 1984](#); [Goodman and Witten, 1985](#)). At present over a dozen groups have deployed or are building terrestrial dark-matter detectors ([Bertone, Hooper, and Silk, 2005](#); [Feng, 2010](#)). These experiments have the potential to probe the local density and velocity dispersion of dark matter at the position of the Earth. By the same token, the interpretation of these experiments and, in particular, the constraints inferred on the mass and scattering cross section of dark-matter candidates depend on astrophysical estimates of the local dark-matter distribution function. Thus, there is a direct link between mass models of the Milky Way and dark-matter detection in the laboratory.

Apart from the dark-matter question, the Milky Way presents an opportunity to observe a “typical” barred spiral galaxy (Hubble classification SBc) from a unique vantage point. Thus, observations of the Milky Way hold a special place in our attempt to understand the formation and structure of spiral galaxies. The remainder of this section focuses on what we know about the distribution of baryons and dark matter in the Galaxy.

Studies of the Milky Way are invariably challenged by our position within it and by our frame of reference, which orbits about the Galactic center. In particular, our distance to the Galactic center and the circular speed at the position of the Sun remain uncertain at the 5% level (Ghez *et al.*, 2008; Bovy, Hogg, and Rix, 2009; Gillessen *et al.*, 2009; Reid *et al.*, 2009; Brunthaler *et al.*, 2011; Schönrich, 2012). These uncertainties enter our interpretation of various observations and our determination of the mass of the Galaxy. On the other hand, the Milky Way offers a unique opportunity to probe the distribution of both visible and dark matter relatively close to the Galactic center. By contrast, for external disk galaxies, rotation curves provide evidence for dark matter only in the outermost regions where dark matter dominates. Estimates of the density of dark matter in the inner regions of large spiral galaxies require accurate assumptions about the shape of the dark halo density profile.

The Milky Way is also unique in that there exist extensive catalogs of halo stars, globular clusters, and satellite galaxies with reliable galactocentric distances and velocities. These tracers provide important constraints on the galactic potential. Moreover, numerous stellar streams, such as the Sagittarius and Monoceros streams, may provide another handle on the galactic potential.

B. Multicomponent models for the Milky Way

The literature is replete with models of the Milky Way. An important early example can be found in Bahcall, Schmidt, and Soneira (1982), hereafter BSS. Their model comprised a double-exponential disk, a (deprojected) de Vaucouleurs stellar halo, a cuspy bulge, and a dark-matter halo. The parameters that described the disk and stellar halo were taken from the earlier work by Bahcall and Soneira (1980), which, in turn, were based on star counts. The BSS model for the dark halo assumed a constant density core and a $r^{-2.7}$ power-law falloff at large radii. Notably, BSS showed that the different components of the Galaxy could “conspire” to produce a flat rotation curve for a wide range of model parameters, particularly the disk mass-to-light ratio and the structural parameters of the halo [see also Bahcall and Casertano (1985) and van Albada *et al.* (1985)]. Blumenthal *et al.* (1984) argued that adiabatic contraction, the response of dark matter to the baryonic component as it condenses and forms the disk and bulge, could “explain” the apparent conspiracy that leads to flat rotation curves. Nevertheless, the disk-halo *conspiracy* in the context of a Λ CDM universe remains an outstanding problem in galactic astronomy while the disk-halo *degeneracy* continues to plague attempts to pin down the structural parameters of dark-matter halos (Dutton *et al.*, 2005).

Sellwood (1985) took the BSS model a step further by realizing it as an N -body distribution and numerically evolving it forward in time. He found that the BSS model was stable against bar formation although it did develop a two-armed spiral. Recall that a self-gravitating disk is generally unstable to the formation of a bar while a disk of particles on circular orbits in a background potential is stable. Disk galaxies lie somewhere between these extremes with the gravitational force felt by the disk particles coming from

both the disk itself and the other components. In the BSS model, the bulge plays the key role in stabilizing the disk.⁷

Another influential model, especially for its focus on the galactic bulge, was devised by Kent (1992). Kent, Dame, and Fazio (1991) constructed a luminosity model for the bulge based on the 2.4 μ m map of the galactic plane from the Spacelab Infrared Telescope. Kent (1992) combined this model with velocity dispersion data to determine the mass-to-light ratio for the galactic bulge. He then constructed disk-bulge-halo mass models designed to fit the rotation curve. The results hinted at the existence of a supermassive black hole in the Galactic center. [For an earlier discussion of the existence of a central supermassive black hole, see Lacy, Townes, and Hollenbach (1982).] Moreover, Kent’s model requires that one allow for noncircular motions in the gas, as in Gerhard and Vietri (1986). The Milky Way is now known to be a barred spiral galaxy (Blitz and Spergel, 1991; Binney, Gerhard, and Spergel, 1997) and mass models that incorporate a bar include Fux (1997, 1999) and Englmaier and Gerhard (2006).

Dehnen and Binney (1998) constructed a suite of disk-bulge-halo galactic mass models. The observational constraints for their work included the circular speed curve, the velocity dispersion toward the bulge, the Oort constants, the local velocity dispersion tensor, and the force and surface density in the solar neighborhood. Dehnen and Binney (1998) surveyed the ten-dimensional parameter space of models using a restricted maximum likelihood analysis in that they considered 25 examples wherein some parameters were held fixed while the remaining parameters are allowed to vary so as to minimize the likelihood function.

Widrow, Pym, and Dubinski (2008) (WPD) constructed dynamical models for the Galaxy using observational constraints similar to those considered by Dehnen and Binney (1998). WPD deployed Bayesian inference and a Markov chain Monte Carlo algorithm to construct the full probability distribution function (PDF) over the model parameter space. The PDF is found to include regions of parameter space in which the model is highly unstable to the formation of a strong bar, so much that the models are almost certainly unphysical. In other regions of parameter space, the models are found to be mildly unstable to the formation of a weak bar and therefore may well represent an axisymmetric, idealized approximation to the Milky Way. Binney (2010a), Binney and McMillan (2011), and McMillan and Binney (2012) have continued to develop observationally motivated models for the Milky Way along similar lines.

As mentioned previously, both Dehnen and Binney (1998) and WPD use the galactic circular speed curve as a model constraint. As with external galaxies, observations of neutral

⁷Ostriker and Peebles (1973) suggested that a dark-matter halo also could stabilize the disk against bar formation, but more modern simulations, including a live halo whose resonances are adequately described, have shown that the halo has a more complex role. During the bar formation phase, a more massive halo slows down the bar formation, but in the later, secular evolution phases, the halo actually helps the bar grow stronger by absorbing a considerable part of the angular momentum emitted by the bar region (Athanasoula, 2002, 2003). See also Sec. III.D.4.

hydrogen provide a measure of the galactic rotation curve, which translates to a circular speed curve provided the gas follows circular orbits. Inside the solar circle, HI observations are usually presented in terms of the so-called terminal velocity v_{term} , which is defined as the peak velocity along a line of sight at galactic coordinates $b = 0$ and $|l| < \pi/2$. If one assumes axisymmetry, then the HI emission corresponding to the peak velocity originates from the galactocentric radius $R = R_0 \sin l$, where R_0 is our distance from the Galactic center. Thus $v_c(R) = v_{\text{term}} + v_c(R_0) \sin l$, where v_c is the circular speed center. Malhotra (1995), for example, determined the terminal velocity to the HI measurements of Weaver and Williams (1973), Bania and Lockman (1984), and Kerr *et al.* (1986) and her measurements were used in both the Dehnen and Binney (1998) and WPD analyses.

The radial velocity of an object at galactic coordinates (l, b) relative to the local standard of rest v_{LSR} is related to the circular velocity via

$$v_{\text{LSR}} = \left\{ \frac{R_0}{R} v_c(R) - v_c(R_0) \right\} \cos b \sin l. \quad (16)$$

Brand and Blitz (1993) considered a sample of HII regions and reflection nebulae with distances and radial velocities that are available and use this method to infer the rotation of the Galaxy out to 17 kpc. Unlike the terminal velocity measurement, R must here be inferred from observations of the heliocentric distance D through the relation $R = (D^2 \cos^2 b + R_0^2 - 2R_0 D \cos b \sin l)^{1/2}$. Dehnen and Binney (1998) and Widrow and Dubinski (2005) presented a statistical method for accomplishing this and incorporated the Brand and Blitz (1993) data into their galactic model constraints. Note that both terminal velocity and outer rotation curve methods require R_0 and $v_c(R_0)$, both of which are uncertain at the 5% level. A proper statistical analysis using these methods therefore requires a marginalization over R_0 and $v_c(R_0)$, subject to prior probabilities for these parameters.

Xue *et al.* (2008) derived a galactic rotation curve out to radius of 60 kpc. Their rotation curve is based on observations of blue horizontal branch (BHB) stars from the Sloan Digital Sky Survey (SDSS) which provided line-of-sight velocity distributions at different galactocentric radii. To construct the rotation curve, they compared these observations with mock observations of simulated Milky Way-like galaxies. Further investigations of halo stars are discussed below.

Figure 14 shows the inner rotation curve as inferred from HI observations by Malhotra (1995), the outer rotation curve inferred from observations of HII regions by Brand and Blitz (1993), and the Xue *et al.* (2008) rotation curve. The upper panel also shows the circular speed curve for one of two mass models from Xue *et al.* (2008). This model assumes a Hernquist bulge, a *sphericalized* exponential disk, and an NFW halo. The lower panel shows one of the more stable examples from the WPD Bayesian analysis. Note that the Xue *et al.* (2008) model was not constrained by Malhotra (1995) or the data of Brand and Blitz (1993) while the WPD model was constructed independent of the Xue *et al.* (2008) results.

Along rather different lines, Klypin, Zhao, and Somerville (2002) constructed mass models for both the Milky Way and M31 that were motivated by disk formation theory in the

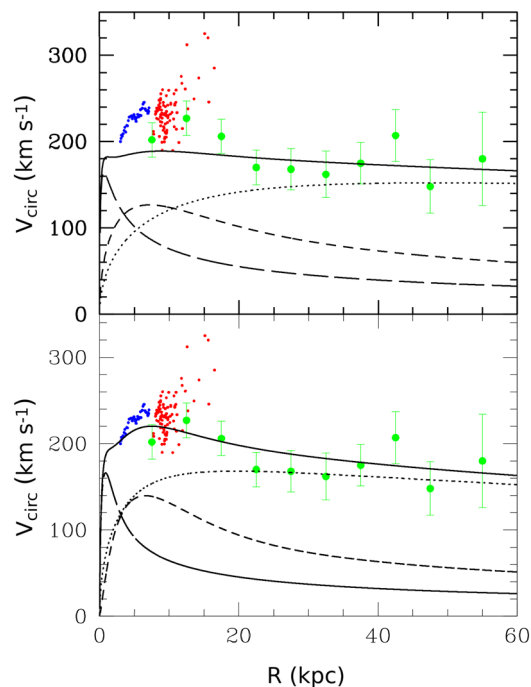


FIG. 14 (color online). Rotation curve, as determined from the analysis of BHB stars by Xue *et al.* (2008), the terminal velocity method by Malhotra (1995), and the analysis of HII regions-reflection nebulae by Brand and Blitz (1993). The upper panel shows the model predictions from Xue *et al.* (2011) for the total rotation curve (solid) and the contributions from the disk (dashed), bulge (long dashed), and halo (dotted). The lower panel shows the WPD model.

standard Λ CDM cosmology. To be precise, they assumed that the protogalaxy has a NFW halo with a concentration parameter in agreement with pure dark-matter simulations. The present-day halo is derived by adiabatically contracting the early-time halo.

In Table I, we present various structural parameters for the models described in Secs. IV.B and IV.C. We include, in addition to the disk, bulge, and halo masses, the local dark-matter density, the key quantity for terrestrial detection experiments. Note that the assumed canonical value for these experiments is $0.0079 M_{\odot} \text{ pc}^{-3} = 0.3 \text{ GeV cm}^{-3}$ (Lewin and Smith, 1996; Bertone, Hooper, and Silk, 2005). The local density of dark matter is of particular interest for direct detection experiments. A more complete discussion of this parameter can be found in Catena and Ullio (2010, 2012) and WPD.

As in Sec. III.D.1, a working definition for the maximal disk hypothesis is that

$$V_{\text{disk}}^2(R_{\text{max}})/V_{\text{tot}}^2(R_{\text{max}}) \geq 0.72.$$

With the exception of a few of the Dehnen and Binney (1998) models and possibly the heavy disk model of Kent (1992), all models shown in Table I find a submaximal disk for the Milky Way. Roughly speaking, systems with smaller values of $V_{\text{disk}}^2/V_{\text{tot}}^2$ will be more stable against bar formation, although this ratio alone is an inadequate predictor of whether a bar will form [see, e.g., Debattista and Sellwood (2000) and WPD].

TABLE I. Selected mass models of the Milky Way as presented in the text. The disk mass M_d , bulge mass M_b , and total mass within 100 kpc M_{100} are given in units of $10^{10} M_\odot$. The disk scale length h is given in units of kpc. Note that [Smith *et al.* \(2007\)](#) assumed a Miyamoto-Nagai model ([Miyamoto and Nagai, 1975](#)) for the disk where the peak in the contribution of the disk to the circular speed curve occurs at $R_{\max} \approx 1.4h$. [Xue *et al.* \(2008\)](#) assumed a “spherical” disk potential where $R_{\max} \approx 1.9h$. All other models assume an exponential disk where $R_{\max} \approx 2.2h$. Column 6 gives the ratio $V_{\text{disk}}^2/V_{\text{tot}}^2$ evaluated at R_{\max} , where V_{tot} and V_{disk} are the total observed velocity and contribution from the baryonic disk, respectively. The final column gives the density of dark matter in the solar neighborhood in units of $M_\odot \text{pc}^{-3}$.

Model	M_d	h	M_b	M_{100}	$V_{\text{disk}}^2/V_{\text{tot}}^2$	$\rho_{DM,\odot}$
BSS	5.6	3.5	1.1	144	0.53	0.009
Kent (1992) —low M_d	3.7	2.8	1.2	125	0.4	0.013
Kent (1992) —high M_d	5.5	2.8	1.2	116	0.67	0.0097
Dehnen and Binney (1998)	0.36–1.5	2–3.4	3.3–5.1	40–75	0.33–0.83	0.009–0.012
Klypin, Zhao, and Somerville (2002)	4.0	3.5	0.8	55	0.37	0.007
Widrow, Pym, and Dubinski (2008) : WPD	4.1	2.8	0.96	40_{-19}^{+22}	0.5	0.008 ± 0.0014
Smith <i>et al.</i> (2007)	5.0	4.0	1.5	55	0.4	0.011
Xue <i>et al.</i> (2008)	5.0	4.0	1.5	49	0.33	0.006
Gnedin <i>et al.</i> (2010)	5.0	3.0	0.5	89	0.33	0.014
McMillan and Binney (2012)	5.7	2.9	0.9	83	0.63	0.0104
Moni Bidin <i>et al.</i> (2012)						0 ± 0.001
Bovy and Tremaine (2012)						0.008 ± 0.003

C. Further observational constraints on the Milky Way potential

1. Circular speed at the Sun’s position in the Galaxy

As mentioned, our position within the Milky Way offers unique observational opportunities. Recently, [Reid *et al.* \(2009\)](#) [see also [Brunthaler *et al.* \(2011\)](#)] reported very long baseline interferometry (VLBI) measurements of trigonometric parallaxes and proper motions for 18 masers located in several of the Galaxy’s spiral arms. These measurements yielded several structural parameters of the Galaxy, most notably, the circular rotation speed at the position of the Sun. Their value $V_c = 254 \pm 16 \text{ km s}^{-1}$ is 15% higher than the standard International Astronomical Union (IAU) 220 km s^{-1} . [[Brunthaler *et al.* \(2011\)](#) analyzed the same VLBI data but with updated values for the solar motion and found $V_t = 239 \pm 7 \text{ km s}^{-1}$.] By contrast, [Koposov, Rix, and Hogg \(2010\)](#) found $V_c = 221 \pm 18 \text{ km s}^{-1}$ by fitting an orbit to the GD-1 stellar stream. Naively, a 15% change in circular speed implies a 33% change in mass, although the implications for the bulge, disk, and halo masses require an analysis that incorporates other constraints such as the ones carried out by [Dehnen and Binney \(1998\)](#) or WPD. Moreover, [Bovy, Hogg, and Rix \(2009\)](#) reanalyzed the maser data and found a somewhat lower value with $V_c = 236 \pm 11$. Their Bayesian analysis differed from that of [Reid *et al.* \(2009\)](#) by assuming a more general orbital distribution for the masers.

Recently, [Schönrich \(2012\)](#) described various ways to determine V_c based on stellar kinematics. The idea is to model the streaming motion of stars using the full phase space information available from the SDSS-SEGUE (Sloan Extension for Galactic Understanding and Exploration) survey. The results are consistent with those described previously and again suggest that V_c is $\sim 10\%$ higher than the standard IAU value.

2. Local escape speed

[Smith *et al.* \(2007\)](#) used a sample of high-velocity stars from the Radial Velocity Experiment (RAVE) ([Steinmetz *et al.*, 2006](#)) to infer that the local escape speed of the Galaxy is $544_{-46}^{+64} \text{ km s}^{-1}$ (90% confidence interval). The fact that the escape speed is significantly higher than $\sqrt{2}V_c$

provides compelling evidence that the Galaxy is embedded in a dark-matter halo that extends well beyond the solar circle. [Smith *et al.* \(2007\)](#) go on to combine their estimate for the escape speed with other kinematic constraints to derive (model-dependent) estimates for the virial radius, virial mass, and concentration of the galactic dark halo. In particular, they considered a model for the Galaxy comprising a [Miyamoto and Nagai \(1975\)](#) disk, a [Hernquist \(1990\)](#) bulge, and an NFW halo. The halo potential can be written as

$$\Phi_{\text{NFW}}(r) = \frac{GM_{\text{vir}}}{\ln(1+c) - c/(1+c)} \frac{1}{r} \ln\left(1 + \frac{r}{r_s}\right), \quad (17)$$

where r_s is the scale radius [see Eq. (11)], $M_{\text{vir}} \equiv M(r = r_{\text{vir}})$ is the virial mass, and $c = r_{\text{vir}}/r_s$ is the concentration parameter. The virial radius r_{vir} is defined such that the mean density within r_{vir} is $\delta_{\text{th}}\rho_{\text{cr}}$, where ρ_{cr} is the background density ([Navarro, Frenk, and White, 1996](#)). The NFW potential has two free parameters. Thus, by combining the escape speed constraint

$$\Phi_{\text{total}} = -\frac{v_{\text{esc}}^2}{2} \quad (18)$$

with the constraint on the local circular speed, one can infer the parameters of the dark halo. [Smith *et al.* \(2007\)](#) assumed $M_d = 5 \times 10^{10} M_\odot$, $M_b = 1.5 \times 10^{10} M_\odot$, $\delta_{\text{th}} = 340$, and $V_c = 220 \text{ km s}^{-1}$ to obtain $M_{\text{vir}} = 0.85_{-0.29}^{+0.55} \times 10^{12} M_\odot$.

3. Kinematic tracers

Yet another route to constraining the mass distribution of the Galaxy, especially beyond the solar circle, is provided by kinematic tracers such as halo stars, globular clusters, and satellite galaxies. Line-of-sight velocities are naturally more easily measured than proper motions. For tracers in the outer parts of the Galaxy, these line-of-sight velocities are primarily radial (with respect to the Galactic center) whereas line-of-sight velocities of tracers in other galaxies will be a mixture of radial and tangential velocities. Thus, the analysis of galactic tracers takes a different form to that for external galaxies.

Early work on dynamical tracers used simple mass estimators such as the following example due to [Lynden-Bell, Cannon, and Godwin \(1983\)](#):

$$M_{\text{est}} = \left(\frac{2}{\langle e^2 \rangle_s} \right) \left(\frac{1}{GN} \sum_{i=1}^N v_{ri}^2 r_i \right), \quad (19)$$

where the sum is over the N objects (satellites, globular clusters, etc.) of the sample. The quantity $\langle e^2 \rangle_s$ is the mean orbital eccentricity ($\langle e^2 \rangle_s = 1/2$ for an isotropic distribution) and encapsulates our ignorance of the orbit distribution. Equation (19) is suitable for a system of objects orbiting a point mass M . Recently, [Watkins, Evans, and An \(2010\)](#) carried out a detailed systematic study of mass estimators for both the Milky Way and Andromeda galaxies based on satellite kinematics. Their results illustrated just how sensitive mass estimates are to assumptions about the velocity structure of the satellite population. In particular, the mass estimates at 100 kpc range from $1.8 \times 10^{11} M_\odot$ to $2.3 \times 10^{12} M_\odot$ depending on the degree of radial velocity anisotropy. A detailed discussion of mass estimators as they might be applied to Gaia data can be found in [An, Evans, and Deason \(2012\)](#).

With enough kinematic tracers, one can determine a velocity dispersion profile. [Battaglia *et al.* \(2005\)](#), for example, derived a radial velocity dispersion profile for the Galaxy from a sample of 240 halo objects (mainly globular clusters and halo stars). The dispersion is roughly constant at 120 km s^{-1} within 30 kpc and then decreases to about 50 km s^{-1} at a galactocentric distance of 120 kpc. These results are consistent with those from a sample of 2400 BHB stars by [Xue *et al.* \(2008\)](#), although that sample extended only to a galactocentric radius of 60 kpc. As discussed above, [Xue *et al.* \(2008\)](#) used the kinematics of BHB stars to derive a rotation curve by comparing their data with mock observations of simulated galaxies. Alternatively, one can model the dispersion profile directly.

The decline in the dispersion profile beyond 30 kpc places constraints on the density profile of the dark halo. In particular, for an isothermal halo, where the density is $\propto r^{-2}$ is inconsistent with the data since the dispersion profile in this case is constant with the radius. [Battaglia *et al.* \(2005\)](#) compared their dispersion profile with model profiles derived from the Jeans equation and found that the data are consistent with an NFW halo that has a relatively high concentration ($c = 18$) and $M_{\text{vir}} \approx 0.8 \times 10^{12} M_\odot$.

[Gnedin *et al.* \(2010\)](#) also used halo stars to infer a rotation curve for the Milky Way. Their analysis was based on the spherical Jeans equation with the assumption that both the density and velocity dispersion profiles for the halo stars are described by power-law functions of radius. They found that the velocity dispersion declines very gradually out to 80 kpc and thus they inferred a shallow slope for the dispersion profile. For this reason, they inferred a larger mass for the virial radius and mass of the galactic halo than [Battaglia *et al.* \(2005\)](#). Best-fit values for their three-component galactic model [motivated, to a large extent, by the [Klypin, Zhao, and Somerville \(2002\)](#) cosmological model] are given in Table I.

In principle, one can model the phase space distribution function (DF) for a set of tracers thereby taking full advantage of the data. This idea was discussed by [Little and Tremaine \(1987\)](#), who also introduced the use of Bayesian statistics to the problem. One begins by calculating the likelihood

function (the probability of the data (e.g., radial velocities and distances for a population of kinematic tracers) given a model for the tracer DF and gravitational potential. Bayes's theorem then allows one to calculate the corresponding probability of the model given the data. In general, since then if one is interested in the potential, one marginalizes over those model parameters that describe the DF. More sophisticated models for the Milky Way potential were considered by [Kochanek \(1996\)](#) and [Wilkinson and Evans \(1999\)](#) who modeled the kinematics of the satellite galaxy population. Similarly, [Deason *et al.* \(2012\)](#) modeled the distribution function of BHB stars to obtain constraints on the galactic potential from 15 to 40 kpc.

4. Vertical force and surface density in the solar neighborhood

The vertical structure of the galactic potential provides a potentially powerful probe of the amount of dark matter in the solar neighborhood. The vertical force is approximately proportional to the surface density, which, in turn, can be compared to the total surface density from stars in the interstellar medium. The classical means of determining the local vertical force requires a sample of stars with known vertical distances and velocities. The first detailed analysis of this type was carried out by [Oort \(1932\)](#) who built upon earlier and important work by [Jeans \(1922\)](#) and [Kapteyn \(1922\)](#). Attempts to understand the local vertical structure of the Galaxy from stellar kinematics have come to be known as the Oort problem.

Of course, in order to infer the local density of dark matter from the vertical structure of the Galaxy near the Sun, one requires a detailed model of the local distribution of visible matter. A detailed model of the visible components in the solar neighborhood can be found in [Flynn *et al.* \(2006\)](#). Note that the total estimated density in visible matter (their Table II) is $0.091 M_\odot \text{ pc}^{-3}$, which is a factor of 6–10 times greater than the predicted local dark-matter density. [Flynn *et al.* \(2006\)](#) also found the local mass-to-light ratios in the B , V , and I bands to be $(M^*/L)_B = 1.4 \pm 0.2$, $(M^*/L)_V = 1.5 \pm 0.2$, and $(M^*/L)_I = 1.2 \pm 0.2$, in good agreement with population synthesis predictions that use typical solar neighborhood IMFs.

In general, the kinematics of the stars in the disk of the galaxy can be described by a phase space DF $f(\mathbf{r}, \mathbf{v}, t)$, which obeys the collisionless Boltzmann equation

$$\frac{\partial f}{\partial t} + \mathbf{v} \cdot \frac{\partial f}{\partial \mathbf{r}} - \frac{\partial f}{\partial \mathbf{v}} \frac{\partial \Phi}{\partial \mathbf{r}} = 0. \quad (20)$$

Typically, one assumes that the stars in the sample are in dynamical equilibrium ($\partial f / \partial t = 0$) and that vertical motions decouple from motions in the disk plane. With these assumptions, $f(\mathbf{r}, \mathbf{v}, t) \propto F(z, v_z)$ and

$$v_z \frac{\partial F}{\partial z} - \frac{\partial F}{\partial v_z} \frac{\partial \Phi}{\partial z} = 0. \quad (21)$$

Finally, Jeans theorem implies $F(z, v_z) = F(E_z)$, where $E_z = v_z^2/2 + \Phi(R_0, z) - \Phi(R_0, 0)$.

Formally, each star in the sample may be viewed as a δ function in z and v_z and therefore the data provide an estimate of F , which, in principle, can be used to infer Φ . In general, restrictive assumptions are required to extract Φ .

For example, the distribution may be assumed to be isothermal so that $F \propto \exp(-E_z/\sigma_z^2)$, where σ_z is the vertical velocity dispersion. One then finds $\Phi(z) = \ln[\nu(z)/\nu(0)]$, where $\nu(z) = \int F dv_z$ is the density run for the tracers. Variations of this method have been used by Oort (1932), Bahcall (1984), and Holmberg and Flynn (2000).

Kuijken and Gilmore (1989) proposed an alternative method which does not rely on the assumption of isothermality. The DF is related to the density and potential through an Abel transform:

$$F(E_z) = \frac{1}{2^{1/2}\pi} \int_{E_z}^{\infty} \frac{d\nu}{d\Phi} \frac{d\Phi}{(\Phi - E_z)^{1/2}}. \quad (22)$$

In order to use this equation, Kuijken and Gilmore made an ansatz for the form of Φ . For each choice of potential, they calculated F and then compared the velocity distribution of the model to that of the data. The best fit over the space of potentials leads to an estimate for Φ . In principle, the local density may be determined from Φ through the Poisson equation. The difficulty is that one requires second derivatives of the potential. An alternative is to determine the local surface density, which is approximately proportional to the force. The dark-matter distribution can then be assumed to be approximately constant close to the galactic plane [i.e., dark matter is distributed in a halo and not a disk, but see Read *et al.* (2008) for an alternative viewpoint].

Recently, Moni Bidin *et al.* (2012) argued that there is little or no dark matter in the solar neighborhood. Their analysis is based on an analysis of some 400 red giant branch stars found in the two micron all sky survey (Skrutskie *et al.*, 2006). The stars in their sample lie in the direction of the south galactic pole between 1.5 and 4.0 kpc from the galactic midplane and are presumably mainly from the thick disk. Their analysis is based on the Poisson and Jeans equations under the assumptions that the stars in the solar neighborhood are in equilibrium and that the Galaxy has azimuthal symmetry. With these assumptions, the integrated surface density within a distance z of the galactic midplane is

$$\Sigma(z) = -\frac{1}{4\pi G} \int_{-z}^z \frac{1}{R} \frac{\partial}{\partial R} (RF_R) dz - 2[F_z(z) - F_z(0)], \quad (23)$$

where F_R and F_z are the radial and vertical components of the force, respectively. They then used the Jeans equation to write these components in terms of radial and vertical derivatives of the components of the velocity dispersion tensor and the density. While z derivatives are estimated from the data, the data are too sparse to provide information about the radial derivatives. Rather, they assumed that all second moments of the velocity dispersion tensor scale as $\exp(-R/h)$, where h is the radial disk scale length for the surface density. Furthermore, they assumed that the rotation curve is locally flat for all z .

With these assumptions, Moni Bidin *et al.* (2012) found that $\Sigma(z = 1.5 \text{ kpc}) \approx 55 M_{\odot} \text{ pc}^{-2}$ and is very nearly flat between 1.5 and 4.0 kpc. In fact, their $\Sigma(z)$ curve is well fitted by the curve for visible mass. By contrast, the standard disk-halo model for the solar neighborhood has $\Sigma(z = 1.5 \text{ kpc}) \approx 75 M_{\odot} \text{ pc}^{-2}$ and rises to $\sim 100 M_{\odot} \text{ pc}^{-2}$ by $z = 4 \text{ kpc}$. Moni Bidin *et al.* (2012) therefore concluded that there is little room for dark matter in the solar neighborhood.

These results have been called into question by Bovy and Tremaine (2012) who pointed out that while the circular speed ($= \sqrt{-RF_R}$) may indeed be locally flat near the midplane, the mean velocity exhibits a significant lag with respect to the local standard of rest due to asymmetric drift. When this effect is taken into account, the data imply a local dark-matter density of $(0.008 \pm 0.002) M_{\odot} \text{ pc}^{-3}$, a result that is consistent with the values shown in Table I. Garbari *et al.* (2012) analyzed kinematic data for 2000 K dwarfs using a method that is also based on the Poisson-Jeans equations and found a relatively high value for the local dark-matter density ($\rho_{DM,\odot} = 0.022_{-0.013}^{+0.015} M_{\odot} \text{ pc}^{-3}$).

Virtually all approaches to the Oort problem rely on the assumption that the stars in the solar neighborhood are in dynamical equilibrium. Widrow *et al.* (2012) found evidence that the disk near the Sun has been perturbed. The results are based on their analysis of solar neighborhood stars from SDSS (Data Release 8; Aihara, Allende Prieto, and An, 2011) and the SEGUE spectroscopic survey (Yanny *et al.*, 2009). The evidence comes in the form of an asymmetry between the number density north and south of the galactic midplane. The asymmetry function (difference between the number density to the north minus the number density to the south divided by the average) has the appearance of a wavelike perturbation. In addition, there appears to be a gradual trend in the bulk velocity across the galactic midplane. This result has also been observed in the RAVE survey (Williams *et al.*, 2013). The perturbations are fairly small (10% or less in the density) and therefore the uncertainty in the surface density due to this effect is likely less than current observational uncertainties. Nevertheless, as the observational situation improves, it may become important to account for departures from equilibrium. In any case, the Widrow *et al.* (2012) result may well represent a new window into the interaction between the disk and halo. In particular, such perturbations may have arisen from a passing satellite or dark-matter subhalo (Widrow *et al.*, 2012; Gómez *et al.*, 2013).

A second issue concerns the assumption that E_z is an integral of motion, at least to a good approximation. Statler (1989) stressed that, for $|z| > 1 \text{ kpc}$, the approximation breaks down and proposed the use of Stäckel potentials, which admit three exact integrals of motion. Unfortunately, the Stäckel potentials are a fairly restricted set and, to date, no realistic disk-bulge-halo model has yet used them.

D. Future prospects

The future for mass modeling of the Milky Way is undoubtedly promising with the anticipated explosion of data from observational programs such as Gaia (Perryman *et al.*, 2001; Wilkinson *et al.*, 2005) and the large synoptic survey telescope (LSST) (Ivezic, Tyson, and Acosta, 2008). Gaia yields distances and proper motions for about 1×10^9 Milky Way stars to its faint limit of $V \sim 20 \text{ mag}$ and also provides radial velocities for about 150×10^6 stars as faint as $V \sim 16 \text{ mag}$. LSST has expected uncertainties in parallax and proper motions that are well matched to those expected for the faintest Gaia stars and provides meaningful measurements down to $r \sim 24 \text{ mag}$. We can therefore expect direct parallax

distances with accuracies better than 10% for turnoff stars to ~ 1 kpc and for bright RGB stars to ~ 10 kpc. Parallax distance accuracies of 10 km s^{-1} are achieved for transverse velocities out to 10 kpc; similar accuracies for larger distances require other (photometric) distance estimates to be folded in. Astronomers then have an unprecedented description of the phase space distribution function for the stellar component of the Galaxy. Major achievable science goals with these data include the discovery of stellar streams from tidally disrupted satellites and new constraints on the local distribution of dark matter. Current Milky Way models may lack the richness and sophistication worthy of the data; several groups have indeed begun laying the groundwork for accurate Milky Way mass models in the era of Gaia and LSST (Binney, 2010b; Sharma *et al.*, 2011; An, Evans, and Deason, 2012; Magorrian, 2013; McMillan and Binney, 2013, and references therein).

V. DYNAMICAL MASSES OF GAS-POOR GALAXIES

A. Introduction

As we go from gas-rich spiral systems to ETGs or dwarf spheroidals (dSphs), common practice is to abandon the systematic use of the extended neutral gas component of the former as a tracer to determine the mass distribution. However, many ETGs have a significant amount of gas, either ionized (Bertola *et al.*, 1984; Fisher, 1997; Sarzi *et al.*, 2006), sometimes molecular (Sage, Welch, and Young, 2007; Young *et al.*, 2011), or even neutral (Knapp, Turner, and Cunniffe, 1985; Morganti *et al.*, 2006; di Serego Alighieri *et al.*, 2007). In such cases, it is possible to conduct parallel approaches to constrain the overall mass profiles of the galaxies. This has been exploited in the context of, say, the search for supermassive black holes (Neumayer, 2010), the kinematics of the central regions (Corsini *et al.*, 1999; Vega Beltrán *et al.*, 2001; Pizzella *et al.*, 2004; Sarzi *et al.*, 2006, and references therein), or large-scale kinematics (Franx, van Gorkom, and de Zeeuw, 1994; Weijmans *et al.*, 2008).

However, the scarcity and complexity of observed gaseous distributions and kinematics and the associated difficulty of properly modeling the dissipative content of galaxies with multicomponent morphologies [although see, e.g., Weiner, Sellwood, and Williams (2001)] has led to further reliance on stellar dynamics: the interpretation of the large- (and small-) scale rotation curves revealed by the emitting gaseous content has thus generally been overtaken by state-of-the-art modeling of one of the existing dissipationless tracers, e.g., old stars, globular clusters, or planetary nebulae. The associated side products, i.e., constraints on the orbital structure of the galaxy under scrutiny, have the advantage of representing a rich source of information to establish its overall formation and evolution history.

In the following sections of Sec. V, we therefore restrict ourselves to briefly introducing the basic ingredients needed for the *kinematic modeling* of dissipationless systems, i.e., the determination of the total mass distribution, thus yielding the DM distribution after subtraction of the visible component. Determining the mass distribution requires extending beyond the simple use of the first velocity moment, the mean velocity

V , as the centered second velocity moment, the stellar velocity dispersion σ , becomes a non-negligible factor. Orbital shapes also depart from the commonly assumed circularity. Kinematic modeling is significantly more accurate through the measurement of the detailed shape of the velocity distribution, which is directly related to the orbital shapes and thus allowing a better understanding of the formation of the galaxies under study.

We first provide some insights on the dependence of mass estimators based on the measurement of the LOS velocity dispersion on details of the probed aperture. We then describe the standard techniques of kinematic modeling, based upon either the Jeans equations of local dynamical equilibrium or the six-dimensional distribution functions and we highlight the recent improvements to these methods. We finally illustrate the power of these methods with recent analyses of observed gas-poor galaxies, often obtaining useful constraints on the compatibility of the DM profiles with those in Λ CDM halos. In several cases, one can also obtain useful constraints on the DM normalization, concentration, inner slope, as well as the orbital *velocity anisotropy* (hereafter anisotropy) in the inner and outer regions. This review does not specifically address the mass modeling of central supermassive black holes (Kormendy and Ho, 2013); however most of the techniques that we discuss here also apply to that problem. See Gerhard (2013) for another recent review on dark-matter profile determinations based on multiple tracers.

B. Simple mass estimators

Before engaging in the complexity of the mass modeling described in Sec. V.C, we review simple mass estimators that have been proposed, all based on the scalar virial theorem (sVT).

The sVT states that for an isolated system in steady state

$$2K + W = 0, \quad (24)$$

where the total kinetic energy $K = \frac{1}{2}M\langle v^2 \rangle$, M is the total galaxy mass, and $\langle v^2 \rangle$ is the mean square velocity of its stars, integrated over the entire galaxy, while W is the total potential energy, which depends on the distribution of the stars and the possible dark matter. This energy budget derives from a time average and depends on the isolation of the dynamical system (to ensure that the tracer is not affected by a neighboring system).

For a nonrotating spherical galaxy, the mean square velocity of the stars is related to the observed LOS velocity dispersion $\langle v^2 \rangle = 3\langle \sigma_{\text{LOS}}^2 \rangle$ (where both averages extend to infinity). Assuming finite mass, Eq. (24) gives

$$M = c \frac{r_r \langle \sigma_{\text{LOS}}^2 \rangle}{G}, \quad (25)$$

where r_r is a characteristic radius of the galaxy, while $c = 6M^2 / \{r_r \int_0^\infty [M(r)/r]^2 dr\}$ in the self-consistent case. When the $\langle v_{\text{LOS}}^2 \rangle$ integral is extended over the entire galaxy, Eq. (25) is completely independent on the radial variation of the stellar anisotropy (Binney and Tremaine, 2008, Sec. 4.8.3). In the general case, the coefficient c depends uniquely on the total (ρ) and tracer (ν , i.e., stellar in galaxies) density profiles of the system.

The practical application of that formula has been the source of some confusion to be addressed before engaging into tentative interpretations. First, the physical radius r_r is measured by the angular radius that it subtends; therefore, it depends directly on the assumed distance D of the object. Any uncertainty on D thus translates linearly into M . Second, there is an inherent uncertainty associated with r_r 's measurement: while it can be strictly defined as, for example, the radius at which half of the galaxy's total light is encompassed, the notion of total light itself is ill defined (it often depends on a subjective extrapolation); the nature of the data also plays a role (e.g., bandpass and signal-to-noise effects). It is thus common to retrieve specific radii values differing by factors of 2 or more for the same well-studied systems (Kormendy *et al.*, 2009; Chen *et al.*, 2010). Both issues should be carefully addressed, especially when considering samples of galaxies for which distances and aperture radii emerge from heterogeneous sources and/or methods. Third, when working at a finite radius r_r , one must add a non-negligible surface term into the virial theorem (The and White, 1986).

The application of Eq. (25) as a robust mass estimator is further compounded by its limited applicability to real stellar systems: one can rarely observe the stellar σ_{LOS} for the entire galaxy, due to the rapid surface brightness drop with galactocentric radii. Therefore, the effect of using a finite aperture must be considered (Michard, 1980; Bailey and MacDonald, 1981; Tonry, 1983). In early works, the coefficient c was determined only for specific galaxy surface brightness profiles (Poveda, 1958; Spitzer, 1969). Using Jeans models, it was realized that the coefficient c , however, depends significantly on the shape of a galaxy surface brightness profile and on the dynamical structure of the galaxy [that is, its anisotropy, see, e.g., Prugniel and Simien (1997) and Bertin, Ciotti, and Del Principe (2002)].

Moreover, galaxies contain unknown amounts of dark matter, making the total mass M an uncertain and ill-defined quantity. For these reasons, following Trujillo, Burkert, and Bell (2004), we rewrite Eq. (25) as

$$M(r_M) = c \frac{r_r \sigma_{\text{ap}}^2(R_\sigma)}{G}, \quad (26)$$

where the σ_{LOS} and mass integrals are restricted to finite radii, and where

$$\sigma_{\text{ap}}^2(R_\sigma) = \frac{\int_0^{R_\sigma} \Sigma(R) \sigma_{\text{LOS}}^2(R) R dR}{\int_0^{R_\sigma} \Sigma(R) R dR} \quad (27)$$

is the squared aperture velocity dispersion averaged over a cylindrical aperture on the sky of projected radius R_σ .

Cappellari *et al.* (2006) calibrated Eq. (26) using the observed surface distributions and integral-field kinematics within typically the *effective radius* containing half the projected luminosity R_e , for a sample of ETGs, in combination with Schwarzschild's axisymmetric dynamical models. They found that the enclosed mass within the effective radius ($r_r = R_e$) of ETGs can be robustly recovered using a best-fitting coefficient⁸ $c \approx 2.5$, which varies little from galaxy to

⁸Their expression for $(M/L)(r_M = R_e)$ was converted to an enclosed mass assuming $(M/L)(r_M = R_e) \approx (M/L)(r_M = r_{1/2})$.

galaxy, with $r_M = r_{1/2}^{\text{light}}$ (the radius of a sphere enclosing half of the galaxy light) and with $r_r = R_\sigma = R_e$ (the radius of a cylinder enclosing half of the galaxy light). Using $r_M = r_{1/2}^{\text{light}}$, $r_r = R_e$, and $R_\sigma \rightarrow \infty$, Wolf *et al.* (2010) analytically derived $c \approx 4.0$ for systems with $\sigma_{\text{LOS}}(R) \approx \text{const}$ and proved that c depends very little on anisotropy (as expected given their infinite aperture for σ_{ap}).⁹

Table II lists the values of c for some popular models of elliptical galaxies for comparison with different predictions (assuming isotropic velocities; anisotropic velocities are discussed later). The values of c are computed by inserting the LOS velocity dispersion of Eq. (34) into Eq. (27), yielding

$$c = 3 \frac{M(r_M) M_p(R_\sigma) / 4\pi r_r}{\int_0^\infty r \nu M dr - \int_{R_\sigma}^\infty (r^2 - R_\sigma^2)^{3/2} \nu M dr / r^2}, \quad (28)$$

where $\nu(r)$ and $M_p(R)$ are the stellar mass density at r and stellar mass enclosed in the cylinder of radius R , and where the denominator is obtained, for isotropic orbits, by Mamon and Łokas (2005a, 2006).¹⁰ Note that our models are idealized as they do not include realistic kinematics, galaxy rotation, or multiple photometric components as in the real stellar systems on which the estimators were originally calibrated. The first four models [from Sersic (1968) and Hernquist (1990)] assume no DM, while the last four include an $m = 6$ Einasto DM model [which Navarro *et al.* (2004) first found to best fit the halos in Λ CDM pure DM simulations], with radius of density slope -2 equal to one-tenth the quasivirial radius r_{200} ,¹¹ within which the DM accounts for 90% of the total.

For the Cappellari *et al.* and especially the Wolf *et al.* estimators, the mass within $r_{1/2}$ depends little on the DM (the Spitzer relation, originally formulated for single-component polytropes, with $r_M = r_{1/2}^{\text{light}}$, matches that of Wolf *et al.*, except for the Hernquist model, where $c = 4.96$). Inclusion of velocity anisotropy, with $\beta = r/2/(r + a_\beta)$ (Mamon and Łokas, 2005b), where $a_\beta = 2R_e$ as found for ellipticals formed by mergers by Dekel *et al.* (2005), makes no difference when $R_\sigma \rightarrow \infty$ (as theoretically expected) and decreases c by typically only 4% for finite R_σ .

In general, galaxies are not spherical and rotate. For this reason, Eq. (26) is not rigorously correct. However, for an aperture that extends to $1R_e$, Eq. (26) was empirically found to still provide a reliable enclosed-mass estimator (Cappellari *et al.*, 2006, 2013b). In this case, σ_e is measured from a single ‘‘effective’’ spectrum within an aperture, centered on the galaxy, enclosing half of the galaxy light. The spectrum can be obtained from integral-field observations for nearby

⁹Churazov *et al.* (2010) suggested a generalization of the approach of Wolf *et al.* (2010) by computing the mass at the radius where mass is least dependent on anisotropy, assuming the three cases of isotropic, radial, and circular orbits.

¹⁰The aperture velocity dispersions generally involve a triple integral. However, for simple anisotropic velocity models, one-third times the denominator of Eq. (28) becomes $\int_0^{R_\sigma} R dR \int_R^\infty K_\beta(r/R, r_a/R) \nu(r) M(r) dr / r$, where K_β is a dimensionless kernel given in Mamon and Łokas (2005b).

¹¹At r_{200} , the mean mass density is defined to be 200 times the critical density of the Universe.

TABLE II. Structural constant $c = GM(r_M)/r_r\sigma_{\text{ap}}^2(R_\sigma)$.

	Spitzer	Cappellari	Wolf	$3R_e$
r_M	∞	$r_{1/2}^{\text{light}}$	$r_{1/2}^{\text{light}}$	$3R_e$
r_r	$r_{1/2}$	R_e	R_e	R_e
R_σ	∞	R_e	r_{vir}	$3R_e$
Predicted	7.5	2.5	4.0	...
Hernquist	7.46	3.31	4.84	5.74
$n = 1.0$ Sérsic	7.19	3.79	4.78	8.56
$n = 2.0$ Sérsic	7.23	3.63	4.85	7.22
$n = 4.0$ Sérsic	6.59	2.96	4.44	5.36
$n = 5.5$ Sérsic	5.91	2.49	3.96	4.37
$n = 1.0$ Sérsic + Einasto DM	112	3.78	4.63	9.53
$n = 2.0$ Sérsic + Einasto DM	112	3.74	4.67	8.38
$n = 4.0$ Sérsic + Einasto DM	103	3.20	4.33	6.70
$n = 5.5$ Sérsic + Einasto DM	94	2.76	3.95	5.70

galaxies, or from a single aperture for high-redshift ones. The resulting σ_e^2 provides a good approximation to the luminosity-weighted velocity second moment $\overline{v_{\text{LOS}}^2} \approx \overline{V^2 + \sigma^2}$ inside the given aperture, where V is the observed mean stellar velocity at a given location and σ is the corresponding dispersion. For this reason, σ_e automatically includes contributions from both rotation and velocity dispersion and is only improperly called σ . The inclusion of rotation is essential for the reliability of the mass estimator.

The Spitzer (1969) and Wolf *et al.* (2010) formulas require kinematic measurements out to the virial radius.¹² Such data can currently be obtained only for dSph’s or globular clusters using individual stellar velocities. When those data are available, the latter formula is weakly sensitive to the differences in the input models. However, the Cappellari *et al.* (2006) formula should be used instead when only central kinematics (within $\sim 1R_e$) is available, as is currently the case for most ETGs. The data in Table II suggest that most of the difference in the coefficients c of Cappellari *et al.* and Wolf *et al.* is attributable to their use of different apertures to measure kinematics. Incidentally, both formulas provide formally correct results for a self-consistent Sérsic model with $m = 5.5$, where the difference in c is entirely explained by the different apertures.

Table II also illustrates the fact that aperture averaged velocity dispersions out to $3R_e$ are insufficient to measure the DM fraction at that radius [which is determined more accurately using the radial profile $\sigma_{\text{LOS}}(R)$ out to $3R_e$].

Next we consider the more refined methods for determining the distribution of the total mass of ETGs lacking a spatially extended gas tracer.

C. Methods based on dynamical modeling

The mass distribution in a gas-poor (and luminous) galaxy is expected to be generally dominated by baryons (mostly stars) in the inner parts and DM dominated in the outskirts. The exact location and shape of the transition between these two regimes has been the subject of an active debate, with

conclusions that seem to depend on the type (and mass) of the sampled galaxies.

The density profiles of DM halos in dissipationless Λ CDM simulations (hereafter Λ CDM halos) seem to converge (Navarro *et al.*, 2004) to the “Einasto” model (Einasto, 1965), which is mathematically “prettier” than the traditional Navarro, Frenk, and White (1996) model as its central density and total mass are both, unlike NFW, finite. These fits are now established from $\approx 10^{-3}$ (Navarro *et al.*, 2010) to 2 or 3 (Prada *et al.*, 2006) virial radii.

The inclusion of dissipative gas in cosmological simulations has the effect of concentrating the baryons in the centers of their structures, where they dominate the gravitational potential and drive the DM component deeper inside. On the scales of ETGs, this effect, commonly referred to as *adiabatic contraction* (Blumenthal *et al.*, 1986; Gnedin *et al.*, 2004), alters the DM density profile toward the singular isothermal ($\rho \propto 1/r^2$) model. This result is, however, expected to be very sensitive to the details of the baryonic feedback processes, and orbit diffusion by the quickly varying potential could be an important agent in flattening of the DM halo cusp (Pontzen and Governato, 2012). See more discussion on this issue in Sec. III.C.1.

For all galaxy types, the dissipative nature of baryons leads them to accumulate in galaxy centers; indeed, if the baryons were negligible everywhere, the Einasto (or NFW) models found in Λ CDM halos would lead to much lower local stellar M/L and aperture velocity dispersion than observed (Mamon and Lokas, 2005a). The dominance of baryons in the center and of DM in the envelopes of ETGs has been confirmed by x-ray measurements (Humphrey *et al.*, 2006; Humphrey and Buote, 2010) and dynamical modeling (Cappellari *et al.*, 2006; Thomas *et al.*, 2011); see Sec. V.E.

In the central region [within $\sim (1-2)R_e$] of an ETG, we rely on a tracer that may generate the majority of the *local* potential, making the stars a nearly *self-consistent* component of the galaxy.¹³ This would contrast with the galaxy’s outskirts, where the potential would be completely dominated by invisible matter, and our visible tracers are merely a set of orbiting entities.

The holy grail of dynamicists is the distribution function (DF) that is the density in phase space (the union of position and velocity spaces) of the observed tracer (luminosity for unresolved ETGs, numbers of stars for resolved dSphs). Its evolution is set by the collisionless Boltzmann equation (CBE), which states the incompressibility of the system in six-dimensional phase space, or in simpler terms in which the DF f is conserved along trajectories ($df/dt = 0$). In vector notation, the CBE reads

$$\frac{\partial f}{\partial t} + \mathbf{v} \cdot \nabla f - \nabla \Phi \cdot \frac{\partial f}{\partial \mathbf{v}} = 0 \quad (\text{CBE}),$$

where Φ is the gravitational potential. In the last term, $-\nabla \Phi$ is the force per unit mass acting on stars (and other bodies). The total density ρ is uniquely determined from Φ through the Poisson equation:

$$\nabla^2 \Phi = 4\pi G \rho \quad (\text{Poisson}).$$

¹²The virial radius is defined to be that where the radial streaming motions are small, typically $4/3$ of r_{200} .

¹³This should never be assumed but rather demonstrated.

Solving the CBE coupled with the Poisson equation is a challenging task, especially since f is a function of at least six variables (three positions, three velocities, ignoring any time dependence), and one can rarely access the tracers representing the total density ρ . A way out of this conundrum is to consider *local variables* to eliminate the direct dependence of f with respect to velocities, as next detailed.

1. Jeans analysis

The traditional simpler approach to mass modeling involves writing the first velocity moments of the CBE, yielding the Jeans equations¹⁴ that specify the local dynamical equilibrium

$$\frac{\partial \bar{\mathbf{v}}}{\partial t} + (\bar{\mathbf{v}} \cdot \nabla) \bar{\mathbf{v}} = -\nabla \Phi - \frac{1}{\nu} \nabla \cdot (\nu \boldsymbol{\sigma}^2), \quad (29)$$

where $\nu = \int f d^3 \mathbf{v}$ is the space density of the tracer, $\boldsymbol{\sigma}^2$ is the tracer's dispersion tensor, whose elements are $\sigma_{ij}^2 = \overline{v_i v_j} - \bar{v}_i \bar{v}_j$, where $\bar{v}_i = \int v_i f d^3 \mathbf{v}$ and $\overline{v_i v_j} = \int v_i v_j f d^3 \mathbf{v}$. The product $\nu \boldsymbol{\sigma}^2$ represents the anisotropic dynamical pressure tensor of the tracer.

The CBE and the Jeans equations [Eq. (29)] apply to all systems, even out of dynamical equilibrium, as long as the tracers behave like test particles in the gravitational potential, and hence do not interact (otherwise the right-hand side of the CBE would be nonzero). In other words, the two-body relaxation time must be much longer than the age of the Universe, as is the case for ETGs, dwarf ellipticals (except in their nuclei) and dSphs. In particular, as mentioned, in both the CBE and the Jeans equations there is no requirement that the observed tracer density ν be proportional to the total mass density ρ .

With the simplifying assumptions of stationarity (ignoring any direct time dependence, i.e., removing the first term on the left-hand side of the CBE), these *stationary* Jeans equations specify the local dynamical equilibrium:

$$\nu (\bar{\mathbf{v}} \cdot \nabla) \bar{\mathbf{v}} + \nabla \cdot (\nu \boldsymbol{\sigma}^2) = -\nu \nabla \Phi. \quad (30)$$

Using the stationary Jeans equations [Eq. (30)], one can relate the orbital properties, contained in the streaming (first) and pressure (second) terms with the mass distribution contained in the potential (right-hand side), through Poisson's equation. Such a Jeans analysis is fairly simple, as it circumvents the difficult problem of recovering the DF, by considering only its first few moments, which more directly relate to real astronomical observable quantities (depending on spatial coordinates). However, one is still left with a degeneracy between the mass and the anisotropy of the pressure tensor, as discussed in the following sections of Sec. V. Moreover, using moments does not guarantee that the DF is positive or null everywhere (Newton and Binney, 1984).

2. Spherical modeling

The small departures from circular symmetry of many astrophysical systems observed in projection, such as globular clusters, dSphs, and the rounder early-type galaxies as well as groups and clusters of galaxies, have encouraged

dynamicalists to often assume spherical symmetry in their kinematic modeling. The stationary nonstreaming spherical Jeans equation can then be simply written as

$$\frac{d(\nu \sigma_r^2)}{dr} + 2 \frac{\beta}{r} \nu \sigma_r^2 = -\nu(r) \frac{v_c^2}{r}, \quad (31)$$

where $\nu \sigma_r^2$ is the radial dynamical pressure (hereafter radial pressure), $v_c^2(r) = GM(r)/r = rd\Phi/dr$ is the squared circular velocity at radius r , while $M(r)$ is the total mass profile, and where

$$\beta(r) = 1 - \frac{\sigma_\theta^2 + \sigma_\phi^2}{2\sigma_r^2} = 1 - \frac{\sigma_\theta^2}{\sigma_r^2} \quad (32)$$

is the tracer's anisotropy profile with $\sigma_r \equiv \sigma_{rr}$, etc., $\sigma_\theta = \sigma_\phi$, by spherical symmetry, and with $\beta = 1, 0, \rightarrow -\infty$ for radial, isotropic, and circular orbits, respectively. The stationary nonstreaming spherical Jeans equation provides an excellent estimate of the mass profile, given all other 3D quantities, in slowly evolving triaxial systems such as Λ CDM halos (Tormen, Bouchet, and White, 1997) and for the stars in ETGs [e.g., formed by mergers of gas-rich spirals in dissipative N -body simulations (Mamon *et al.*, 2006)].

As one is left with two unknown quantities, the radial profiles of mass and anisotropy, linked by a single equation, one must contend with a nefarious mass-anisotropy degeneracy (MAD). The simplest and most popular approach to circumvent the MAD is to assume simply parametrized forms for both the mass and anisotropy profiles. One can then express the product of the observable quantities: the surface density profile $\Sigma(R)$ and the line-of-sight square velocity dispersion profile $\sigma_{\text{LOS}}^2(R)$ versus projected radius R through the anisotropic kinematic projection equation (Binney and Mamon, 1982) expressing the observed quantity

$$\Sigma(R) \sigma_{\text{LOS}}^2(R) = 2 \int_R^\infty \left(1 - \beta \frac{R^2}{r^2}\right) \nu \sigma_r^2 \frac{r dr}{\sqrt{r^2 - R^2}}. \quad (33)$$

One can insert the radial pressure from the spherical stationary Jeans equation (31) into Eq. (33) to determine the LOS velocity dispersions through a double integration over $\nu M dr$. Mamon and Łokas (2005b) simplified the problem by writing the projected pressure as a single integral

$$\Sigma(R) \sigma_{\text{LOS}}^2(R) = 2G \int_R^\infty K_\beta \left(\frac{r}{R}, \frac{r_\beta}{R}\right) \nu(r) M(r) \frac{dr}{r}, \quad (34)$$

where they determined simple analytical expressions for the dimensionless kernel K_β for several popular analytical formulations of $\beta(r; r_\beta)$ [Tremaine *et al.* (1994) previously derived $K_\beta(r, R) = \sqrt{1 - R^2/r^2}$ for $\beta = 0$]. The number density ν is obtained by Abel inversion

$$\nu(r) = -(1/\pi) \int_r^\infty (d\Sigma_{\text{tot}}/dR) dR / \sqrt{R^2 - r^2}.$$

When both $\rho(r)$ and $\nu(r)$ are expanded as sums of spherical Gaussian functions (Bendinelli, 1991), Eq. (34) can be applied to the individual Gaussians, which can have different β values. This leads to an expression involving a single quadrature for nearly general $\beta(r)$ profiles (Cappellari, 2008).

The next step in complexity is the nonparametric *mass inversion*, where $\beta(r)$ is assumed, involving first the anisotropic kinematic deprojection by inverting Eq. (33) (Mamon

¹⁴The Jeans equations are also called ‘‘equations of stellar hydrodynamics’’ or ‘‘hydrostatic equations.’’

and Boué, 2010; Wolf *et al.*, 2010) and then directly obtaining the mass profile by inserting the derived radial pressure into the Jeans equation (31). For simple $\beta(r)$ models, the mass profile can be written as a single integral (Mamon and Boué, 2010). Interestingly, for systems with roughly constant $\sigma_{\text{LOS}}(R)$ (as is the case for most galaxies), the mass profile at the half-light radius $r_{1/2} \approx 1.3R_e$ is almost independent of the assumed $\beta(r)$, as analytically derived by Wolf *et al.* (2010).

Alternatively, a mass profile is assumed and one directly determines the anisotropy profile through the nonparametric *anisotropy inversion*, first derived by Binney and Mamon (1982), with other algorithms by Tonry (1983), Bicknell *et al.* (1989), Dejonghe and Merritt (1992), and especially Solanes and Salvador-Solé (1990).

None of these approaches can lift the MAD. One promising alternative approach is to consider the variation with projected radius of the LOS velocity dispersion and *kurtosis* (Łokas, 2002; Łokas and Mamon, 2003). This method has been successfully tested (Sanchis, Łokas, and Mamon, 2004) on Λ CDM halos viewed in projection, despite the fact that these halos are triaxial (Jing and Suto, 2002a, and references therein), with anisotropy that increases with radius (Mamon and Łokas, 2005b, and references therein), substructures, and streaming motions. Unfortunately, the LOS projection of the fourth order Jeans equation, required in the dispersion-kurtosis method, is possible only when $\beta = \text{const}$, whereas ETGs formed by major mergers show rapidly increasing $\beta(r)$ (Dekel *et al.*, 2005). Nevertheless, Richardson and Fairbairn (2013a) recently generalized this approach for systems where the fourth order anisotropy is a function of the usual second order one, as is indeed seen in Λ CDM halos (Wojtak *et al.*, 2008).

3. Axisymmetric modeling

The large majority of the galaxies in the Universe are to first order axisymmetric (except for spiral arms and bars) and possess disks even for ETGs (Krajnović *et al.*, 2011; McDonald *et al.*, 2011). This includes fast rotators (Cappellari *et al.*, 2007; Emsellem *et al.*, 2007, 2011) and spirals.

If we rewrite the stationary CBE in cylindrical coordinates (R, z, ϕ) and assume *axial symmetry* and steady state, we obtain two nontrivial Jeans equations (Jeans, 1922; Binney and Tremaine, 2008, Eq. 4.222b,c) that are functions of four unknowns σ_R^2 , σ_z^2 , $\overline{v_\phi^2}$, and $\overline{v_R v_z}$ and do not uniquely specify a solution. By assuming that the velocity ellipsoid is aligned with the cylindrical coordinates, we further simplify such equations as

$$\frac{\nu\sigma_R^2 - \nu\overline{v_\phi^2}}{R} + \frac{\partial(\nu\sigma_R^2)}{\partial R} = -\nu \frac{\partial\Phi}{\partial R}, \quad (35)$$

$$\frac{\partial(\nu\sigma_z^2)}{\partial z} = -\nu \frac{\partial\Phi}{\partial z}. \quad (36)$$

The two equations (35) and (36) now depend only on σ_R^2 , σ_z^2 , and $\overline{v_\phi^2}$, but one must still specify at least one function of (R, z) for a unique solution.

The generality of such equations can be maintained by writing a direct dependence between the two dispersions in

the meridional plane via a function b such that $\sigma_R^2 = b\sigma_z^2$, with the boundary condition $\nu\sigma_z^2 = 0$ as $z \rightarrow \infty$. This yields (Cappellari, 2008)

$$\nu\sigma_z^2(R, z) = \int_z^\infty \nu \frac{\partial\Phi}{\partial z} dz, \quad (37)$$

$$\overline{\nu v_\phi^2}(R, z) = b \left[R \frac{\partial(\nu\sigma_z^2)}{\partial R} + \nu\sigma_z^2 \right] + R\nu \frac{\partial\Phi}{\partial R}. \quad (38)$$

For a given observed surface brightness and assumed total mass distribution, when Eqs. (37) and (38) are projected onto the plane of the sky and integrated along the LOS, they produce a unique prediction for the observed second moment $\overline{v_{\text{LOS}}^2}$, as a function of b and the inclination i . The second moment $\overline{v_{\text{LOS}}^2}$ is empirically well approximated by $v_{\text{rms}}^2 \equiv V^2 + \sigma^2$ (the squares of the centroid of a Gaussian fit to the LOS velocity profile and of its dispersion), which is easily observed in galaxies. This implies that V and σ do not provide separately any extra information on the galaxy mass that is not already contained in their quadratic sum. It also implies that, when galaxy rotation V is significant, one cannot neglect its contribution to the galaxy-mass determination, and that one needs to know the inclination of the galaxy accurately. The dependence of the mass distribution on V_{rms} alone can be physically understood: for a given dynamical model, any star along a given orbit can have its sense of rotation reversed without altering $\overline{v_{\text{LOS}}^2}$ (or the mass).

To predict galaxy rotations from the Jeans equations one must make an extra assumption on how the second moments around the symmetry axis $\overline{v_\phi^2}$ divide into ordered and random motions $\overline{v_\phi^2} = \overline{v_\phi^2} + \sigma_\phi^2$. The simplest assumption to define this division is to adopt an oblate velocity ellipsoid (OVE), namely, assume $\sigma_\phi = \sigma_R > \sigma_z$ (Cappellari, 2008). This OVE model has a streaming velocity uniquely defined by

$$\overline{v_\phi^2} = \overline{v_\phi^2} - b\sigma_z^2, \quad (39)$$

with $\overline{v_\phi^2}$ and σ_z^2 as given in Eqs. (37) and (38).

With $b = 1$, Eqs. (37) and (38) define a circular velocity ellipsoid in the (v_R, v_z) plane: this is the historical semi-isotropic assumption that implies $\sigma_R = \sigma_z$ (and $\overline{v_R v_z} = 0$), and is sufficient to “close” the set of equations to provide a unique solution for the remaining variables σ_z^2 and $\overline{v_\phi^2}$ (Nagai and Miyamoto, 1976; Satoh, 1980; Binney, Davies, and Illingworth, 1990; van der Marel, Binney, and Davies, 1990; Emsellem, Monnet, and Bacon, 1994). If we consider Eq. (39), we retrieve the special case of the classic isotropic rotator (Binney, 1978).

When the total mass and surface brightness are described via the multi-Gaussian expansion (MGE) method of Emsellem, Monnet, and Bacon (1994), the potential and Jeans equations can be expressed in a simple form and $\overline{v_{\text{LOS}}^2}$ requires only a single quadrature for the semi-isotropic case (Emsellem, Monnet, and Bacon, 1994; Emsellem, Dejonghe, and Bacon, 1999). This is also true for the general case $\sigma_R \neq \sigma_z \neq \sigma_\phi$, and for all six projected second moments, including radial velocities and proper motions, as demonstrated by Cappellari (2008). This flexibility can be

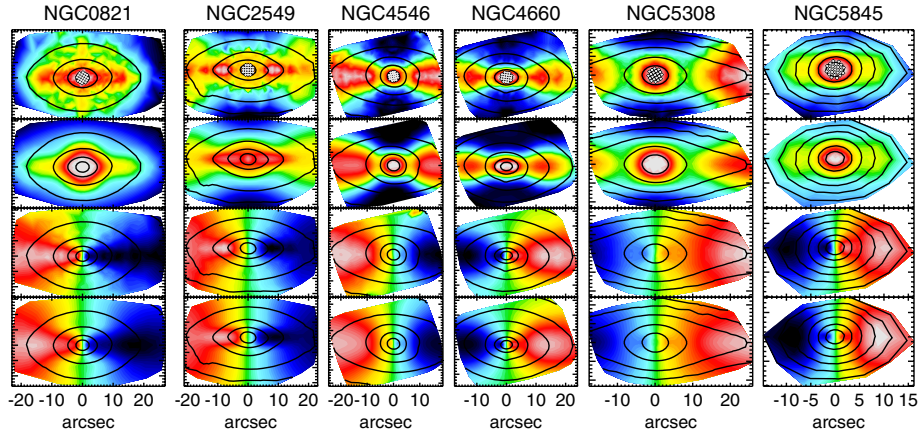


FIG. 15 (color online). Data-model comparison of six fast-rotator galaxies (previously classified as either E’s and S0’s) using the “Jeans anisotropic MGE” (JAM) method. From top to bottom: bi-symmetrized observations of $V_{\text{rms}} \equiv \sqrt{V^2 + \sigma^2}$, model of the same, bi-symmetrized observations of V , model of V . The contours show the isophotes. The models generally agree with the original nonsymmetrized data within the statistical errors. From Cappellari, 2008.

more practically witnessed when using an implementation of the “Jeans anisotropic MGE” (JAM) modeling method (Cappellari, 2008) augmented by the possibility to probe the parameter space within a Bayesian framework (see, e.g., Sec. II.C.2). A key feature of the OVE rotator with constant $b = (\sigma_R/\sigma_z)^2$ is that it maintains the simplicity of the isotropic (or semi-isotropic) rotator, but contrary to the latter, it provides a remarkably good description of the observations. In fact, these suggest that both fast-rotator ETGs (Cappellari *et al.*, 2007; Thomas *et al.*, 2009) and disk galaxies have a dynamical structure roughly characterized by a flattening of the velocity ellipsoid in the z direction parallel to the galaxy symmetry axis (Gerssen, Kuijken, and Merrifield, 1997, 2000; Shapiro, Gerssen, and van der Marel, 2003; Noordermeer, Merrifield, and Aragón-Salamanca, 2008). Indeed, once an accurate description of the surface brightness of the galaxies is provided via the MGE, the OVE rotator with constant b accurately predicts (Fig. 15) both the first (V) and second ($V_{\text{rms}} = \sqrt{V_{\text{rot}}^2 + \sigma^2}$) moment of the LOS velocity as inferred with state-of-the-art integral-field observations of the stellar kinematics of large samples of fast-rotator ETGs (Cappellari, 2008; Scott *et al.*, 2009; Cappellari *et al.*, 2013b). The success of the cylindrical oriented approximation may be related to the disklike nature of the majority of the galaxies in the Universe, where this particular alignment of the velocity ellipsoid appears natural (Richstone, 1984).

Real galaxies need not have accurately cylindrically oriented velocity ellipsoids. In fact, theoretical arguments and numerical experiments suggest the velocity ellipsoid cannot be perfectly cylindrically oriented (Dehnen and Gerhard, 1993). However, comparison with realistic N -body simulations of galaxies indicates that the cylindrically oriented velocity ellipsoid approximation can be used to reliably measure the mean values of the internal anisotropy or to recover mean M/L even in realistic situations where the anisotropy is not constant (Lablanche *et al.*, 2012).

D. Distribution function analysis

Although the Jeans analysis is simple and fast, it has two disadvantages: first, the second LOS velocity moment does

not describe the full information of projected phase space (PPS) $(\alpha, \delta, v_{\text{LOS}})$, where (α, δ) are the equatorial sky coordinates and v_{LOS} is the LOS velocity, and even the inclusion of the higher order moments (Magorrian and Binney, 1994; Magorrian, 1995) is less informative than using the full PPS. Second, for spherically modeled galaxies, the solutions of the Jeans analysis depend on the required radial binning of the velocity moments. Moreover, the variation of the velocity moments with projected radius is often noisy, requiring smoothing of the data. We now describe a more general family of mass modeling methods, which solves for the gravitational potential and the DF, by fitting the PPS distribution predicted for combinations of gravitational potential and DF to the observed PPS distribution.

1. Spherical distribution function modeling

In spherical symmetry, the PPS is simply (R, v_{LOS}) , where R is the projected radius, and the DF projects onto PPS as a triple integral (Dejonghe and Merritt, 1992):

$$g(R, v_{\text{LOS}}) = 2 \int_R^\infty \frac{r dr}{\sqrt{r^2 - R^2}} \int_{-\infty}^{+\infty} dv_\perp \int_{-\infty}^{+\infty} f(r, \mathbf{v}) dv_\phi. \quad (40)$$

So, with the knowledge of the DF shape, one can fit its parameters to match the PPS.

In spherical systems with isotropic nonstreaming velocities, the DF is a function of energy only, i.e., $f = f(E)$, while in anisotropic nonstreaming (e.g., nonrotating) spherical systems it is a function of energy and the modulus of the angular momentum. The PPS distribution in isotropic systems is (Strigari, Frenk, and White, 2010)

$$g(R, v_{\text{LOS}}) = 4\pi \int_R^\infty \frac{r dr}{\sqrt{r^2 - R^2}} \int_{\Phi(r) + v_{\text{LOS}}^2/2}^0 f(E) dE, \quad (41)$$

where the DF is given by the Eddington formula (Eddington, 1916).

However, Λ CDM halos are anisotropic (Colín, Klypin, and Kravtsov, 2000; Ascasibar and Gottlöber, 2008). Wojtak *et al.* (2008) recently showed that Λ CDM halos have DFs that are

separable in energy and angular momentum, with $f(E, L) = f_E(E)L^{2(\beta_\infty - \beta_0)}(1 + L^2/L_0^2)^{-\beta_0}$, with $\beta_0 = \beta(0)$ and $\beta_\infty = \lim_{r \rightarrow \infty} \beta$, and where L_0 is a free parameter related to the “anisotropy radius” where $\beta(r) = (\beta_0 + \beta_\infty)/2$. Unfortunately, the energy part of the DF is nonanalytical, although Wojtak *et al.* showed how it can be efficiently evaluated numerically [they also provide an analytical approximation for $f_E(E)$]. This Λ CDM halo-based DF can then be applied to fit the distribution of objects in PPS using Eq. (40), as shown by Wojtak *et al.* (2009).

For quasispherical galaxies, where, in contrast to clusters and Λ CDM halos, dissipation ought to play an important role, it is not yet clear that the DF is separable in energy and angular momentum as Wojtak *et al.* (2008) have found for Λ CDM halos. Moreover, the triple integral in Eq. (40) makes the Λ CDM halo DF method computationally intensive. The simplest and popular alternative is to fit the PPS assuming a Gaussian distribution for the LOS velocities, and the radial profiles of mass and anisotropy (Battaglia *et al.*, 2008; Strigari *et al.*, 2008; Wolf *et al.*, 2010). Unfortunately, this method provides very weak constraints on the anisotropy (Walker *et al.*, 2009).¹⁵ One can assume instead a Gaussian shape for the 3D velocity distribution, as in the Modeling Anisotropy and Mass Profiles of Observed Spherical Systems (MAMPOSSt) method of Mamon, Biviano, and Boué (2013), again adopting radial profiles of mass and anisotropy, and fitting the predicted distribution of particles in PPS. This operation involves only a single integral.

Both the Λ CDM halo DF and MAMPOSSt methods have been successfully tested on Λ CDM halos viewed in projection (Wojtak *et al.*, 2009; Mamon, Biviano, and Boué, 2013, respectively). They both yield useful constraints on both the mass and anisotropy profiles: with ~ 500 tracers, the mass M_{200} within the (quasivirial) radius r_{200} and the outer anisotropy are recovered with $\sim 30\%$ and $\sim 20\%$ relative accuracy, while the scale radius of the DM is obtained to within a factor of 1.5. The bias in the recovered M_{200} correlates with the ratio of LOS velocity dispersion measured within the virial sphere, estimated along the LOS to that measured in 3D (corrected by $\sqrt{3}$) so that the limiting factor for accurate mass measurements is the triaxiality of Λ CDM halos (Mamon, Biviano, and Boué, 2013).

2. Toward flattened systems

The majority of the gas-poor ETGs have important elongation in the plane of the sky. A number of methods have been developed and tested in an attempt to retrieve the full DF for flattened systems. In the case of the semi-isotropic approximation, Hunter and Qian (1993), expanding upon the Eddington formula for spherical systems, demonstrated that a direct inversion of the mass density ρ can be obtained analytically, which can then be applied to galaxies with complex morphologies (Emsellem, Dejonghe, and Bacon, 1999). Besides the fact that this involves analytic extrapolations of functions into the complex plane, flattened systems do not seem consistent with the semi-isotropic hypothesis. It may

therefore be worth reexamining this technique with the OVE assumption in mind.

Other techniques based on, for instance, the expansion of the DF into a set of basis functions (Dejonghe, 1989) have enjoyed some success (Kuijken, 1995; Gerhard *et al.*, 1998; Emsellem, Dejonghe, and Bacon, 1999). When the potential is of the Stäckel form, the DF can be readily expressed (de Zeeuw, 1985; Arnold, de Zeeuw, and Hunter, 1994), and the orbital structure is then a simple function of basic building blocks corresponding to explicit integrals of motion [see applications in Hunter and de Zeeuw (1992) and Statler (2001)]. For these specific cases, the general solution of the Jeans equations providing the moments in terms of standard integrals has even been worked out by van de Ven *et al.* (2003). Unfortunately, the difficulty of choosing a relevant set of basis functions for the DF, or to design models that fit specific galaxies from the very center to the outer parts, has led modelers to consider other more natural methods that treat a galaxy as the sum of well-chosen orbits: this is the subject of the following section.

3. General orbit-based modeling

A popular approach to nonspherical potentials (as well as spherical ones) is that of *orbit modeling* (Schwarzschild, 1979; Richstone and Tremaine, 1984). In the axisymmetric case, one considers orbits of given E , L_z , and I_3 (a nonclassical integral of motion) in a given potential (i.e., the DF is made of delta functions in E , L_z , and I_3). One searches for a linear combination of these orbits that minimizes the residuals between predicted and true observables, enforcing positive weights. These weights are obtained either by averaging the observables over an orbit (Schwarzschild) or by continuously updating them [Syer and Tremaine, 1996; NMAGIC code of de Lorenzi *et al.* (2007); Dehnen, 2009; Long and Mao, 2010)]. Such a technique can also be generalized to triaxial systems (van den Bosch *et al.*, 2008). Although more challenging to implement than Jeans analyses, orbit-based and particle-based methods constitute the state-of-the-art methods of kinematic modeling.

Because of its generality, the Schwarzschild method is more robust to the biases that may affect some of the other methods. It can also handle observable quantities more effectively, such as higher order Gauss-Hermite moments, while Jeans analyses are mostly concerned with the first two exact velocity moments. The robust measurement of the latter can be challenging given the complex LOS velocity distributions. The Schwarzschild method has been used extensively to measure masses of supermassive black holes in galaxies (van der Marel *et al.*, 1998; Cretton and van den Bosch, 1999; Verolme *et al.*, 2002; Gebhardt *et al.*, 2003; Valluri, Merritt, and Emsellem, 2004), to measure M/L or DM profiles (Cappellari *et al.*, 2006; Thomas *et al.*, 2007; Weijmans *et al.*, 2009), or to study the orbital anisotropy (Cappellari *et al.*, 2007; van den Bosch *et al.*, 2008; Thomas *et al.*, 2009).

The generality of the Schwarzschild method is linked with the presence of degeneracies in the recovered parameters, and with the general need to regularize the sampling of the PPS by adding minimization constraints. Indeed, the unknown three-dimensional shape and using plane-of-sky velocities makes the dimension of the observable projected phase space too low. In fact, observations can at best provide a 3D quantity,

¹⁵Walker *et al.* (2009) did not fit the PPS but $\sigma_{\text{LOS}}(R)$.

namely, the line-of-sight velocity distribution (LOSVD) at every projected location on the sky plane. This observable has the same dimension as the DF which, for Jeans's theorem, generally depends on the three isolating integrals of motion. The dimensionality equivalence between the observables and the DF explains why one can uniquely recover the DF from the data, when all other model parameters are known (Thomas *et al.*, 2004; Krajnović *et al.*, 2005; van de Ven, de Zeeuw, and van den Bosch, 2008; Morganti and Gerhard, 2012). However it is unlikely to robustly constrain additional quantities from the same 3D data (Valluri, Merritt, and Emsellem, 2004), namely, the 3D total mass distribution and the angles at which it is observed. Important degeneracies are indeed found when trying to measure the galaxy shape (Krajnović *et al.*, 2005; van den Bosch and van de Ven, 2009) or mass distributions (de Lorenzi *et al.*, 2009; see also Fig. 17) with very general approaches.

E. Results

As emphasized in Sec. V.D.1, the CBE can be applied to any tracer, as long as the system is sufficiently isolated. The choice of tracers typically involves the old stellar population, the globular cluster or planetary nebula systems, satellite galaxies, or x-ray emission from hot gas when present.¹⁶ Leaving the analysis of resolved dwarf spheroidal galaxies for Sec. V.E.5, nearly all kinematic studies of ETGs have focused on the bright end of the luminosity function, as dwarf ellipticals are often too difficult to study.¹⁷

1. Integrated stellar light: The inner regions and the IMF

The integrated stellar light component is the prime choice of tracer when considering regions within $\approx (1 - 2)R_e$ (see Fig. 15) and relatively luminous galaxies. Most of the observations then generally extend beyond the first two velocity moments (van der Marel *et al.*, 1994), which often helps to break the MAD (Gerhard *et al.*, 1998; Napolitano *et al.*, 2011). For galaxies that are intrinsically flattened or with complex morphologies, it is critical to make use of the two-dimensional kinematic maps provided by, for instance, integral-field spectroscopy as shown by Cappellari and McDermid (2005) and Krajnović *et al.* (2005). Progress can also be made by comparing dynamical and stellar population estimates to infer DM fractions and more generally the mass distribution in the central regions of galaxies (Gerhard *et al.*, 2001; Cappellari *et al.*, 2006; Napolitano, Romanowsky, and Tortora, 2010; Thomas *et al.*, 2011; Wegner *et al.*, 2012). Among others, these works confirm that the total M/L in the inner region of ETGs does not agree with the one predicted using stellar population models with a universal IMF. This can be interpreted as evidence for a variation in the dark-matter fraction in the galaxy's central regions, if the IMF is universal, or that the IMF is not universal and likely a function of total mass.

¹⁶See also the use of low-mass x-ray binaries as mass or dynamical tracers in dSph galaxies by Dehnen and King (2006).

¹⁷The more rapidly declining surface brightness profiles of dwarf ellipticals relative to their giant counterparts makes the spectroscopic measurements at several R_e especially challenging.

The most extensive set of detailed dynamical models to date, accurately reproducing both the galaxy photometry and the integral-field stellar kinematics, was constructed for the 260 ETGs of the ATLAS^{3D} survey (Cappellari *et al.*, 2013b). This study used axisymmetric anisotropic models based on the Jeans equations (JAM in Sec. V.C.3) and includes a rather general dark halo, where both its slope and normalization are varied to reproduce the data within a Bayesian framework. The halo inner logarithmic slope is allowed to vary from the values predicted by halo contraction models (Abadi *et al.*, 2010) to the nearly constant density profiles expected from halo expansion models (Pontzen and Governato, 2012). The median fraction of dark matter inferred from the models, within a sphere of radius $r = R_e$, is just 10%–20%. Cappellari *et al.* (2013b) found this dark-matter fraction to be consistent with predictions for the same galaxies inferred by linking NFW halos to the real galaxies and assuming halo masses via the halo abundance matching technique (Behroozi, Conroy, and Wechsler, 2010). Using satellites as tracers of the gravitational potential, the NFW model of Wojtak and Mamon (2013) extrapolates¹⁸ to a similar DM fraction within R_e for red galaxies of masses $(1.6-5) \times 10^{11} M_\odot$ (see Fig. 17), but to much larger dark-matter fractions for lower and higher mass red galaxies.

The study of Cappellari *et al.* (2012) found that dark matter cannot explain the systematic increase in the total M/L with the galaxy's velocity dispersion σ_e . This implies a systematic variation of the stellar IMF with σ_e , with the mass normalization changing by a factor up to 2–3, or from Chabrier (2003) or Kroupa (2001) to heavier than Salpeter (1955) over the full galaxy population (Fig. 16; Cappellari *et al.*, 2012). The Salpeter or heavier IMF for the most massive ETGs is consistent with recent findings from the analysis of IMF sensitive spectral features (van Dokkum and Conroy, 2010; Conroy and van Dokkum, 2012; Spiniello *et al.*, 2012) and with strong lensing results (Auger, Treu, Gavazzi *et al.*, 2010; Treu *et al.*, 2010; Dutton *et al.*, 2013 and discussion in Sec. VII), under the assumption of cosmologically motivated dark-matter halos. This result also smoothly bridges the gap between the IMF inferred for massive ETGs and the lighter Chabrier or Kroupa inferred for spiral galaxies (Bell and de Jong, 2001, see Sec. III).

Alternatives to a nonuniversal IMF do exist to explain the dynamical or lensing results, but they require that either (i) all current stellar population models (Sec. II) systematically and severely underpredict the M/L for the galaxies with the largest σ , which are characterized by the largest metallicities, or (ii) the dark matter accurately follows the stellar distribution, contrary to what all simulations predict. Moreover, the IMF trends inferred from spectral absorption features need to be explained by a conspiracy of chemical abundance variation with galaxy σ . There is currently no evidence for any of these effects, but further investigations in these directions are still important.

Several recent studies provided kinematic measurements of the integrated stellar light of ETGs beyond $(3-4)R_e$, using long-slit (Thomas *et al.*, 2007; Proctor *et al.*, 2009; Coccato *et al.*, 2010; Arnold *et al.*, 2011) or two-dimensional

¹⁸The projected radii of the satellite galaxies analyzed by Wojtak and Mamon (2013) begin at $5R_e$.

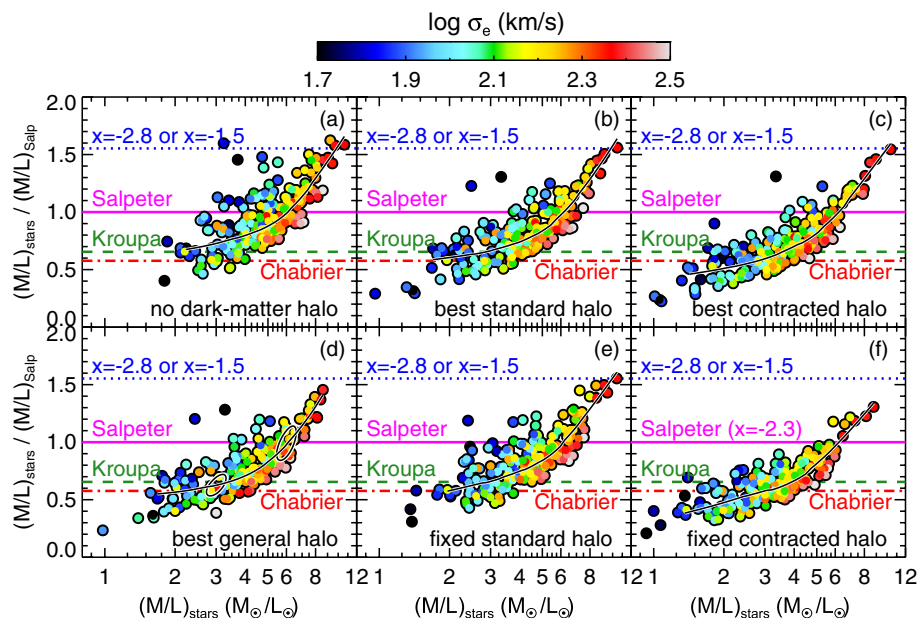


FIG. 16 (color online). Systematic variation of the stellar IMF in ETGs. The six panels show the ratio between the $(M/L)_{\text{stars}}$ of the stellar component, determined using dynamical models, and the $(M/L)_{\text{Salp}}$ of the stellar population, measured via stellar population models with a Salpeter IMF, as a function of $(M/L)_{\text{stars}}$. The solid lines are a local plot smoothing (LOESS) nonparametric regression to the data. Colors indicate the galaxies' stellar velocity dispersion σ_e , which is related to the galaxy mass. The horizontal lines indicate the expected values for the ratio if the galaxy had (i) a Chabrier IMF (dash-dotted line); (ii) a Kroupa IMF (dashed line); (iii) a Salpeter IMF ($x = -2.3$, solid line) and two additional power-law IMFs with (iv) $x = -2.8$ and (v) $x = -1.5$, respectively (dotted line). Different panels correspond to different assumptions for the dark-matter halos employed in the dynamical models as written in the black titles. A curved relation is clearly visible in all panels. From Cappellari *et al.*, 2012.

spectroscopy (Weijmans *et al.*, 2009). This, however, remains a rather challenging task, and as we probe outward we must consider more discrete tracers such as globular clusters and planetary nebulae (see Sec. V.E.2). The results obtained so far provided a picture where ETGs are dominated by the stellar mass out to $(1-3)R_e$, thus playing the counterpart of the *maximum disk* hypothesis in gas-rich systems (see Sec. III.D.1) but for hotter stellar systems, while the outer halos are generally consistent with Λ CDM predictions.

2. Globular clusters and planetary nebulae: The outer regions

In order to probe the distant radii beyond $\approx 4R_e$, observations from individual globular clusters (Pota *et al.*, 2013) or planetary nebulae (Douglas *et al.*, 2007; Coccato *et al.*, 2009; Napolitano *et al.*, 2011) become essential, even though these populations are often scarce. See Gerhard (2013) for a recent review.

GCs have been used extensively to probe the mass distribution of the outer halos of ETGs (Côté *et al.*, 2003; Hwang *et al.*, 2008; Lee *et al.*, 2010, and references therein). There are three drawbacks to adopting GCs as dynamical tracers. (1) As most GCs are red and very old, they have orbited many times around their host galaxy, and the most adventurous ones with the smallest pericenters will have been progressively tidally stripped by the potential of the host galaxy. Therefore, for a given apocenter, the GCs with the largest pericenters will have survived, leading to a bias toward more circular orbits (in comparison with the underlying stellar population). (2) Their dynamics is thought to originate from rather violent physical processes (early collapse, gas-rich mergers) and may

therefore not be strictly linked with the orbital structure of the old stellar population (Bournaud, Duc, and Emsellem, 2008). (3) A bimodality in the color distribution of GCs in bright ETGs is often observed (Brodie and Strader, 2006), which may then call for several decoupled dynamical components in the final modeling. As for any tracer embedded in the outermost regions of a galaxy potential, it is sometimes difficult to assess the steady-state and dynamically relaxed nature of a certain tracer, and address whether or not the observations still probe the galaxy potential or lie beyond the boundary with the intracluster potential (Doherty *et al.*, 2009).

One of the most thorough studies of a GC system by Schubert *et al.* (2010) includes nearly 700 GCs for the central Fornax cluster massive early-type galaxy NGC 1399. Using a $\beta = \text{const}$ Jeans analysis, they showed that the red GC population traces very well the field stellar population, while the blue one appears to be the superposition of several subpopulations including accreted or true cluster members. A similar study of the same galaxy with (4 times fewer) PNe by McNeil *et al.* (2010) illustrates the relative merits of using GCs and PNe as tracers of the gravitational potential.

It is fortunate that PNe do not suffer from the three drawbacks affecting GCs. PNe are generally thought to represent the distribution and dynamics of the galactic stellar halos with high fidelity [see, however, Méndez *et al.* (2001) and Sambhus, Gerhard, and Méndez (2006)]. Moreover, they are easy to observe, especially thanks to their very strong [OIII] emission line at 5007 \AA . Henceforth, several dynamical studies have targeted PNe around bright ETGs using multislit or slitless spectroscopy, or with the dedicated planetary nebulae spectrograph (Douglas *et al.*, 2002).

First analyses (Méndez *et al.*, 2001; Romanowsky *et al.*, 2003; Douglas *et al.*, 2007) based on Jeans analysis and Schwarzschild modeling suggested surprisingly little evidence for dark matter in the host galaxies studied. However, recent results (Das *et al.*, 2011) strongly confirm and quantify the discrepancy between the observed dynamics and that expected from the sole stellar light in giant ETGs such as NGC 4649. The extracted PNe luminosity distribution has also served to improve the distance estimated to that galaxy (Teodorescu *et al.*, 2011). Although PN-based kinematic modeling is usually limited by the number of tracers (typically 100 to 200), the Planetary Nebula Spectrograph (PN.S) team has performed an observational program observing PNe in the outer regions of a dozen ETGs, with detailed results on a number of prototypical systems such as NGC 4374 in the Virgo cluster, reaching out to $\approx 5R_e$ (Napolitano *et al.*, 2011). This kinematic modeling usually assumes spherical symmetry, but there now exist several studies using axisymmetric models: e.g., NGC 4697 (de Lorenzi *et al.*, 2008), NGC 3379 (de Lorenzi *et al.*, 2009), and NGC 4494 (Morganti *et al.*, 2013).

The main limitation of such studies is the often assumed hypothesis of spherical symmetry for the mass distribution, but these results can still serve as strong guidelines to constrain the presence of dark matter in the outer halos of ETGs.

3. Other tracers and combined approaches

At such large radii reached by the GC populations, as in NGC 1399, many studies take advantage of the presence of large x-ray halos around specific ETGs to constrain the corresponding radial mass and make direct comparisons (Humphrey *et al.*, 2006; Schuberth *et al.*, 2010; Das *et al.*, 2011; Gerhard, 2013). A number of galaxies have been surveyed, mostly massive ETGs as they are more often embedded within such x-ray halos (Fukazawa *et al.*, 2006; Nagino and Matsushita, 2009). The assumed hypothesis of hydrostatic equilibrium for the hot gas may sometimes hamper the robustness of such conclusions, but these effects are generally thought to be small. This is convincingly confirmed by comparing several concomitant tracers (Churazov *et al.*, 2008; Humphrey and Buote, 2010; Humphrey *et al.*, 2011), although some discrepancies have been reported, sometimes suggesting a transition from the galaxy halo to the cluster intergalactic medium (Schuberth *et al.*, 2010), or sometimes not yielding firm conclusions on their origins (Romanowsky *et al.*, 2009).

As also mentioned, even ETGs have sufficiently abundant (and well-behaved) gas components that can be used to constrain mass profiles out to large radii (Franx, van Gorkom, and de Zeeuw, 1994; Weijmans *et al.*, 2008).

Orbits of individual satellites may further help to constrain the potential around a galaxy (Geehan *et al.*, 2006; van der Marel and Guhathakurta, 2008). Prada *et al.* (2003) and Klypin and Prada (2009) used the SDSS to stack the PPS built from the satellites of thousands of otherwise fairly isolated galaxies and found it to be consistent with the predictions of Λ CDM simulations. Conroy *et al.* (2007) and More *et al.* (2011b) analyzed galaxy satellites based on SDSS data and derived the variation of virial mass with host galaxy luminosity, separating red and blue galaxies. They both found that red host galaxies have typically double the halo mass as their blue

counterparts of the same stellar mass. These two studies make assumptions that thwart the derivation of useful constraints on the anisotropy. Using the Λ CDM halo DF model (Wojtak *et al.*, 2008) on a larger SDSS sample, Wojtak and Mamon (2013) were able to obtain more reliable relations between halo and stellar mass or luminosity, confirming to first order the results of Conroy *et al.* and More *et al.* The stellar fractions within the virial radius of red galaxies with $\log M_{\text{stars}} > 10$ exceed 1%, peaking at 2% for $\log M_{\text{stars}} \approx 11.9$, and decreasing again to 1% at larger masses. However, Wojtak and Mamon also found that red galaxies have more concentrated halos than blue galaxies of the same stellar or halo mass, and that the inner and outer orbits of satellites around red galaxies are somewhat radial. One can consult Secs. VI and VII on lensing for further details about the galaxy-mass profiles at large radii.

As hinted above, a promising path toward robust mass profiles comes from the simultaneous use of all available tracers, hoping for a consistent picture to emerge. Many studies have been conducted toward this end, mostly targeting ETGs (Pota *et al.*, 2013) and more specifically very massive ones (Woodley *et al.*, 2010; Arnold *et al.*, 2011; Das *et al.*, 2011; Murphy, Gebhardt, and Adams, 2011). In agreement with results stated above, the overall impression from these studies calls for ETGs as being dominated by baryons within $1R_e$, with dark matter representing about half of the mass within $(2-4)R_e$ and dominating at larger radii.

4. The mass-anisotropy degeneracy

The results presented in this section appear robust in a statistical sense. However, on an individual basis, measuring the mass profile in gas-poor galaxies is intrinsically difficult due to the degeneracy in the stellar dynamical models. The MAD is best broken by the joint use of several tracers, especially if they probe the same region of the potential. The use of tracers with very different orbital anisotropies can also be very useful to lift the MAD.

As an illustration of this MAD problem, Fig. 17 shows the wide variety of solutions for the nearby apparently roundish ETG, NGC 3379, which had been the test bed for the putative suggestion that ETGs have relatively poor or diffuse dark-matter halos (Romanowsky *et al.*, 2003; Douglas *et al.*, 2007). One notices highly discrepant conclusions from various modeling attempts, in particular, at the outer limit of spectroscopic observations ($\sim 200''$ or $\approx 4R_e$). The MAD is clearly present as the higher DM fractions indicate fairly radial orbits in the outer regions, while the lower ones come with isotropic orbits (de Lorenzi *et al.*, 2009): this emphasizes the fact that specific tracers may constrain the mass distribution with uncertainties of different amplitude and nature. Moreover, there is a wide range of theoretical predictions. Also, some of the orbit solutions of Romanowsky *et al.* (2003) indicated “normal” levels of DM at large radii (Mamon and Łokas, 2005b). In fact, all recent observational modeling of NGC 3379 leads to an increased fraction of DM at increasing large radii. If NGC 3379, which has quasicircular isophotes, were a nearly face-on S0 (Capaccioli *et al.*, 1991), as suggested by its classification as a fast rotator (Emsellem *et al.*, 2007), one would expect lower DM fractions (Magorrian and Ballantyne, 2001).

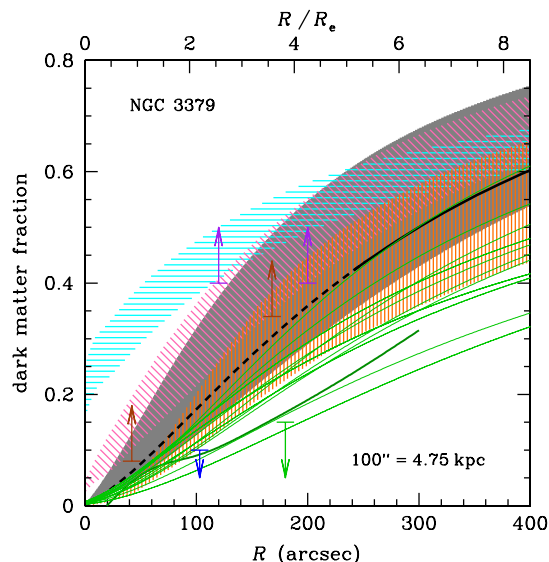


FIG. 17 (color online). Dark-matter fraction vs physical radius in NGC 3379 [assuming $R_e = 47''$ and Sérsic index $n = 4.74$, following Douglas *et al.* (2007)]. The light upper limit and light curves, respectively, show the Jeans (PNe) and orbit-modeling solutions of Romanowsky *et al.* (2003) (stars + PNe), while the other upper limit is the DF modeling (stars) of Kronawitter *et al.* (2000). The medium-thickness dark curve shows the spherical Jeans solution (stars + PNe) with double the number of PNe (Douglas *et al.*, 2007). The vertically shaded region gives the limits of NMAGIC orbit modeling (stars + PNe) (de Lorenzi *et al.*, 2009). The lower limits show the orbit modeling (stars) by Weijmans *et al.* (2009) and the isotropic Jeans analysis (globular clusters) of Pierce *et al.* (2006). The horizontal- and oblique-shaded regions give the predictions (Dekel *et al.*, 2005) from equal-mass merger SPH + cooling + feedback simulations (Cox *et al.*, 2004) of, respectively, gas-poor and gas-rich spirals embedded in dark-matter halos. The curve is from the satellite kinematics study of Wojtak and Mamon (2013), adopting the mean of their third and fourth stellar mass bins for red hosts (the stellar mass of NGC 3379 is in between), dashes for the extrapolation within the smallest satellite radii analyzed, while the shaded region represents the 1σ confidence from their Monte Carlo Markov chain analysis.

5. Discrete star velocities for dwarf spheroidal galaxies

Relative to giant ETGs, dSphs constitute the other mass extreme. The study of such low luminosity objects and very faint galaxies relies mostly on very nearby (local group) galaxies and largely in the context of resolved stellar populations (Gilmore *et al.*, 2007). Mass modeling is feasible thanks to ambitious observational programs to measure the stellar kinematics of hundreds and sometimes several thousands of individual stars¹⁹ (Tolstoy *et al.*, 2004; Łokas, Mamon, and Prada, 2005; Simon and Geha, 2007; Walker, Mateo, and Olszewski, 2009; Geha *et al.*, 2010; Battaglia *et al.*, 2011; Simon *et al.*, 2011). See the detailed review by Battaglia, Helmi, and Breddels (2013).

An example of this method is shown in Fig. 18 for the Sculptor dwarf spheroidal galaxy, studied in detail by Battaglia *et al.* (2008), who fitted the PPS assuming

¹⁹Similar methods apply to the study of Milky Way stars; see Sec. IV.

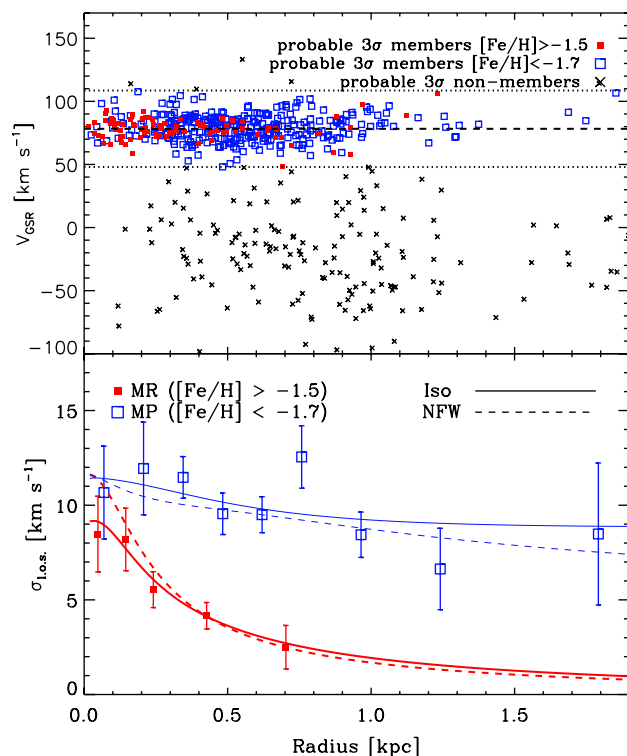


FIG. 18 (color online). Very large telescope and FLAMES velocity measurements for individual stars along the line of sight to the Sculptor dwarf spheroidal galaxy (dSph). Top panel: Line-of-sight velocities in the galactic standard of rest vs projected radius for probable members to the Sculptor dSph (the filled and open squares show probable members with metallicity $[\text{Fe}/\text{H}] > -1.5$ and < -1.7 , respectively) and for probable nonmembers (crosses). The region of probable membership is indicated by the two horizontal dotted lines, while the dashed line indicates the systemic velocity of the galaxy. Bottom panel: Line-of-sight velocity dispersion profiles for the metal-rich ($[\text{Fe}/\text{H}] > -1.5$) and metal-poor stars ($[\text{Fe}/\text{H}] < -1.7$), as shown by the filled and open squares with error bars, respectively. The solid and dashed lines show the LOS velocity dispersion profiles for the best-fitting pseudoisothermal (cored) and NFW (cusped) dark-matter models. Adapted from Battaglia *et al.*, 2008.

Gaussian LOS velocity distributions (adding a component for contamination by our Milky Way). By disentangling the metal-poor and metal-rich stellar subpopulations, they were able to show that, if physically meaningful, these two sub-systems were compatible with the same potential (best fitted by an isothermal DM profile) but with different anisotropy, providing some clues about their origin, as the metal-rich subpopulation appears to show a faster transition to radial orbits than the metal-poor one. The resulting dynamical mass-to-light ratio M/L reached values in excess of 150 inside ~ 2 kpc, demonstrating the dominance of DM at all radii in such low surface brightness objects. Walker and Peñarrubia (2011) used a similar two-population analysis to constrain the slopes of the mass profiles of the Fornax and Sculptor dSph galaxies, ruling out cusps as steep as -1 (NFW) for both and favoring inner slopes of -0.4 ± 0.4 (Fornax) and -0.5 ± 0.5 (Sculptor).

The DM core in Sculptor was recently confirmed by Richardson and Fairbairn (2013b) using their new

dispersion-kurtosis analysis with general anisotropy (Richardson and Fairbairn, 2013a). Amorisco and Evans (2012) noted that Fornax has three distinct stellar populations (with different metallicities), and, with this constraint, Amorisco, Agnello, and Evans (2013) showed that Fornax must indeed have a core of $1_{-0.4}^{+0.8}$ kpc or else an NFW model with an unlikely very large scale radius. However, orbit modeling allows a cusp for Sculptor (Breddels *et al.*, 2013) and Fornax (Jardel and Gebhardt, 2012). Indeed, using orbit modeling, Breddels and Helmi (2013) concluded that while Fornax, Sculptor, Carina, and Sextans can each accommodate either a cusp or a core, cores are unlikely when these four dSph galaxies are considered together. The debate between halo cusps and cores is thus still ongoing, largely because studies often group together different stellar populations that share different kinematics and neglect small but non-negligible rotation, and because nonspherical modeling increases the space of acceptable solutions.

Strigari, Frenk, and White (2010) used an isotropic analysis [with Eq. (41) and Eddington’s formula, and extracted the dispersion and kurtosis profiles from the former] to show that the classical dSph galaxies have LOS velocity dispersion, kurtosis, and even distributions that are consistent with their surface density and with subhalos taken from the Aquarius Λ CDM simulation of the Milky Way (Springel *et al.*, 2008), with dynamical masses between $2 \times 10^8 M_\odot$ and $15 \times 10^8 M_\odot$. More generally, it is believed (Mateo, 1998, and references therein) that most dSphs have very high virial-theorem M/L s. Recently, Walker *et al.* (2009) and Wolf *et al.* (2010) found that dSph M/L ’s within the half-light radius increase toward lower masses down to the lowest mass *ultrafaint dwarfs* (UFDs). Although extrapolating these systems to their virial radii may be ill advised, the data are consistent with all dSphs (including UFDs) having virial masses above $10^8 M_\odot$ (Walker *et al.*, 2009; Wolf *et al.*, 2010).

However, the detailed modeling of dSphs is challenging because of Milky Way contamination (Lokas, Mamon, and Prada, 2005) and because their likely tidal tails are expected to lie very close to the LOS (Klimontowski *et al.*, 2009), which could then lead to an overestimate of their mass (Klimontowski *et al.*, 2007).

Furthermore, when the stellar velocity dispersion reaches extremely low values, additional ingredients such as the contribution of binary systems must be taken into account for proper dynamical modeling, in particular, for ultrafaint dwarf galaxies (Martinez *et al.*, 2011, and references therein). N -body models may be required for an accurate dynamical modeling of these objects.

F. Future prospects

We reviewed the basic methods to determine the distribution of total mass in gas-poor galaxies, while addressing a number of intrinsic degeneracies that may affect current determinations. We see two main directions for future applications of the discussed techniques.

On the one hand, for local group galaxies, the dynamical degeneracies can be alleviated by increasing the dimension of the observable space, namely, by observing proper motions together with radial velocities of individual stars. At present,

this can be done for nearby star clusters by including plane-of-sky velocities from stellar proper motions in the dynamical models (van de Ven *et al.*, 2006; van den Bosch *et al.*, 2006; van der Marel and Anderson, 2010).

The global space astrometry satellite Gaia (Perryman *et al.*, 2001) provides proper motions with unprecedented accuracy. Unfortunately, the classical dSph galaxies are so distant that the error on proper motions from Gaia will be of the order of their internal velocity dispersions (Battaglia, Helmi, and Breddels, 2013), so the gain from proper motions with Gaia may be significant only for the closest dSph galaxies. However, the future generation of 30–40 m telescopes should roughly double the Gaia precision on proper motions (with a 5-year base line, Davies and Genzel, 2010) and lead to much more accurate mass and orbital modeling [as first suggested by Leonard and Merritt (1989)].

These data require and exploit the full generality and sophistication of the models. However, it is likely that such a wealth of data will also reveal new degeneracies associated with the subpopulations of stars in galaxies, themselves reflecting their complex formation and evolution history.

Meanwhile, if the increase in computing power grows at the current rate, one should be able to increasingly resort to N -body modeling (or associated techniques) to determine the distribution of mass in ETGs and dSphs that are not in perfect dynamical equilibrium and possibly address such models in some restricted cosmological context.

On the other hand, the same simpler techniques that are being applied today to relatively small samples of nearby galaxies will be used to study much larger samples of galaxies with two-dimensional stellar (and gaseous) kinematics and at increasingly larger redshift. The current state of the art is defined by the ATLAS^{3D} (Cappellari *et al.*, 2011) and CALIFA surveys (Sánchez *et al.*, 2012), which have mapped a few hundred galaxies via integral-field spectroscopy. Ongoing surveys, such as the SAMI (PI: Scott Croom) and MaNGA (PI: Kevin Bundy), will extend the sample size by about 2 orders of magnitude, using multiobject two-dimensional spectrographs on dedicated telescopes. Accurate masses, which themselves rely on accurate distances, will still be a critical ingredient to study galaxy formation from these larger samples. Finally, the next frontier will involve constructing dynamical models of galaxies at significant redshift, to trace the assembly of galaxy masses over time. This will also make use of multiobject spectrographs, optimized for near-infrared wavelengths, to effectively reduce the exposure times by orders of magnitude, mounted on future generation very large telescopes. Within the next ten years (i.e., ~ 2024), we may be able to approach the quality of the stellar kinematics of galaxies obtainable today in the Virgo cluster, up to the key redshift $z \sim 2$, when the Universe was just one-quarter of its current age and much of the galaxy mass was being assembled.

VI. WEAK LENSING BY GALAXIES

A. Introduction

Most methods to constrain or measure the masses of galaxies are limited to relatively small radii, where baryons

are dominant. This is because these methods probe the gravitational potential through the dynamics of visible tracers. Although it is safe to assume that galaxies are virialized, uncertainties in the mass estimates remain, for instance due to anisotropies in the velocity distributions. Furthermore, these baryon-dominated regions are not yet fully understood, which complicates a direct comparison of the models of galaxy formation to observational data. We note, however, that predictions from cosmological numerical simulations keep improving. Nonetheless, it would be advantageous to have observational constraints that can be robustly measured from numerical simulations. The virial mass of the galaxy is an obvious choice, but it is difficult to measure using dynamical methods. To date, only satellite galaxies have provided some information using data from large redshift surveys such as the SDSS (McKay *et al.*, 2002; Prada *et al.*, 2003).

In this section we focus on a direct probe of the matter distribution in the Universe, which provides us with a unique opportunity to probe the outer regions of galaxies. It makes use of the fact that inhomogeneities in the matter distribution, such as the halos around galaxies, perturb the paths of photons emitted by distant sources: it is as if we are viewing these sources with a spatially varying index of refraction. As a result, the images of the distant galaxies typically appear slightly distorted (and magnified), an effect that is known as weak gravitational lensing. The amplitude of the distortion provides us with a direct measurement of the gravitational tidal field, which in turn can be used to “image” the distribution of dark matter *directly* (Kaiser and Squires, 1993). If the distortion is large enough, multiple images of the source can be observed. This strong lensing provides accurate constraints on the mass distribution on small scales and its applications are discussed in Sec. VII.

The applications of weak lensing are not limited to galaxy-galaxy lensing, which is the study of the properties of galaxy dark-matter halos. In fact, the first detections were made by searching for the lensing-induced alignments of galaxies behind massive clusters of galaxies where the lensing signal is larger (Tyson, Wenk, and Valdes, 1990; Fahlman *et al.*, 1994). In recent years the focus has shifted to the measurement of the statistical properties of the large-scale structure: this cosmic shear is a promising probe of dark energy and has been detected with high significance (Fu *et al.*, 2008). This application is driving much of the development in improving measurement techniques, but also in terms of survey requirements. Consequently, galaxy-galaxy lensing studies benefit as well, because the data requirements are rather similar: we need to survey large areas of the sky, preferably in multiple bands in order to derive photometric redshifts. Such data sets are becoming available, and significant progress is expected in the coming years as the analyses of the first multicolor cosmic shear surveys are completed.

The first attempt to measure the weak-lensing signal around galaxies²⁰ was made by Tyson *et al.* (1984) using data from photographic plates with fairly poor image quality. As discussed next in more detail, the determination of the lensing signal requires careful measurements of the shapes of

faint galaxies which benefit greatly from good image quality. Consequently, the first detection was reported over a decade later by Brainerd, Blandford, and Smail (1996) using deep ground-based CCD images. Soon after Hudson *et al.* (1998) exploited the combination of deep Hubble Space Telescope (HST) imaging and photometric redshifts in the northern Hubble deep field.

An accurate determination of the galaxy-galaxy lensing not only requires good image quality. As next explained, the signal around an individual galaxy is too low to be detected. Instead we stack the signals for a large ensemble of lenses to improve the signal-to-noise ratio of the measurement. The early studies were all based on small survey areas, thus yielding small numbers of lens-source pairs. This changed with the start of the SDSS: Fischer *et al.* (2000) used only 225 deg² of commissioning data and detected a significant galaxy-galaxy lensing signal out to 1 Mpc. The SDSS data are relatively shallow, but the large survey area provides the large number of lens-source pairs to measure the lensing signal with high accuracy. Another important feature of the SDSS is the availability of redshifts for the lenses (spectroscopic as well as photometric), which has been used by McKay *et al.* (2001), Guzik and Seljak (2002), and Mandelbaum, Seljak *et al.* (2006).

In the case of deep observations the reduction in the number of lenses (due to a smaller survey area) is compensated by the increase in the number of sources, which are also more distant. Hence, even by imaging tens of square degrees the galaxy-galaxy lensing signal can be measured accurately (Hoekstra, Yee, and Gladders, 2004; Parker *et al.*, 2007). Such surveys typically lack spectroscopic redshift information for the lenses and use photometric redshifts instead [but see van Uitert *et al.* (2011) for an example that combines SDSS spectroscopy with deeper imaging].

Next we provide a brief introduction to weak galaxy-galaxy lensing and present a number of highlights, demonstrating the potential of this technique. However, it is important to stress that this is a field that is still developing, and many exciting results are expected from the next generations of surveys.

B. Theory of weak lensing

Because of space limitations, we can provide only the most basic discussion of weak gravitational lensing. We refer the interested reader to a recent review by Hoekstra and Jain (2008) or the thorough introductions by Bartelmann and Schneider (2001) or Schneider (2006b).

Inhomogeneities along the line of sight deflect photons originating from distant galaxies. As these sources are typically small, the resulting effect is a remapping of f^s , the surface brightness distribution of the source:

$$f^{\text{obs}}(x_i) = f^s(\mathcal{A}_{ij}x_j), \quad (42)$$

where \mathbf{x} is the position on the sky and \mathcal{A} is the distortion matrix (i.e., the Jacobian of the transformation), which is specified by the projected surface density of the lens and the redshifts of the lens and the source. It is convenient to introduce the deflection potential Ψ :

$$\Psi(\mathbf{x}) = \frac{1}{\pi} \int d^2\mathbf{x}' \kappa(\mathbf{x}') \ln|\mathbf{x} - \mathbf{x}'|, \quad (43)$$

²⁰In fact, it was the first attempt ever to measure a weak-lensing signal.

where the convergence κ is the ratio of the projected surface density $\Sigma(\mathbf{x})$ and the critical surface density Σ_{crit} :

$$\kappa(\mathbf{x}) = \frac{\Sigma(\mathbf{x})}{\Sigma_{\text{crit}}}, \quad (44)$$

with Σ_{crit} defined as

$$\Sigma_{\text{crit}} = \frac{c^2}{4\pi G} \frac{D_s}{D_l D_{ls}}. \quad (45)$$

Here D_s , D_l , and D_{ls} correspond to the angular diameter distances between the observer and the source, the observer and the lens, and the lens and the source. Hence, the lensing signal depends on both the redshifts of the lenses and the sources. Note that, in particular, the sources are too faint to determine spectroscopic redshifts, and photometric redshifts are used instead. Early galaxy-galaxy lensing studies lacked redshift information for both lenses and sources and average redshift distributions were used to infer masses (Hoekstra, Yee, and Gladders, 2004; Parker *et al.*, 2007). Redshift information is particularly useful for the lenses, as it allows one to study the lensing signal as a function of baryonic content and environment. Often photometric redshifts are also used for the lenses (Hoekstra *et al.*, 2005; Kleinheinrich *et al.*, 2006), with the notable exception of the SDSS (Mandelbaum, Seljak *et al.*, 2006; van Uitert *et al.*, 2011).

Redshifts for individual sources are not critical, provided their redshift distribution is known. However, if such information is lacking, faint satellite galaxies associated with the lens will dilute the lensing signal, if left unaccounted for. Furthermore, if these galaxies align their major axis toward the host galaxies, they will bias the signal (Agustsson and Brainerd, 2006).

The distortion matrix \mathcal{A} can be written in terms of the second derivatives of the deflection potential Ψ :

$$\mathcal{A} = \delta_{ij} - \frac{\partial^2 \Psi}{\partial \theta_i \partial \theta_j} = \begin{pmatrix} 1 - \kappa - \gamma_1 & -\gamma_2 \\ -\gamma_2 & 1 - \kappa + \gamma_1 \end{pmatrix}, \quad (46)$$

where we used $\kappa = \frac{1}{2} \nabla^2 \Psi$ and introduced the complex shear $\gamma \equiv \gamma_1 + i\gamma_2$, which are related to the deflection potential through

$$\gamma_1 = \frac{1}{2}(\Psi_{,11} - \Psi_{,22}) \quad \text{and} \quad \gamma_2 = \Psi_{,12}. \quad (47)$$

If κ and $\gamma \ll 1$ (i.e., the weak-lensing regime), the effect of the remapping by \mathcal{A} is to transform a circular source into an ellipse, with axis ratio $\sim (1 - |\gamma|)/(1 + |\gamma|)$ and position angle $\alpha = \arctan(\gamma_2/\gamma_1)/2$. In addition, the source is magnified by a factor

$$\mu = \frac{1}{\det \mathcal{A}} = \frac{1}{(1 - \kappa)^2 - |\gamma|^2}, \quad (48)$$

boosting the flux by the same amount. To first order, the magnification depends on the convergence only. Both the shearing and magnification of sources are observable effects, although both are quite different in terms of techniques and systematics.

C. Shear

To study the dark-matter distribution in the Universe, the measurement of the shearing of background galaxies is most commonly used, because of the better signal-to-noise ratio that can be achieved per lens-source pair when compared to the effect of magnification. It involves the measurement of the shapes of the faint background galaxies. Under the assumption that galaxies are randomly oriented in the absence of lensing, the strength of the tidal gravitational field can be inferred from the measured ellipticities of an ensemble of sources.

If we consider an isolated lens, the effect of weak lensing is a systematic (purely) tangential alignment of the images of the background galaxies with respect to the lens galaxy. The average tangential distortion, defined as

$$\gamma_T = -(\gamma_1 \cos 2\phi + \gamma_2 \sin 2\phi), \quad (49)$$

can then be used to quantify the lensing signal. Here ϕ is the azimuthal angle with respect to the lensing galaxy. For any mass distribution the azimuthally averaged tangential shear can be interpreted as a mass contrast:

$$\langle \gamma_T \rangle(r) = \bar{\kappa}(<r) - \bar{\kappa}(r). \quad (50)$$

A simple model to compare to the data is the singular isothermal sphere (SIS) with $\rho(r) = \sigma^2/(2\pi G r^2)$, where σ is the line-of-sight velocity dispersion. For this mass distribution we obtain

$$\gamma_T(r) = \kappa(r) = \frac{r_E}{2r}, \quad (51)$$

where r_E is the Einstein radius, which can be expressed in terms of σ and $\beta = \langle D_{ls}/D_s \rangle$:

$$r_E = \beta \left(\frac{\sigma}{186 \text{ km/s}} \right)^2 \text{ arcsec}. \quad (52)$$

If we fitted the model to the data from R_0 to R , the corresponding error is

$$\sigma_{r_E} = \sqrt{\frac{1}{\pi \bar{n} \ln(R/R_0)}} \sigma_{\text{gal}}, \quad (53)$$

where \bar{n} is the number density of sources and σ_{gal} is their intrinsic ellipticity ($\sigma_{\text{gal}} \sim 0.3$). For deep ground-based observations $\bar{n} \sim 10\text{--}20 \text{ arc min}^{-2}$. As discussed later, we should consider only the signal at $R < 120''$ and $R > 5''$ (because the lens light should not interfere with our shape measurement). For a galaxy with a velocity dispersion of 150 km/s, we obtain a typical signal-to-noise ratio of $r_E/\sigma_{r_E} \sim 0.39/1.4 \sim 0.28$ (adopting a typical value of $\beta = 0.6$). Even with the much higher source density in HST observations the best we can achieve is $S/N \sim 1$. Hence the signal of an individual lens galaxy is by far too small to be detected. Instead we have to average the signals for an ensemble of lenses to improve the signal-to-noise ratio.

Furthermore, the induced lensing signal is small, much smaller than the typical observational distortions that affect the observed shapes of the galaxies. The most relevant ones are the circularization by the point spread function (PSF) (seeing) and PSF anisotropy. The former lowers the signal

(if uncorrected for) and the latter can mimic a lensing signal. Much effort has been spent on understanding and correcting these sources of systematics. A major driver has been the study of lensing by large-scale structure, aka cosmic shear, which is an important way to study dark energy [see [Hoekstra and Jain \(2008\)](#) for a review] and extremely sensitive to residual systematics. In galaxy-galaxy lensing, however, one averages the signal perpendicular to lines connecting many lens-source pairs, which are randomly oriented with respect to the direction of PSF anisotropy. As a result any residual systematics are suppressed. The measurement of halo shapes is somewhat more sensitive, but as shown in [Hoekstra, Yee, and Gladders \(2004\)](#) current results are not affected and it is possible to reduce the impact further, albeit at the expense of increasing the noise ([Mandelbaum, Hirata *et al.*, 2006](#); [van Uitert *et al.*, 2012](#)).

D. Magnification

The measurement of the magnification provides a complementary way to study the mass distribution. The actual magnification cannot be measured because the intrinsic fluxes of the sources are unknown. Instead, the signal can be inferred from the change in the source number counts. Such a change arises from the balance between two competing effects. On the one hand, the actual volume that is surveyed is reduced, because the solid angle behind the cluster is enlarged. However, the fluxes of the sources in this smaller volume are boosted, thus increasing the limiting magnitude. As a consequence, the net change in source surface density depends not only on the mass of the lens, but also on the steepness of the intrinsic luminosity function of the sources. If it is steep, the increase in limiting magnitude wins over the reduction in solid angle, and an excess of sources is observed. If the number counts are shallow, a reduction in the source number density is observed.

The uncertainty in the measurement is determined by variations in the number density (i.e., a combination of Poisson noise and the clustering of the sources). A correct interpretation of the results requires only accurate photometry and knowledge of the (unlensed) luminosity function. Therefore the requirements on the PSF are much less stringent compared to the shear-based approach.

The magnification has been measured for quasars in the SDSS ([Scranton *et al.*, 2005](#); [Ménard *et al.*, 2008](#)) and Lyman-break galaxies in the Canada-France-Hawaii Telescope (CFHT) Legacy Survey by [Hildebrandt, van Waerbeke, and Erben \(2009\)](#). The latter study is of particular interest, because these dropout galaxies are readily identified in deep wide-field imaging surveys. Furthermore, as the sources are all at high redshift, this approach provides a unique way to study the masses of high redshift ($z \sim 1$) galaxies using ground-based data.

E. Galaxy-mass cross-correlation function

If galaxies are well separated, or randomly distributed, the observed lensing signal can be directly related to the ensemble averaged dark-matter distribution. In the real Universe, however, galaxies are clustered. This complicates such a simple interpretation of the data. On sufficiently small scales the

lensing signal is dominated by individual halos, but on larger scales we measure the combined signals from many halos. An example is shown in [Fig. 19](#), which shows results from the analysis of 334 deg² of data from the RCS2 ([van Uitert *et al.*, 2011](#)); see also, e.g., [Fischer *et al.* \(2000\)](#), [Hoekstra, Yee, and Gladders \(2004\)](#), and [Sheldon *et al.* \(2004\)](#). A significant signal is measured out to 30' from the lenses, which corresponds to ~ 9 Mpc. [Figure 19](#) also shows the best-fit NFW profile (to data between 0.2 and 0.6 arc min), which drops below the observations for scales larger than 1' (~ 300 kpc). Hence on these larger scales the clustering of the lenses is important to interpret the data. [van Uitert *et al.* \(2011\)](#) also compared the data to a SIS model and found that it also fits the data well out to ~ 300 kpc, indicating that it is typically difficult to distinguish between profiles. We note that [Gavazzi *et al.* \(2007\)](#) used a combination of strong- and weak-lensing measurements around massive ellipticals and found that a SIS model provides a good fit to the data. As discussed later, this does not imply that the density profile is isothermal. Rather, it is believed to be the result of the clustering of galaxies, which themselves have NFW density profiles.

It is therefore more appropriate to think of the galaxy-galaxy lensing signal as a measurement of the cross correlation between the galaxy and mass distribution: the galaxy-mass cross-correlation function. This observable provides additional constraints for models of galaxy formation and can be used to study the bias parameter as a function of scale ([Van Waerbeke, 1998](#)). In particular, it allows us to study whether the (small scale) bias is nonlinear and/or stochastic ([Pen, 1998](#); [Dekel and Lahav, 1999](#)).

The galaxy-mass cross-correlation function is closely related to the galaxy two-point correlation function and the cosmic shear signal, as they all provide ways to study the growth of structures via gravitational instability. On large scales the biasing is (close to) linear and the galaxy and dark-matter distributions are well correlated. In this situation

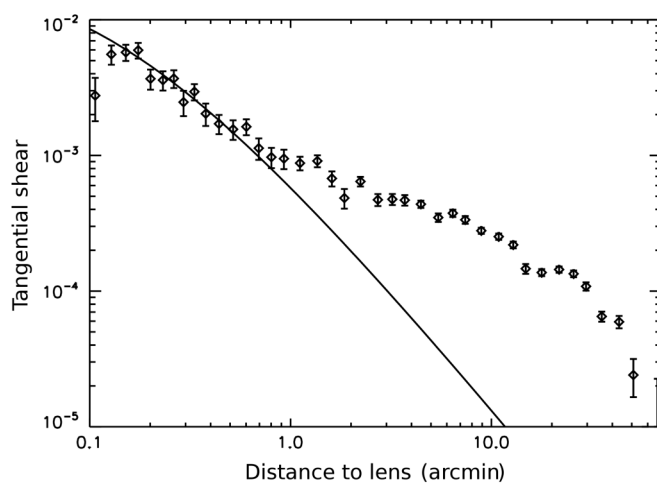


FIG. 19. Ensemble averaged tangential shear plotted as a function of distance from the lens using 334 deg² of r' data from the RCS2 ([van Uitert *et al.*, 2011](#)). The lenses are selected to have apparent magnitudes $19.5 < m_r < 21.5$ and the sources $22 < m_r < 24$. For reference the best-fit NFW profile is also drawn, which shows that on scales beyond 1' (~ 300 kpc) the clustering of the lenses becomes important.

the galaxy power spectrum is b^2 times the matter power spectrum $P(k)$ which can be measured through cosmic shear studies (Fu *et al.*, 2008; Hoekstra and Jain, 2008). The value of the bias parameter b is not known *a priori*. Similarly, the galaxy-mass cross-power spectrum will be $b \times r \times P(k)$, where r is the cross-correlation coefficient. The observed tangential shear measurement can be expressed as an integral over the power spectrum multiplied by a filter [see Guzik and Seljak (2001) and Hoekstra *et al.* (2002) for more details].

The combination of the galaxy two-point correlation function and the galaxy-galaxy lensing signal provides a direct measurement of the ratio b/r as a function of scale. This ratio was first measured by Hoekstra, Yee, and Gladders (2001), who later extended the analysis to the full red-sequence cluster survey (RCS) data in Hoekstra *et al.* (2002). They found that b/r is constant out to ~ 7 Mpc with an average value of 1.09 ± 0.035 for $\sim L_*$ galaxies. Sheldon *et al.* (2004) found similar results using SDSS data. Hoekstra *et al.* (2002) also included cosmic shear measurements from the VIRMOS-Desart survey (Van Waerbeke *et al.*, 2002) to study the scale dependence of b and r separately. Although Hoekstra *et al.* (2002) found tentative evidence for a variation of b and r with scale, this result needs to be confirmed as residual systematics in the cosmic shear signal may have affected the results (Van Waerbeke, Mellier, and Hoekstra, 2005).

Finally, Reyes *et al.* (2010) recently showed how general relativity (GR) can be tested by combining the observed galaxy-galaxy lensing signal with measurements of redshift-space distortions and the clustering of galaxies. This measurement combines three probes of large-scale structure to compare the two scalar potentials in the gravitational metric (ψ and ϕ). In Λ CDM and GR, both scalar potentials are equal. The lensing signal is sensitive to the sum of these, whereas the clustering measurements are sensitive only to the Newtonian potential ϕ . Although each of the observational probes depends on the value of the bias and the normalization of the power spectrum, the combination of these probes does not. Reyes *et al.* (2010) used data from the SDSS and found good agreement with GR on scales ranging from ~ 2 to 40 Mpc. The results cannot yet rule out $f(R)$ gravity models, but do disfavor some TeVeS models.

F. Properties of dark-matter halos

Although the study of the galaxy-mass cross-correlation function can provide useful constraints for models of galaxy formation, one would also like to learn more about the properties of the galaxy dark-matter halos themselves. This requires us to “separate” the contributions from individual halos from the clustering of the lenses. There are a number of ways this can be done. For instance, we can use the actual positions of the lenses and make the simplifying assumption that the observed signal arises only from the dark-matter halos associated with those lenses. Hence this approach does not describe well the situation in clusters or the large-scale structure. Furthermore, it is computationally expensive, in particular, if the model is extended to include more parameters. An advantage, however, is that it uses the two-dimensional shear field around the lenses, which is compared

to the observations in a maximum likelihood fashion. The maximum likelihood method, however, has not been studied in detail using numerical simulations and it is currently unclear to what extent the simplifying assumptions bias the results. Such tests are needed before this approach can be applied to modern, large data sets.

The maximum likelihood method was used by Hoekstra, Yee, and Gladders (2004) to examine the extent of dark-matter halos around galaxies [see also, e.g., Brainerd, Blandford, and Smail (1996) and Hudson *et al.* (1998)]. The lack of color information limited the analysis, but Hoekstra, Yee, and Gladders (2004) were able to constrain for the first time the sizes of the dark-matter halos. Figure 20 shows the result when an NFW model is assumed (Navarro, Frenk, and White, 1997). The mass and scale radius r_s are free parameters in the model, which are well constrained. Numerical simulations of cold dark matter (Navarro, Frenk, and White, 1997) predict a correlation between these parameters and the dashed line shows this prediction, which is in excellent agreement with these measurements. However, the mass-concentration relation depends on cosmology (in particular, the normalization of the matter power spectrum σ_8), which has changed over the years. Furthermore, larger numerical simulations have been used to examine the relations between halo properties and their evolution. The original results presented by Hoekstra, Yee, and Gladders (2004) used $\sigma_8 = 0.85$, but updated results with both lower and higher figures yield larger values for r_s . We therefore also show in Fig. 20 the expectations for Neto *et al.* (2007) who used $\sigma_8 = 0.9$ and Duffy *et al.* (2008) who used $\sigma_8 = 0.8$; given the limited investigations on the merits of the maximum likelihood method, it is unclear whether or not there is tension between the data and the predictions. It does suggest that this is an avenue worth pursuing.

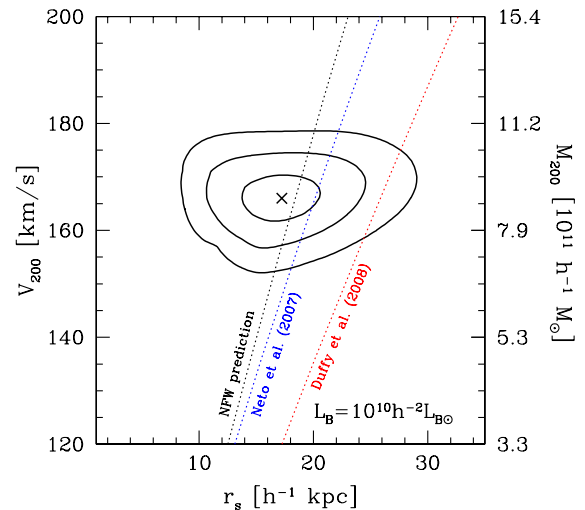


FIG. 20 (color online). Joint constraints on the scale radius r_s and mass M_{200} (and corresponding rotation velocity V_{200} for a galaxy with an NFW profile and a fiducial luminosity $L_B = 10^{10} h^{-2} L_{B0}$). The contours indicate the 68%, 95%, and 99.7% confidence on two parameters jointly. The dotted lines indicate the predictions from the numerical simulations by NFW (Hoekstra, Yee, and Gladders, 2004). Our updated version of this figure shows expectations from works by Neto *et al.* (2007) and Duffy *et al.* (2008).

In high density regions, such as clusters of galaxies, the galaxy dark-matter halos are expected to be tidally stripped due to the interaction with the tidal field of the smooth cluster mass distribution. Galaxy-galaxy lensing studies provide the only way to examine the sizes of the dark-matter halos as a function of the cluster-centric radius (Natarajan and Kneib, 1997; Natarajan *et al.*, 1998). A complication is that the signal arises from a combination of the stripped halos and the global cluster mass distribution. The various components can be modeled by a maximum likelihood method. To minimize contamination by field galaxies, with their much more extended halos, early work was confined to early-type galaxies (Natarajan *et al.*, 1998; Limousin *et al.*, 2007), but recently Natarajan *et al.* (2009) were able to study late-type galaxies as well. These studies have shown that dark-matter halos of cluster galaxies are tidally truncated (Limousin *et al.*, 2007; Natarajan *et al.*, 2009), which is also observed in strong lensing studies (Halkola, Seitz, and Pannella, 2007).

The clustering of dark-matter halos as a function of mass is well understood. This knowledge can be used to predict the galaxy-mass cross-correlation function, by relating the dark-matter distribution statistically to the observable galaxies through a halo occupation distribution (Seljak, 2000); for a review, see Cooray and Sheth (2002). This halo model approach is a powerful and natural way to interpret the data as it provides a natural way to account for the fact that the clustering depends on mass and that more massive halos host more than one galaxy (i.e., groups and clusters of galaxies). A minor drawback is that it uses only the tangential component of the shear. For isolated lenses the signal is indeed purely tangential, but this is no longer the case for an ensemble of lenses. The halo model was used by Guzik and Seljak (2002) and Mandelbaum, Seljak *et al.* (2006) to interpret the results from the SDSS and constrain the fraction of satellite galaxies. A similar study was carried out by van Uitert *et al.* (2011) who complemented the SDSS spectroscopic data with deep imaging data from the second red-sequence cluster survey (RCS2). This improved constraints for the massive galaxies, which on average are at higher redshifts.

The former studies focus only on the galaxy-mass cross-correlation function, but a consistent model for galaxy formation also makes predictions for the clustering of galaxies and the luminosity and/or stellar mass functions. Combining the information of these complementary probes can improve the constraints on the halo model parameters (Leauthaud *et al.*, 2011). Such a joint analysis was performed recently by Leauthaud *et al.* (2012) using data from the COSMOS survey. The high-quality lensing data, in combination with unprecedented wavelength coverage, allowed Leauthaud *et al.* (2012) to study the evolution of the stellar-to-halo mass relation from $z = 0.2$ out to $z = 1$. They found that the halo mass scales with stellar mass $\propto M_*^{0.46}$ for galaxies with $M_* < 5 \times 10^{10} M_\odot$ over the redshift range studied, whereas the slope of the relation steepens for higher masses.

One can also attempt to “avoid” the complication caused by the clustering of the lenses by considering only relatively “isolated” lenses. In this case the observed lensing signal is dominated by only a single galaxy. Such a selection, which requires (photometric) redshift information, was used by Hoekstra *et al.* (2005) to study the relation between the virial

mass and the luminosity. They limited the sample to galaxies that are more than $30''$ away from a brighter galaxy. For these galaxies Hoekstra *et al.* (2005) found that the virial mass scales with luminosity as $\propto L^{1.5}$, in agreement with the results from Guzik and Seljak (2002) and Mandelbaum, Seljak *et al.* (2006) who used the halo model to interpret the SDSS data. For a galaxy with fiducial luminosity of $L_B = 10^{10} h^{-2} L_{B\odot}$, Hoekstra *et al.* (2005) obtained a virial mass $M_{\text{vir}} = 9.9_{-1.3}^{+1.5} \times 10^{11} M_\odot$, also in good agreement with Mandelbaum, Seljak *et al.* (2006).

If we assume that baryons do not escape the dark-matter overdensity they are associated with, the ratio of M_b , the mass in baryons, to the virial total mass of the halo is $M_b/M_{\text{vir}} = \Omega_b/\Omega_m$. Furthermore, the amount of cold gas is negligible for massive galaxies. Therefore, by comparing the stellar mass of the lenses to the virial mass determined by weak lensing, the efficiency with which baryons are converted into stars can be constrained. Hoekstra *et al.* (2005) found that late types convert a ~ 2 times larger fraction of baryons into stars compared to early-type galaxies. The measurement of Hoekstra *et al.* (2005) is mostly constrained by relatively luminous galaxies. Mandelbaum, Seljak *et al.* (2006) found that the conversion efficiencies are independent of a morphological type for stellar masses less than $\sim 7 \times 10^{10} M_\odot$, but also found that later-type galaxies appear more efficient for higher stellar masses. Heymans *et al.* (2006) used data from the GEMS survey (Rix *et al.*, 2004) to study the mean virial-to-stellar-mass ratio for a complete sample of massive galaxies out to $z \sim 0.8$. The results, which agreed well with Hoekstra *et al.* (2005) and Mandelbaum, Seljak *et al.* (2006), showed little evidence for evolution. Leauthaud *et al.* (2012) also studied the stellar mass fraction as a function of mass finding a minimum at a halo mass of $\sim 1.2 \times 10^{12} M_\odot$.

These studies demonstrate the potential of weak-lensing results for the study of galaxy evolution. We note, however, the accuracy of the halo model is limited, and that measurements soon will be limited by this.

G. Halo shapes

The average shape of dark-matter halos can provide another way to learn more about the nature of dark matter (and the interaction with baryons). Numerical simulations of CDM have shown that the resulting dark-matter halos are triaxial with a typical ellipticity of ~ 0.3 (Dubinski and Carlberg, 1991; Jing and Suto, 2002b; Hayashi, Navarro, and Springel, 2007). In the case of self-interacting dark matter, the predicted halos are more spherical, although this difference is more pronounced on small scales (Davé *et al.*, 2001). We also note that hydrodynamic simulations suggest that baryonic effects cause dark-matter halos to evolve more oblate configurations at all radii, even if the effect of baryons is most prominent in the inner parts (Kazantzidis *et al.*, 2004; Kazantzidis, Abadi, and Navarro, 2010).

The small scales, which are baryon dominated, are best probed by strong lensing studies or dynamical studies. The latter approach has been extended to larger scales through the study of streams of stars in the Milky Way (Helmi, 2004; Koposov, Rix, and Hogg, 2010). On large scales, which are best constrained by numerical simulations, only

weak-lensing studies can provide observational constraints on the shapes of dark-matter halos. The measurement, however, is difficult: we now need to measure an azimuthal variation in the, already small, galaxy-galaxy lensing signal. The azimuthal variation is measured with respect to the major axis of the light distribution, i.e., we assume that the halos are aligned with the lens. If halos are flattened, but not aligned with the light distribution, the resulting lensing signal will be isotropic. Hence, any misalignment will reduce the amplitude of the azimuthal variation and the weak-lensing constraints are in effect lower limits on the shapes. Such misalignments might result from baryonic effects. For instance, [Bailin *et al.* \(2005\)](#) found in their hydrodynamic simulations of disk galaxies that the outer part of the halo is not well aligned with the inner regions, which show a good alignment between disk and inner halo [see also, e.g., [Abadi *et al.* \(2010\)](#)].

Weak-lensing studies of dark-matter halo shapes are more sensitive to systematic effects or errors compared to the measurement of the galaxy-mass cross-correlation function. For instance, residual PSF anisotropy leads to correlations between the lenses and sources, biasing the dark-matter halo shape determination ([Hoekstra, Yee, and Gladders, 2004](#); [Mandelbaum, Hirata *et al.*, 2006](#)). However, even in the absence of residual systematics, lensing by lower redshift structures can align the lens and the source, reducing the signature of an anisotropic halo. This cosmic shear contribution is described by [Mandelbaum, Hirata *et al.* \(2006\)](#) [see also [Brainerd \(2010\)](#) and [Howell and Brainerd \(2010\)](#) who discuss this problem]. This source of bias becomes more prominent with increasing lens redshift and will need to be taken into account when interpreting the current generation of surveys. Fortunately, [Mandelbaum, Hirata *et al.* \(2006\)](#) provided a method to suppress this signal, although this can be applied reliably only on relatively small scales and with limited accuracy ([van Uitert *et al.*, 2012](#)).

A successful measurement of the halo shapes requires a much larger number of lens-source pairs, as the signal-to-noise ratio is about one-tenth of that of the tangential shear signal and limited to small scales ([van Uitert *et al.*, 2012](#)). In recent years a number of pioneering studies have been carried out, but the results are still inconclusive. The first claim of elliptical dark-matter halos using weak lensing was presented by [Hoekstra, Yee, and Gladders \(2004\)](#) using 42 deg² of data from the RCS. The lenses were selected based on their apparent magnitude and early-type galaxies contribute most of the signal. [Hoekstra, Yee, and Gladders \(2004\)](#) found that the halos are aligned with the light distribution and estimated an ellipticity of $\langle e_{\text{halo}} \rangle = 0.33_{-0.09}^{+0.07}$. These results are in fair agreement with the results from [Parker *et al.* \(2007\)](#), who used 22 deg² of deep *i'* data from the CFHT Legacy Survey and also inferred an ellipticity ~ 0.3 .

The analysis of SDSS data by [Mandelbaum, Hirata *et al.* \(2006\)](#) did not detect an azimuthal variation in the lensing signal when considering the full sample of lens galaxies. However, when restricting the sample to bright early-type galaxies, the results of [Mandelbaum, Hirata *et al.* \(2006\)](#) suggest that the halos are aligned with the light. Recently, [van Uitert *et al.* \(2012\)](#) completed the analysis of 800 deg² of RCS2 data, but did not detect a significant anisotropy signal.

Part of the loss of precision is caused by a careful accounting for possible systematic effects.

An interesting, still open question is whether the alignments are the same for different types of galaxies. The possible differences between the various analyses need to be investigated further, but it is clear that significant progress will be possible only with the next generation of deep, multi-color surveys which provide redshift information for the lenses. The latter is important because of the scale dependence of the anisotropy signal ([Mandelbaum, Hirata *et al.*, 2006](#); [van Uitert *et al.*, 2012](#)).

H. Future prospects

Early weak galaxy-galaxy studies have already provided unique constraints on the properties of dark-matter halos, such as constraints on their extent and shapes, as well as masses. The SDSS results have demonstrated the usefulness of multicolor data and redshift information for the lenses. Of particular interest would be studies that complement the SDSS with deeper imaging. The precision of photometric redshifts limits their usefulness at low redshifts, but for the study of lenses with $z > 0.3$ the excellent statistics that can be achieved from the next generation surveys are expected to outweigh the limitations. For instance, the KiloDegree Survey (KiDS) which started observations in the fall of 2011 will cover 1500 deg² in nine filters. The extensive wavelength coverage will yield accurate photometric redshifts for the lenses. As a result statistical errors will be reduced by a factor of ~ 4 over current results and provide the first opportunity to study in detail the properties of dark-matter halos as a function of density and baryon contents. The Dark Energy Survey, which recently started taking data, will image 5000 deg².

Another major step forward will come from the LSST which plans to start surveying $\sim 20\,000$ deg² around the turn of this decade and space-based dark energy projects, such as the recently approved Euclid mission ([Laureijs *et al.*, 2011](#)), which is scheduled for launch in 2020. The excellent statistics provided by the latter projects will allow for the study of the galaxy lensing signal over a wide range in physical properties and redshift. Thanks to these developments galaxy-galaxy lensing will continue to develop into an important tool to study galaxy masses as a function of their observable baryonic properties.

VII. THE DARK AND LUMINOUS MASS DISTRIBUTION OF EARLY-TYPE GALAXIES USING STRONG GRAVITATIONAL LENSING

A. Introduction

Despite being a fundamental parameter required to test galaxy formation models ([White and Rees, 1978](#); [Blumenthal *et al.*, 1984](#)), the measurement of galaxy masses with few percent accuracy on any scale is notoriously difficult. This is particularly the case for ETGs which are not rotationally supported and generally lack gas-dynamical tracers. As seen in previous sections, a wide range of methods, or their combinations, have been employed to measure galaxy total

masses on very different scales: e.g., stellar and gas dynamics, hydrostatic equilibrium of x-ray emitting gas, and weak gravitational lensing. Whereas each of these methodologies have their own advantages and limitations, they also all have varying levels of precision and varying scales within which a mass can be measured.

In general, however, none of these methods reach the percent-level precision which is often required to accurately measure, for instance, the contribution of dark matter to the inner regions of galaxies where both baryons and dark matter interact and possibly play equal partners in galaxy formation models (Bertin, Saglia, and Stiavelli, 1992; Saglia, Bertin, and Stiavelli, 1992; Loewenstein and White III, 1999; Keeton, 2001; Padmanabhan *et al.*, 2004). In addition to degeneracies, some methods also become problematic beyond the local universe considering the limited signal-to-noise ratio of observations with present-day telescopes.

In this section, we focus on strong gravitational lensing (plus stellar dynamics) as a probe of the mass of galaxies out to tens of kpc scales, covering their inner regions to several effective radii (and beyond in combination with weak lensing). In addition, we discuss the use of gravitational lensing to quantify the level of mass substructure in the dark-matter halos (e.g., CDM substructure or dwarf satellites). The basics of strong lensing theory and the ability to measure galaxy masses to percent-level accuracy on different scales is introduced. This is exemplified with several recent highlights, mostly based on the largest strong lensing survey to date: the Sloan Lens ACS (SLACS) Survey (Bolton, Burles *et al.*, 2006). This section is neither complete nor unbiased and we refer to Schneider (2006a) and Treu (2010) for more thorough theoretical and observational overviews.

B. Basic lensing theory

Strong gravitational lensing can, to very good approximation, be regarded as geometric optics in curved spacetime (Schneider, Ehlers, and Falco, 1992; Kochanek, 2006), with the usual conservation of surface brightness. We also assume in nearly all astrophysical circumstances that the gravitational field that causes lensing (weak or strong) satisfies $|\phi|/c^2 \ll 1$ and that perturbations from the FRW metric of the Universe are small. As in geometric optics, curved spacetime can heuristically be associated with a refractive index $n = 1 + 2|\phi|/c^2$ for each point in space. A change in refractive index leads to a deflection of the light ray by

$$\vec{\alpha} = \int \vec{\nabla}_{\perp} n dl = \frac{2}{c^2} \int \vec{\nabla}_{\perp} \phi dl. \quad (54)$$

Hence an observer sees the light ray from a different direction than where it originated. In summary, two parallel rays of light (or wave fronts; Kayser and Refsdal, 1983) originating from slightly different positions will in general not remain parallel and can either diverge or converge. Similarly, rays of light being emitted in different directions from a single source can sometimes end up crossing each other again. If an observer (e.g., on Earth) happens to be at that crossing point, the emitting source will be seen multiple times. The deflection can be used to learn more about the mass

distribution of the deflector (e.g., galaxy, cluster, stars, etc.). It is worth noting that the concepts of time delay and deflection can be unified in the generalization of the concept of ‘‘Fermat’s principle’’ (Schneider, 1985; Blandford and Narayan, 1986), where lensed images form on extrema of a so-called time-delay surface.

1. The thin-lens approximation

Before coming up with a general equation for strong lensing, we illustrate some of these aspects in case of a point mass (e.g., a star or stellar remnant) with gravitational potential

$$\phi(\xi, z) = \frac{GM}{\sqrt{\xi^2 + z^2}}, \quad (55)$$

where ξ and z are the distances perpendicular and parallel to the line of sight from the point mass to the observer, respectively, and G and M are the gravitational constant and mass of the lens. One finds (note that $\xi^2 = \vec{\xi} \cdot \vec{\xi}$ and then the gradient is carried out with respect to $\vec{\xi}$)

$$\vec{\nabla}_{\perp} \phi = \frac{GM\vec{\xi}}{(\xi^2 + z^2)^{3/2}}. \quad (56)$$

Integrating this along the LOS, assuming z goes from minus to plus infinity, the deflection angle for a point mass is

$$\hat{\alpha} = \frac{4GM}{c^2\xi} = \frac{2R_s}{\xi}, \quad (57)$$

where $R_s = 2GM/c^2$ is the Schwarzschild radius. In general the impact parameter $b \gg R_s$, hence the deflection angles are far smaller than unity (weak deflection), justifying the approximations that were made so far.

We now also note that in general the distance Δz over which light is substantially deflected is much smaller than the distance of the lensed source of light to the deflector and the deflector to the source. In that case, we can approximate any extended lens by the ‘‘thin-lens approximation,’’ where the density distribution (ρ) is collapsed along the line of sight in to a surface density $\Sigma(\vec{\xi}) = \int \rho(\vec{\xi}, z) dz$. The latter is often the only mass-related quantity that can be determined. Deflection is assumed to occur effectively instantaneously in the lens plane of the deflector. The thin-lens approximation is practically always justified for describing the main deflector. However, whenever very high accuracy is required it should be kept in mind that the Universe is not exactly homogeneous and isotropic on large scales and therefore describing the intervening space between the source and the deflector and between the deflector and the observer with a standard Robertson-Walker metric is only an approximation. In reality, photons will propagate through overdensities and underdensities, resulting effectively in additional distortion (shear) and focus or defocus in addition to the one provided by the main deflector (see Sec. VI). This effect is usually accounted for as external shear and convergence and result in typical corrections of the order of a few percent to the strong lensing inference (Keeton, Kochanek, and Seljak, 1997; Treu *et al.*, 2009; Suyu and Halkola, 2010; Suyu *et al.*, 2013).

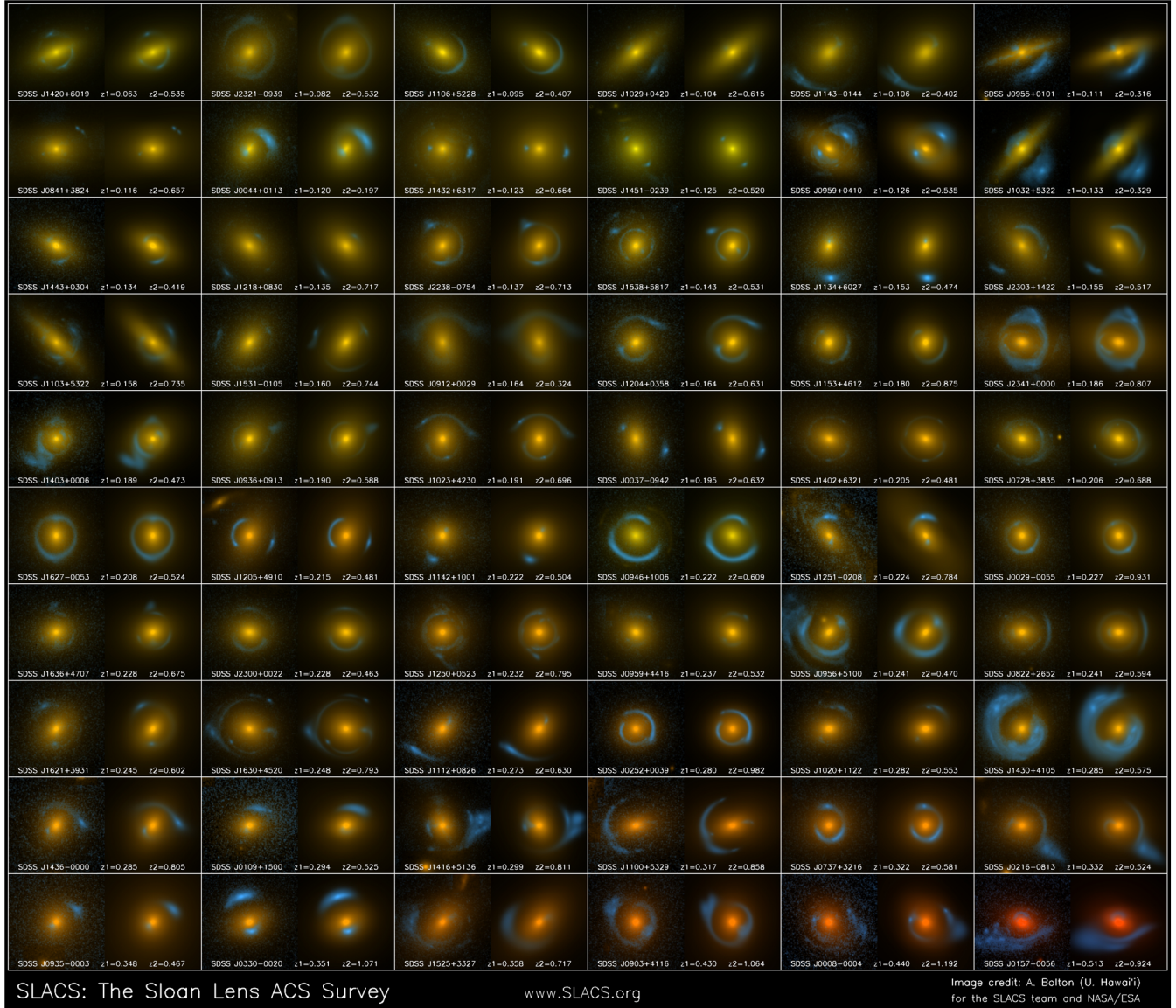


FIG. 21 (color online). A subsample of SLACS lenses in false color. Each panel shows the data on the left and a model of the system on the right. From Adam Bolton.

Extending now from the point-source deflector to a general (surface) mass distribution, using $M \rightarrow \Sigma(\vec{\xi})d^2\xi$, one readily finds that

$$\vec{\alpha}(\vec{\xi}) = \frac{4G}{c^2} \iint \frac{\Sigma(\vec{\xi}')(\vec{\xi} - \vec{\xi}')}{|\vec{\xi} - \vec{\xi}'|^2} d^2\xi'. \quad (58)$$

For circularly symmetric lenses with $\xi = |\vec{\xi}|$ we have

$$\vec{\alpha}(\xi) = \frac{4GM(\leq \xi)\vec{\xi}}{c^2\xi^2} \quad (59)$$

with

$$M(\leq \xi) = 2\pi \int_0^\xi \Sigma(\xi')\xi' d\xi'. \quad (60)$$

We are now ready to introduce the lens equation which forms the basis of lensing theory.

2. The lens equation

Now that the deflection for any general and circularly symmetric mass distribution can be calculated, we can relate any point in plane (at a distance D_s) where the emitting source is to a point at $\vec{\theta} = \vec{\xi}/D_d$ in the plane of the deflector (at a distance D_d) as seen by the observer. We also assume that the distance from the deflector to the source is D_{ds} , which in GR is not necessarily equal to $D_s - D_d$. In that case (Fig. 21), we readily find in scalar notation $\theta D_s = \beta D_s + \hat{\alpha} D_{ds}$, assuming the small-angle approximation, or equivalently

$$\vec{\beta} = \vec{\theta} - \frac{D_{ds}}{D_s} \vec{\alpha}, \quad (61)$$

where $\vec{\beta}$ is the vector angle to the source as it would be seen (with respect to some arbitrary coordinate origin, usually chosen to the deflector centroid) if not lensed and $\vec{\theta}$ is the vector angle of the lensed image(s) as observed. Defining the

reduced deflection angle as $\vec{\alpha} \equiv (D_{ds}/D_s)\vec{\hat{\alpha}}$, we arrive at the standard nonlinear lens equation

$$\vec{\beta}(\vec{\theta}) = \vec{\theta} - \vec{\alpha}(\vec{\theta}). \quad (62)$$

We note here that the nonlinearity of $\vec{\alpha}(\vec{\theta})$ can lead to multiple solutions of $\vec{\theta}$ of the lens equation for a given source position $\vec{\beta}$; hence multiple imaging (strong lensing) occurs (note that this equation holds for each position of an extended source and that image surface brightness for each solution $\vec{\theta}$ is identical to that of the source at $\vec{\beta}$). The extreme case of multiple imaging is the creation of the ‘‘Einstein ring’’ for circularly symmetric lenses, for which

$$\beta = \theta - \frac{4GM(\theta)D_{ds}}{c^2D_dD_s} \frac{1}{\theta}. \quad (63)$$

Defining the Einstein radius

$$\theta_E \equiv \left[\frac{4GM(\theta)D_{ds}}{c^2D_dD_s} \right]^{1/2}, \quad (64)$$

the lens equation for $\beta = 0$ has the solution $\theta = \pm\theta_E$. Because of symmetry, a source aligned with the source-deflector line will be imaged into a perfect Einstein ring.

We can take one more step to simplify the equations. We do this assuming the deflector has constant density (a ‘‘mass sheet’’). In that case

$$\alpha(\theta) = \left[\frac{4\pi G\Sigma D_d D_{ds}}{c^2 D_s} \right] \theta = \left[\frac{\Sigma}{\Sigma_{\text{crit}}} \right] \theta, \quad (65)$$

with $\Sigma_{\text{crit}} \equiv c^2 D_s / 4\pi G D_d D_{ds}$. We further define the so-called ‘‘convergence’’ $\kappa \equiv \Sigma / \Sigma_{\text{crit}}$. Hence, the deflection angle is linear and $\beta = (1 - \kappa)\theta$. For $\kappa = 1$, parallel rays converge to a single focus, making the transition from $\kappa < 1$ to $\kappa > 1$ special. The mass sheet with $\kappa = 1$ is a perfect focusing lens. Whereas this is not the case for general lenses, it turns out that lenses with $\kappa > 1$ at any point, can create multiple images because of overfocusing. With this definition the deflection angle becomes

$$\vec{\alpha}(\vec{\theta}) = \frac{1}{\pi} \iint \frac{\kappa(\vec{\theta}')(\vec{\theta} - \vec{\theta}')}{|\vec{\theta} - \vec{\theta}'|^2} d^2\vec{\theta}'. \quad (66)$$

It can be shown that the average convergence inside the Einstein radius of any circularly symmetric deflector is exactly equal to 1. Thus for lens systems with a (near) Einstein ring, the mass inside the Einstein radius is $M_E \equiv \pi(D_d\theta_E)\Sigma_{\text{crit}}$ independent of the density profile of the deflector. In fact, deviations from symmetry are only secondary effects. Hence the masses of strong lenses can be determined to rather exquisite accuracy if a reasonable Einstein radius can be defined.

3. Axisymmetric lenses

Whereas lens modeling can be rather complex, in general axisymmetric (in 2D) lenses give good insight into the processes that are important in lensing. This is because many lenses are ETGs, which generally have round mass distributions and potential with small ellipticities. It is therefore useful to derive some properties for these types of lenses, giving first-order results for other lenses as well.

We thus assume $\kappa(\theta) = \kappa(|\vec{\theta}|)$ and $\alpha(\theta) = |\vec{\alpha}(|\vec{\theta}|)|$. It is then easy to show that

$$\alpha(\theta) = \frac{M(<\theta)}{\theta} = \langle \kappa \rangle(\theta)\theta, \quad (67)$$

with

$$M(<\theta) \equiv 2 \int_0^\theta d\theta' \theta' \kappa(\theta') \quad (68)$$

and

$$\langle \kappa \rangle(\theta) = \frac{M(<\theta)}{\theta^2}. \quad (69)$$

Hence the deflection angle then reduces to

$$\beta = [1 - \langle \kappa \rangle(\theta)]\theta. \quad (70)$$

This immediately shows that for an Einstein ring with $\beta = 0$ that $\langle \kappa \rangle(\theta) = 1$. Hence for any axisymmetric lens the average convergence inside the Einstein radius is unity. The enclosed mass can thus be inferred independent of the density profile. In physical units

$$M_E = \pi\theta_E^2 D_d^2 \Sigma_{\text{crit}}, \quad (71)$$

or conversely

$$\theta_E = \left(\frac{4GM_E D_{ds}}{c^2 D_d D_s} \right)^{1/2}. \quad (72)$$

Then if the Einstein radius can be determined, the mass can be determined.

4. Lensing and stellar dynamics

A powerful complementary constraint that is worth mentioning is the combination of the precise total mass measurement using strong gravitational lensing with stellar kinematic measurements. Whereas this combination can become rather complex for two or three integral (nonspherical) models, here we illustrate the basic idea assuming spherical symmetry and power-law density and luminosity-density models (Treu and Koopmans, 2002a; Koopmans, 2004; Bolton, Rappaport, and Burles, 2006). Despite these simplifications, these toy models give rather robust results for the density slopes of ETGs.

We suppose that the stellar component has a luminosity density $\nu_l(r) = \nu_{l,o} r^{-\delta}$ and is a trace component embedded in a total (i.e., luminous plus dark-matter) mass distribution with a density $\nu_\rho(r) = \nu_{\rho,o} r^{-\gamma'}$. In addition, we assume that the anisotropy of the stellar component $\beta = 1 - (\overline{\sigma_\theta^2}/\overline{\sigma_r^2})$ is constant with radius. For a lens galaxy with a projected mass M_E inside the Einstein radius R_E , the luminosity-weighted average line-of-sight velocity dispersion inside an aperture R_A is given, after solving the spherical Jeans equations, by

$$\langle \sigma_{\parallel}^2 \rangle(\leq R_A) = \frac{1}{\pi} \left[\frac{GM_E}{R_E} \right] f(\gamma', \delta, \beta) \left(\frac{R_A}{R_E} \right)^{2-\gamma'} \quad (73)$$

with

$$f(\gamma', \delta, \beta) = 2\sqrt{\pi} \left(\frac{\delta - 3}{(\xi - 3)(\xi - 2\beta)} \right) \times \left\{ \frac{\Gamma[(\xi - 1)/2]}{\Gamma[\xi/2]} - \beta \frac{\Gamma[(\xi + 1)/2]}{\Gamma[(\xi + 2)/2]} \right\} \times \left\{ \frac{\Gamma[\delta/2]\Gamma[\gamma'/2]}{\Gamma[(\delta - 1)/2]\Gamma[(\gamma' - 1)/2]} \right\} \quad (74)$$

and $\xi = \gamma' + \delta - 2$. Similarly,

$$\sigma_{\parallel}^2(R) = \frac{1}{\pi} \left[\frac{GM_E}{R_E} \right] \left(\frac{\xi - 3}{\delta - 3} \right) f(\gamma', \delta, \beta) \left(\frac{R}{R_E} \right)^{2-\gamma'}. \quad (75)$$

In the simple case of a SIS with $\gamma' = \delta = \xi = 2$ and $\beta = 0$, we recover the well-known result

$$\sigma_{\parallel}^2(R) = \frac{1}{\pi} \left[\frac{GM_E}{R_E} \right] \quad (\text{SIS}). \quad (76)$$

From Eq. (73), one sees that the radial dependence of the stellar velocity dispersion depends on γ' only. All other parameters (i.e., δ , β , etc.) enter only into the normalization. Since the luminosity density (i.e., δ) and M_E are measured with little uncertainty, the measurement of $\langle \sigma_{\parallel}^2 \rangle (\leq R_A \neq R_E)$ immediately gives the density slope $\gamma'(\beta)$ (where β in general plays only a minor role). This is the basis of combining stellar dynamics with gravitational lensing to obtain not only the mass but also the density slope of ETGs.

We can estimate the change $\delta\gamma'$ from the observables. One finds to first order (assuming fixed values of β and δ)

$$\begin{aligned} \frac{\delta\sigma_{\parallel}}{\sigma_{\parallel}} (\leq R_A) &= \frac{1}{2} \frac{\delta M_E}{M_E} + \frac{1}{2} \left(\frac{\partial \log f}{\partial \log \gamma'} - \gamma' \log \left[\frac{R_A}{R_E} \right] \right) \frac{\delta\gamma'}{\gamma'} \\ &\equiv \frac{1}{2} \left(\frac{\delta M_E}{M_E} + \alpha_g \frac{\delta\gamma'}{\gamma'} \right). \end{aligned} \quad (77)$$

The second term in this equation was already derived by [Treu and Koopmans \(2002a\)](#). If we further assume the errors on M_E and σ_{\parallel} to be independent,

$$\langle \delta_{\gamma'}^2 \rangle \approx \alpha_g^{-2} \{ \langle \delta_{M_E}^2 \rangle + 4 \langle \delta_{\sigma_{\parallel}}^2 \rangle \}, \quad (78)$$

where δ_{\dots} indicate fractional errors. Since in general $\delta_{M_E} \ll \delta_{\sigma_{\parallel}}$, one finds the simple rule of thumb that the error $\delta_{\gamma'} \sim \delta_{\sigma_{\parallel}}$ for close-to-isothermal mass models, since $\alpha_g \sim 2$. This estimate is in very good agreement with the results from properly solving the Jeans equations for two-component mass models and justifies neglecting the mass errors ([Treu and Koopmans, 2004](#)).

C. Observational results

In this section we highlight some recent results on the study of early-type galaxies using strong gravitational lensing.

We focus on two aspects of strong gravitational lensing that have recently progressed rapidly and that have great promise in future galaxy structure and evolutions studies: (i) The combination of strong lensing, stellar kinematics, and stellar populations to constrain the inner stellar and dark-matter mass profiles of ETGs as a function of their mass and redshift and (ii) the use of simply parametrized and grid-based modeling of strong lenses to constrain the

level mass substructure in the inner regions of ETGs. We illustrate how lensing can address these two science drivers based mostly on recent results from the SLACS.

1. Sloan Lens ACS Survey

The SLACS gravitational lenses ([Bolton, Burles *et al.*, 2006, 2008](#); [Koopmans *et al.*, 2006](#); [Treu *et al.*, 2006, 2009](#); [Gavazzi *et al.*, 2007, 2008](#); [Bolton, Treu *et al.*, 2008](#); [Auger *et al.*, 2009](#); [Auger, Treu, Bolton *et al.*, 2010](#); [Newton *et al.*, 2011](#)) were selected from the spectroscopic data base of the SDSS based on the presence of absorption-dominated galaxy continuum at one redshift and nebular emission lines (Balmer series, [OII] 3727, or [OIII] 5007) at a higher redshift. The spectroscopic lens survey technique was first envisioned by [Warren *et al.* \(1998\)](#) and [Hewett *et al.* \(2000\)](#) following the discovery of the gravitational lens 0047 – 2808 through the presence of high-redshift Lyman- α emission in the spectrum of the targeted lower redshift elliptical galaxy. Further details of the SLACS approach are provided in [Bolton *et al.* \(2004, 2005\)](#). The SLACS survey includes candidates from the SDSS MAIN galaxy sample ([Strauss *et al.*, 2002](#)) in addition to candidates from the SDSS luminous red galaxy sample ([Eisenstein *et al.*, 2001](#)). Most candidates were selected on the basis of multiple emission lines, although several lens candidates were observed on the basis of secure [OII] 3727 line detections alone. By virtue of this spectroscopic selection method, all SLACS lenses and lens candidates have secure foreground (“lens”) and background (“source”) redshifts from the outset. Accurate redshifts such as these are essential for most quantitative scientific applications of strong lensing, as they are required to convert angles into physical lengths.

2. The density profiles of ETGs

When combining the total mass inside the Einstein radius given by detailed lensing modeling, usually accurate to a few percent ([Kochanek, 1991](#)), with measurements of stellar kinematics (either inside an aperture, along a slit, or through a 2D IFU measurement), a powerful constraint can be set on the average kinematically weighted density profile of ETGs inside the Einstein radius (or effective radius whichever is larger). This methodology, shortly outlined in Sec. VII.C.1, has been successfully applied initially by the lenses structure and dynamics (LSD) survey ([Koopmans and Treu, 2002, 2003](#); [Treu and Koopmans, 2002a, 2002b, 2004](#)) and more recently by the SLACS, the Boss Emission Line Lens 23 Survey (BELLS) ([Bolton *et al.*, 2012](#); [Brownstein *et al.*, 2012](#)), the Strong Lensing in the Legacy Survey (SL2S) ([Ruff *et al.*, 2011](#); [Gavazzi *et al.*, 2012](#)), and the Sloan Wide field camera Edge-on Late-type Lens Survey (SWELLS) ([Treu *et al.*, 2011](#)) for the case of spiral deflectors. Whereas the quality of the kinematic profiles in general cannot compete with that obtained for local ETGs (Sec. V), the combination of these data with strong lensing at higher redshifts has several major advantages.

First, even “low quality” lensing information combined with a single measurement of the stellar velocity dispersion can often be obtained out to $z \sim 1$ without a major telescope investment. This allows their inner mass profiles to be

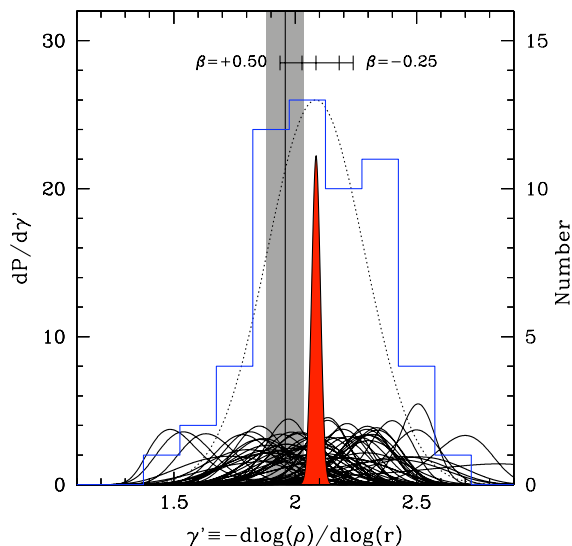


FIG. 22 (color online). The logarithmic density slopes of 58 SLACS early-type galaxies (thin solid curves). The filled curve is the joint posterior probability distribution of the average density slope of the sample. The histogram indicates the distribution of median values of the density slopes. The dotted Gaussian curve indicates the intrinsic scatter in γ'_{LD} (see text). We assume a Hernquist luminosity-density profile and no anisotropy (i.e., $\beta_r = 0$). The small dashes indicate the shift in average density slope for $\beta_r = +0.50, +0.25, -0.50$, and -0.25 (left to right), respectively. Note the reversal of the $\beta_r = -0.50$ and -0.25 dashes. The vertical solid line and gray region indicates the best-fit value and 68% C.L. interval, respectively, of the average density derived from scaling relations.

determined even at half the age of the Universe. Hence, evolution (in the ensemble average properties) of ETGs can be studied (Ruff *et al.*, 2011; Bolton *et al.*, 2012). Second, the additional use of strong lensing masses (plus constraints on its density slope near the Einstein radius) helps break the mass-sheet and mass-anisotropy degeneracies.

The results of the SLACS survey based on the combination of lensing and kinematic constraints for ~ 60 ETGs lenses have been described (Koopmans *et al.*, 2006, 2009; Czoske *et al.*, 2008; Barnabè *et al.*, 2009, 2010; Auger, Treu, Gavazzi *et al.*, 2010). Regarding the total mass-density profile, Koopmans *et al.* (2009) and Auger, Treu, Gavazzi *et al.* (2010) found that inside one effective radius massive elliptical galaxies with $M_{\text{eff}} \geq 3 \times 10^{10} M_{\odot}$ are well approximated by a power-law ellipsoid with an average logarithmic density slope of $\langle \gamma'_{LD} \rangle \equiv -d\log(\rho_{\text{tot}})/d\log(r) = 2.078 \pm 0.027$ (random error on mean) with an intrinsic scatter of 0.16 ± 0.02 (for isotropic orbits; results change as shown in Fig. 22 for reasonable amounts of anisotropy). Whereas this result is based on a separate analysis of the lensing and stellar kinematics and assumes spherical symmetry (or simple scaling relations), it has been confirmed by more sophisticated joint and self-consistent lensing and dynamical analysis methods based on axisymmetric mass distributions and two integral Schwarzschild modelings of the full lensing data and two-dimensional velocity fields (Czoske *et al.*, 2008; Barnabè *et al.*, 2009). Based on a subset of 16 lens ETGs with deep integral-field spectroscopy Barnabè *et al.* (2011) found

$\langle \gamma' \rangle = 2.074^{+0.043}_{-0.041}$ with an intrinsic scatter of $0.143^{+0.054}_{-0.014}$. Overall the internal structure of the SLACS ETGs at $z = 0.1-0.4$ is found to be perfectly consistent with that found for their nearby counterparts, as described in Sec. V.

The addition of weak gravitational lensing data to the strong lensing and dynamics analysis allows one to extend the measurement of the total mass-density profile well beyond the effective radii in an ensemble sense. With HST data, the weak-lensing signal is measurable for a sample of just a few tens of ETGs in the redshift range $z = 0.1-0.8$ (Gavazzi *et al.*, 2007; Auger, Treu, Gavazzi *et al.*, 2010; Lagattuta *et al.*, 2010). The two main results of the combined weak, strong, and dynamics analyses are that SLACS lenses have average virial mass $\sim 2 \times 10^{13} M_{\odot}$ and that their total mass-density profile is well described by a single isothermal sphere $\gamma' \approx 2$ out to ~ 100 effective radii. This result is remarkable because neither the stellar component nor the dark-matter halo are well described by single power laws, and yet their sum is. This total mass profile is well reproduced by the combination of a stellar component and a standard NFW halo (Gavazzi *et al.*, 2007) for sensible values of stellar mass-to-light ratio. This is very different from what is found at higher and lower masses (clusters and dwarfs) where typically a single isothermal sphere is not a good description of the total mass-density profile. The simplicity of the total mass-density profiles of ETGs has been sometimes called the “bulge-halo” conspiracy (Dutton and Treu, 2013), and it provides important constraints on theoretical models of ETGs formation, especially on parameters that drive the star formation efficiency like supernovae and nuclear feedback (Dubois *et al.*, 2013; Remus *et al.*, 2013).

The conclusion that can be drawn from these analyses is that ETGs on average have density profiles that are close to isothermal. However, one needs to keep in mind that there is an intrinsic scatter of $\sim 10\%$ in the logarithmic density slope between galaxies (i.e., they do not all have similar density profiles), which could be due to their formation history. This intrinsic scatter is comparable to studies of nearby galaxies (Gerhard *et al.*, 2001) based on stellar kinematics alone. The only dependence on third parameters identified so far is that between the slope and the stellar mass density inside the effective radius, where higher stellar mass density ETGs have steeper density slopes (Dutton and Treu, 2013). This tantalizing result is confirmed by the self-consistent axisymmetric modeling technique (Barnabè and Koopmans, 2007; Barnabè *et al.*, 2012) and proves that ETGs are at least a two parameter family even when it comes to their internal mass structure.

3. The stellar IMF and dark-matter fraction in ETGs

Strong lensing can accurately constrain the mass inside the Einstein radius. In combination with the luminosity inside the Einstein radius this yields a firm upper limit on the stellar mass-to-light ratio inside that radius (Brewer *et al.*, 2012). As discussed in Sec. II, given an optical infrared spectral energy distribution, modern stellar population synthesis models are believed to provide estimates of the stellar mass-to-light ratio that are accurate to within roughly old stellar populations like the one found in massive ETGs. In this case, the main source of uncertainty is the shape of the stellar initial mass function,

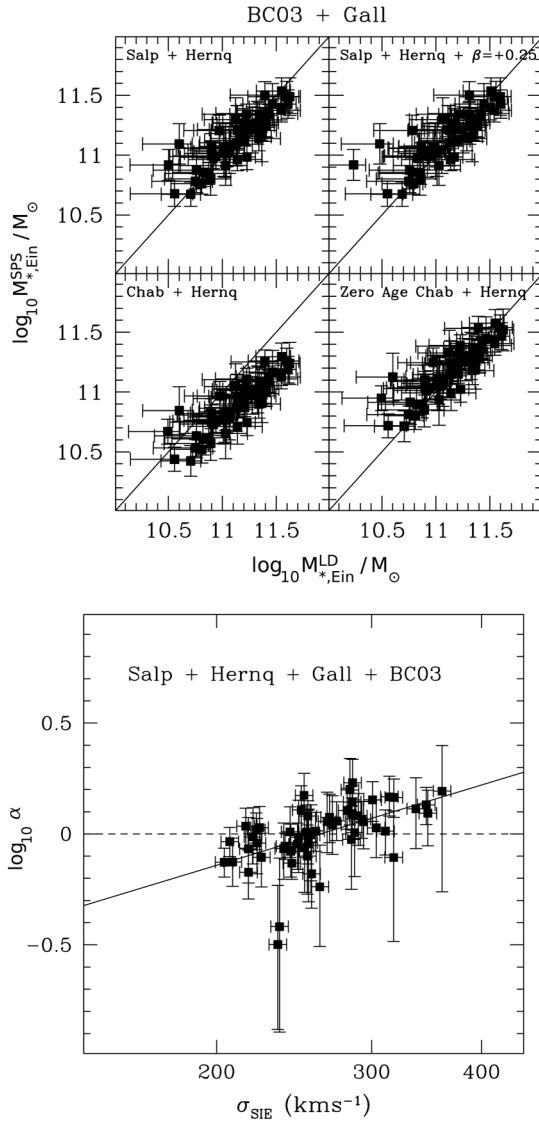


FIG. 23. Top: Comparison between stellar mass in the cylinder of radius equal to the Einstein radius as inferred from lensing and dynamical models (x axis) and that inferred from fitting stellar population synthesis models to the observed spectral energy distribution (y axis). The solid line indicates the identity. Stellar population synthesis models by [Bruzual and Charlot \(2003\)](#) are assumed together with an informative metallicity prior to [Gallazzi *et al.* \(2005\)](#). Bottom: Template mismatch parameter $\alpha \equiv M_{*,\text{Ein}}^{\text{LD}}/M_{*,\text{Ein}}^{\text{SPS}}$ for Salpeter IMF as a function of lensing velocity dispersion (left), stellar velocity dispersion (center), and V -band luminosity corrected to $z = 0.2$. A tentative positive trend with velocity dispersion is observed (solid line). The dashed line represents the trend expected for a universal Salpeter IMF.

which is needed to convert the observed luminosity (dominated by a small range of stellar masses) to the total mass in stars and stellar remnants. Thus, by combining gravitational lensing, stellar kinematics, and stellar population synthesis modeling, powerful new constraints can be set on the stellar IMF and the fraction of dark matter in the inner regions of ETGs (see Fig. 24). By means of additional information, like spatially resolved kinematics and/or simple assumptions on the functional form of the dark-matter density profile, one can break in part the degeneracy between the stellar IMF and the

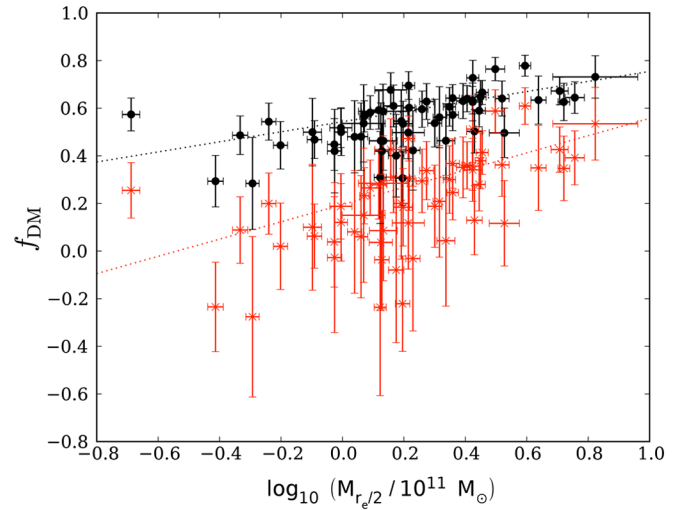


FIG. 24 (color online). Relations between the projected dark-matter fraction within half of the effective radius and M_*/r_e . Gray points are for a Salpeter IMF and black points are for a Chabrier IMF.

dark-matter fraction and derive realistic limits on either one ([Treu and Koopmans, 2004](#)) for limits on the dark-matter fraction inside the Einstein radius out to $z \sim 1$.

[Treu *et al.* \(2010\)](#) studied the stellar initial mass function of ETGs by comparing the stellar mass fraction inside one effective radius determined solely from lensing and stellar dynamics with that inferred from stellar population synthesis models. Whereas these limits are rather weak on a system-to-system basis, the combination of 56 SLACS ETGs allows a rather detailed comparison. The main result is that bottom-heavy IMFs such as those measured by [Salpeter \(1955\)](#) are strongly preferred over lightweight IMFs such as those proposed by [Chabrier \(2003\)](#), assuming standard NFW dark-matter density profiles. This result is further strengthened by [Auger, Treu, Gavazzi *et al.* \(2010\)](#) who modeled these systems in detail, including adiabatic contraction and weak-lensing constraints, and found that only heavy Salpeter-type IMF are consistent with the observed properties of ETGs. In combination with standard results based on spiral galaxy rotation curves (see Sec. III) and dynamical measurements of early-type galaxies (see Sec. V), these results indicated that the stellar initial mass function cannot be universal.

The lensing and kinematic studies by themselves ([Treu *et al.*, 2010](#)) also suggest that the IMF normalization varies with galaxy mass within the sample of SLACS lenses, if NFW halos are allowed (Fig. 23). However, the mass dependency within the SLACS sample becomes insignificant if the halos are allowed to contract in response to baryonic physics ([Auger, Treu, Gavazzi *et al.*, 2010](#)).

Several subsequent studies also point toward nonuniversal IMFs using independent techniques. For example, based on detailed modeling of weak stellar absorption features, [van Dokkum and Conroy \(2010\)](#) confirmed the lensing result in which the IMF of massive early-type galaxies are inconsistent with Chabrier. In addition, they provided the crucial suggestion that the extra mass is to be attributed to low-mass stars, with an overall IMF shape similar to Salpeter's. Detailed stellar dynamical modeling of spatially resolved velocity

fields of ETGs also adds important information. First, it provides an independent confirmation of the initial lensing results that Chabrier-like IMFs are disfavored for massive ETGs. Second, the local galaxy samples cover a large enough range in stellar mass to detect a trend in stellar mass-to-light normalization within ETGs themselves, assuming the inner mass-density profiles of their dark-matter halos can be modeled as power laws which are allowed to vary within a fixed range across the sample (Cappellari *et al.*, 2012, 2013a).

Overall there is good agreement between the dynamical, lensing, and stellar population probes (Dutton *et al.*, 2013). Given its broad implications, it is reassuring that many independent lines of evidence (Zaritsky *et al.*, 2012) contradict the simple hypothesis of a universal IMF, which has been a central tenet of extragalactic astronomy for the few past decades. Much work is currently under way to determine the exact form of the IMF, clarify systematic uncertainties, and investigate possible variations with morphology or other parameters [see, e.g., Spiniello *et al.* (2011, 2012, 2013), Dutton, Mendel, and Simard (2012), Sonnenfeld *et al.* (2012), Conroy *et al.* (2013), Ferreras *et al.* (2013), Goudfrooij and Kruijssen (2013), and Smith and Lucey (2013)].

4. Mass substructure in ETGs

Whereas the results described previously are concerned with the smooth mass distributions of ETGs, gravitational lensing can also measure the level of mass-density fluctuations, and, in particular, the amount of substructure in their inner regions. Thus, gravitational lensing provides an opportunity to directly measure the mass function of subhalos, irrespective of their stellar content. This is a stringent test of the nature of dark matter, since cold dark matter predicts that the subhalo mass function should go as $dN/nM \propto M^{-1.9}$ down to very small masses (Springel *et al.*, 2008).

The first lensing studies of this topic, based on the so-called flux-ratio anomalies (Mao and Schneider, 1998; Metcalf and Madau, 2001) of radio-loud lenses quasars from the Cosmic Lens All-Sky Survey (CLASS) (Dalal and Kochanek, 2002), indicated a level of substructure broadly consistent with the expectations of CDM cosmology. In the following decade, much work was devoted to understanding the systematic uncertainties associated with this method (Koopmans *et al.*, 2003; Kochanek and Dalal, 2004; Dobler and Keeton, 2006; Shin and Evans, 2008; Metcalf and Amara, 2012), but overall progress has been limited mostly by the small number of known quadruply imaged radio-loud quasars. Detailed comparisons with cosmological numerical simulations are challenging, owing to the need for high resolution and approximations related to the implementation of baryonic physics (Kochanek and Dalal, 2004; Mao *et al.*, 2004; Macciò *et al.*, 2006; Xu *et al.*, 2009, 2012). It also remains an open question whether some of these anomalies are caused by dark or luminous substructure (More *et al.*, 2008, 2009; Jackson *et al.*, 2010; Nierenberg *et al.*, 2012).

To overcome some of the limitations of flux-ratio anomaly systems (e.g., the position and mass of the substructure are highly degenerate so only statistical constraints can really be placed currently) and exploit the large samples of galaxy-galaxy strong lens systems, Koopmans (2005) developed a

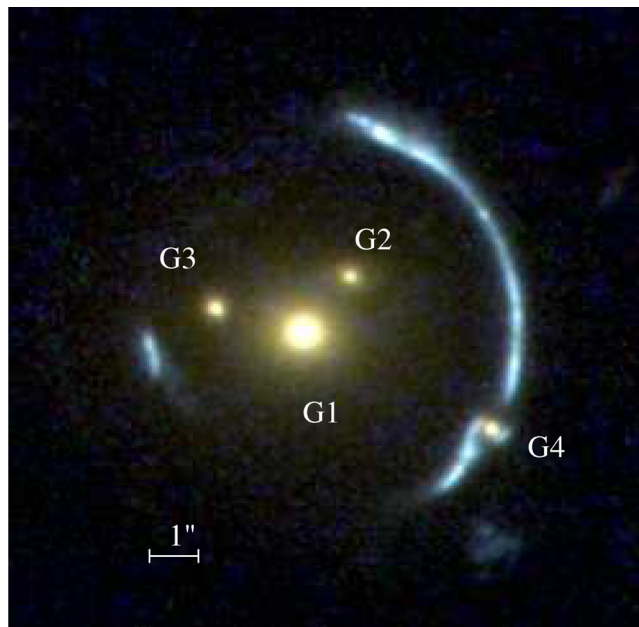


FIG. 25 (color online). Overview of the lens system the “Clone.” This false-color image was created from HST and WFPC2 images through filters F450W, F606W, and F814W.

new method based on the entire surface brightness distribution of the extended lens source. The information contained in thousands of pixels allows one to reconstruct the surface mass density of the deflector, pinpoint the position of possible substructures, and determine their masses [see also Vegetti and Koopmans (2009) for a complete Bayesian extension of this method]. Alternative methods have been developed by other groups to reconstruct on a grid the surface mass density of gravitational lenses, or their gravitational potential, albeit mostly with the goal of studying cosmology from gravitational time delays. The method developed by Suyu *et al.* (2009) is very similar in spirit to that of Vegetti and Koopmans (2009), while the one developed and applied by Saha *et al.* (2006) differs substantially. In the latter method the mass distribution is reconstructed on a grid using only multiple image positions as constraints. Thus the amount of freedom in the models is substantially larger and the choice of geometric priors becomes more important. Putting this class of model into a statistical framework is challenging although efforts are underway (Coles, 2008).

5. Luminous dwarf galaxies

A nice demonstration of these methodologies is provided by known luminous substructures in gravitational lens systems. For example, the system shown in Fig. 25 was discovered by Lin *et al.* (2009) and shows a bright arc with a dwarf galaxy (G4) splitting the giant arc on the sub-arcsec scale. Whereas this anomaly of the arc is caused by the dwarf galaxy, similar anomalies could in principle also be caused by dark substructure and be used to reconstruct their mass and position. Not all such cases, however, are as obvious as this case. The best reconstruction of the lensed arcs is shown in Fig. 26 (a galaxy surface brightness model has been subtracted) and a grid-based reconstruction of the potential and

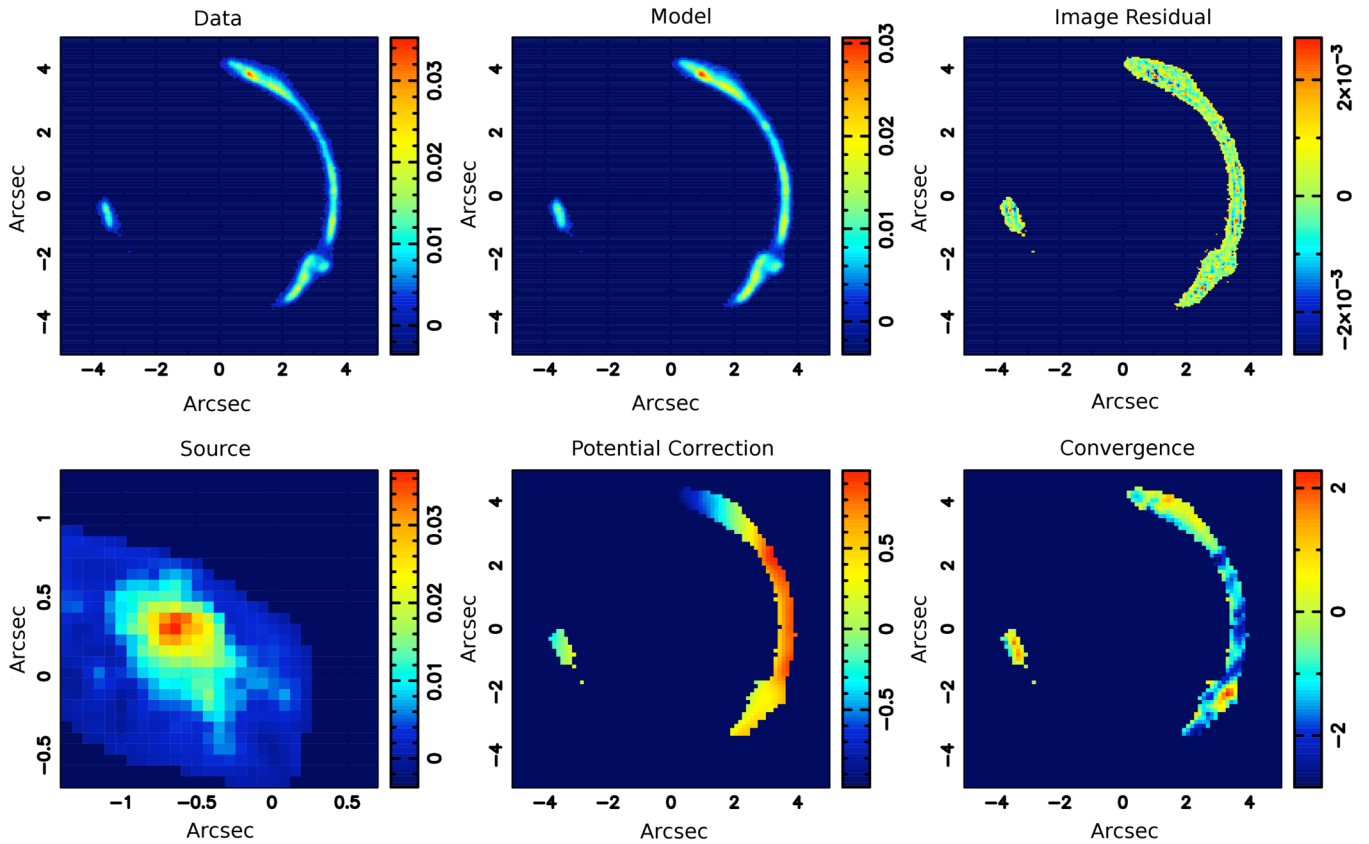


FIG. 26 (color online). Illustration of pixelized reconstruction of the source surface brightness and lens potential corrections of the lens system shown in Fig. 25 using the gravitational imaging technique. The top-left panel shows the data, consisting of the surface brightness of a highly distorted lensed source. The top-middle panel shows the model surface brightness, while the top-right one shows the image residuals (data model). The bottom-left panel shows the source surface brightness distribution reconstructed in the source plane (i.e., after “delensing”; note the zoomed-in angular scale). The bottom-middle panel shows the corrections to the gravitational potential, with respect to a smooth simply parametrized mass distribution. The bottom-right panel shows the inferred convergence, i.e., the projected surface mass distribution. Note the peak at the lower-right corner of the image corresponding to the satellite responsible for the curvature in the arc.

surface density (lower-right panel) has been constructed (Vegetti, Czoske, and Koopmans, 2010). A high overdensity is clearly visible at the position of the anomaly. Replacing this object by a tidally truncated pseudo-Jaffe mass model, a mass of $M_{\text{sub}} = (2.75 \pm 0.04) \times 10^{10} M_{\odot}$ inside its tidal radius of $r_t = 0.68$ arc sec is found. This result is robust against changes in the lens model. The satellite luminosity is $L_B = (1.6 \pm 0.8) \times 10^9 L_{\odot}$, leading to a total mass-to-light ratio within the tidal radius of $(M/L)_B = [(17.2 \pm 8.5) M/L_{\odot}] / L_{\odot}$. While this mass-to-light ratio is high compared to early-type dwarfs, it is also an upper limit since the extended emission is hard to measure due to the arc. Another demonstration of the power of this method is given by the analysis of the system SL2SJ08544-0121 by Suyu and Halkola (2010).

6. Dark substructures

A method is currently being applied to the SLACS lenses with the goal of quantifying the abundance of substructures independent of their luminosity. Two detections have been reported so far.

The first substructure detected via gravitational imaging is in the Jackpot system (Gavazzi *et al.*, 2008), which shows two concentric rings of sources at two redshifts. The inner ring of

this system, even though rather smooth, has a very high signal-to-noise ratio and is therefore quite suitable for the grid-based analysis method.

A simply parametrized elliptical power-law density model plus external shear provides a good fit to the data, but for a rather structured source model (Vegetti *et al.*, 2010). Figure 27 shows a reconstruction of the system down to the noise level where the source is more smooth, but a perturbation of the lensing potential is required at 4.3 kpc projected distance from the lens center (the feature in the upper left of the lower-right panel shows the corresponding overdensity).

Whereas there is a tradeoff between the complexity of the source and that of the lens potential, this can objectively be assessed through the Bayesian evidence (i.e., the probability of the data when marginalizing over the full posterior probability function) and the smooth-source plus more complex lens model is preferred at a (rough) equivalent of 16 σ significance (Vegetti *et al.*, 2010).

This detection is confirmed by modeling the substructure with a tidally truncated pseudo-Jaffe density profile (Vegetti *et al.*, 2010). The substructure mass is $M_{\text{sub}} = (3.51 \pm 0.15) \times 10^9 M_{\odot}$. A lower limit of $(M/L)_{V,\odot} \geq 120 M_{\odot} / L_{V,\odot}$ (3σ) is set inside a sphere of 0.3 kpc centered on the substructure ($r_{\text{tidal}} = 1.1$ kpc). This implies a projected dark-matter mass

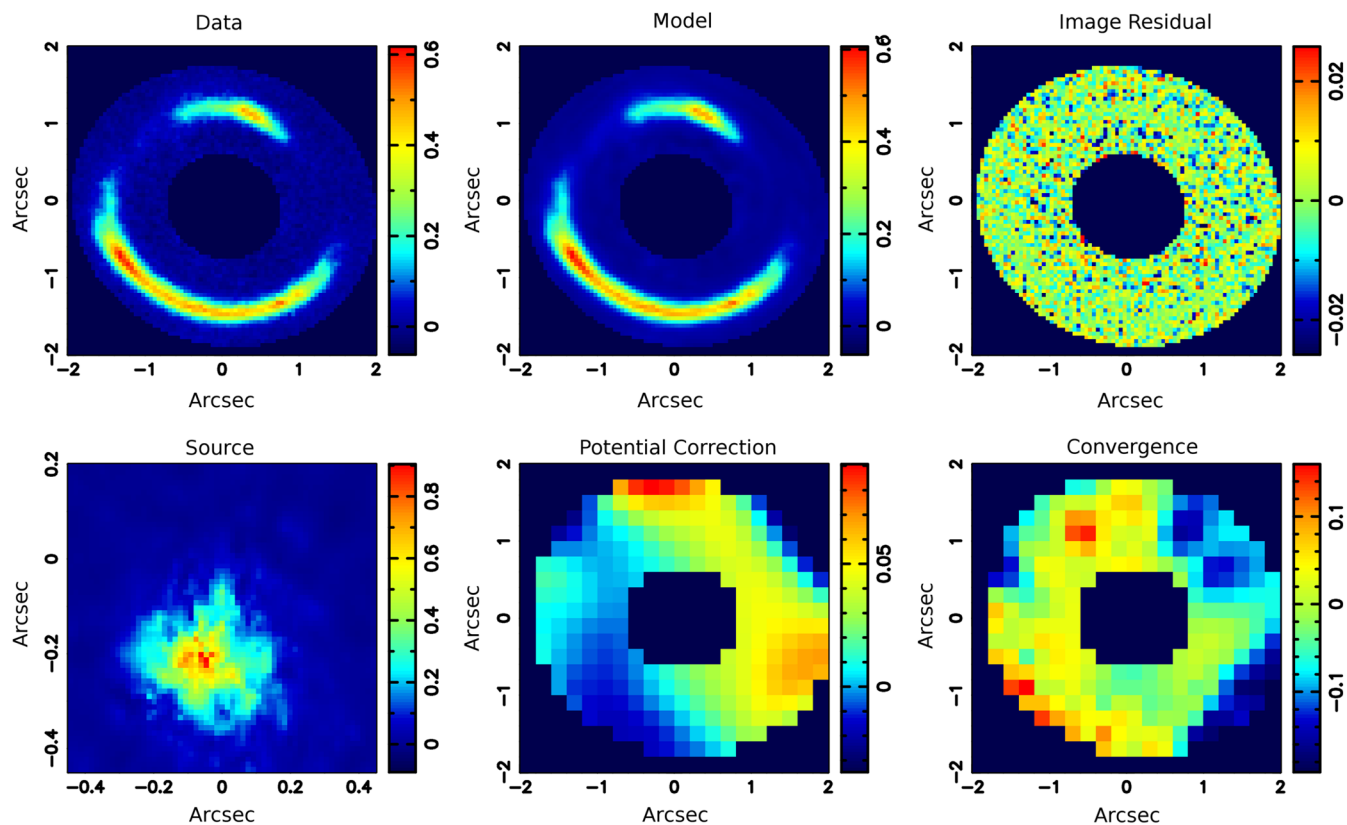


FIG. 27 (color online). Gravitational imaging analysis of the Jackpot gravitational lens system. The panels are as in Fig. 25. Note the convergence peak in the top-right portion of the bottom-right panel, corresponding to the detected substructure.

fraction in substructure at the radius of the inner Einstein ring of $f = 2.15^{+2.05}_{-1.25}\%$ (68% C.L.) in the mass range $4 \times 10^6 M_\odot$ to $4 \times 10^9 M_\odot$, assuming $\alpha = 1.9 \pm 0.1$ (with $dN/dm \propto m^{-\alpha}$). Assuming a flat prior on α , between 1.0 and 3.0, increases this to $f = 2.56^{+3.26}_{-1.50}\%$ (68% C.L.). The likelihood ratio is ~ 0.5 between these fractions and that from simulations ($f_{N\text{-body}} \approx 0.003$). More recently, a second detection has been reported in the CLASS gravitational lens system B1938 + 666 based on HST and Keck adaptive optics images (Vegetti *et al.*, 2012). Remarkably the satellite mass is only $2 \times 10^8 M_\odot$ and yet it is detected at redshift 0.881.

The inference on the substructure mass function based on just two systems is uncertain (Vegetti *et al.*, 2012), but so far the results are broadly consistent with those expected from numerical simulations. Effort is under way to refine those measurements by applying the gravitational imaging technique to larger samples of lenses (Vegetti *et al.*, 2012). Proving that the substructure is inside the ETG and not along the line of sight is actually challenging (Chen, Kravtsov, and Keeton, 2003; Chen, Koushiappas, and Zentner, 2011). At the moment the level of line-of-sight contamination is ill constrained.

D. Future prospects

The method of strong gravitational lensing has progressed significantly in the past decade, proving to be a fundamental tool for precision astrophysics and cosmology. Progress in the field has come from new observations of unprecedentedly large samples of lensed systems, a growing synergy with other

techniques (stellar kinematic and stellar population studies), and the development of new methodologies such as self-consistent lensing and dynamics and grid-based strong lensing. Whereas this research area is just too extensive for an exhaustive review here, we tried to illustrate the progress and potential of strong lensing by highlighting some recent results from the largest galaxy-scale strong lens survey to date, the SLACS survey. These examples demonstrate that valuable constraints can be set on the inner density profiles of ETGs as well as on their dark-matter mass fraction as a function of galaxy mass and cosmic time, their stellar IMF, and the level of mass substructure.

One obvious concern is that strong gravitational lenses are rare in the sky (approximately fewer than 1/100–1/1000 massive ETGs can be detected as strong lenses, depending on resolution and depth). However, even in an era when exquisite data can be gathered for much larger samples of nonlens galaxies, strong lensing still brings unique and extremely precise measurements of mass (typically to a few percent) which are independent of the standard assumptions and uncertainties of other more traditional methods, as discussed here. By combining strong gravitational lensing information with that inferred from other methods one can break many of the traditional degeneracies (e.g., mass anisotropy, IMF versus stellar mass) and achieve new insights into the formation and evolution of early-type galaxies. Furthermore strong lensing thrives at cosmological distances where other methods suffer from the inevitable loss in sensitivity and angular resolution. For example, as discussed, only by using strong lensing information can one determine, as a

function of cosmic time accurate mass profiles, the normalization of the stellar IMF and the abundance of dark substructures. Thus, strong lensing is an essential tool for any evolutionary study of the mass structure of ETGs.

Furthermore, the upcoming decade will see a revolution in the study of strong gravitational lens systems. At the moment, most strong lensing applications are limited by the number of known strong lens systems suitable for that particular application. The current samples, limited to only a few hundred galaxy-scale lenses, are insufficient to explore detailed trends in mass, redshifts, and other potentially illuminating parameters. However, the current and next generation of wide-field sky surveys (e.g., from Herschel-ALMA, DES, LSST, PanSTARRS, LOFAR, Euclid, KiDS, SKA, etc.) will enable the discovery of 10^3 – 10^5 galaxy-scale lens systems thus removing the limitations stemming from sample size once and for all. With only limited resources for detailed follow-up of individual sources at present, strong lenses will clearly become a high-priority target given the high density of information that they provide.

ACKNOWLEDGMENTS

We are grateful to Lia Athanassoula, Giuseppina Battaglia, Matt Bershady, James Bullock, Laurent Chemin, Enrico Maria Corsini, Nathan Deg, Ken Freeman, Dimitri Gadotti, Ortwin Gerhard, Stacy McGaugh, Kristine Spekkens, and Piet van der Kruit for useful discussions. Laurent Chemin, Octavio Valenzuela, and Giuseppina Battaglia are also thanked for providing Figs. 10, 11, and 18, respectively. Cory Wagner kindly improved the presentation of various figures, and two diligent referees provided valuable comments that improved various parts of this review. S. C. and L. M. W. acknowledge the support of the Natural Sciences and Engineering Research Council of Canada through respective Discovery grants. M. C. acknowledges support from a Royal Society University Research Fellowship. A. A. D. acknowledges support from the Canadian Institute for Theoretical Astrophysics (CITA) National Fellows program. H. H. and L. V. E. K. acknowledge support by NWO VIDI grants, while T. T. acknowledges support from the Packard Foundation through a Packard Research Fellowship.

REFERENCES

- Abadi, M. G., J. F. Navarro, M. Fardal, A. Babul, and M. Steinmetz, 2010, “Galaxy-induced transformation of dark matter haloes,” *Mon. Not. R. Astron. Soc.* **407**, 435.
- Agustsson, I., and T. G. Brainerd, 2006, “The Orientation of Satellite Galaxies: Evidence of Elongation in the Direction of the Host,” *Astrophys. J.* **644**, L25.
- Aihara, H., C. Allende Prieto, and D. e. An, 2011, “The Eighth Data Release of the Sloan Digital Sky Survey: First Data from SDSS-III,” *Astrophys. J. Suppl. Ser.* **193**, 29.
- Alaghband-Zadeh, S., *et al.*, 2012, “Integral field spectroscopy of $2.0 < z < 2.7$ submillimetre galaxies: gas morphologies and kinematics,” *Mon. Not. R. Astron. Soc.* **424**, 2232.
- Amorisco, N. C., A. Agnello, and N. W. Evans, 2013, “The core size of the Fornax dwarf spheroidal,” *Mon. Not. R. Astron. Soc.* **429**, L89.
- Amorisco, N. C., and N. W. Evans, 2012, “A Troublesome Past: Chemodynamics of the Fornax Dwarf Spheroidal,” *Astrophys. J.* **756**, L2.
- An, J., N. W. Evans, and A. J. Deason, 2012, “Mass estimators in the Gaia era,” *Mon. Not. R. Astron. Soc.* **420**, 2562.
- Andersen, D. R., and M. A. Bershady, 2013, “The Photometric and Kinematic Structure of Face-on Disk Galaxies. III. Kinematic Inclinations from H α Velocity Fields,” *Astrophys. J.* **768**, 41.
- Andersen, D. R., M. A. Bershady, L. S. Sparke, J. S. Gallagher III, E. M. Wilcots, W. van Driel, and D. Monnier-Ragaine, 2006, “The Photometric and Kinematic Structure of Face-on Disk Galaxies. I. Sample Definition, H α Integral Field Spectroscopy, and H I Line Widths,” *Astrophys. J. Suppl. Ser.* **166**, 505.
- Arnold, J. A., A. J. Romanowsky, J. P. Brodie, L. Chomiuk, L. R. Spitler, J. Strader, A. J. Benson, and D. A. Forbes, 2011, “The Fossil Record of Two-phase Galaxy Assembly: Kinematics and Metallicities in the Nearest S0 Galaxy,” *Astrophys. J.* **736**, L26.
- Arnold, R., P. T. de Zeeuw, and C. Hunter, 1994, “Orbital Content and Velocity Fields of Triaxial Galaxies,” *Mon. Not. R. Astron. Soc.* **271**, 924 [<http://adsabs.harvard.edu/abs/1994MNRAS.271..924A>].
- Ascasibar, Y., and S. Gottlöber, 2008, “The dynamical structure of dark matter haloes,” *Mon. Not. R. Astron. Soc.* **386**, 2022.
- Athanassoula, E., 1983, Ed., “Internal kinematics and dynamics of galaxies,” *Proceedings of the Symposium, Université de Franche-Comte, Besancon, France, 1982*, IAU Symposium, No. 100 (Reidel, Dordrecht) [<http://adsabs.harvard.edu/abs/1983IAUS..100.....A>].
- Athanassoula, E., 2002, “Bar-Halo Interaction and Bar Growth,” *Astrophys. J.* **569**, L83.
- Athanassoula, E., 2003, “What determines the strength and the slowdown rate of bars?,” *Mon. Not. R. Astron. Soc.* **341**, 1179.
- Athanassoula, E., R. E. G. Machado, and S. A. Rodionov, 2013, “Bar formation and evolution in disc galaxies with gas and a triaxial halo: morphology, bar strength and halo properties,” *Mon. Not. R. Astron. Soc.* **429**, 1949.
- Auger, M. W., T. Treu, A. S. Bolton, R. Gavazzi, L. V. E. Koopmans, P. J. Marshall, K. Bundy, and L. A. Moustakas, 2009, “The Sloan Lens ACS Survey. IX. Colors, Lensing, and Stellar Masses of Early-Type Galaxies,” *Astrophys. J.* **705**, 1099.
- Auger, M. W., T. Treu, A. S. Bolton, R. Gavazzi, L. V. E. Koopmans, P. J. Marshall, L. A. Moustakas, and S. Burles, 2010, “The Sloan Lens ACS Survey. X. Stellar, Dynamical, and Total Mass Correlations of Massive Early-type Galaxies,” *Astrophys. J.* **724**, 511.
- Auger, M. W., T. Treu, R. Gavazzi, A. S. Bolton, L. V. E. Koopmans, and P. J. Marshall, 2010, “Dark Matter Contraction and the Stellar Content of Massive Early-type Galaxies: Disfavoring ‘Light’ Initial Mass Functions,” *Astrophys. J.* **721**, L163.
- Baade, W., 1944, “The Resolution of Messier 32, NGC 205, and the Central Region of the Andromeda Nebula,” *Astrophys. J.* **100**, 137.
- Bahcall, J. N., 1984, “K giants and the total amount of matter near the sun,” *Astrophys. J.* **287**, 926.
- Bahcall, J. N., and S. Casertano, 1985, “Some possible regularities in the missing mass problem,” *Astrophys. J.* **293**, L7.
- Bahcall, J. N., M. Schmidt, and R. M. Soneira, 1982, “On the interpretation of rotation curves measured at large galactocentric distances,” *Astrophys. J.* **258**, L23.
- Bahcall, J. N., and R. M. Soneira, 1980, “The universe at faint magnitudes. I - Models for the galaxy and the predicted star counts,” *Astrophys. J. Suppl. Ser.* **44**, 73.
- Bailey, M. E., and J. MacDonald, 1981, “A comparison between velocity dispersion profiles of de Vaucouleurs and King galaxy models,” *Mon. Not. R. Astron. Soc.* **194**, 195 [<http://adsabs.harvard.edu/abs/1981MNRAS.194..195B>].

- Bailin, J., *et al.*, 2005, “Internal Alignment of the Halos of Disk Galaxies in Cosmological Hydrodynamic Simulations,” *Astrophys. J.* **627**, L17.
- Bania, T.M., and F.J. Lockman, 1984, “A survey of the latitude structure of galactic H I on small angular scales,” *Astrophys. J. Suppl. Ser.* **54**, 513.
- Bardeen, J.M., J.R. Bond, N. Kaiser, and A.S. Szalay, 1986, “The statistics of peaks of Gaussian random fields,” *Astrophys. J.* **304**, 15.
- Barnabè, M., M.W. Auger, T. Treu, L.V.E. Koopmans, A.S. Bolton, O. Czoske, and R. Gavazzi, 2010, “The non-evolving internal structure of early-type galaxies: the case study SDSSJ0728 + 3835 at $z = 0.206$,” *Mon. Not. R. Astron. Soc.* **406**, 2339.
- Barnabè, M., O. Czoske, L.V.E. Koopmans, T. Treu, and A.S. Bolton, 2011, “Two-dimensional kinematics of SLACS lenses - III. Mass structure and dynamics of early-type lens galaxies beyond $z \sim 0.1$,” *Mon. Not. R. Astron. Soc.* **415**, 2215.
- Barnabè, M., O. Czoske, L.V.E. Koopmans, T. Treu, A.S. Bolton, and R. Gavazzi, 2009, “Two-dimensional kinematics of SLACS lenses - II. Combined lensing and dynamics analysis of early-type galaxies at $z = 0.08-0.33$,” *Mon. Not. R. Astron. Soc.* **399**, 21.
- Barnabè, M., A.A. Dutton, P.J. Marshall, M.W. Auger, B.J. Brewer, T. Treu, A.S. Bolton, D.C. Koo, and L.V.E. Koopmans, 2012, “The SWELLS survey - IV. Precision measurements of the stellar and dark matter distributions in a spiral lens galaxy,” *Mon. Not. R. Astron. Soc.* **423**, 1073.
- Barnabè, M., and L.V.E. Koopmans, 2007, “A Unifying Framework for Self-consistent Gravitational Lensing and Stellar Dynamics Analyses of Early-Type Galaxies,” *Astrophys. J.* **666**, 726.
- Bartelmann, M., and P. Schneider, 2001, “Weak gravitational lensing,” *Phys. Rep.* **340**, 291.
- Battaglia, G., A. Helmi, and M. Breddels, 2013, “Internal kinematics and dynamical models of dwarf spheroidal galaxies around the Milky Way,” [arXiv:1305.5965](https://arxiv.org/abs/1305.5965).
- Battaglia, G., A. Helmi, H. Morrison, P. Harding, E.W. Olszewski, M. Mateo, K.C. Freeman, J. Norris, and S.A. Shectman, 2005, “The radial velocity dispersion profile of the Galactic halo: constraining the density profile of the dark halo of the Milky Way,” *Mon. Not. R. Astron. Soc.* **364**, 433.
- Battaglia, G., A. Helmi, E. Tolstoy, M. Irwin, V. Hill, and P. Jablonka, 2008, “The Kinematic Status and Mass Content of the Sculptor Dwarf Spheroidal Galaxy,” *Astrophys. J.* **681**, L13.
- Battaglia, G., E. Tolstoy, A. Helmi, M. Irwin, P. Parisi, V. Hill, and P. Jablonka, 2011, “Study of the Sextans dwarf spheroidal galaxy from the DART Ca II triplet survey,” *Mon. Not. R. Astron. Soc.* **411**, 1013.
- Baugh, C.M., C.G. Lacey, C.S. Frenk, G.L. Granato, L. Silva, A. Bressan, A.J. Benson, and S. Cole, 2007, in *The Nature of (Sub) millimeter Galaxies in Hierarchical Models*, edited by A.J. Baker, J. Glenn, A.I. Harris, J.G. Mangum, and M.S. Yun, Astronomical Society of the Pacific Conference Series Vol. 375, From Z-Machines to ALMA: (Sub)Millimeter Spectroscopy of Galaxies, p. 7 [<http://adsabs.harvard.edu/abs/2007ASPC..375....7B>].
- Behroozi, P.S., C. Conroy, and R.H. Wechsler, 2010, “A Comprehensive Analysis of Uncertainties Affecting the Stellar Mass-Halo Mass Relation for $0 < z < 4$,” *Astrophys. J.* **717**, 379.
- Behroozi, P.S., R.H. Wechsler, and C. Conroy, 2013, “The Average Star Formation Histories of Galaxies in Dark Matter Halos from $z = 0-8$,” *Astrophys. J.* **770**, 57.
- Bell, E.F., and R.S. de Jong, 2000, “The stellar populations of spiral galaxies,” *Mon. Not. R. Astron. Soc.* **312**, 497.
- Bell, E.F., and R.S. de Jong, 2001, “Stellar Mass-to-Light Ratios and the Tully-Fisher Relation,” *Astrophys. J.* **550**, 212.
- Bell, E.F., D.H. McIntosh, N. Katz, and M.D. Weinberg, 2003, “The Optical and Near-Infrared Properties of Galaxies. I. Luminosity and Stellar Mass Functions,” *Astrophys. J. Suppl. Ser.* **149**, 289.
- Beninelli, O., 1991, “Abel integral equation inversion and deconvolution by multi-Gaussian approximation,” *Astrophys. J.* **366**, 599.
- Bershady, M.A., T.P.K. Martinsson, M.A.W. Verheijen, K.B. Westfall, D.R. Andersen, and R.A. Swaters, 2011, “Galaxy Disks are Submaximal,” *Astrophys. J.* **739**, L47.
- Bershady, M.A., M.A.W. Verheijen, R.A. Swaters, D.R. Andersen, K.B. Westfall, and T. Martinsson, 2010, “The DiskMass Survey. I. Overview,” *Astrophys. J.* **716**, 198.
- Bershady, M.A., M.A.W. Verheijen, K.B. Westfall, D.R. Andersen, R.A. Swaters, and T. Martinsson, 2010, “The DiskMass Survey. II. Error Budget,” *Astrophys. J.* **716**, 234.
- Bertin, G., L. Ciotti, and M. Del Principe, 2002, “Weak homology of elliptical galaxies,” *Astron. Astrophys.* **386**, 149.
- Bertin, G., R.P. Saglia, and M. Stiavelli, 1992, “Elliptical galaxies with dark matter. I - Self-consistent models. II - Optimal luminous-dark matter decomposition for a sample of bright objects,” *Astrophys. J.* **384**, 423.
- Bertola, F., D. Bettoni, L. Rusconi, and G. Sedmak, 1984, “Stellar versus gaseous kinematics in E and SO galaxies,” *Astron. J.* **89**, 356.
- Bertone, G., D. Hooper, and J. Silk, 2005, “Particle dark matter: evidence, candidates and constraints,” *Phys. Rep.* **405**, 279.
- Bezanson, R., *et al.*, 2011, “Redshift Evolution of the Galaxy Velocity Dispersion Function,” *Astrophys. J.* **737**, L31.
- Bica, E., and D. Alloin, 1986, “A base of star clusters for stellar population synthesis,” *Astron. Astrophys.* **162**, 21 [<http://adsabs.harvard.edu/abs/1986A%26A...162...21B>].
- Bicknell, G.V., T.E.G. Bruce, D. Carter, and N.E.B. Killeen, 1989, “The stellar dynamics of NGC 1399,” *Astrophys. J.* **336**, 639.
- Binney, J., 1978, “On the rotation of elliptical galaxies,” *Mon. Not. R. Astron. Soc.* **183**, 501 [<http://adsabs.harvard.edu/abs/1978MNRAS.183..501B>].
- Binney, J., 2010a, “Distribution functions for the Milky Way,” *Mon. Not. R. Astron. Soc.* **401**, 2318.
- Binney, J., O. Gerhard, and D. Spergel, 1997, “The photometric structure of the inner Galaxy,” *Mon. Not. R. Astron. Soc.* **288**, 365.
- Binney, J., and G.A. Mamon, 1982, “M/L and velocity anisotropy from observations of spherical galaxies, or must M87 have a massive black hole?,” *Mon. Not. R. Astron. Soc.* **200**, 361 [<http://adsabs.harvard.edu/abs/1982MNRAS.200..361B>].
- Binney, J., and P. McMillan, 2011, “Models of our Galaxy - II,” *Mon. Not. R. Astron. Soc.* **413**, 1889.
- Binney, J., and S. Tremaine, 2008, *Galactic Dynamics* (Princeton University Press, Princeton, NJ), 2nd ed.
- Binney, J.J., 2010b, “Joint Discussion 5 Modelling the Milky Way in the Era of Gaia,” *Highlights of Astronomy* **15**, 173.
- Binney, J.J., R.L. Davies, and G.D. Illingworth, 1990, “Velocity mapping and models of the elliptical galaxies NGC 720, NGC 1052, and NGC 4697,” *Astrophys. J.* **361**, 78.
- Blais-Ouellette, S., 2000, “Distribution de la matière sombre dans les galaxies spirales,” Ph.D. thesis (Université de Montréal).
- Blandford, R., and R. Narayan, 1986, “Fermat’s principle, caustics, and the classification of gravitational lens images,” *Astrophys. J.* **310**, 568.
- Blanton, M.R., and S. Roweis, 2007, “K-Corrections and Filter Transformations in the Ultraviolet, Optical, and Near-Infrared,” *Astron. J.* **133**, 734.
- Blitz, L., and D.N. Spergel, 1991, “Direct evidence for a bar at the Galactic center,” *Astrophys. J.* **379**, 631.

- Blumenthal, G. R., S. M. Faber, R. Flores, and J. R. Primack, 1986, “Contraction of dark matter galactic halos due to baryonic infall,” *Astrophys. J.* **301**, 27.
- Blumenthal, G. R., S. M. Faber, J. R. Primack, and M. J. Rees, 1984, “Formation of galaxies and large-scale structure with cold dark matter,” *Nature (London)* **311**, 517.
- Bolatto, A. D., A. K. Leroy, E. Rosolowsky, F. Walter, and L. Blitz, 2008, “The Resolved Properties of Extragalactic Giant Molecular Clouds,” *Astrophys. J.* **686**, 948.
- Bolton, A. S., S. Burles, L. V. E. Koopmans, T. Treu, R. Gavazzi, L. A. Moustakas, R. Wayth, and D. J. Schlegel, 2008, “The Sloan Lens ACS Survey. V. The Full ACS Strong-Lens Sample,” *Astrophys. J.* **682**, 964.
- Bolton, A. S., S. Burles, L. V. E. Koopmans, T. Treu, and L. A. Moustakas, 2005, “SDSS J140228.22 + 632133.3: A New Spectroscopically Selected Gravitational Lens,” *Astrophys. J.* **624**, L21.
- Bolton, A. S., S. Burles, L. V. E. Koopmans, T. Treu, and L. A. Moustakas, 2006, “The Sloan Lens ACS Survey. I. A Large Spectroscopically Selected Sample of Massive Early-Type Lens Galaxies,” *Astrophys. J.* **638**, 703.
- Bolton, A. S., S. Burles, D. J. Schlegel, D. J. Eisenstein, and J. Brinkmann, 2004, “Sloan Digital Sky Survey Spectroscopic Lens Search. I. Discovery of Intermediate-Redshift Star-forming Galaxies behind Foreground Luminous Red Galaxies,” *Astron. J.* **127**, 1860.
- Bolton, A. S., S. Rappaport, and S. Burles, 2006, Constraint on the post-Newtonian parameter γ on galactic size scales, *Phys. Rev. D* **74**, 061501.
- Bolton, A. S., T. Treu, L. V. E. Koopmans, R. Gavazzi, L. A. Moustakas, S. Burles, D. J. Schlegel, and R. Wayth, 2008, “The Sloan Lens ACS Survey. VII. Elliptical Galaxy Scaling Laws from Direct Observational Mass Measurements,” *Astrophys. J.* **684**, 248.
- Bolton, A. S., *et al.*, 2012, “The BOSS Emission-Line Lens Survey. II. Investigating Mass-density Profile Evolution in the SLACS + BELLS Strong Gravitational Lens Sample,” *Astrophys. J.* **757**, 82.
- Bosma, A., 1978, “The distribution and kinematics of neutral hydrogen in spiral galaxies of various morphological types,” Ph.D. thesis (University of Groningen).
- Bosma, A., Y. Byun, K. C. Freeman, and E. Athanassoula, 1992, “The opacity of spiral disks,” *Astrophys. J.* **400**, L21.
- Bottema, R., 1993, “The Stellar Kinematics of Galactic Disks,” *Astron. Astrophys.* **275**, 16 [<http://adsabs.harvard.edu/abs/1993A%26A...275...16B>].
- Bournaud, F., P. A. Duc, and E. Emsellem, 2008, “High-resolution simulations of galaxy mergers: resolving globular cluster formation,” *Mon. Not. R. Astron. Soc.* **389**, L8.
- Bovy, J., D. W. Hogg, and H. W. Rix, 2009, “Galactic Masers and the Milky Way Circular Velocity,” *Astrophys. J.* **704**, 1704.
- Bovy, J., and S. Tremaine, 2012, “On the Local Dark Matter Density,” *Astrophys. J.* **756**, 89.
- Braine, J., *et al.*, 1993, “A CO(1-0) and CO(2-1) survey of nearby spiral galaxies. I - Data and observations,” *Astron. Astrophys. Suppl. Ser.* **97**, 887 [<http://adsabs.harvard.edu/abs/1993A%26AS...97..887B>].
- Brainerd, T. G., 2010, “Multiple Weak Deflections in Galaxy-Galaxy Lensing,” *Astrophys. J.* **713**, 603.
- Brainerd, T. G., R. D. Blandford, and I. Smail, 1996, “Weak Gravitational Lensing by Galaxies,” *Astrophys. J.* **466**, 623.
- Brand, J., and L. Blitz, 1993, “The Velocity Field of the Outer Galaxy,” *Astron. Astrophys.* **275**, 67 [<http://adsabs.harvard.edu/abs/1993A%26A...275...67B>].
- Breddels, M. A., and A. Helmi, 2013, “Model comparison of the dark matter profiles of Fornax, Sculptor, Carina and Sextans,” [arXiv:1304.2976](https://arxiv.org/abs/1304.2976).
- Breddels, M. A., A. Helmi, R. C. E. van den Bosch, G. van de Ven, and G. Battaglia, 2013, “Orbit-based dynamical models of the Sculptor dSph galaxy,” *Mon. Not. R. Astron. Soc.* **433**, 3173.
- Brewer, B. J., A. A. Dutton, T. Treu, M. W. Auger, P. J. Marshall, M. Barnabè, A. S. Bolton, D. C. Koo, and L. V. E. Koopmans, 2012, “The SWELLS survey - III. Disfavouring ‘heavy’ initial mass functions for spiral lens galaxies,” *Mon. Not. R. Astron. Soc.* **422**, 3574.
- Briggs, F. H., 1990, “Rules of behavior for galactic WARPS,” *Astrophys. J.* **352**, 15.
- Brodie, J. P., and J. Strader, 2006, “Extragalactic Globular Clusters and Galaxy Formation,” *Annu. Rev. Astron. Astrophys.* **44**, 193.
- Brownstein, J. R., *et al.*, 2012, “The BOSS Emission-Line Lens Survey (BELLS). I. A Large Spectroscopically Selected Sample of Lens Galaxies at Redshift 0.5,” *Astrophys. J.* **744**, 41.
- Brunthaler, A., *et al.*, 2011, “The Bar and Spiral Structure Legacy (BeSSeL) survey: Mapping the Milky Way with VLBI astrometry,” *Astron. Nachr.* **332**, 461.
- Bruzual, G., 1983, “Spectral evolution of galaxies. I - Early-type systems,” *Astrophys. J.* **273**, 105.
- Bruzual, G., 2007, “Stellar Populations: High Spectral Resolution Libraries. Improved TP-AGB Treatment,” edited by A. Vallenari, R. Tantalo, L. Portinari, and A. Moretti, in *From Stars to Galaxies: Building the Pieces to Build Up the Universe*, Astronomical Society of the Pacific Conference Series Vol. 374, p. 303 [<http://adsabs.harvard.edu/abs/2007ASPC..374..303B>].
- Bruzual, G., and S. Charlot, 1993, “Spectral evolution of stellar populations using isochrone synthesis,” *Astrophys. J.* **405**, 538.
- Bruzual, G., and S. Charlot, 2003, “Stellar population synthesis at the resolution of 2003,” *Mon. Not. R. Astron. Soc.* **344**, 1000.
- Bundy, K., R. S. Ellis, C. J. Conselice, J. E. Taylor, M. C. Cooper, C. N. A. Willmer, B. J. Weiner, A. L. Coil, K. G. Noeske, and P. R. M. Eisenhardt, 2006, “The Mass Assembly History of Field Galaxies: Detection of an Evolving Mass Limit for Star-Forming Galaxies,” *Astrophys. J.* **651**, 120.
- Burbidge, E. M., and G. R. Burbidge, 1975, “The Masses of Galaxies,” in *Galaxies and the Universe* (University of Chicago Press, Chicago, IL), p. 81 [<http://adsabs.harvard.edu/abs/1975gaun.book...81B>].
- Burkert, A., 1995, “The Structure of Dark Matter Halos in Dwarf Galaxies,” *Astrophys. J.* **447**, L25.
- Buzzoni, A., 1989, “Evolutionary population synthesis in stellar systems. I - A global approach,” *Astrophys. J. Suppl. Ser.* **71**, 817.
- Capaccioli, M., M. Vietri, E. V. Held, and H. Lorenz, 1991, “Is the standard elliptical NGC 3379 a triaxial disk galaxy?,” *Astrophys. J.* **371**, 535.
- Cappellari, M., 2008, “Measuring the inclination and mass-to-light ratio of axisymmetric galaxies via anisotropic Jeans models of stellar kinematics,” *Mon. Not. R. Astron. Soc.* **390**, 71.
- Cappellari, M., and R. M. McDermid, 2005, “The nuclear orbital distribution in galaxies as a fossil record of black hole formation from integral-field spectroscopy,” *Classical Quantum Gravity* **22**, S347.
- Cappellari, M., *et al.*, 2006, “The SAURON project - IV. The mass-to-light ratio, the virial mass estimator and the Fundamental Plane of elliptical and lenticular galaxies,” *Mon. Not. R. Astron. Soc.* **366**, 1126 [<http://adsabs.harvard.edu/abs/2006MNRAS.366.1126C>].
- Cappellari, M., *et al.*, 2007, “The SAURON project - X. The orbital anisotropy of elliptical and lenticular galaxies: revisiting the $(V/\sigma, \epsilon)$ diagram with integral-field stellar kinematics,” *Mon. Not. R. Astron. Soc.* **379**, 418.

- Cappellari, M., *et al.*, 2011, “The ATLAS^{3D} project - I. A volume-limited sample of 260 nearby early-type galaxies: science goals and selection criteria,” *Mon. Not. R. Astron. Soc.* **413**, 813.
- Cappellari, M., *et al.*, 2012, “Systematic variation of the stellar initial mass function in early-type galaxies,” *Nature (London)* **484**, 485.
- Cappellari, M., *et al.*, 2013a, “The ATLAS^{3D} project - XX. Mass-size and mass- σ distributions of early-type galaxies: bulge fraction drives kinematics, mass-to-light ratio, molecular gas fraction and stellar initial mass function,” *Mon. Not. R. Astron. Soc.* **432**, 1862.
- Cappellari, M., *et al.*, 2013b, “The ATLAS^{3D} project - XV. Benchmark for early-type galaxies scaling relations from 260 dynamical models: mass-to-light ratio, dark matter, Fundamental Plane and Mass Plane,” *Mon. Not. R. Astron. Soc.* **432**, 1709.
- Carignan, C., and K. C. Freeman, 1985, “Basic parameters of dark halos in late-type spirals,” *Astrophys. J.* **294**, 494.
- Casertano, S., 1983, “Rotation curve of the edge-on spiral galaxy NGC 5907: disc and halo masses,” *Mon. Not. R. Astron. Soc.* **203**, 735 [<http://adsabs.harvard.edu/abs/1983MNRAS.203..735C>].
- Cassisi, S., M. Castellani, and V. Castellani, 1997, “Intermediate-age metal deficient stellar populations: the case of metallicity $Z = 0.00001$,” *Astron. Astrophys.* **317**, 108 [<http://adsabs.harvard.edu/abs/1997A%26A...317..108C>].
- Catena, R., and P. Ullio, 2010, “A novel determination of the local dark matter density,” *J. Cosmol. Astropart. Phys.* **08**, 004.
- Catena, R., and P. Ullio, 2012, “The local dark matter phase-space density and impact on WIMP direct detection,” *J. Cosmol. Astropart. Phys.* **05**, 005.
- Catinella, B., M. P. Haynes, and R. Giovanelli, 2007, “Rotational Widths for Use in the Tully-Fisher Relation. II. The Impact of Surface Brightness,” *Astron. J.* **134**, 334.
- Cayatte, V., C. Kotanyi, C. Balkowski, and J. H. van Gorkom, 1994, “A very large array survey of neutral hydrogen in Virgo Cluster spirals. 3: Surface density profiles of the gas,” *Astron. J.* **107**, 1003.
- Chabrier, G., 2003, “Galactic Stellar and Substellar Initial Mass Function,” *Publ. Astron. Soc. Pac.* **115**, 763.
- Charlot, S., and A. G. Bruzual, 1991, “Stellar population synthesis revisited,” *Astrophys. J.* **367**, 126.
- Charlot, S., G. Worthey, and A. Bressan, 1996, “Uncertainties in the Modeling of Old Stellar Populations,” *Astrophys. J.* **457**, 625.
- Chemin, L., C. Carignan, N. Drouin, and K. C. Freeman, 2006, “HI Studies of the Sculptor Group Galaxies. VIII. The Background Galaxies: NGC 24 and NGC 45,” *Astron. J.* **132**, 2527.
- Chemin, L., C. Carignan, and T. Foster, 2009, “HI Kinematics and Dynamics of Messier 31,” *Astrophys. J.* **705**, 1395.
- Chemin, L., and O. Hernandez, 2009, “A slow bar in a dark matter dominated galaxy,” *Astron. Astrophys.* **499**, L25.
- Chemin, L., *et al.*, 2006, “A Virgo high-resolution $H\alpha$ kinematical survey - II. The Atlas,” *Mon. Not. R. Astron. Soc.* **366**, 812 [<http://adsabs.harvard.edu/abs/2006MNRAS.366..812C>].
- Chen, C. W., P. Côté, A. A. West, E. W. Peng, and L. Ferrarese, 2010, “Homogeneous UGRIZ Photometry for ACS Virgo Cluster Survey Galaxies: A Non-parametric Analysis from SDSS Imaging,” *Astrophys. J. Suppl. Ser.* **191**, 1.
- Chen, J., S. M. Koushiappas, and A. R. Zentner, 2011, “The Effects of Halo-to-halo Variation on Substructure Lensing,” *Astrophys. J.* **741**, 117.
- Chen, J., A. V. Kravtsov, and C. R. Keeton, 2003, “Lensing Optical Depths for Substructure and Isolated Dark Matter Halos,” *Astrophys. J.* **592**, 24.
- Chen, Y. M., *et al.*, 2012, “Evolution of the most massive galaxies to $z = 0.6$ - I. A new method for physical parameter estimation,” *Mon. Not. R. Astron. Soc.* **421**, 314 [<http://adsabs.harvard.edu/abs/2012MNRAS.421..314C>].
- Churazov, E., W. Forman, A. Vikhlinin, S. Tremaine, O. Gerhard, and C. Jones, 2008, “Measuring the non-thermal pressure in early-type galaxy atmospheres: a comparison of X-ray and optical potential profiles in M87 and NGC 1399,” *Mon. Not. R. Astron. Soc.* **388**, 1062.
- Churazov, E., S. Tremaine, W. Forman, O. Gerhard, P. Das, A. Vikhlinin, C. Jones, H. Böhringer, and K. Gebhardt, 2010, “Comparison of approximately isothermal gravitational potentials of elliptical galaxies based on X-ray and optical data,” *Mon. Not. R. Astron. Soc.* **404**, 1165 [<http://adsabs.harvard.edu/abs/2010MNRAS.404.1165C>].
- Cimatti, A., *et al.*, 2008, “GMASS ultradeep spectroscopy of galaxies at $z \sim 2$. II. Superdense passive galaxies: how did they form and evolve?,” *Astron. Astrophys.* **482**, 21.
- Coccatto, L., M. Arnaboldi, O. Gerhard, K. C. Freeman, G. Ventimiglia, and N. Yasuda, 2010, “Kinematics and line strength indices in the halos of the Coma brightest cluster galaxies NGC 4874 and NGC 4889,” *Astron. Astrophys.* **519**, A95.
- Coccatto, L., *et al.*, 2009, “Kinematic properties of early-type galaxy haloes using planetary nebulae,” *Mon. Not. R. Astron. Soc.* **394**, 1249.
- Coles, J., 2008, “A New Estimate of the Hubble Time with Improved Modeling of Gravitational Lenses,” *Astrophys. J.* **679**, 17.
- Colín, P., A. A. Klypin, and A. V. Kravtsov, 2000, “Velocity Bias in a Λ Cold Dark Matter Model,” *Astrophys. J.* **539**, 561.
- Conroy, C., 2013, “Modeling the Panchromatic Spectral Energy Distributions of Galaxies,” *Annu. Rev. Astron. Astrophys.* **51**, 393.
- Conroy, C., A. A. Dutton, G. J. Graves, J. T. Mendel, and P. G. van Dokkum, 2013, “Dynamical Versus Stellar Masses in Compact Early-Type Galaxies: Further Evidence for Systematic Variation in the Stellar Initial Mass Function,” [arXiv:1306.2316](https://arxiv.org/abs/1306.2316).
- Conroy, C., and J. E. Gunn, 2010, “The Propagation of Uncertainties in Stellar Population Synthesis Modeling. III. Model Calibration, Comparison, and Evaluation,” *Astrophys. J.* **712**, 833.
- Conroy, C., J. E. Gunn, and M. White, 2009, “The Propagation of Uncertainties in Stellar Population Synthesis Modeling. I. The Relevance of Uncertain Aspects of Stellar Evolution and the Initial Mass Function to the Derived Physical Properties of Galaxies,” *Astrophys. J.* **699**, 486.
- Conroy, C., and P. G. van Dokkum, 2012, “The Stellar Initial Mass Function in Early-type Galaxies From Absorption Line Spectroscopy. II. Results,” *Astrophys. J.* **760**, 71.
- Conroy, C., *et al.*, 2007, “Evolution in the Halo Masses of Isolated Galaxies between $z \sim 1$ and $z \sim 0$: From DEEP2 to SDSS,” *Astrophys. J.* **654**, 153.
- Cooray, A., and R. Sheth, 2002, “Halo models of large scale structure,” *Phys. Rep.* **372**, 1.
- Corsini, E. M., 2011, “Direct measurements of bar pattern speeds,” *Memorie della Societa Astronomica Italiana Supplementi* **18**, 23 [<http://adsabs.harvard.edu/abs/2011MSAIS..18..23C>].
- Corsini, E. M., A. Pizzella, M. Sarzi, P. Cinzano, J. C. Vega Beltrán, J. G. Funes, F. Bertola, M. Persic, and P. Salucci, 1999, “Dark matter in early-type spiral galaxies: the case of NGC 2179 and of NGC 2775,” *Astron. Astrophys.* **342**, 671 [<http://adsabs.harvard.edu/abs/1999A%26A...342..671C>].
- Côté, P., D. E. McLaughlin, J. G. Cohen, and J. P. Blakeslee, 2003, “Dynamics of the Globular Cluster System Associated with M49 (NGC 4472): Cluster Orbital Properties and the Distribution of Dark Matter,” *Astrophys. J.* **591**, 850.

- Courteau, S., 1992, “Tully-Fisher distances and motions in the northern sky,” Ph.D. thesis (University of California, Santa Cruz).
- Courteau, S., 1997, “Optical Rotation Curves and Linewidths for Tully-Fisher Applications,” *Astron. J.* **114**, 2402.
- Courteau, S., D. R. Andersen, M. A. Bershad, L. A. MacArthur, and H. W. Rix, 2003, “The Tully-Fisher Relation of Barred Galaxies,” *Astrophys. J.* **594**, 208.
- Courteau, S., and H. W. Rix, 1999, “Maximal Disks and the Tully-Fisher Relation,” *Astrophys. J.* **513**, 561.
- Courteau, S., and Y.J. Sohn, 2003, “Galaxy Evolution from Emission Linewidths,” in *The Mass of Galaxies at Low and High Redshift*, edited by R. Bender and A. Renzini (Springer-Verlag, Berlin), p. 204 [<http://adsabs.harvard.edu/abs/2003mgllh.conf..204C>].
- Courteau, S., and S. van den Bergh, 1999, “The Solar Motion Relative to the Local Group,” *Astron. J.* **118**, 337.
- Courteau, S., L. M. Widrow, M. McDonald, P. Guhathakurta, K. M. Gilbert, Y. Zhu, R. L. Beaton, and S. R. Majewski, 2011, “The Luminosity Profile and Structural Parameters of the Andromeda Galaxy,” *Astrophys. J.* **739**, 20.
- Cox, T.J., J. Primack, P. Jonsson, and R. S. Somerville, 2004, “Generating Hot Gas in Simulations of Disk-Galaxy Major Mergers,” *Astrophys. J.* **607**, L87.
- Cretton, N., and F.C. van den Bosch, 1999, “Evidence for a Massive Black Hole in the S0 Galaxy NGC 4342,” *Astrophys. J.* **514**, 704.
- Czoske, O., M. Barnabè, L. V.E. Koopmans, T. Treu, and A. S. Bolton, 2008, “Two-dimensional kinematics of SLACS lenses - I. Phase-space analysis of the early-type galaxy SDSSJ2321-097 at $z \sim 0.1$,” *Mon. Not. R. Astron. Soc.* **384**, 987.
- Daddi, E., *et al.*, 2005, “Passively Evolving Early-Type Galaxies at $1.4 < z < 2.5$ in the Hubble Ultra Deep Field,” *Astrophys. J.* **626**, 680.
- Dai, X., M.E. Anderson, J.N. Bregman, and J.M. Miller, 2012, “XMM-Newton Detects a Hot Gaseous Halo in the Fastest Rotating Spiral Galaxy UGC 12591,” *Astrophys. J.* **755**, 107.
- Dalal, N., and C. S. Kochanek, 2002, “Direct Detection of Cold Dark Matter Substructure,” *Astrophys. J.* **572**, 25.
- Das, P., O. Gerhard, R. H. Mendez, A. M. Teodorescu, and F. de Lorenzi, 2011, “Using NMAGIC to probe the dark matter halo and orbital structure of the X-ray bright, massive elliptical galaxy, NGC 4649,” *Mon. Not. R. Astron. Soc.* **415**, 1244.
- Davé, R., D. N. Spergel, P. J. Steinhardt, and B. D. Wandelt, 2001, “Halo Properties in Cosmological Simulations of Self-interacting Cold Dark Matter,” *Astrophys. J.* **547**, 574.
- Davies, R., and R. Genzel, 2010, “MICADO: The Multi-adaptive Optics Imaging Camera for Deep Observations,” *The Messenger* **140**, 32 [<http://adsabs.harvard.edu/abs/2010Msngr.140..32D>].
- Deason, A. J., V. Belokurov, N. W. Evans, and J. An, 2012, “Broken degeneracies: the rotation curve and velocity anisotropy of the Milky Way halo,” *Mon. Not. R. Astron. Soc.* **424**, L44.
- Debbastista, V.P., and J.A. Sellwood, 2000, “Constraints from Dynamical Friction on the Dark Matter Content of Barred Galaxies,” *Astrophys. J.* **543**, 704.
- de Blok, W. J. G., 2010, “The Core-Cusp Problem,” *Adv. Astron.* **2010**, 789293.
- de Blok, W. J. G., F. Walter, E. Brinks, C. Trachternach, S. H. Oh, and R. C. Kennicutt, Jr., 2008, “High-Resolution Rotation Curves and Galaxy Mass Models from THINGS,” *Astron. J.* **136**, 2648.
- Dehnen, W., 2009, “Tailoring triaxial N-body models via a novel made-to-measure method,” *Mon. Not. R. Astron. Soc.* **395**, 1079.
- Dehnen, W., and J. Binney, 1998, “Mass models of the Milky Way,” *Mon. Not. R. Astron. Soc.* **294**, 429.
- Dehnen, W., and O. E. Gerhard, 1993, “Three-integral models of oblate elliptical galaxies,” *Mon. Not. R. Astron. Soc.* **261**, 311 [<http://adsabs.harvard.edu/abs/1993MNRAS.261..>].
- Dehnen, W., and A. King, 2006, “Probing dark matter with X-ray binaries,” *Mon. Not. R. Astron. Soc.* **367**, L29.
- de Jong, R. S., 1996, “Near-infrared and optical broadband surface photometry of 86 face-on disk dominated galaxies. II. A two-dimensional method to determine bulge and disk parameters.,” *Astron. Astrophys. Suppl. Ser.* **118**, 557.
- de Jong, R. S., and E. F. Bell, 2007, “Comparing Dynamical and Stellar Population Mass-To-Light Ratio Estimates,” *Island Universes - Structure and Evolution of Disk Galaxies*, Astrophysics and Space Science Proceedings (Springer, New York), p. 107 [<http://adsabs.harvard.edu/abs/2007iuse.book..107D>].
- de Jong, R. S., and R. L. Davies, 1997, “The Shapes and Ages of Elliptical Galaxies,” *Mon. Not. R. Astron. Soc.* **285**, L1.
- Dejonghe, H., 1989, “A quadratic programming technique for modeling gravitating systems,” *Astrophys. J.* **343**, 113.
- Dejonghe, H., and D. Merritt, 1992, “Inferring the mass of spherical stellar systems from velocity moments,” *Astrophys. J.* **391**, 531.
- Dekel, A., and O. Lahav, 1999, “Stochastic Nonlinear Galaxy Biasing,” *Astrophys. J.* **520**, 24.
- Dekel, A., F. Stoehr, G. A. Mamon, T. J. Cox, G. S. Novak, and J. R. Primack, 2005, “Lost and found dark matter in elliptical galaxies,” *Nature (London)* **437**, 707.
- de Lorenzi, F., V. P. Debbastista, O. Gerhard, and N. Sambhus, 2007, “NMAGIC: a fast parallel implementation of a χ^2 -made-to-measure algorithm for modelling observational data,” *Mon. Not. R. Astron. Soc.* **376**, 71.
- de Lorenzi, F., O. Gerhard, R. P. Saglia, N. Sambhus, V. P. Debbastista, M. Pannella, and R. H. Méndez, 2008, “Dark matter content and internal dynamics of NGC 4697: NMAGIC particle models from slit data and planetary nebula velocities,” *Mon. Not. R. Astron. Soc.* **385**, 1729.
- de Lorenzi, F., *et al.*, 2009, “Dearth of dark matter or massive dark halo? Mass-shape-anisotropy degeneracies revealed by NMAGIC dynamical models of the elliptical galaxy NGC 3379,” *Mon. Not. R. Astron. Soc.* **395**, 76.
- De Lucia, G., *et al.*, 2007, “The build-up of the colour-magnitude relation in galaxy clusters since $z \sim 0.8$,” *Mon. Not. R. Astron. Soc.* **374**, 809.
- de Zeeuw, T., 1985, “Elliptical galaxies with separable potentials,” *Mon. Not. R. Astron. Soc.* **216**, 273 [<http://adsabs.harvard.edu/abs/1985MNRAS.216..273D>].
- di Serego Alighieri, S., *et al.*, 2007, “The HI content of early-type galaxies from the ALFALFA survey. I. Catalogued HI sources in the Virgo cluster,” *Astron. Astrophys.* **474**, 851.
- Dobler, G., and C. R. Keeton, 2006, “Finite source effects in strong lensing: implications for the substructure mass scale,” *Mon. Not. R. Astron. Soc.* **365**, 1243.
- Doherty, M., M. Arnaboldi, P. Das, O. Gerhard, J. A. L. Aguerri, R. Ciardullo, J. J. Feldmeier, K. C. Freeman, G. H. Jacoby, and G. Murante, 2009, “The edge of the M 87 halo and the kinematics of the diffuse light in the Virgo cluster core,” *Astron. Astrophys.* **502**, 771.
- Douglas, N. G., *et al.*, 2002, “The Planetary Nebula Spectrograph: The Green Light for Galaxy Kinematics,” *Publ. Astron. Soc. Pac.* **114**, 1234.
- Douglas, N. G., *et al.*, 2007, “The PN.S Elliptical Galaxy Survey: Data reduction, planetary nebula catalog, and basic dynamics for NGC 3379,” *Astrophys. J.* **664**, 257.
- Drukier, A., and L. Stodolsky, 1984, “Principles and applications of a neutral-current detector for neutrino physics and astronomy,” *Phys. Rev. D* **30**, 2295.

- Dubinski, J., and R. G. Carlberg, 1991, “The structure of cold dark matter halos,” *Astrophys. J.* **378**, 496.
- Dubois, Y., R. Gavazzi, S. Peirani, and J. Silk, 2013, “AGN-driven quenching of star formation: morphological and dynamical implications for early-type galaxies,” *Mon. Not. R. Astron. Soc.* **433**, 3297.
- Duffy, A. R., J. Schaye, S. T. Kay, and C. Dalla Vecchia, 2008, “Dark matter halo concentrations in the Wilkinson Microwave Anisotropy Probe year 5 cosmology,” *Mon. Not. R. Astron. Soc.* **390**, L64.
- Duffy, A. R., J. Schaye, S. T. Kay, C. Dalla Vecchia, R. A. Battye, and C. M. Booth, 2010, “Impact of baryon physics on dark matter structures: a detailed simulation study of halo density profiles,” *Mon. Not. R. Astron. Soc.* **405**, 2161 [<http://adsabs.harvard.edu/abs/2010MNRAS.405.2161D>].
- Dutton, A. A., B. J. Brewer, P. J. Marshall, M. W. Auger, T. Treu, D. C. Koo, A. S. Bolton, B. P. Holden, and L. V. E. Koopmans, 2011, “The SWELLS survey - II. Breaking the disc-halo degeneracy in the spiral galaxy gravitational lens SDSS J2141-0001,” *Mon. Not. R. Astron. Soc.* **417**, 1621.
- Dutton, A. A., C. Conroy, F. C. van den Bosch, F. Prada, and S. More, 2010, “The kinematic connection between galaxies and dark matter haloes,” *Mon. Not. R. Astron. Soc.* **407**, 2.
- Dutton, A. A., C. Conroy, F. C. van den Bosch, L. Simard, J. T. Mendel, S. Courteau, A. Dekel, S. More, and F. Prada, 2011, “Dark halo response and the stellar initial mass function in early-type and late-type galaxies,” *Mon. Not. R. Astron. Soc.* **416**, 322 [<http://adsabs.harvard.edu/abs/2011MNRAS.416.322D>].
- Dutton, A. A., S. Courteau, R. de Jong, and C. Carignan, 2005, “Mass Modeling of Disk Galaxies: Degeneracies, Constraints, and Adiabatic Contraction,” *Astrophys. J.* **619**, 218.
- Dutton, A. A., A. V. Macciò, J. T. Mendel, and L. Simard, 2013, “Universal IMF versus dark halo response in early-type galaxies: breaking the degeneracy with the Fundamental Plane,” *Mon. Not. R. Astron. Soc.* **432**, 2496.
- Dutton, A. A., J. T. Mendel, and L. Simard, 2012, “Evidence for a non-universal stellar initial mass function in low-redshift high-density early-type galaxies,” *Mon. Not. R. Astron. Soc.* **422**, L33.
- Dutton, A. A., and T. Treu, 2013, “The bulge-halo conspiracy in massive elliptical galaxies: implications for the stellar initial mass function and halo response to baryonic processes,” [arXiv:1303.4389](https://arxiv.org/abs/1303.4389).
- Dutton, A. A., F. C. van den Bosch, A. Dekel, and S. Courteau, 2007, “A Revised Model for the Formation of Disk Galaxies: Low Spin and Dark Halo Expansion,” *Astrophys. J.* **654**, 27.
- Eddington, A. S., 1916, “The distribution of stars in globular clusters,” *Mon. Not. R. Astron. Soc.* **76**, 572 [<http://adsabs.harvard.edu/abs/1916MNRAS..76.572E>].
- Einasto, J., 1965, “On the Construction of a Composite Model for the Galaxy and on the Determination of the System of Galactic Parameters,” *Trudy Inst. Astroz. Alma-Ata* **5**, 87 [<http://adsabs.harvard.edu/abs/1965TrAlm...5...87E>].
- Eisenstein, D. J., *et al.*, 2001, “Spectroscopic Target Selection for the Sloan Digital Sky Survey: The Luminous Red Galaxy Sample,” *Astron. J.* **122**, 2267.
- El-Zant, A., I. Shlosman, and Y. Hoffman, 2001, “Dark Halos: The Flattening of the Density Cusp by Dynamical Friction,” *Astrophys. J.* **560**, 636.
- Emsellem, E., H. Dejonghe, and R. Bacon, 1999, “Dynamical models of NGC 3115,” *Mon. Not. R. Astron. Soc.* **303**, 495.
- Emsellem, E., G. Monnet, and R. Bacon, 1994, “The multi-gaussian expansion method: a tool for building realistic photometric and kinematical models of stellar systems I. The formalism,” *Astron. Astrophys.* **285**, 723 [<http://adsabs.harvard.edu/abs/1994A%26A...285..723E>].
- Emsellem, E., *et al.*, 2007, “The SAURON project - IX. A kinematic classification for early-type galaxies,” *Mon. Not. R. Astron. Soc.* **379**, 401.
- Emsellem, E., *et al.*, 2011, “The ATLAS^{3D} project - III. A census of the stellar angular momentum within the effective radius of early-type galaxies: unveiling the distribution of fast and slow rotators,” *Mon. Not. R. Astron. Soc.* **414**, 888.
- Englmaier, P., and O. Gerhard, 1999, “Gas dynamics and large-scale morphology of the Milky Way galaxy,” *Mon. Not. R. Astron. Soc.* **304**, 512.
- Englmaier, P., and O. Gerhard, 2006, “Milky Way Gas Dynamics,” *Celest. Mech. Dyn. Astron.* **94**, 369.
- Faber, S. M., 1972, “Quadratic programming applied to the problem of galaxy population synthesis,” *Astron. Astrophys.* **20**, 361 [<http://adsabs.harvard.edu/abs/1972A%26A....20.361F>].
- Faber, S. M., and J. S. Gallagher, 1979, “Masses and mass-to-light ratios of galaxies,” *Annu. Rev. Astron. Astrophys.* **17**, 135.
- Fahlman, G., N. Kaiser, G. Squires, and D. Woods, 1994, “Dark matter in MS 1224 from distortion of background galaxies,” *Astrophys. J.* **437**, 56.
- Famaey, B., and S. S. McGaugh, 2012, “Modified Newtonian Dynamics (MOND): Observational Phenomenology and Relativistic Extensions,” *Living Rev. Relativity* **15**, 10.
- Feng, J. L., 2010, “Dark Matter Candidates from Particle Physics and Methods of Detection,” *Annu. Rev. Astron. Astrophys.* **48**, 495.
- Féron, C., J. Hjorth, J. P. McKean, and J. Samsing, 2009, “A Search for Disk-Galaxy Lenses in the Sloan Digital Sky Survey,” *Astrophys. J.* **696**, 1319.
- Ferreras, I., F. La Barbera, I. G. de la Rosa, A. Vazdekis, R. R. de Carvalho, J. Falcón-Barroso, and E. Ricciardelli, 2013, “Systematic variation of the stellar initial mass function with velocity dispersion in early-type galaxies,” *Mon. Not. R. Astron. Soc.* **429**, L15.
- Fioc, M., and B. Rocca-Volmerange, 1997, “PEGASE: a UV to NIR spectral evolution model of galaxies. Application to the calibration of bright galaxy counts,” *Astron. Astrophys.* **326**, 950 [<http://adsabs.harvard.edu/abs/1997A%26A...326..950F>].
- Fischer, P., *et al.* (SDSS Collaboration), 2000, “Weak Lensing with Sloan Digital Sky Survey Commissioning Data: The Galaxy-Mass Correlation Function to 1 H⁻¹ Mpc,” *Astron. J.* **120**, 1198.
- Fisher, D., 1997, “Kinematic Profiles of SO Galaxies,” *Astron. J.* **113**, 950.
- Flynn, C., J. Holmberg, L. Portinari, B. Fuchs, and H. Jahreiß, 2006, “On the mass-to-light ratio of the local Galactic disc and the optical luminosity of the Galaxy,” *Mon. Not. R. Astron. Soc.* **372**, 1149.
- Förster Schreiber, N. M., *et al.*, 2006, “SINFONI Integral Field Spectroscopy of $z \sim 2$ UV-selected Galaxies: Rotation Curves and Dynamical Evolution,” *Astrophys. J.* **645**, 1062.
- Franz, M., J. H. Gorkom, and T. de Zeeuw, 1994, “Evidence for axisymmetric halos: The case of IC 2006,” *Astrophys. J.* **436**, 642.
- Freeman, K. C., 1970, “On the Disks of Spiral and SO Galaxies,” *Astrophys. J.* **160**, 811.
- Fu, L., *et al.*, 2008, “Very weak lensing in the CFHTLS wide: cosmology from cosmic shear in the linear regime,” *Astron. Astrophys.* **479**, 9.
- Fukazawa, Y., J. G. Botoya-Nonesa, J. Pu, A. Ohto, and N. Kawano, 2006, “Scaling Mass Profiles around Elliptical Galaxies Observed with Chandra and XMM-Newton,” *Astrophys. J.* **636**, 698.

- Fux, R., 1997, “3D self-consistent N-body barred models of the Milky Way. I. Stellar dynamics,” *Astron. Astrophys.* **327**, 983 [<http://adsabs.harvard.edu/abs/1997A%26A...327..983F>].
- Fux, R., 1999, “3D self-consistent N-body barred models of the Milky Way. II. Gas dynamics,” *Astron. Astrophys.* **345**, 787 [<http://adsabs.harvard.edu/abs/1999A%26A...345..787F>].
- Gallazzi, A., and E.F. Bell, 2009, “Stellar Mass-to-Light Ratios from Galaxy Spectra: How Accurate Can They Be?,” *Astrophys. J. Suppl. Ser.* **185**, 253.
- Gallazzi, A., S. Charlot, J. Brinchmann, S. D. M. White, and C. A. Tremonti, 2005, “The ages and metallicities of galaxies in the local universe,” *Mon. Not. R. Astron. Soc.* **362**, 41.
- Garbari, S., C. Liu, J.I. Read, and G. Lake, 2012, “A new determination of the local dark matter density from the kinematics of K dwarfs,” *Mon. Not. R. Astron. Soc.* **425**, 1445.
- Gavazzi, R., T. Treu, L. V. E. Koopmans, A. S. Bolton, L. A. Moustakas, S. Burles, and P. J. Marshall, 2008, “The Sloan Lens ACS Survey. VI. Discovery and Analysis of a Double Einstein Ring,” *Astrophys. J.* **677**, 1046.
- Gavazzi, R., T. Treu, P. J. Marshall, F. Brault, and A. Ruff, 2012, “The SL2S Galaxy-scale Gravitational Lens Sample. I. The Alignment of Mass and Light in Massive Early-type Galaxies at $z = 0.2-0.9$,” *Astrophys. J.* **761**, 170.
- Gavazzi, R., T. Treu, J. D. Rhodes, L. V. E. Koopmans, A. S. Bolton, S. Burles, R. J. Massey, and L. A. Moustakas, 2007, “The Sloan Lens ACS Survey. IV. The Mass Density Profile of Early-Type Galaxies out to 100 Effective Radii,” *Astrophys. J.* **667**, 176.
- Gebhardt, K., *et al.*, 2003, “Axisymmetric Dynamical Models of the Central Regions of Galaxies,” *Astrophys. J.* **583**, 92.
- Geehan, J. J., M. A. Fardal, A. Babul, and P. Guhathakurta, 2006, “Investigating the Andromeda stream - I. Simple analytic bulge-disc-halo model for M31,” *Mon. Not. R. Astron. Soc.* **366**, 996 [<http://adsabs.harvard.edu/abs/2006MNRAS.366..996G>].
- Geha, M., R. P. van der Marel, P. Guhathakurta, K. M. Gilbert, J. Kalirai, and E. N. Kirby, 2010, “Local Group Dwarf Elliptical Galaxies. II. Stellar Kinematics to Large Radii in NGC 147 and NGC 185,” *Astrophys. J.* **711**, 361.
- Gerhard, O., 2013, “Dark matter in massive galaxies,” *Proceedings of the International Astronomical Union, The Intriguing Life of Massive Galaxies*, IAU Symposium, Vol. 295, p. 211 [<http://adsabs.harvard.edu/abs/2013IAUS..295..211G>].
- Gerhard, O., G. Jeske, R. P. Saglia, and R. Bender, 1998, “Breaking the degeneracy between anisotropy and mass - The dark halo of the E0 galaxy NGC 6703,” *Mon. Not. R. Astron. Soc.* **295**, 197 [<http://adsabs.harvard.edu/abs/1998MNRAS.295..197G>].
- Gerhard, O., A. Kronawitter, R. P. Saglia, and R. Bender, 2001, “Dynamical Family Properties and Dark Halo Scaling Relations of Giant Elliptical Galaxies,” *Astron. J.* **121**, 1936.
- Gerhard, O. E., and M. Vietri, 1986, “The Peculiar Shape of the Inner Galactic Rotation Curve,” *Mon. Not. R. Astron. Soc.* **223**, 377 [<http://adsabs.harvard.edu/abs/1986MNRAS.223..377G>].
- Gerssen, J., K. Kuijken, and M. R. Merrifield, 1997, “The shape of the velocity ellipsoid in NGC 488,” *Mon. Not. R. Astron. Soc.* **288**, 618.
- Gerssen, J., K. Kuijken, and M. R. Merrifield, 2000, “Disc heating in NGC 2985,” *Mon. Not. R. Astron. Soc.* **317**, 545.
- Ghez, A. M., *et al.*, 2008, “Measuring Distance and Properties of the Milky Way’s Central Supermassive Black Hole with Stellar Orbits,” *Astrophys. J.* **689**, 1044.
- Gillessen, S., *et al.*, 2009, “Monitoring Stellar Orbits Around the Massive Black Hole in the Galactic Center,” *Astrophys. J.* **692**, 1075.
- Gilmore, G., M. I. Wilkinson, R. F. G. Wyse, J. T. Kleyna, A. Koch, N. W. Evans, and E. K. Grebel, 2007, “The Observed Properties of Dark Matter on Small Spatial Scales,” *Astrophys. J.* **663**, 948.
- Giovanelli, R., and M. P. Haynes, 2002, “The Inner Scale Length of Spiral Galaxy Rotation Curves,” *Astrophys. J.* **571**, L107.
- Giovanelli, R., M. P. Haynes, V. C. Rubin, and W. K. Ford, Jr., 1986, “UGC 12591 - The most rapidly rotating disk galaxy,” *Astrophys. J.* **301**, L7.
- Gnedin, O. Y., W. R. Brown, M. J. Geller, and S. J. Kenyon, 2010, “The Mass Profile of the Galaxy to 80 kpc,” *Astrophys. J.* **720**, L108.
- Gnedin, O. Y., A. V. Kravtsov, A. A. Klypin, and D. Nagai, 2004, “Response of Dark Matter Halos to Condensation of Baryons: Cosmological Simulations and Improved Adiabatic Contraction Model,” *Astrophys. J.* **616**, 16.
- Gómez, F. A., I. Minchev, B. W. O’Shea, T. C. Beers, J. S. Bullock, and C. W. Purcell, 2013, “Vertical density waves in the Milky Way disc induced by the Sagittarius dwarf galaxy,” *Mon. Not. R. Astron. Soc.* **429**, 159.
- Goodman, M. W., and E. Witten, 1985, “Detectability of certain dark-matter candidates,” *Phys. Rev. D* **31**, 3059.
- Goudfrooij, P., and J. M. D. Kruijssen, 2013, “The Optical Colors of Giant Elliptical Galaxies and their Metal-Rich Globular Cluster s Indicate a Bottom-Heavy Initial Mass Function,” *Astrophys. J.* **762**, 107.
- Governato, F., A. Zolotov, A. Pontzen, C. Christensen, S. H. Oh, A. M. Brooks, T. Quinn, S. Shen, and J. Wadsley, 2012, “Cuspy no more: how outflows affect the central dark matter and baryon distribution in Λ cold dark matter galaxies,” *Mon. Not. R. Astron. Soc.* **422**, 1231.
- Graff, P., M. P. Hobson, and A. Lasenby, 2011, “An investigation into the Multiple Optimised Parameter Estimation and Data compression algorithm,” *Mon. Not. R. Astron. Soc.* **413**, L66.
- Greggio, L., and A. Renzini, 2011, *Stellar Populations. A User Guide from Low to High Redshift*.
- Guzik, J., and U. Seljak, 2001, “Galaxy-dark matter correlations applied to galaxy-galaxy lensing: predictions from the semi-analytic galaxy formation models,” *Mon. Not. R. Astron. Soc.* **321**, 439.
- Guzik, J., and U. Seljak, 2002, “Virial masses of galactic haloes from galaxy-galaxy lensing: theoretical modelling and application to Sloan Digital Sky Survey data,” *Mon. Not. R. Astron. Soc.* **335**, 311.
- Halkola, A., S. Seitz, and M. Pannella, 2007, “The Sizes of Galaxy Halos in Galaxy Cluster Abell 1689,” *Astrophys. J.* **656**, 739.
- Hall, M., S. Courteau, A. A. Dutton, M. McDonald, and Y. Zhu, 2012, “An investigation of Sloan Digital Sky Survey imaging data and multiband scaling relations of spiral galaxies,” *Mon. Not. R. Astron. Soc.* **425**, 2741.
- Hayashi, E., J. F. Navarro, and V. Springel, 2007, “The shape of the gravitational potential in cold dark matter haloes,” *Mon. Not. R. Astron. Soc.* **377**, 50.
- Haynes, M. P., and R. Giovanelli, 1984, “Neutral hydrogen in isolated galaxies. IV - Results for the Arecibo sample,” *Astron. J.* **89**, 758.
- Helmi, A., 2004, “Is the dark halo of our Galaxy spherical?,” *Mon. Not. R. Astron. Soc.* **351**, 643.
- Hernquist, L., 1990, “An analytical model for spherical galaxies and bulges,” *Astrophys. J.* **356**, 359.
- Hewett, P. C., S. J. Warren, J. P. Willis, J. Bland-Hawthorn, and G. F. Lewis, 2000, in “High-Redshift Gravitationally Lensed Galaxies and Tunable Filter Imaging,” edited by W. van Breugel and J. Bland-Hawthorn, *Imaging the Universe in Three Dimensions*, Astronomical Society of the Pacific Conference Series Vol. 195, p. 94 [<http://adsabs.harvard.edu/abs/2000ASPC..195..94H>].
- Heymans, C., *et al.*, 2006, “A weak lensing estimate from GEMS of the virial to stellar mass ratio in massive galaxies to $z \sim 0.8$,” *Mon. Not. R. Astron. Soc.* **371**, L60.

- Hildebrandt, H., L. van Waerbeke, and T. Erben, 2009, “CARS: The CFHTLS-Archive-Research Survey. III. First detection of cosmic magnification in samples of normal high- z galaxies,” *Astron. Astrophys.* **507**, 683.
- Hoekstra, H., B. C. Hsieh, H. K. C. Yee, H. Lin, and M. D. Gladders, 2005, “Virial Masses and the Baryon Fraction in Galaxies,” *Astrophys. J.* **635**, 73.
- Hoekstra, H., and B. Jain, 2008, “Weak Gravitational Lensing and Its Cosmological Applications,” *Annu. Rev. Nucl. Part. Sci.* **58**, 99.
- Hoekstra, H., L. van Waerbeke, M. D. Gladders, Y. Mellier, and H. K. C. Yee, 2002, “Weak Lensing Study of Galaxy Biasing,” *Astrophys. J.* **577**, 604.
- Hoekstra, H., H. K. C. Yee, and M. D. Gladders, 2001, “Measurement of the Bias Parameter from Weak Lensing,” *Astrophys. J.* **558**, L11.
- Hoekstra, H., H. K. C. Yee, and M. D. Gladders, 2004, “Properties of Galaxy Dark Matter Halos from Weak Lensing,” *Astrophys. J.* **606**, 67.
- Holmberg, J., and C. Flynn, 2000, “The local density of matter mapped by Hipparcos,” *Mon. Not. R. Astron. Soc.* **313**, 209.
- Howell, P. J., and T. G. Brainerd, 2010, “Galaxy-galaxy lensing by non-spherical haloes - I. Theoretical considerations,” *Mon. Not. R. Astron. Soc.* **407**, 891.
- Huchra, J., M. Gorenstein, S. Kent, I. Shapiro, G. Smith, E. Horine, and R. Perley, 1985, “2237 + 0305: A new and unusual gravitational lens,” *Astron. J.* **90**, 691.
- Hudson, M. J., S. D. J. Gwyn, H. Dahle, and N. Kaiser, 1998, “Galaxy-Galaxy Lensing in the Hubble Deep Field: The Halo Tully-Fisher Relation at Intermediate Redshift,” *Astrophys. J.* **503**, 531.
- Humphrey, P. J., and D. A. Buote, 2010, “The slope of the mass profile and the tilt of the Fundamental Plane in early-type galaxies,” *Mon. Not. R. Astron. Soc.* **403**, 2143.
- Humphrey, P. J., D. A. Buote, C. R. Canizares, A. C. Fabian, and J. M. Miller, 2011, “A Census of Baryons and Dark Matter in an Isolated, Milky Way Sized Elliptical Galaxy,” *Astrophys. J.* **729**, 53.
- Humphrey, P. J., D. A. Buote, F. Gastaldello, L. Zappacosta, J. S. Bullock, F. Brighenti, and W. G. Mathews, 2006, “A Chandra View of Dark Matter in Early-Type Galaxies,” *Astrophys. J.* **646**, 899.
- Hunter, C., and P. T. de Zeeuw, 1992, “Triaxial galaxy models with thin tube orbits,” *Astrophys. J.* **389**, 79.
- Hunter, C., and E. Qian, 1993, “Two-integral distribution functions for axisymmetric galaxies,” *Mon. Not. R. Astron. Soc.* **262**, 401 [<http://adsabs.harvard.edu/abs/1993MNRAS.262..401H>].
- Hwang, H. S., M. G. Lee, H. S. Park, S. C. Kim, J. H. Park, Y. J. Sohn, S. G. Lee, S. C. Rey, Y. W. Lee, and H. I. Kim, 2008, “The Globular Cluster System of M60 (NGC 4649). II. Kinematics of the Globular Cluster System,” *Astrophys. J.* **674**, 869.
- Ilbert, O., *et al.*, 2010, “Galaxy Stellar Mass Assembly Between $0.2 < z < 2$ from the S-COSMOS Survey,” *Astrophys. J.* **709**, 644.
- Ivezic, Z., J. A. Tyson, and E. Acosta (LSST Collaboration), 2008, “LSST: from Science Drivers to Reference Design and Anticipated Data Products,” [arXiv:0805.2366](http://arxiv.org/abs/0805.2366).
- Jackson, N., S. E. Bryan, S. Mao, and C. Li, 2010, “Satellites in the field and lens galaxies: SDSS/COSMOS versus SLACS/CLASS,” *Mon. Not. R. Astron. Soc.* **403**, 826.
- Jardel, J. R., and K. Gebhardt, 2012, “The Dark Matter Density Profile of the Fornax Dwarf,” *Astrophys. J.* **746**, 89.
- Jaunsen, A. O., and J. Hjorth, 1997, “Detection of a spiral lens galaxy and optical variability in the gravitational lens system B1600 + 434,” *Astron. Astrophys.* **317**, L39 [<http://adsabs.harvard.edu/abs/1997A%26A...317L..39J>].
- Jeans, J. H., 1922, “The motions of stars in a Kapteyn universe,” *Mon. Not. R. Astron. Soc.* **82**, 122 [<http://adsabs.harvard.edu/abs/1922MNRAS...82..122J>].
- Jing, Y. P., and Y. Suto, 2002a, “Triaxial Modeling of Halo Density Profiles with High-Resolution N-Body Simulations,” *Astrophys. J.* **574**, 538.
- Jing, Y. P., and Y. Suto, 2002b, “Triaxial Modeling of Halo Density Profiles with High-Resolution N-Body Simulations,” *Astrophys. J.* **574**, 538.
- Johansson, P. H., A. Burkert, and T. Naab, 2009, “The Evolution of Black Hole Scaling Relations in Galaxy Mergers,” *Astrophys. J.* **707**, L184.
- Kahn, F. D., and L. Woltjer, 1959, “Intergalactic Matter and the Galaxy,” *Astrophys. J.* **130**, 705.
- Kaiser, N., and G. Squires, 1993, “Mapping the dark matter with weak gravitational lensing,” *Astrophys. J.* **404**, 441.
- Kapteyn, J. C., 1922, “First Attempt at a Theory of the Arrangement and Motion of the Sidereal System,” *Astrophys. J.* **55**, 302.
- Kassin, S. A., R. S. de Jong, and B. J. Weiner, 2006, “Dark and Baryonic Matter in Bright Spiral Galaxies. II. Radial Distributions for 34 Galaxies,” *Astrophys. J.* **643**, 804.
- Kauffmann, G., *et al.*, 2003, “The host galaxies of active galactic nuclei,” *Mon. Not. R. Astron. Soc.* **346**, 1055.
- Kayser, R., and S. Refsdal, 1983, “The difference in light travel time between gravitational lens images. I - Generalization of the wavefront method to arbitrary deflectors and inhomogeneous universes,” *Astron. Astrophys.* **128**, 156 [<http://adsabs.harvard.edu/abs/1983A%26A...128..156K>].
- Kazantzidis, S., M. G. Abadi, and J. F. Navarro, 2010, “The Sphericalization of Dark Matter Halos by Galaxy Disks,” *Astrophys. J.* **720**, L62.
- Kazantzidis, S., A. V. Kravtsov, A. R. Zentner, B. Allgood, D. Nagai, and B. Moore, 2004, “The Effect of Gas Cooling on the Shapes of Dark Matter Halos,” *Astrophys. J.* **611**, L73.
- Keeton, C. R., 2001, “Cold Dark Matter and Strong Gravitational Lensing: Concord or Conflict?,” *Astrophys. J.* **561**, 46.
- Keeton, C. R., C. S. Kochanek, and U. Seljak, 1997, “Shear and Ellipticity in Gravitational Lenses,” *Astrophys. J.* **482**, 604.
- Kennicutt, R. C., 1983, “On the evolution of the spiral galaxies in the Virgo cluster,” *Astron. J.* **88**, 483.
- Kent, S. M., 1986, “Dark matter in spiral galaxies. I - Galaxies with optical rotation curves,” *Astron. J.* **91**, 1301.
- Kent, S. M., 1987, “Dark matter in spiral galaxies. II - Galaxies with H I rotation curves,” *Astron. J.* **93**, 816.
- Kent, S. M., 1992, “Galactic structure from the spacelab infrared telescope. III - A dynamical model for the Milky Way bulge,” *Astrophys. J.* **387**, 181.
- Kent, S. M., T. M. Dame, and G. Fazio, 1991, “Galactic structure from the Spacelab infrared telescope. II - Luminosity models of the Milky Way,” *Astrophys. J.* **378**, 131.
- Kerr, F. J., P. F. Bowers, P. D. Jackson, and M. Kerr, 1986, “Fully sampled neutral hydrogen survey of the southern Milky Way,” *Astron. Astrophys. Suppl. Ser.* **66**, 373 [<http://adsabs.harvard.edu/abs/1986A%26AS...66..373K>].
- Kleinheinrich, M., *et al.*, 2006, “Weak lensing measurements of dark matter halos of galaxies from COMBO-17,” *Astron. Astrophys.* **455**, 441.
- Klimontowski, J., E. L. Łokas, S. Kazantzidis, L. Mayer, G. A. Mamon, and F. Prada, 2009, “The orientation and kinematics of inner tidal tails around dwarf galaxies orbiting the Milky Way,” *Mon. Not. R. Astron. Soc.* **400**, 2162.

- Klimontowski, J., E. L. Łokas, S. Kazantzidis, F. Prada, L. Mayer, and G. A. Mamon, 2007, “Mass modelling of dwarf spheroidal galaxies: the effect of unbound stars from tidal tails and the Milky Way,” *Mon. Not. R. Astron. Soc.* **378**, 353.
- Klypin, A., and F. Prada, 2009, “Testing Gravity With Motion of Satellites Around Galaxies: Newtonian Gravity Against Modified Newtonian Dynamics,” *Astrophys. J.* **690**, 1488.
- Klypin, A., H. Zhao, and R. S. Somerville, 2002, “ Λ CDM-based Models for the Milky Way and M31. I. Dynamical Models,” *Astrophys. J.* **573**, 597.
- Knapp, G. R., E. L. Turner, and P. E. Cuniffe, 1985, “The statistical distribution of the neutral-hydrogen content of elliptical galaxies,” *Astron. J.* **90**, 454.
- Kochanek, C. S., 1991, “The implications of lenses for galaxy structure,” *Astrophys. J.* **373**, 354.
- Kochanek, C. S., 1996, “The Mass of the Milky Way,” *Astrophys. J.* **457**, 228.
- Kochanek, C. S., 2006, “Part 2: Strong Gravitational Lensing,” *Gravitational lensing: strong, weak and micro*, Saas-Fee Advanced Course 33 (Springer, Berlin), p. 91 [<http://adsabs.harvard.edu/abs/2006glsw.conf...91K>].
- Kochanek, C. S., and N. Dalal, 2004, “Tests for Substructure in Gravitational Lenses,” *Astrophys. J.* **610**, 69.
- Koopmans, L., 2004, “Dark-Matter and Baryons in Early-type Lens Galaxies,” in *Proceedings of Baryons in Dark Matter Halos*, edited by R. Dettmar, U. Klein, and P. Salucci (SISSA) [<http://adsabs.harvard.edu/abs/2004bdmh.confE..66K>].
- Koopmans, L. V. E., 2005, “Gravitational imaging of cold dark matter substructures,” *Mon. Not. R. Astron. Soc.* **363**, 1136.
- Koopmans, L. V. E., A. Biggs, R. D. Blandford, I. W. A. Browne, N. J. Jackson, S. Mao, P. N. Wilkinson, A. G. de Bruyn, and J. Wambsganss, 2003, “Extrinsic Radio Variability of JVAS/CLASS Gravitational Lenses,” *Astrophys. J.* **595**, 712.
- Koopmans, L. V. E., A. Bolton, T. Treu, O. Czoske, M. W. Auger, M. Barnabè, S. Vegetti, R. Gavazzi, L. A. Moustakas, and S. Burles, 2009, “The Structure and Dynamics of Massive Early-Type Galaxies: On Homology, Isothermality, and Isotropy Inside One Effective Radius,” *Astrophys. J.* **703**, L51.
- Koopmans, L. V. E., A. G. de Bruyn, and N. Jackson, 1998, “The edge-on spiral gravitational lens B1600 + 434,” *Mon. Not. R. Astron. Soc.* **295**, 534.
- Koopmans, L. V. E., and T. Treu, 2002, “The Stellar Velocity Dispersion of the Lens Galaxy in MG 2016 + 112 at $z = 1.004$,” *Astrophys. J.* **568**, L5.
- Koopmans, L. V. E., and T. Treu, 2003, “The Structure and Dynamics of Luminous and Dark Matter in the Early-Type Lens Galaxy of 0047–281 at $z = 0.485$,” *Astrophys. J.* **583**, 606.
- Koopmans, L. V. E., T. Treu, A. S. Bolton, S. Burles, and L. A. Moustakas, 2006, “The Sloan Lens ACS Survey. III. The Structure and Formation of Early-Type Galaxies and Their Evolution since $z \sim 1$,” *Astrophys. J.* **649**, 599.
- Koposov, S. E., H. W. Rix, and D. W. Hogg, 2010, “Constraining the Milky Way Potential with a Six-Dimensional Phase-Space Map of the GD-1 Stellar Stream,” *Astrophys. J.* **712**, 260.
- Kormendy, J., D. B. Fisher, M. E. Cornell, and R. Bender, 2009, “Structure and Formation of Elliptical and Spheroidal Galaxies,” *Astrophys. J. Suppl. Ser.* **182**, 216.
- Kormendy, J., and L. C. Ho, 2013, “Coevolution (Or Not) of Supermassive Black Holes and Host Galaxies,” *Annu. Rev. Astron. Astrophys.* **51**, 511.
- Krajnović, D., M. Cappellari, E. Emsellem, R. M. McDermid, and P. T. de Zeeuw, 2005, “Dynamical modelling of stars and gas in NGC 2974: determination of mass-to-light ratio, inclination and orbital structure using the Schwarzschild method,” *Mon. Not. R. Astron. Soc.* **357**, 1113.
- Krajnović, D., *et al.*, 2011, “The ATLAS^{3D} project - II. Morphologies, kinematic features and alignment between photometric and kinematic axes of early-type galaxies,” *Mon. Not. R. Astron. Soc.* **414**, 2923.
- Kranz, T., A. Slyz, and H. W. Rix, 2003, “Dark Matter within High Surface Brightness Spiral Galaxies,” *Astrophys. J.* **586**, 143.
- Kravtsov, A. V., A. A. Klypin, J. S. Bullock, and J. R. Primack, 1998, “The Cores of Dark Matter-dominated Galaxies: Theory versus Observations,” *Astrophys. J.* **502**, 48.
- Kregel, M., P. C. van der Kruit, and K. C. Freeman, 2005, “Structure and kinematics of edge-on galaxy discs - V. The dynamics of stellar discs,” *Mon. Not. R. Astron. Soc.* **358**, 503.
- Kronawitter, A., R. P. Saglia, O. Gerhard, and R. Bender, 2000, “Orbital structure and mass distribution in elliptical galaxies,” *Astron. Astrophys. Suppl. Ser.* **144**, 53.
- Kroupa, P., 2001, “On the variation of the initial mass function,” *Mon. Not. R. Astron. Soc.* **322**, 231.
- Kuijken, K., 1995, “An Axisymmetric Distribution Function for the Galactic Bulge,” *Astrophys. J.* **446**, 194.
- Kuijken, K., and G. Gilmore, 1989, “The Mass Distribution in the Galactic Disc - II - Determination of the Surface Mass Density of the Galactic Disc Near the Sun,” *Mon. Not. R. Astron. Soc.* **239**, 605 [<http://adsabs.harvard.edu/abs/1989MNRAS.239..605K>].
- Kuzio de Naray, R., C. A. Arsenault, K. Spekkens, J. A. Sellwood, M. McDonald, J. D. Simon, and P. Teuben, 2012, “Searching for non-axisymmetries in NGC 6503: a weak end-on bar,” *Mon. Not. R. Astron. Soc.* **427**, 2523.
- Lablanche, P. Y., *et al.*, 2012, “The ATLAS 3D project - XII. Recovery of the mass-to-light ratio of simulated early-type barred galaxies with axisymmetric dynamical models,” *Mon. Not. R. Astron. Soc.* **424**, 1495.
- Lacy, J. H., C. H. Townes, and D. J. Hollenbach, 1982, “The nature of the central parsec of the Galaxy,” *Astrophys. J.* **262**, 120.
- Lagattuta, D. J., C. D. Fassnacht, M. W. Auger, P. J. Marshall, M. Bradač, T. Treu, R. Gavazzi, T. Schrabback, C. Faure, and T. Anguita, 2010, “Cosmic Evolution of Virial and Stellar Mass in Massive Early-type Galaxies,” *Astrophys. J.* **716**, 1579.
- Laureijs, R., *et al.*, 2011, Euclid Definition Study Report, [arXiv:1110.3193](https://arxiv.org/abs/1110.3193).
- Leauthaud, A., J. Tinker, P. S. Behroozi, M. T. Busha, and R. H. Wechsler, 2011, “A Theoretical Framework for Combining Techniques that Probe the Link Between Galaxies and Dark Matter,” *Astrophys. J.* **738**, 45.
- Leauthaud, A., *et al.*, 2012, “New Constraints on the Evolution of the Stellar-to-dark Matter Connection: A Combined Analysis of Galaxy-Galaxy Lensing, Clustering, and Stellar Mass Functions from $z = 0.2$ to $z = 1$,” *Astrophys. J.* **744**, 159.
- Lee, M. G., H. S. Park, H. S. Hwang, N. Arimoto, N. Tamura, and M. Onodera, 2010, “The Globular Cluster System of the Virgo Giant Elliptical Galaxy NGC 4636. II. Kinematics of the Globular Cluster System,” *Astrophys. J.* **709**, 1083.
- Leitherer, C., and S. Ekström, 2012, in “Population synthesis at the crossroads,” *Proceedings of the IAU Symposium Vol. 284*, edited by R. J. Tuffs and C. C. Popescu, p. 2 [<http://adsabs.harvard.edu/abs/2012IAUS..284....2L>].
- Leonard, P. J. T., and D. Merritt, 1989, “The mass of the open star cluster M35 as derived from proper motions,” *Astrophys. J.* **339**, 195.
- Lewin, J. D., and P. F. Smith, 1996, “Review of mathematics, numerical factors, and corrections for dark matter experiments based on elastic nuclear recoil,” *Astropart. Phys.* **6**, 87.
- Limousin, M., J. P. Kneib, S. Bardeau, P. Natarajan, O. Czoske, I. Smail, H. Ebeling, and G. P. Smith, 2007, “Truncation of galaxy

- dark matter halos in high density environments,” *Astron. Astrophys.* **461**, 881.
- Lin, H., *et al.*, 2009, “Discovery of a Very Bright, Strongly Lensed $z = 2$ Galaxy in the SDSS DR5,” *Astrophys. J.* **699**, 1242.
- Lindblad, P. A. B., P. O. Lindblad, and E. Athanassoula, 1996, “Hydrodynamical simulations of the barred spiral galaxy NGC 1365. Dynamical interpretation of observations,” *Astron. Astrophys.* **313**, 65 [<http://adsabs.harvard.edu/abs/1996A%26A...313...65L>].
- Little, B., and S. Tremaine, 1987, “Distant satellites as probes of our Galaxy’s mass distribution,” *Astrophys. J.* **320**, 493.
- Loewenstein, M., and R. E. White III, 1999, “Prevalence and Properties of Dark Matter in Elliptical Galaxies,” *Astrophys. J.* **518**, 50.
- Lokas, E. L., 2002, “Dark matter distribution in dwarf spheroidal galaxies,” *Mon. Not. R. Astron. Soc.* **333**, 697.
- Lokas, E. L., and G. A. Mamon, 2003, “Dark matter distribution in the Coma cluster from galaxy kinematics: breaking the mass-anisotropy degeneracy,” *Mon. Not. R. Astron. Soc.* **343**, 401.
- Lokas, E. L., G. A. Mamon, and F. Prada, 2005, “Dark matter distribution in the Draco dwarf from velocity moments,” *Mon. Not. R. Astron. Soc.* **363**, 918.
- Long, R. J., and S. Mao, 2010, “Made-to-measure galaxy models - I. Methodology,” *Mon. Not. R. Astron. Soc.* **405**, 301 [<http://adsabs.harvard.edu/abs/2010MNRAS.405..301L>].
- Lynden-Bell, D., R. D. Cannon, and P. J. Godwin, 1983, “Slippery evidence on the Galaxy’s invisible heavy halo,” *Mon. Not. R. Astron. Soc.* **204**, 87P [<http://adsabs.harvard.edu/abs/1983MNRAS.204P.87L>].
- Lyubenova, M., H. Kuntschner, M. Rejkuba, D. R. Silva, M. Kissler-Patig, and L. E. Tacconi-Garman, 2012, “Integrated J- and H-band spectra of globular clusters in the LMC: implications for stellar population models and galaxy age dating,” *Astron. Astrophys.* **543**, A75.
- MacArthur, L. A., 2005, “Dust Sensitivity of Absorption-Line Indices,” *Astrophys. J.* **623**, 795.
- MacArthur, L. A., S. Courteau, E. Bell, and J. A. Holtzman, 2004, “Structure of Disk-dominated Galaxies. II. Color Gradients and Stellar Population Models,” *Astrophys. J. Suppl. Ser.* **152**, 175.
- MacArthur, L. A., J. J. González, and S. Courteau, 2009, “Stellar population and kinematic profiles in spiral bulges and discs: population synthesis of integrated spectra,” *Mon. Not. R. Astron. Soc.* **395**, 28.
- MacArthur, L. A., M. McDonald, S. Courteau, and J. Jesús González, 2010, “Integrated Stellar Populations: Confronting Photometry with Spectroscopy,” *Astrophys. J.* **718**, 768.
- Macciò, A. V., A. A. Dutton, and F. C. van den Bosch, 2008, “Concentration, spin and shape of dark matter haloes as a function of the cosmological model: WMAP1, WMAP3 and WMAP5 results,” *Mon. Not. R. Astron. Soc.* **391**, 1940.
- Macciò, A. V., B. Moore, J. Stadel, and J. Diemand, 2006, “Radial distribution and strong lensing statistics of satellite galaxies and substructure using high-resolution Λ CDM hydrodynamical simulations,” *Mon. Not. R. Astron. Soc.* **366**, 1529 [<http://adsabs.harvard.edu/abs/2006MNRAS.366.1529M>].
- Macciò, A. V., G. Stinson, C. B. Brook, J. Wadsley, H. M. P. Couchman, S. Shen, B. K. Gibson, and T. Quinn, 2012, “Halo Expansion in Cosmological Hydro Simulations: Toward a Baryonic Solution of the Cusp/Core Problem in Massive Spirals,” *Astrophys. J.* **744**, L9.
- Magorrian, J., 1995, “Reconstructing Two-Integral Distribution Functions from Moments,” *Mon. Not. R. Astron. Soc.* **277**, 1185 [<http://adsabs.harvard.edu/abs/1995MNRAS.277.1185M>].
- Magorrian, J., 2013, “Bayes versus the virial theorem: inferring the potential of a galaxy from a kinematical snapshot,” [arXiv:1303.6099](https://arxiv.org/abs/1303.6099).
- Magorrian, J., and D. Ballantyne, 2001, “Mass profiles and anisotropies of early-type galaxies,” *Mon. Not. R. Astron. Soc.* **322**, 702.
- Magorrian, J., and J. Binney, 1994, “Predicting line-of-sight velocity distributions of elliptical galaxies,” *Mon. Not. R. Astron. Soc.* **271**, 949 [<http://adsabs.harvard.edu/abs/1994MNRAS.271..949M>].
- Malhotra, S., 1995, “The Vertical Distribution and Kinematics of H I and Mass Models of the Galactic Disk,” *Astrophys. J.* **448**, 138.
- Maller, A. H., L. Simard, P. Guhathakurta, J. Hjorth, A. O. Jaunsen, R. A. Flores, and J. R. Primack, 2000, “Breaking the Disk/Halo Degeneracy with Gravitational Lensing,” *Astrophys. J.* **533**, 194.
- Mamon, G. A., A. Biviano, and G. Boué, 2013, “MAMPOSS: Modelling Anisotropy and Mass Profiles of Observed Spherical Systems - I. Gaussian 3D velocities,” *Mon. Not. R. Astron. Soc.* **429**, 3079.
- Mamon, G. A., and G. Boué, 2010, “Kinematic deprojection and mass inversion of spherical systems of known velocity anisotropy,” *Mon. Not. R. Astron. Soc.* **401**, 2433.
- Mamon, G. A., E. Łokas, A. Dekel, F. Stoehr, and T. J. Cox, 2006, “Kinematical and Dynamical Modeling of Elliptical Galaxies,” *EAS Publications Series* **20**, 139.
- Mamon, G. A., and E. L. Łokas, 2005a, “Dark matter in elliptical galaxies - I. Is the total mass density profile of the NFW form or even steeper?,” *Mon. Not. R. Astron. Soc.* **362**, 95.
- Mamon, G. A., and E. L. Łokas, 2005b, “Dark matter in elliptical galaxies: II. Estimating the mass within the virial radius,” *Mon. Not. R. Astron. Soc.* **363**, 705.
- Mamon, G. A., and E. L. Łokas, 2006, “Erratum: Dark matter in elliptical galaxies - I. Is the total mass density profile of the NFW form or even steeper?,” *Mon. Not. R. Astron. Soc.* **370**, 1581.
- Mandelbaum, R., C. M. Hirata, T. Broderick, U. Seljak, and J. Brinkmann, 2006, “Ellipticity of dark matter haloes with galaxy-galaxy weak lensing,” *Mon. Not. R. Astron. Soc.* **370**, 1008.
- Mandelbaum, R., U. Seljak, G. Kauffmann, C. M. Hirata, and J. Brinkmann, 2006, “Galaxy halo masses and satellite fractions from galaxy-galaxy lensing in the Sloan Digital Sky Survey: stellar mass, luminosity, morphology and environment dependencies,” *Mon. Not. R. Astron. Soc.* **368**, 715.
- Mao, S., Y. Jing, J. P. Ostriker, and J. Weller, 2004, “Anomalous Flux Ratios in Gravitational Lenses: For or against Cold Dark Matter?,” *Astrophys. J.* **604**, L5.
- Mao, S., and P. Schneider, 1998, “Evidence for substructure in lens galaxies?,” *Mon. Not. R. Astron. Soc.* **295**, 587.
- Maraston, C., 1998, “Evolutionary synthesis of stellar populations: a modular tool,” *Mon. Not. R. Astron. Soc.* **300**, 872.
- Maraston, C., 2005, “Evolutionary population synthesis: models, analysis of the ingredients and application to high- z galaxies,” *Mon. Not. R. Astron. Soc.* **362**, 799.
- Maraston, C., L. Greggio, A. Renzini, S. Ortolani, R. P. Saglia, T. H. Puzia, and M. Kissler-Patig, 2003, “Integrated spectroscopy of bulge globular clusters and fields. II. Implications for population synthesis models and elliptical galaxies,” *Astron. Astrophys.* **400**, 823.
- Maraston, C., M. Kissler-Patig, J. P. Brodie, P. Barmby, and J. P. Huchra, 2001, “The AGB phase-transition outside the local group: K-band observations of young star clusters in NGC 7252,” *Astron. Astrophys.* **370**, 176.
- Maraston, C., *et al.*, 2006, “Evidence for TP-AGB Stars in High-Redshift Galaxies, and Their Effect on Deriving Stellar Population Parameters,” *Astrophys. J.* **652**, 85.
- Maraston, C., J. Pforr, A. Renzini, E. Daddi, M. Dickinson, A. Cimatti, and C. Tonini, 2010, “Star formation rates and masses of

- $z \sim 2$ galaxies from multicolour photometry,” *Mon. Not. R. Astron. Soc.* **407**, 830.
- Maraston, C., and D. Thomas, 2000, “Strong Balmer Lines in Old Stellar Populations: No Need for Young Ages in Ellipticals?,” *Astrophys. J.* **541**, 126.
- Maraston, C., *et al.*, 2012, “Stellar masses of SDSS-III BOSS galaxies at $z \sim 0.5$ and constraints to galaxy formation models,” *Mon. Not. R. Astron. Soc.* (to be published) [[arXiv:1207.6114](https://arxiv.org/abs/1207.6114)].
- Marigo, P., L. Girardi, A. Bressan, M. A. T. Groenewegen, L. Silva, and G. L. Granato, 2008, “Evolution of asymptotic giant branch stars. II. Optical to far-infrared isochrones with improved TP-AGB models,” *Astron. Astrophys.* **482**, 883.
- Martinez, G. D., Q. E. Minor, J. Bullock, M. Kaplinghat, J. D. Simon, and M. Geha, 2011, “A Complete Spectroscopic Survey of the Milky Way Satellite Segue 1: Dark Matter Content, Stellar Membership, and Binary Properties from a Bayesian Analysis,” *Astrophys. J.* **738**, 55.
- Martizzi, D., R. Teyssier, B. Moore, and T. Wentz, 2012, “The effects of baryon physics, black holes and active galactic nucleus feedback on the mass distribution in clusters of galaxies,” *Mon. Not. R. Astron. Soc.* **422**, 3081.
- Mateo, M. L., 1998, “Dwarf Galaxies of the Local Group,” *Annu. Rev. Astron. Astrophys.* **36**, 435.
- Mathewson, D. S., V. L. Ford, and M. Buchhorn, 1992, “A southern sky survey of the peculiar velocities of 1355 spiral galaxies,” *Astrophys. J. Suppl. Ser.* **81**, 413.
- McDonald, M., S. Courteau, R. B. Tully, and J. Roediger, 2011, “A survey of 286 Virgo cluster galaxies at optical griz and near-IR H band: surface brightness profiles and bulge-disc decompositions,” *Mon. Not. R. Astron. Soc.* **414**, 2055.
- McKay, T. A., *et al.*, 2001, “Galaxy Mass and Luminosity Scaling Laws Determined by Weak Gravitational Lensing,” [arXiv:astro-ph/0108013](https://arxiv.org/abs/astro-ph/0108013).
- McKay, T. A., *et al.*, 2002, “Dynamical Confirmation of Sloan Digital Sky Survey Weak-lensing Scaling Laws,” *Astrophys. J.* **571**, L85.
- McMillan, P. J., and J. Binney, 2012, “Analysing surveys of our Galaxy - I. Basic astrometric data,” *Mon. Not. R. Astron. Soc.* **419**, 2251.
- McMillan, P. J., and J. J. Binney, 2013, “Analysing surveys of our Galaxy - II. Determining the potential,” *Mon. Not. R. Astron. Soc.* **433**, 1411.
- McNeil, E. K., M. Arnaboldi, K. C. Freeman, O. E. Gerhard, L. Coccatto, and P. Das, 2010, “Counter-dispersed slitless-spectroscopy technique: planetary nebula velocities in the halo of NGC 1399,” *Astron. Astrophys.* **518**, A44.
- Ménard, B., D. Nestor, D. Turnshek, A. Quider, G. Richards, D. Chelouche, and S. Rao, 2008, “Lensing, reddening and extinction effects of MgII absorbers from $z = 0.4$ to 2,” *Mon. Not. R. Astron. Soc.* **385**, 1053.
- Méndez, R. H., A. Riffeser, R. P. Kudritzki, M. Matthias, K. C. Freeman, M. Arnaboldi, M. Cappacioli, and O. E. Gerhard, 2001, “Detection, Photometry, and Slitless Radial Velocities of 535 Planetary Nebulae in the Flattened Elliptical Galaxy NGC 4697,” *Astrophys. J.* **563**, 135.
- Metcalf, R. B., and A. Amara, 2012, “Small-scale structures of dark matter and flux anomalies in quasar gravitational lenses,” *Mon. Not. R. Astron. Soc.* **419**, 3414.
- Metcalf, R. B., and P. Madau, 2001, “Compound Gravitational Lensing as a Probe of Dark Matter Substructure within Galaxy Halos,” *Astrophys. J.* **563**, 9.
- Michard, R., 1980, “On the M/L ratios in elliptical galaxies,” *Astron. Astrophys.* **91**, 122 [[http://adsabs.harvard.edu/abs/1980A%26A....91..122M](https://adsabs.harvard.edu/abs/1980A%26A....91..122M)].
- Milgrom, M., 1983, “A modification of the Newtonian dynamics as a possible alternative to the hidden mass hypothesis,” *Astrophys. J.* **270**, 365.
- Miyamoto, M., and R. Nagai, 1975, “Three-dimensional models for the distribution of mass in galaxies,” *Publ. Astron. Soc. Jpn.* **27**, 533 [[http://adsabs.harvard.edu/abs/1975PASJ...27..533M](https://adsabs.harvard.edu/abs/1975PASJ...27..533M)].
- Mo, H., F. C. van den Bosch, and S. White, 2010, *Galaxy Formation and Evolution* (Cambridge University Press, Cambridge, England).
- Moni Bidin, C., G. Carraro, R. A. Méndez, and R. Smith, 2012, “Kinematical and Chemical Vertical Structure of the Galactic Thick Disk. II. A Lack of Dark Matter in the Solar Neighborhood,” *Astrophys. J.* **751**, 30.
- More, A., J. P. McKean, S. More, R. W. Porcas, L. V. E. Koopmans, and M. A. Garrett, 2009, “The role of luminous substructure in the gravitational lens system MG 2016 + 112,” *Mon. Not. R. Astron. Soc.* **394**, 174.
- More, A., J. P. McKean, T. W. B. Muxlow, R. W. Porcas, C. D. Fassnacht, and L. V. E. Koopmans, 2008, “Probing a massive radio galaxy with gravitational lensing,” *Mon. Not. R. Astron. Soc.* **384**, 1701.
- More, S., F. C. van den Bosch, M. Cacciato, R. Skibba, H. J. Mo, and X. Yang, 2011a, “Satellite kinematics - III. Halo masses of central galaxies in SDSS,” *Mon. Not. R. Astron. Soc.* **410**, 210.
- Morganti, L., and O. Gerhard, 2012, “Regularizing made-to-measure particle models of galaxies,” *Mon. Not. R. Astron. Soc.* **422**, 1571.
- Morganti, L., O. Gerhard, L. Coccatto, I. Martínez-Valpuesta, and M. Arnaboldi, 2013, “Elliptical galaxies with rapidly decreasing velocity dispersion profiles: NMAGIC models and dark halo parameter estimates for NGC 4494,” *Mon. Not. R. Astron. Soc.* **431**, 3570.
- Morganti, R., P. T. de Zeeuw, T. A. Oosterloo, R. M. McDermid, D. Krajnović, M. Cappellari, F. Kenn, A. Weijmans, and M. Sarzi, 2006, “Neutral hydrogen in nearby elliptical and lenticular galaxies: the continuing formation of early-type galaxies,” *Mon. Not. R. Astron. Soc.* **371**, 157.
- Murphy, J. D., K. Gebhardt, and J. J. Adams, 2011, “Galaxy Kinematics with VIRUS-P: The Dark Matter Halo of M87,” *Astrophys. J.* **729**, 129.
- Nagai, R., and M. Miyamoto, 1976, “A family of self-gravitating stellar systems with axial symmetry,” *Publ. Astron. Soc. Jpn.* **28**, 1 [[http://adsabs.harvard.edu/abs/1976PASJ...28....1N](https://adsabs.harvard.edu/abs/1976PASJ...28....1N)].
- Nagino, R., and K. Matsushita, 2009, “Gravitational potential and X-ray luminosities of early-type galaxies observed with XMM-Newton and Chandra,” *Astron. Astrophys.* **501**, 157.
- Napolitano, N. R., *et al.*, 2011, “The PN.S Elliptical Galaxy Survey: a standard Λ CDM halo around NGC 4374?,” *Mon. Not. R. Astron. Soc.* **411**, 2035.
- Napolitano, N. R., A. J. Romanowsky, and C. Tortora, 2010, “The central dark matter content of early-type galaxies: scaling relations and connections with star formation histories,” *Mon. Not. R. Astron. Soc.* **405**, 2351 [[http://adsabs.harvard.edu/abs/2010MNRAS.405.2351N](https://adsabs.harvard.edu/abs/2010MNRAS.405.2351N)].
- Natarajan, P., and J. Kneib, 1997, “Lensing by galaxy haloes in clusters of galaxies,” *Mon. Not. R. Astron. Soc.* **287**, 833.
- Natarajan, P., J. Kneib, I. Smail, and R. S. Ellis, 1998, “The Mass-to-Light Ratio of Early-Type Galaxies: Constraints from Gravitational Lensing in the Rich Cluster AC 114,” *Astrophys. J.* **499**, 600.
- Natarajan, P., J. Kneib, I. Smail, T. Treu, R. Ellis, S. Moran, M. Limousin, and O. Czoske, 2009, “The Survival of Dark Matter Halos in the Cluster Cl 0024 + 16,” *Astrophys. J.* **693**, 970.
- Navarro, J. F., V. R. Eke, and C. S. Frenk, 1996, “The cores of dwarf galaxy haloes,” *Mon. Not. R. Astron. Soc.* **283**, L72.

- Navarro, J. F., C. S. Frenk, and S. D. M. White, 1996, “The Structure of Cold Dark Matter Halos,” *Astrophys. J.* **462**, 563.
- Navarro, J. F., C. S. Frenk, and S. D. M. White, 1997, “A Universal Density Profile from Hierarchical Clustering,” *Astrophys. J.* **490**, 493.
- Navarro, J. F., E. Hayashi, C. Power, A. R. Jenkins, C. S. Frenk, S. D. M. White, V. Springel, J. Stadel, and T. R. Quinn, 2004, “The inner structure of Λ CDM haloes - III. Universality and asymptotic slopes,” *Mon. Not. R. Astron. Soc.* **349**, 1039.
- Navarro, J. F., A. Ludlow, V. Springel, J. Wang, M. Vogelsberger, S. D. M. White, A. Jenkins, C. S. Frenk, and A. Helmi, 2010, “The diversity and similarity of simulated cold dark matter haloes,” *Mon. Not. R. Astron. Soc.* **402**, 21.
- Neto, A. F., L. Gao, P. Bett, S. Cole, J. F. Navarro, C. S. Frenk, S. D. M. White, V. Springel, and A. Jenkins, 2007, “The statistics of Λ CDM halo concentrations,” *Mon. Not. R. Astron. Soc.* **381**, 1450.
- Neumayer, N., 2010, “The Supermassive Black Hole at the Heart of Centaurus A: Revealed by the Kinematics of Gas and Stars,” *Pub. Astron. Soc. Aust.* **27**, 449.
- Newton, A. J., and J. Binney, 1984, “Constructing distribution functions for spherical galaxies,” *Mon. Not. R. Astron. Soc.* **210**, 711 [<http://adsabs.harvard.edu/abs/1984MNRAS.210.711N>].
- Newton, E. R., P. J. Marshall, T. Treu, M. W. Auger, R. Gavazzi, A. S. Bolton, L. V. E. Koopmans, and L. A. Moustakas, 2011, “The Sloan Lens ACS Survey. XI. Beyond Hubble Resolution: Size, Luminosity, and Stellar Mass of Compact Lensed Galaxies at Intermediate Redshift,” *Astrophys. J.* **734**, 104.
- Nierenberg, A. M., M. W. Auger, T. Treu, P. J. Marshall, C. D. Fassnacht, and M. T. Busha, 2012, “Luminous Satellites. II. Spatial Distribution, Luminosity Function, and Cosmic Evolution,” *Astrophys. J.* **752**, 99.
- Noordermeer, E., M. R. Merrifield, and A. Aragón-Salamanca, 2008, “Exploring disc galaxy dynamics using integral field unit data,” *Mon. Not. R. Astron. Soc.* **388**, 1381 [<http://adsabs.harvard.edu/abs/2008MNRAS.388.1381N>].
- Noordermeer, E., J. M. van der Hulst, R. Sancisi, R. S. Swaters, and T. S. van Albada, 2007, “The mass distribution in early-type disc galaxies: declining rotation curves and correlations with optical properties,” *Mon. Not. R. Astron. Soc.* **376**, 1513.
- Nordsieck, K. H., 1973, “The Angular Momentum of Spiral Galaxies. Methods of Rotation-Curve Analysis,” *Astrophys. J.* **184**, 719.
- O’Connell, R. W., 1976, “Galaxy spectral synthesis. I - Stellar populations in the nuclei of giant ellipticals,” *Astrophys. J.* **206**, 370.
- Oort, J. H., 1926, “Asymmetry in the distribution of stellar velocities,” *Observatory* **49**, 302 [<http://adsabs.harvard.edu/abs/1926Obs...49..302O>].
- Oort, J. H., 1932, “The force exerted by the stellar system in the direction perpendicular to the galactic plane and some related problems,” *Bull. Astron. Inst. Neth.* **6**, 249 [<http://adsabs.harvard.edu/abs/1932BAN.....6..249O>].
- Oort, J. H., 1965, “Stellar Dynamics,” in *Galactic Structure*, edited by A. Blaauw and M. Schmidt (University of Chicago Press, Chicago), p. 455 [<http://adsabs.harvard.edu/abs/1965gast.conf..455O>].
- Opik, E., 1922, “An estimate of the distance of the Andromeda Nebula,” *Astrophys. J.* **55**, 406.
- Ostriker, J. P., and P. J. E. Peebles, 1973, “A Numerical Study of the Stability of Flattened Galaxies: or, can Cold Galaxies Survive?,” *Astrophys. J.* **186**, 467.
- Padmanabhan, N., *et al.*, 2004, “Stellar and dynamical masses of ellipticals in the Sloan Digital Sky Survey,” *New Astron.* **9**, 329.
- Panter, B., R. Jimenez, A. F. Heavens, and S. Charlot, 2007, “The star formation histories of galaxies in the Sloan Digital Sky Survey,” *Mon. Not. R. Astron. Soc.* **378**, 1550.
- Papastergis, E., A. Cattaneo, S. Huang, R. Giovanelli, and M. P. Haynes, 2012, “A Direct Measurement of the Baryonic Mass Function of Galaxies and Implications for the Galactic Baryon Fraction,” *Astrophys. J.* **759**, 138.
- Papastergis, E., A. M. Martin, R. Giovanelli, and M. P. Haynes, 2011, “The Velocity Width Function of Galaxies from the 40% ALFALFA Survey: Shedding Light on the Cold Dark Matter Overabundance Problem,” *Astrophys. J.* **739**, 38.
- Parker, L. C., H. Hoekstra, M. J. Hudson, L. van Waerbeke, and Y. Mellier, 2007, “The Masses and Shapes of Dark Matter Halos from Galaxy-Galaxy Lensing in the CFHT Legacy Survey,” *Astrophys. J.* **669**, 21.
- Partridge, C., O. Lahav, and Y. Hoffman, 2013, “Weighing the Local Group in the presence of dark energy,” *Mon. Not. R. Astron. Soc.* **436**, L45.
- Pease, F. G., 1918, “The Rotation and Radial Velocity of the Central Part of the Andromeda nebula,” *Proc. Natl. Acad. Sci. U.S.A.* **4**, 21.
- Peebles, P. J. E., 1989, “Tracing galaxy orbits back in time,” *Astrophys. J.* **344**, L53.
- Pen, U., 1998, “Reconstructing Nonlinear Stochastic Bias from Velocity Space Distortions,” *Astrophys. J.* **504**, 601.
- Perryman, M. A. C., *et al.*, 2001, “GAIA: Composition, formation and evolution of the Galaxy,” *Astron. Astrophys.* **369**, 339.
- Pfarr, J., C. Maraston, and C. Tonini, 2012, “Recovering galaxy stellar population properties from broad-band spectral energy distribution fitting,” *Mon. Not. R. Astron. Soc.* **422**, 3285.
- Phelps, S., A. Nusser, and V. Desjacques, 2013, “The mass of the Milky Way and M31 using the method of least action,” [arXiv:1306.4013](https://arxiv.org/abs/1306.4013).
- Pickles, A. J., 1985, “Differential population synthesis of early-type galaxies. III - Synthesis results,” *Astrophys. J.* **296**, 340.
- Pierce, M., *et al.*, 2006, “Gemini/GMOS spectra of globular clusters in the Leo group elliptical NGC 3379,” *Mon. Not. R. Astron. Soc.* **366**, 1253.
- Pizzella, A., E. M. Corsini, J. C. Vega Beltrán, and F. Bertola, 2004, “Ionized gas and stellar kinematics of seventeen nearby spiral galaxies,” *Astron. Astrophys.* **424**, 447.
- Pontzen, A., and F. Governato, 2012, “How supernova feedback turns dark matter cusps into cores,” *Mon. Not. R. Astron. Soc.* **421**, 3464.
- Pota, V., *et al.*, 2013, “The SLUGGS Survey: kinematics for over 2500 globular clusters in 12 early-type galaxies,” *Mon. Not. R. Astron. Soc.* **428**, 389.
- Poveda, A., 1958, The Masses of Spherical Galaxies M32. A likely application, *Boletín de los Observatorios Tonantzintla y Tacubaya* **2**, 3 [<http://adsabs.harvard.edu/abs/1958BOTT....2q...3P>].
- Pozzetti, L., *et al.*, 2010, “zCOSMOS - 10k-bright spectroscopic sample. The bimodality in the galaxy stellar mass function: exploring its evolution with redshift,” *Astron. Astrophys.* **523**, A13.
- Prada, F., A. A. Klypin, E. Simonneau, J. Betancort-Rijo, S. Patiri, S. Gottlöber, and M. A. Sanchez-Conde, 2006, “How Far Do They Go? The Outer Structure of Galactic Dark Matter Halos,” *Astrophys. J.* **645**, 1001.
- Prada, F., M. Vitvitska, A. Klypin, J. A. Holtzman, D. J. Schlegel, E. K. Grebel, H. W. Rix, J. Brinkmann, T. A. McKay, and I. Csabai, 2003, “Observing the Dark Matter Density Profile of Isolated Galaxies,” *Astrophys. J.* **598**, 260.
- Press, W. H., and P. Schechter, 1974, “Formation of Galaxies and Clusters of Galaxies by Self-Similar Gravitational Condensation,” *Astrophys. J.* **187**, 425.

- Proctor, R. N., D. A. Forbes, A. J. Romanowsky, J. P. Brodie, J. Strader, M. Spolaor, J. T. Mendel, and L. Spitler, 2009, “Probing the 2D kinematic structure of early-type galaxies out to three effective radii,” *Mon. Not. R. Astron. Soc.* **398**, 91.
- Prugniel, P., and F. Simien, 1997, “The fundamental plane of early-type galaxies: non-homology of the spatial structure.,” *Astron. Astrophys.* **321**, 111 [<http://adsabs.harvard.edu/abs/1997A%26A...321..111P>].
- Read, J. I., G. Lake, O. Agertz, and V. P. Debattista, 2008, “Thin, thick and dark discs in Λ CDM,” *Mon. Not. R. Astron. Soc.* **389**, 1041.
- Reid, M. J., *et al.*, 2009, “Trigonometric Parallaxes of Massive Star-Forming Regions. VI. Galactic Structure, Fundamental Parameters, and Noncircular Motions,” *Astrophys. J.* **700**, 137.
- Remus, R. S., A. Burkert, K. Dolag, P. H. Johansson, T. Naab, L. Oser, and J. Thomas, 2013, “The Dark Halo—Spheroid Conspiracy and the Origin of Elliptical Galaxies,” *Astrophys. J.* **766**, 71.
- Renzini, A., 1981, “Energetics of stellar populations,” *Ann. Phys. (Paris)* **6**, 87 [<http://adsabs.harvard.edu/abs/1981AnPh....6...87R>].
- Renzini, A., and A. Buzzoni, 1986, “Global properties of stellar populations and the spectral evolution of galaxies, Spectral evolution of galaxies,” *Proceedings of the Fourth Workshop, Erice, Italy, 1985 (A87-20001 07-90)* (D. Reidel Publishing Co., Dordrecht), pp. 195–235.
- Renzini, A., and L. Ciotti, 1993, “Transverse Dissections of the Fundamental Planes of Elliptical Galaxies and Clusters of Galaxies,” *Astrophys. J.* **416**, L49.
- Renzini, A., and M. Voli, 1981, “Advanced evolutionary stages of intermediate-mass stars. I - Evolution of surface compositions,” *Astron. Astrophys.* **94**, 175 [<http://adsabs.harvard.edu/abs/1981A%26A....94..175R>].
- Reyes, R., R. Mandelbaum, J. E. Gunn, J. Pizagno, and C. N. Lackner, 2011, “Calibrated Tully-Fisher relations for improved estimates of disc rotation velocities,” *Mon. Not. R. Astron. Soc.* **417**, 2347.
- Reyes, R., R. Mandelbaum, U. Seljak, T. Baldauf, J. E. Gunn, L. Lombiser, and R. E. Smith, 2010, “Confirmation of general relativity on large scales from weak lensing and galaxy velocities,” *Nature (London)* **464**, 256.
- Rhee, G., O. Valenzuela, A. Klypin, J. Holtzman, and B. Moorthy, 2004, “The Rotation Curves of Dwarf Galaxies: A Problem for Cold Dark Matter?,” *Astrophys. J.* **617**, 1059.
- Richardson, T., and M. Fairbairn, 2013a, “Analytical solutions to the mass-anisotropy degeneracy with higher order Jeans analysis: a general method,” *Mon. Not. R. Astron. Soc.* **432**, 3361.
- Richardson, T., and M. Fairbairn, 2013b, “Cores in Classical Dwarf Spheroidal Galaxies? A Dispersion-Kurtosis Jeans Analysis Without Restricted Anisotropy,” [arXiv:1305.0670](https://arxiv.org/abs/1305.0670).
- Richstone, D. O., 1984, “Scale-free models of galaxies. III - A survey of the oblate E6 solution set,” *Astrophys. J.* **281**, 100.
- Richstone, D. O., and S. Tremaine, 1984, “A general method for constructing spherical galaxy models,” *Astrophys. J.* **286**, 27.
- Rix, H.-W., *et al.*, 2004, “GEMS: Galaxy Evolution from Morphologies and SEDs,” *Astrophys. J. Suppl. Ser.* **152**, 163.
- Roberts, M. S., and R. N. Whitehurst, 1975, “The rotation curve and geometry of M31 at large galactocentric distances,” *Astrophys. J.* **201**, 327.
- Roediger, J. C., S. Courteau, L. A. MacArthur, and M. McDonald, 2011, “The formation and evolution of Virgo cluster galaxies - II. Stellar populations,” *Mon. Not. R. Astron. Soc.* **416**, 1996.
- Rogstad, D. H., and G. S. Shostak, 1972, “Gross Properties of Five Scd Galaxies as Determined from 21-centimeter Observations,” *Astrophys. J.* **176**, 315.
- Romanowsky, A. J., N. G. Douglas, M. Arnaboldi, K. Kuijken, M. R. Merrifield, N. R. Napolitano, M. Capaccioli, and K. C. Freeman, 2003, “A Dearth of Dark Matter in Ordinary Elliptical Galaxies,” *Science* **301**, 1696.
- Romanowsky, A. J., J. Strader, L. R. Spitler, R. Johnson, J. P. Brodie, D. A. Forbes, and T. Ponman, 2009, “Mapping The Dark Side with DEIMOS: Globular Clusters, X-Ray Gas, and Dark Matter in the NGC 1407 Group,” *Astron. J.* **137**, 4956.
- Rubin, V. C., J. Burley, A. Kiasatpoor, B. Klock, G. Pease, E. Rutscheidt, and C. Smith, 1962, “Kinematic studies of early-type stars. I. Photometric survey, space motions, and comparison with radio observations,” *Astron. J.* **67**, 491.
- Rubin, V. C., D. Burstein, W. K. Ford, Jr., and N. Thonnard, 1985, “Rotation velocities of 16 SA galaxies and a comparison of Sa, Sb, and SC rotation properties,” *Astrophys. J.* **289**, 81.
- Rubin, V. C., and W. K. Ford, Jr., 1970, “Rotation of the Andromeda Nebula from a Spectroscopic Survey of Emission Regions,” *Astrophys. J.* **159**, 379.
- Ruff, A. J., R. Gavazzi, P. J. Marshall, T. Treu, M. W. Auger, and F. Brault, 2011, “The SL2S Galaxy-scale Lens Sample. II. Cosmic Evolution of Dark and Luminous Mass in Early-type Galaxies,” *Astrophys. J.* **727**, 96.
- Rupen, M. P., 1991, “Neutral hydrogen observations of NGC 4565 and NGC 891,” *Astron. J.* **102**, 48.
- Sackett, P. D., 1997, “Does the Milky Way Have a Maximal Disk?,” *Astrophys. J.* **483**, 103.
- Sage, L. J., G. A. Welch, and L. M. Young, 2007, “The Cool ISM in Elliptical Galaxies. I. A Survey of Molecular Gas,” *Astrophys. J.* **657**, 232.
- Saglia, R. P., G. Bertin, and M. Stiavelli, 1992, “Elliptical Galaxies with Dark Matter. II. Optimal Luminous–Dark Matter Decomposition for a Sample of Bright Objects,” *Astrophys. J.* **384**, 433.
- Saha, P., J. Coles, A. V. Macciò, and L. L. R. Williams, 2006, “The Hubble Time Inferred from 10 Time Delay Lenses,” *Astrophys. J.* **650**, L17.
- Salpeter, E. E., 1955, “The Luminosity Function and Stellar Evolution,” *Astrophys. J.* **121**, 161.
- Sambhus, N., O. Gerhard, and R. H. Méndez, 2006, “Kinematic Evidence for Different Planetary Nebula Populations in the Elliptical Galaxy NGC 4697,” *Astron. J.* **131**, 837.
- Sánchez, S. F., *et al.*, 2012, “CALIFA, the Calar Alto Legacy Integral Field Area survey. I. Survey presentation,” *Astron. Astrophys.* **538**, A8.
- Sanchis, T., E. L. Lokas, and G. A. Mamon, 2004, “The reliability of the kinematical evidence for dark matter: the effects of non-sphericity, substructure and streaming motions,” *Mon. Not. R. Astron. Soc.* **347**, 1198.
- Sandage, A., 1986a, “Star formation rates, galaxy morphology, and the Hubble sequence,” *Astron. Astrophys.* **161**, 89 [<http://adsabs.harvard.edu/abs/1986A%26A...161..89S>].
- Sandage, A., 1986b, “The redshift-distance relation. IX - Perturbation of the very nearby velocity field by the mass of the Local Group,” *Astrophys. J.* **307**, 1.
- Sarzi, M., *et al.*, 2006, “The SAURON project - V. Integral-field emission-line kinematics of 48 elliptical and lenticular galaxies,” *Mon. Not. R. Astron. Soc.* **366**, 1151 [<http://adsabs.harvard.edu/abs/2006MNRAS.366.1151S>].
- Sato, C., 1980, “Dynamical Models of Axisymmetric Galaxies and Their Applications to the Elliptical Galaxy NGC4697,” *Publ. Astron. Soc. Jpn.* **32**, 41 [<http://adsabs.harvard.edu/abs/1980PASJ...32..41S>].
- Scalo, J. M., 1986, “The stellar initial mass function,” *Fundam. Cosm. Phys.* **11**, 1 [<http://adsabs.harvard.edu/abs/1986FCPh...11....1S>].
- Scheiner, J., 1899, “On the spectrum of the great nebula in Andromeda,” *Astrophys. J.* **9**, 149.

- Schneider, P., 1985, “A new formulation of gravitational lens theory, time-delay, and Fermat’s principle,” *Astron. Astrophys.* **143**, 413 [<http://adsabs.harvard.edu/abs/1985A%26A...143..413S>].
- Schneider, P., 2006a, in “Part 1: Introduction to gravitational lensing and cosmology,” *Gravitational Lensing: Strong, Weak and Micro*, Saas-Fee Advanced Course 33, edited by G. Meylan, P. Jetzer, P. North, P. Schneider, C. S. Kochanek, and J. Wambsganss (Springer, New York), p. 1 [<http://adsabs.harvard.edu/abs/2006glsw.conf....1S>].
- Schneider, P., 2006b, in “Part 3: Weak gravitational lensing,” *Saas-Fee Advanced Course 33: Gravitational Lensing: Strong, Weak and Micro*, Saas-Fee Advanced Course 33, edited by G. Meylan, P. Jetzer, P. North, P. Schneider, C. S. Kochanek, and J. Wambsganss (Springer, New York), p. 269 [<http://adsabs.harvard.edu/abs/2006glsw.conf..269S>].
- Schneider, P., J. Ehlers, and E. E. Falco, 1992, *Gravitational Lenses* (Springer-Verlag, Berlin) [<http://adsabs.harvard.edu/abs/1992grle.book.....S>].
- Schönrich, R., 2012, “Galactic rotation and solar motion from stellar kinematics,” *Mon. Not. R. Astron. Soc.* **427**, 274.
- Schuberth, Y., T. Richtler, M. Hilker, B. Dirsch, L. P. Bassino, A. J. Romanowsky, and L. Infante, 2010, “The globular cluster system of NGC 1399. V. dynamics of the cluster system out to 80 kpc,” *Astron. Astrophys.* **513**, A52.
- Schwarzschild, M., 1979, “A numerical model for a triaxial stellar system in dynamical equilibrium,” *Astrophys. J.* **232**, 236.
- Scott, N., *et al.*, 2009, “The SAURON Project - XIV. No escape from V_{esc} : a global and local parameter in early-type galaxy evolution,” *Mon. Not. R. Astron. Soc.* **398**, 1835.
- Scranton, R., *et al.*, 2005, “Detection of Cosmic Magnification with the Sloan Digital Sky Survey,” *Astrophys. J.* **633**, 589.
- Seljak, U., 2000, “Analytic model for galaxy and dark matter clustering,” *Mon. Not. R. Astron. Soc.* **318**, 203.
- Sellwood, J. A., 1985, “The global stability of our Galaxy,” *Mon. Not. R. Astron. Soc.* **217**, 127 [<http://adsabs.harvard.edu/abs/1985MNRAS.217..127S>].
- Sellwood, J. A., and S. S. McGaugh, 2005, “The Compression of Dark Matter Halos by Baryonic Infall,” *Astrophys. J.* **634**, 70.
- Sellwood, J. A., and R. Z. Sánchez, 2010, “Quantifying non-circular streaming motions in disc galaxies,” *Mon. Not. R. Astron. Soc.* **404**, 1733 [<http://adsabs.harvard.edu/abs/2010MNRAS.404.1733S>].
- Sersic, J. L., 1968, *Atlas de Galaxias Australes*, Observatorio Astronomico, Cordoba, Argentina.
- Shapiro, K. L., J. Gerssen, and R. P. van der Marel, 2003, “Observational Constraints on Disk Heating as a Function of Hubble Type,” *Astron. J.* **126**, 2707.
- Shapley, A. E., C. C. Steidel, D. K. Erb, N. A. Reddy, K. L. Adelberger, M. Pettini, P. Barmby, and J. Huang, 2005, “Ultraviolet to Mid-Infrared Observations of Star-forming Galaxies at $z \sim 2$: Stellar Masses and Stellar Populations,” *Astrophys. J.* **626**, 698.
- Sharma, S., J. Bland-Hawthorn, K. V. Johnston, and J. Binney, 2011, “Galaxia: A Code to Generate a Synthetic Survey of the Milky Way,” *Astrophys. J.* **730**, 3.
- Sheldon, E. S., *et al.*, 2004, “The Galaxy-Mass Correlation Function Measured from Weak Lensing in the Sloan Digital Sky Survey,” *Astron. J.* **127**, 2544.
- Sheth, K., J. Melbourne, D. M. Elmegreen, B. G. Elmegreen, E. Athanassoula, R. G. Abraham, and B. J. Weiner, 2012, “Hot Disks and Delayed Bar Formation,” *Astrophys. J.* **758**, 136.
- Shin, E. M., and N. W. Evans, 2008, “The effect of satellite galaxies on gravitational lensing flux ratios,” *Mon. Not. R. Astron. Soc.* **385**, 2107.
- Shu, F. H., R. V. Stachnik, and J. C. Yost, 1971, “On the Density-Wave Theory of Galactic Spirals. III. Comparisons with External Galaxies,” *Astrophys. J.* **166**, 465.
- Simon, J. D., A. D. Bolatto, A. Leroy, and L. Blitz, 2003, “High-Resolution Measurements of the Dark Matter Halo of NGC 2976: Evidence for a Shallow Density Profile,” *Astrophys. J.* **596**, 957.
- Simon, J. D., A. D. Bolatto, A. Leroy, L. Blitz, and E. L. Gates, 2005, “High-Resolution Measurements of the Halos of Four Dark Matter-Dominated Galaxies: Deviations from a Universal Density Profile,” *Astrophys. J.* **621**, 757.
- Simon, J. D., and M. Geha, 2007, “The Kinematics of the Ultrafaint Milky Way Satellites: Solving the Missing Satellite Problem,” *Astrophys. J.* **670**, 313.
- Simon, J. D., *et al.*, 2011, “A Complete Spectroscopic Survey of the Milky Way Satellite Segue 1: The Darkest Galaxy,” *Astrophys. J.* **733**, 46.
- Skrutskie, M. F., *et al.*, 2006, “The Two Micron All Sky Survey (2MASS),” *Astron. J.* **131**, 1163.
- Slipher, V. M., 1914, “The Radial Velocity of the Andromeda Nebula,” *Popular Astronomy* **22**, 19 [<http://adsabs.harvard.edu/abs/1914PA.....22...19S>].
- Smith, M. C., *et al.*, 2007, “The RAVE survey: constraining the local Galactic escape speed,” *Mon. Not. R. Astron. Soc.* **379**, 755.
- Smith, R. J., and J. R. Lucey, 2013, “A giant elliptical galaxy with a lightweight initial mass function,” *Mon. Not. R. Astron. Soc.* **434**, 1964.
- Sofue, Y., and V. Rubin, 2001, “Rotation Curves of Spiral Galaxies,” *Annu. Rev. Astron. Astrophys.* **39**, 137.
- Solanes, J. M., and E. Salvador-Solé, 1990, “Analytical anisotropic models of clusters of galaxies,” *Astron. Astrophys.* **234**, 93 [<http://adsabs.harvard.edu/abs/1990A%26A...234..93S>].
- Sonnenfeld, A., T. Treu, R. Gavazzi, P. J. Marshall, M. W. Auger, S. H. Suyu, L. V. E. Koopmans, and A. S. Bolton, 2012, “Evidence for Dark Matter Contraction and a Salpeter Initial Mass Function in a Massive Early-type Galaxy,” *Astrophys. J.* **752**, 163.
- Spekkens, K., R. Giovanelli, and M. P. Haynes, 2005, “The Cusp/Core Problem in Galactic Halos: Long-Slit Spectra for a Large Dwarf Galaxy Sample,” *Astron. J.* **129**, 2119.
- Spekkens, K., and J. A. Sellwood, 2007, “Modeling Noncircular Motions in Disk Galaxies: Application to NGC 2976,” *Astrophys. J.* **664**, 204.
- Spiniello, C., L. V. E. Koopmans, S. C. Trager, O. Czoske, and T. Treu, 2011, “The X-Shooter Lens Survey - I. Dark matter domination and a Salpeter-type initial mass function in a massive early-type galaxy,” *Mon. Not. R. Astron. Soc.* **417**, 3000.
- Spiniello, C., S. Trager, L. V. E. Koopmans, and C. Conroy, 2013, “The stellar IMF determined in early-type galaxies from a non-degenerate set of optical line indices,” [arXiv:1305.2873](https://arxiv.org/abs/1305.2873).
- Spiniello, C., S. C. Trager, L. V. E. Koopmans, and Y. P. Chen, 2012, “Evidence for a Mild Steepening and Bottom-heavy Initial Mass Function in Massive Galaxies from Sodium and Titanium-oxide Indicators,” *Astrophys. J.* **753**, L32.
- Spinrad, H., and B. J. Taylor, 1971, “The Stellar Content of the Nuclei of Nearby Galaxies. I. M31, M32, and M81,” *Astrophys. J. Suppl. Ser.* **22**, 445.
- Spitzer, L., 1969, “Equipartition and the formation of compact nuclei in spherical stellar systems,” *Astrophys. J.* **158**, L139.
- Springel, V., J. Wang, M. Vogelsberger, A. Ludlow, A. Jenkins, A. Helmi, J. F. Navarro, C. S. Frenk, and S. D. M. White, 2008, “The Aquarius Project: the subhaloes of galactic haloes,” *Mon. Not. R. Astron. Soc.* **391**, 1685.
- Springob, C. M., M. P. Haynes, R. Giovanelli, and B. R. Kent, 2005, “A Digital Archive of H I 21 Centimeter Line Spectra of Optically Targeted Galaxies,” *Astrophys. J. Suppl. Ser.* **160**, 149.

- Statler, T. S., 1989, “Problems in determining the surface density of the Galactic disk,” *Astrophys. J.* **344**, 217.
- Statler, T. S., 2001, “The Shape and Orientation of NGC 3379: Implications for Nuclear Decoupling,” *Astron. J.* **121**, 244.
- Steinmetz, M., *et al.*, 2006, “The Radial Velocity Experiment (RAVE): First Data Release,” *Astron. J.* **132**, 1645.
- Strauss, M. A., *et al.*, 2002, “Spectroscopic Target Selection in the Sloan Digital Sky Survey: The Main Galaxy Sample,” *Astron. J.* **124**, 1810.
- Strigari, L. E., J. S. Bullock, M. Kaplinghat, J. D. Simon, M. Geha, B. Willman, and M. G. Walker, 2008, “A common mass scale for satellite galaxies of the Milky Way,” *Nature (London)* **454**, 1096.
- Strigari, L. E., C. S. Frenk, and S. D. M. White, 2010, “Kinematics of Milky Way satellites in a Lambda cold dark matter universe,” *Mon. Not. R. Astron. Soc.* **408**, 2364.
- Suyu, S. H., and A. Halkola, 2010, “The halos of satellite galaxies: the companion of the massive elliptical lens SL2S J08544-0121,” *Astron. Astrophys.* **524**, A94.
- Suyu, S. H., P. J. Marshall, R. D. Blandford, C. D. Fassnacht, L. V. E. Koopmans, J. P. McKean, and T. Treu, 2009, “Dissecting the Gravitational Lens B1608 + 656. I. Lens Potential Reconstruction,” *Astrophys. J.* **691**, 277.
- Suyu, S. H., *et al.*, 2013, “Two Accurate Time-delay Distances from Strong Lensing: Implications for Cosmology,” *Astrophys. J.* **766**, 70.
- Swaters, R. A., R. Sancisi, T. S. van Albada, and J. M. van der Hulst, 2011, “Are Dwarf Galaxies Dominated by Dark Matter?,” *Astrophys. J.* **729**, 118.
- Syer, D., and S. Tremaine, 1996, “Made-to-measure N-body systems,” *Mon. Not. R. Astron. Soc.* **282**, 223.
- Syget, J. F., H. Tu, B. Fort, and R. Gavazzi, 2010, “A search for edge-on galaxy lenses in the CFHT Legacy Survey,” *Astron. Astrophys.* **517**, A25.
- Tamm, A., E. Tempel, P. Tenjes, O. Tihhonova, and T. Tuvikene, 2012, “Stellar mass map and dark matter distribution in M 31,” *Astron. Astrophys.* **546**, A4.
- Taylor, E. N., M. Franx, J. Brinchmann, A. van der Wel, and P. G. van Dokkum, 2010, “On the Masses of Galaxies in the Local Universe,” *Astrophys. J.* **722**, 1.
- Taylor, E. N., *et al.*, 2011, “Galaxy And Mass Assembly (GAMA): stellar mass estimates,” *Mon. Not. R. Astron. Soc.* **418**, 1587.
- Teodorescu, A. M., R. H. Méndez, F. Bernardi, J. Thomas, P. Das, and O. Gerhard, 2011, “Planetary Nebulae in the Elliptical Galaxy NGC 4649 (M60): Kinematics and Distance Redetermination,” *Astrophys. J.* **736**, 65.
- Teuben, P. J., 2002, in “Velocity Fields of Disk Galaxies,” *Disks of Galaxies: Kinematics, Dynamics and Perturbations*, edited by E. Athanassoula, A. Bosma, and R. Mujica, Astronomical Society of the Pacific Conference Series, Vol. 275 (Astronomical Society of the Pacific, San Francisco), p. 217 [<http://adsabs.harvard.edu/abs/2002ASPC..275..217T>].
- The, L. S., and S. D. M. White, 1986, “The mass of the Coma cluster,” *Astron. J.* **92**, 1248.
- Thomas, D., C. Maraston, and J. Johansson, 2011, “Flux-calibrated stellar population models of Lick absorption-line indices with variable element abundance ratios,” *Mon. Not. R. Astron. Soc.* **412**, 2183.
- Thomas, D., C. Maraston, and A. Korn, 2004, “Higher-order Balmer line indices in α /Fe-enhanced stellar population models,” *Mon. Not. R. Astron. Soc.* **351**, L19.
- Thomas, J., *et al.*, 2009, “The flattening and the orbital structure of early-type galaxies and collisionless N-body binary disc mergers,” *Mon. Not. R. Astron. Soc.* **393**, 641.
- Thomas, J., R. P. Saglia, R. Bender, D. Thomas, K. Gebhardt, J. Magorrian, E. M. Corsini, and G. Wegner, 2007, “Dynamical modelling of luminous and dark matter in 17 Coma early-type galaxies,” *Mon. Not. R. Astron. Soc.* **382**, 657.
- Thomas, J., R. P. Saglia, R. Bender, D. Thomas, K. Gebhardt, J. Magorrian, E. M. Corsini, G. Wegner, and S. Seitz, 2011, “Dynamical masses of early-type galaxies: a comparison to lensing results and implications for the stellar initial mass function and the distribution of dark matter,” *Mon. Not. R. Astron. Soc.* **415**, 545.
- Thomas, J., R. P. Saglia, R. Bender, D. Thomas, K. Gebhardt, J. Magorrian, and D. Richstone, 2004, “Mapping stationary axisymmetric phase-space distribution functions by orbit libraries,” *Mon. Not. R. Astron. Soc.* **353**, 391.
- Tinker, J., A. V. Kravtsov, A. Klypin, K. Abazajian, M. Warren, G. Yepes, S. Gottlöber, and D. E. Holz, 2008, “Toward a Halo Mass Function for Precision Cosmology: The Limits of Universality,” *Astrophys. J.* **688**, 709.
- Tinsley, B. M., 1972, “Galactic Evolution,” *Astron. Astrophys.* **20**, 383 [<http://adsabs.harvard.edu/abs/1972A%26A....20..383T>].
- Tinsley, B. M., and J. E. Gunn, 1976, “Evolutionary synthesis of the stellar population in elliptical galaxies. I - Ingredients, broad-band colors, and infrared features,” *Astrophys. J.* **203**, 52.
- Tojeiro, R., A. F. Heavens, R. Jimenez, and B. Panter, 2007, “Recovering galaxy star formation and metallicity histories from spectra using VESPA,” *Mon. Not. R. Astron. Soc.* **381**, 1252.
- Tojeiro, R., S. Wilkins, A. F. Heavens, B. Panter, and R. Jimenez, 2009, “A Public Catalog of Stellar Masses, Star Formation and Metallicity Histories, and Dust Content from the Sloan Digital Sky Survey using VESPA,” *Astrophys. J. Suppl. Ser.* **185**, 1.
- Tolstoy, E., *et al.*, 2004, “Two Distinct Ancient Components in the Sculptor Dwarf Spheroidal Galaxy: First Results from the Dwarf Abundances and Radial Velocities Team,” *Astrophys. J.* **617**, L119.
- Tonry, J. L., 1983, “Anisotropic velocity dispersions in spherical galaxies,” *Astrophys. J.* **266**, 58.
- Toomre, A., 1963, “On the Distribution of Matter Within Highly Flattened Galaxies,” *Astrophys. J.* **138**, 385.
- Tormen, G., F. R. Bouchet, and S. D. M. White, 1997, “The structure and dynamical evolution of dark matter haloes,” *Mon. Not. R. Astron. Soc.* **286**, 865.
- Tortora, C., A. J. Romanowsky, and N. R. Napolitano, 2013, “An Inventory of the Stellar Initial Mass Function in Early-type Galaxies,” *Astrophys. J.* **765**, 8.
- Trager, S. C., S. M. Faber, G. Worthey, and J. J. González, 2000, “The Stellar Population Histories of Early-Type Galaxies. II. Controlling Parameters of the Stellar Populations,” *Astron. J.* **120**, 165.
- Tremaine, S., D. O. Richstone, Y. I. Byun, A. Dressler, S. M. Faber, C. Grillmair, J. Kormendy, and T. R. Lauer, 1994, “A family of models for spherical stellar systems,” *Astron. J.* **107**, 634.
- Treu, T., 2010, “Strong Lensing by Galaxies,” *Annu. Rev. Astron. Astrophys.* **48**, 87.
- Treu, T., M. W. Auger, L. V. E. Koopmans, R. Gavazzi, P. J. Marshall, and A. S. Bolton, 2010, “The Initial Mass Function of Early-Type Galaxies,” *Astrophys. J.* **709**, 1195.
- Treu, T., A. A. Dutton, M. W. Auger, P. J. Marshall, A. S. Bolton, B. J. Brewer, D. C. Koo, and L. V. E. Koopmans, 2011, “The SWELLS survey - I. A large spectroscopically selected sample of edge-on late-type lens galaxies,” *Mon. Not. R. Astron. Soc.* **417**, 1601.
- Treu, T., R. Gavazzi, A. Gorecki, P. J. Marshall, L. V. E. Koopmans, A. S. Bolton, L. A. Moustakas, and S. Burles, 2009, “The SLACS

- Survey. VIII. The Relation between Environment and Internal Structure of Early-Type Galaxies,” *Astrophys. J.* **690**, 670.
- Treu, T., L. V. Koopmans, A. S. Bolton, S. Burles, and L. A. Moustakas, 2006, “The Sloan Lens ACS Survey. II. Stellar Populations and Internal Structure of Early-Type Lens Galaxies,” *Astrophys. J.* **640**, 662.
- Treu, T., and L. V. E. Koopmans, 2002a, “The Internal Structure and Formation of Early-Type Galaxies: The Gravitational Lens System MG 2016 + 112 at $z = 1.004$,” *Astrophys. J.* **575**, 87.
- Treu, T., and L. V. E. Koopmans, 2002b, “The internal structure of the lens PG1115 + 080: breaking degeneracies in the value of the Hubble constant,” *Mon. Not. R. Astron. Soc.* **337**, L6.
- Treu, T., and L. V. E. Koopmans, 2004, “Massive Dark Matter Halos and Evolution of Early-Type Galaxies to $z \approx 1$,” *Astrophys. J.* **611**, 739.
- Trott, C. M., T. Treu, L. V. E. Koopmans, and R. L. Webster, 2010, “Stars and dark matter in the spiral gravitational lens 2237 + 0305,” *Mon. Not. R. Astron. Soc.* **401**, 1540.
- Trott, C. M., and R. L. Webster, 2002, “Dissecting a galaxy: mass distribution of 2237 + 0305,” *Mon. Not. R. Astron. Soc.* **334**, 621.
- Trujillo, I., A. Burkert, and E. F. Bell, 2004, “The Tilt of the Fundamental Plane: Three-Quarters Structural Nonhomology, One-Quarter Stellar Population,” *Astrophys. J.* **600**, L39.
- Trujillo-Gomez, S., A. Klypin, J. Primack, and A. J. Romanowsky, 2011, “Galaxies in Λ CDM with Halo Abundance Matching: Luminosity-Velocity Relation, Baryonic Mass-Velocity Relation, Velocity Function, and Clustering,” *Astrophys. J.* **742**, 16.
- Tyson, J. A., F. Valdes, J. F. Jarvis, and A. P. Mills, Jr., 1984, “Galaxy mass distribution from gravitational light deflection,” *Astrophys. J.* **281**, L59.
- Tyson, J. A., R. A. Wenk, and F. Valdes, 1990, “Detection of systematic gravitational lens galaxy image alignments-Mapping dark matter in galaxy clusters,” *Astrophys. J.* **349**, L1.
- Valenzuela, O., and A. Klypin, 2003, “Secular bar formation in galaxies with a significant amount of dark matter,” *Mon. Not. R. Astron. Soc.* **345**, 406.
- Valenzuela, O., G. Rhee, A. Klypin, F. Governato, G. Stinson, T. Quinn, and J. Wadsley, 2007, “Is There Evidence for Flat Cores in the Halos of Dwarf Galaxies? The Case of NGC 3109 and NGC 6822,” *Astrophys. J.* **657**, 773.
- Valluri, M., D. Merritt, and E. Emsellem, 2004, “Difficulties with Recovering the Masses of Supermassive Black Holes from Stellar Kinematical Data,” *Astrophys. J.* **602**, 66.
- van Albada, T. S., J. N. Bahcall, K. Begeman, and R. Sancisi, 1985, “Distribution of dark matter in the spiral galaxy NGC 3198,” *Astrophys. J.* **295**, 305.
- van den Bosch, F. C., and R. A. Swaters, 2001, “Dwarf galaxy rotation curves and the core problem of dark matter haloes,” *Mon. Not. R. Astron. Soc.* **325**, 1017.
- van den Bosch, R., T. de Zeeuw, K. Gebhardt, E. Noyola, and G. van de Ven, 2006, “The Dynamical Mass-to-Light Ratio Profile and Distance of the Globular Cluster M15,” *Astrophys. J.* **641**, 852.
- van den Bosch, R. C. E., and G. van de Ven, 2009, “Recovering the intrinsic shape of early-type galaxies,” *Mon. Not. R. Astron. Soc.* **398**, 1117.
- van den Bosch, R. C. E., G. van de Ven, E. K. Verolme, M. Cappellari, and P. T. de Zeeuw, 2008, “Triaxial orbit based galaxy models with an application to the (apparent) decoupled core galaxy NGC 4365,” *Mon. Not. R. Astron. Soc.* **385**, 647.
- van der Kruit, P. C., 1988, “The three-dimensional distribution of light and mass in disks of spiral galaxies,” *Astron. Astrophys.* **192**, 117 [<http://adsabs.harvard.edu/abs/1988A%26A...192..117V>].
- van der Kruit, P. C., and R. J. Allen, 1978, “The kinematics of spiral and irregular galaxies,” *Annu. Rev. Astron. Astrophys.* **16**, 103.
- van der Kruit, P. C., and K. C. Freeman, 2011, “Galaxy Disks,” *Annu. Rev. Astron. Astrophys.* **49**, 301.
- van der Marel, R. P., and J. Anderson, 2010, “New Limits on an Intermediate-Mass Black Hole in Omega Centauri. II. Dynamical Models,” *Astrophys. J.* **710**, 1063.
- van der Marel, R. P., J. Binney, and R. L. Davies, 1990, “Models of Elliptical Galaxies - NGC3379, NGC4261, NGC4278 and NGC4472,” *Mon. Not. R. Astron. Soc.* **245**, 582 [<http://adsabs.harvard.edu/abs/1990MNRAS.245..582V>].
- van der Marel, R. P., N. Cretton, P. T. de Zeeuw, and H. W. Rix, 1998, “Improved Evidence for a Black Hole in M32 from HST/FOS Spectra. II. Axisymmetric Dynamical Models,” *Astrophys. J.* **493**, 613.
- van der Marel, R. P., M. Fardal, G. Besla, R. L. Beaton, S. T. Sohn, J. Anderson, T. Brown, and P. Guhathakurta, 2012, “The M31 Velocity Vector. II. Radial Orbit toward the Milky Way and Implied Local Group Mass,” *Astrophys. J.* **753**, 8.
- van der Marel, R. P., and P. Guhathakurta, 2008, “M31 Transverse Velocity and Local Group Mass from Satellite Kinematics,” *Astrophys. J.* **678**, 187.
- van der Marel, R. P., H. W. Rix, D. Carter, M. Franx, S. D. M. White, and T. de Zeeuw, 1994, “Velocity Profiles of Galaxies with Claimed Black-Holes - Part One - Observations of M31 M32 NGC3115 and NGC4594,” *Mon. Not. R. Astron. Soc.* **268**, 521 [<http://adsabs.harvard.edu/abs/1994MNRAS.268..521V>].
- van de Ven, G., P. T. de Zeeuw, and R. C. E. van den Bosch, 2008, “Recovery of the internal orbital structure of galaxies,” *Mon. Not. R. Astron. Soc.* **385**, 614.
- van de Ven, G., C. Hunter, E. K. Verolme, and P. T. de Zeeuw, 2003, “General solution of the Jeans equations for triaxial galaxies with separable potentials,” *Mon. Not. R. Astron. Soc.* **342**, 1056.
- van de Ven, G., R. C. E. van den Bosch, E. K. Verolme, and P. T. de Zeeuw, 2006, “The dynamical distance and intrinsic structure of the globular cluster ω Centauri,” *Astron. Astrophys.* **445**, 513.
- van Dokkum, P. G., 2008, “Evidence of Cosmic Evolution of the Stellar Initial Mass Function,” *Astrophys. J.* **674**, 29.
- van Dokkum, P. G., and C. Conroy, 2010, “A substantial population of low-mass stars in luminous elliptical galaxies,” *Nature (London)* **468**, 940.
- van Dokkum, P. G., and C. Conroy, 2012, “The Stellar Initial Mass Function in Early-type Galaxies from Absorption Line Spectroscopy. I. Data and Empirical Trends,” *Astrophys. J.* **760**, 70.
- van Uitert, E., H. Hoekstra, T. Schrabback, D. G. Gilbank, M. D. Gladders, and H. K. C. Yee, 2012, “Constraints on the shapes of galaxy dark matter haloes from weak gravitational lensing,” *Astron. Astrophys.* **545**, A71.
- van Uitert, E., H. Hoekstra, M. Velander, D. G. Gilbank, M. D. Gladders, and H. K. C. Yee, 2011, “Galaxy-galaxy lensing constraints on the relation between baryons and dark matter in galaxies in the Red Sequence Cluster Survey 2,” *Astron. Astrophys.* **534**, A14.
- Van Waerbeke, L., 1998, “Scale dependence of the bias investigated by weak lensing,” *Astron. Astrophys.* **334**, 1 [<http://adsabs.harvard.edu/abs/1998A%26A...334...1V>].
- Van Waerbeke, L., Y. Mellier, and H. Hoekstra, 2005, “Dealing with systematics in cosmic shear studies: New results from the VIRMOS-DESCART survey,” *Astron. Astrophys.* **429**, 75.
- Van Waerbeke, L., Y. Mellier, R. Pelló, U. Pen, H. J. McCracken, and B. Jain, 2002, “Likelihood analysis of cosmic shear on simulated and VIRMOS-DESCART data,” *Astron. Astrophys.* **393**, 369.
- Vazdekis, A., E. Casuso, R. F. Peletier, and J. E. Beckman, 1996, “A New Chemo-evolutionary Population Synthesis Model for

- Early-Type Galaxies. I. Theoretical Basis,” *Astrophys. J. Suppl. Ser.* **106**, 307.
- Vega Beltrán, J. C., A. Pizzella, E. M. Corsini, J. G. Funes, W. W. Zeilinger, J. E. Beckman, and F. Bertola, 2001, “Kinematic properties of gas and stars in 20 disc galaxies,” *Astron. Astrophys.* **374**, 394.
- Vegetti, S., O. Czoske, and L. V. E. Koopmans, 2010, “Quantifying dwarf satellites through gravitational imaging: the case of SDSSJ120602.09 + 514229.5,” *Mon. Not. R. Astron. Soc.* **407**, 225.
- Vegetti, S., and L. V. E. Koopmans, 2009, “Bayesian strong gravitational-lens modelling on adaptive grids: objective detection of mass substructure in Galaxies,” *Mon. Not. R. Astron. Soc.* **392**, 945.
- Vegetti, S., L. V. E. Koopmans, A. Bolton, T. Treu, and R. Gavazzi, 2010, “Detection of a dark substructure through gravitational imaging,” *Mon. Not. R. Astron. Soc.* **408**, 1969.
- Vegetti, S., D. J. Lagattuta, J. P. McKean, M. W. Auger, C. D. Fassnacht, and L. V. E. Koopmans, 2012, “Gravitational detection of a low-mass dark satellite galaxy at cosmological distance,” *Nature (London)* **481**, 341.
- Verolme, E. K., M. Cappellari, Y. Copin, R. P. van der Marel, R. Bacon, M. Bureau, R. L. Davies, B. M. Miller, and P. T. de Zeeuw, 2002, “A SAURON study of M32: measuring the intrinsic flattening and the central black hole mass,” *Mon. Not. R. Astron. Soc.* **335**, 517.
- Walcher, J., B. Groves, T. Budavári, and D. Dale, 2011, “Fitting the integrated spectral energy distributions of galaxies,” *Astrophys. Space Sci.* **331**, 1.
- Walker, M. G., M. Mateo, and E. W. Olszewski, 2009, “Stellar Velocities in the Carina, Fornax, Sculptor, and Sextans dSph Galaxies: Data From the Magellan/MMFS Survey,” *Astron. J.* **137**, 3100.
- Walker, M. G., M. Mateo, E. W. Olszewski, J. Peñarrubia, N. Wyn Evans, and G. Gilmore, 2009, “A Universal Mass Profile for Dwarf Spheroidal Galaxies?,” *Astrophys. J.* **704**, 1274.
- Walker, M. G., and J. Peñarrubia, 2011, “A Method for Measuring (Slopes of) the Mass Profiles of Dwarf Spheroidal Galaxies,” *Astrophys. J.* **742**, 20.
- Warren, S. J., A. Iovino, P. C. Hewett, and P. A. Shaver, 1998, “Spectroscopy of the optical Einstein ring 0047-2808,” *Mon. Not. R. Astron. Soc.* **299**, 1215.
- Watkins, L. L., N. W. Evans, and J. H. An, 2010, “The masses of the Milky Way and Andromeda galaxies,” *Mon. Not. R. Astron. Soc.* **406**, 264.
- Weaver, H., and D. R. W. Williams, 1973, “The Berkeley low-latitude survey of neutral hydrogen Part I. Profiles,” *Astron. Astrophys. Suppl. Ser.* **8**, 1 [<http://adsabs.harvard.edu/abs/1973A%26AS....8....1W>].
- Wegner, G. A., E. M. Corsini, J. Thomas, R. P. Saglia, R. Bender, and S. B. Pu, 2012, “Further Evidence for Large Central Mass-to-light Ratios in Early-type Galaxies: The Case of Ellipticals and Lenticulars in the A262 Cluster,” *Astron. J.* **144**, 78.
- Weijmans, A., M. Cappellari, R. Bacon, P. T. de Zeeuw, E. Emsellem, J. Falcón-Barroso, H. Kuntschner, R. M. McDermid, R. C. E. van den Bosch, and G. van de Ven, 2009, “Stellar velocity profiles and line strengths out to four effective radii in the early-type galaxies NGC3379 and 821,” *Mon. Not. R. Astron. Soc.* **398**, 561.
- Weijmans, A. M., D. Krajnović, G. van de Ven, T. A. Oosterloo, R. Morganti, and P. T. de Zeeuw, 2008, “The shape of the dark matter halo in the early-type galaxy NGC 2974,” *Mon. Not. R. Astron. Soc.* **383**, 1343.
- Weinberg, M. D., 1985, “Evolution of barred galaxies by dynamical friction,” *Mon. Not. R. Astron. Soc.* **213**, 451 [<http://adsabs.harvard.edu/abs/1985MNRAS.213..451W>].
- Weiner, B. J., J. A. Sellwood, and T. B. Williams, 2001, “The Disk and Dark Halo Mass of the Barred Galaxy NGC 4123. II. Fluid-Dynamical Models,” *Astrophys. J.* **546**, 931.
- Westfall, K. B., M. A. Bershad, M. A. W. Verheijen, D. R. Andersen, T. P. K. Martinson, R. A. Swaters, and A. Schechtman-Rook, 2011, “The DiskMass Survey. IV. The Dark-matter-dominated Galaxy UGC 463,” *Astrophys. J.* **742**, 18.
- Wevers, B. M. H. R., 1984, “A study of spiral galaxies using HI synthesis observations and photographic surface photometry,” Ph.D. thesis (Groningen University).
- White, S. D. M., and M. J. Rees, 1978, “Core condensation in heavy halos - A two-stage theory for galaxy formation and clustering,” *Mon. Not. R. Astron. Soc.* **183**, 341 [<http://adsabs.harvard.edu/abs/1978MNRAS.183..341W>].
- Widrow, L. M., and J. Dubinski, 2005, “Equilibrium Disk-Bulge-Halo Models for the Milky Way and Andromeda Galaxies,” *Astrophys. J.* **631**, 838.
- Widrow, L. M., S. Gardner, B. Yanny, S. Dodelson, and H. Y. Chen, 2012, “Galactoseismology: Discovery of Vertical Waves in the Galactic Disk,” *Astrophys. J.* **750**, L41.
- Widrow, L. M., B. Pym, and J. Dubinski, 2008, “Dynamical Blueprints for Galaxies,” *Astrophys. J.* **679**, 1239.
- Wilkins, S. M., V. Gonzalez-Perez, C. M. Baugh, C. G. Lacey, and J. Zuntz, 2013, “Single-colour diagnostics of the mass-to-light ratio - I. Predictions from galaxy formation models,” *Mon. Not. R. Astron. Soc.* **431**, 430.
- Wilkinson, M. I., and N. W. Evans, 1999, “The present and future mass of the Milky Way halo,” *Mon. Not. R. Astron. Soc.* **310**, 645.
- Wilkinson, M. I., *et al.*, 2005, “Spectroscopic survey of the Galaxy with Gaia- II. The expected science yield from the Radial Velocity Spectrometer,” *Mon. Not. R. Astron. Soc.* **359**, 1306.
- Williams, M. E. K., *et al.*, 2013, “The wobbly Galaxy: kinematics north and south with RAVE red clump giants,” [arXiv:1302.2468](https://arxiv.org/abs/1302.2468).
- Wojtak, R., E. L. Łokas, G. A. Mamon, and S. Gottlöber, 2009, “The mass and anisotropy profiles of galaxy clusters from the projected phase-space density: testing the method on simulated data,” *Mon. Not. R. Astron. Soc.* **399**, 812.
- Wojtak, R., E. L. Łokas, G. A. Mamon, S. Gottlöber, A. Klypin, and Y. Hoffman, 2008, “The distribution function of dark matter particles in massive haloes,” *Mon. Not. R. Astron. Soc.* **388**, 815.
- Wojtak, R., and G. A. Mamon, 2013, “Physical properties underlying observed kinematics of satellite galaxies,” *Mon. Not. R. Astron. Soc.* **428**, 2407.
- Wolf, J., G. D. Martinez, J. S. Bullock, M. Kaplinghat, M. Geha, R. R. Muñoz, J. D. Simon, and F. F. Avedo, 2010, “Accurate masses for dispersion-supported galaxies,” *Mon. Not. R. Astron. Soc.* **406**, 1220.
- Woodley, K. A., M. Gómez, W. E. Harris, D. Geisler, and G. L. H. Harris, 2010, “The Kinematics of the Globular Cluster System of NGC 5128 with a New Large Sample of Radial Velocity Measurements,” *Astron. J.* **139**, 1871.
- Worthey, G., 1994, “Comprehensive stellar population models and the disentanglement of age and metallicity effects,” *Astrophys. J. Suppl. Ser.* **95**, 107.
- Worthey, G., and D. L. Ottaviani, 1997, “H gamma and H delta Absorption Features in Stars and Stellar Populations,” *Astrophys. J. Suppl. Ser.* **111**, 377.
- Xu, D. D., S. Mao, A. P. Cooper, L. Gao, C. S. Frenk, R. E. Angulo, and J. Helly, 2012, “On the effects of line-of-sight structures on lensing flux-ratio anomalies in a Λ CDM universe,” *Mon. Not. R. Astron. Soc.* **421**, 2553.
- Xu, D. D., S. Mao, J. Wang, V. Springel, L. Gao, S. D. M. White, C. S. Frenk, A. Jenkins, G. Li, and J. F. Navarro, 2009, “Effects of dark matter substructures on gravitational lensing: results from the Aquarius simulations,” *Mon. Not. R. Astron. Soc.* **398**, 1235.

- Xue, X. X., *et al.*, 2008, “The Milky Way’s Circular Velocity Curve to 60 kpc and an Estimate of the Dark Matter Halo Mass from the Kinematics of 2400 SDSS Blue Horizontal-Branch Stars,” *Astrophys. J.* **684**, 1143.
- Xue, X. X., *et al.*, 2011, “Quantifying Kinematic Substructure in the Milky Way’s Stellar Halo,” *Astrophys. J.* **738**, 79.
- Yang, X., H. J. Mo, and F. C. van den Bosch, 2009, “Galaxy Groups in the SDSS DR4. III. The Luminosity and Stellar Mass Functions,” *Astrophys. J.* **695**, 900.
- Yanny, B., *et al.*, 2009, “SEGUE: A Spectroscopic Survey of 240,000 Stars with $g = 14\text{--}20$,” *Astron. J.* **137**, 4377.
- Yegorova, I. A., A. Pizzella, and P. Salucci, 2011, “Probing dark matter haloes of spiral galaxies at poorly explored distances using satellite kinematics,” *Astron. Astrophys.* **532**, A105.
- Young, L. M., *et al.*, 2011, “The ATLAS^{3D} project - IV. The molecular gas content of early-type galaxies,” *Mon. Not. R. Astron. Soc.* **414**, 940.
- Zaritsky, D., J. E. Colucci, P. M. Pessev, R. A. Bernstein, and R. Chandar, 2012, “Evidence for Two Distinct Stellar Initial Mass Functions,” *Astrophys. J.* **761**, 93.
- Zibetti, S., S. Charlot, and H. W. Rix, 2009, “Resolved stellar mass maps of galaxies - I. Method and implications for global mass estimates,” *Mon. Not. R. Astron. Soc.* **400**, 1181.
- Zibetti, S., A. Gallazzi, S. Charlot, D. Pierini, and A. Pasquali, 2013, “Near-infrared spectroscopy of post-starburst galaxies: a limited impact of TP-AGB stars on galaxy spectral energy distributions,” *Mon. Not. R. Astron. Soc.* **428**, 1479.
- Zwaan, M. A., J. M. van der Hulst, W. J. G. de Blok, and S. S. McGaugh, 1995, “The Tully-Fisher relation for low surface brightness galaxies: implications for galaxy evolution,” *Mon. Not. R. Astron. Soc.* **273**, L35 [<http://adsabs.harvard.edu/abs/1995MNRAS.273L..35Z>].
- Zwicky, F., 1933, “Die Rotverschiebung von extragalaktischen Nebeln,” *Helv. Phys. Acta* **6**, 110 [<http://adsabs.harvard.edu/abs/1933AcHP...6..110Z>].